

DECISION MAKING TOOL FOR PIPELINES VULNERABILITY ASSESSMENT WITH EXTERNAL CORROSION, STRESS CORROSION CRACKING CONSIDERATION AND GEO-HAZARD

Dr. Solomon Tesfamariam, P.Eng. (Professor, School of Engineering, UBC)

Haile Woldesellasse (PhD student, UBC)

Dr. Asselin, Edouard, P.Eng. (Professor, Department of Materials Engineering, UBC)

Dr. Min Xu (PDF, Department of Materials Engineering, UBC)

Dr. Dharma Wijewickreme, P.Eng. (Professor, Department of Civil Engineering, UBC)

Dr. Prajakta Jadhav; (PDF, Department of Civil Engineering, UBC)

Final Report

June 2022

Prepared for:

The BC Oil and Gas Research and Innovation Society (BC OGRIS)

PO Box 9331 Stn Prov Govt, Victoria, BC V8W 9N3

Disclaimer

The research team acknowledges the BC Oil and Gas Research and Innovation Society (BC OGRIS) and Mitacs for funding this project. The team also acknowledges Dr. Gouri Bhuyan, P.Eng., from BC Oil and Gas Commission, for the input and direction during the project and for reviews of the report. We also acknowledge contribution of Dr. Balekelayi Ngandu, Dr. Souvik Chakraborty, and Edel R. Martínez.

Disclaimer

THIS VULNERABILITY SOFTWARE IS PROVIDED BY THE RESEARCH TEAM IS “AS IS” AND ANY EXPRESS OR IMPLIED WARRANTIES, INCLUDING, BUT NOT LIMITED TO, THE IMPLIED WARRANTIES OF MERCHANTABILITY AND FITNESS FOR A PARTICULAR PURPOSE ARE DISCLAIMED. IN NO EVENT SHALL THE RESEARCH TEAM’S BE LIABLE FOR ANY DIRECT, INDIRECT, INCIDENTAL, SPECIAL, EXEMPLARY, OR CONSEQUENTIAL DAMAGES (INCLUDING, BUT NOT LIMITED TO, PROCUREMENT OF SUBSTITUTE GOODS OR SERVICES; LOSS OF USE, DATA, OR PROFITS; OR BUSINESS INTERRUPTION) HOWEVER CAUSED AND ON ANY THEORY OF LIABILITY, WHETHER IN CONTRACT, STRICT LIABILITY, OR TORT (INCLUDING NEGLIGENCE OR OTHERWISE) ARISING IN ANY WAY OUT OF THE USE OF THIS SOFTWARE, EVEN IF ADVISED OF THE POSSIBILITY OF SUCH DAMAGE.

Executive Summary

The reliability of oil and gas pipelines is compromised due to deterioration processes, coupled with exposure to natural and human induced hazards. This report has been prepared as a part of the research proposal submitted by researchers at The University of British Columbia (UBC) dated 14 January 2019 on “*Decision Making Tool for Pipelines Vulnerability Assessment with Multi-hazards (Corrosion and Geo-Hazard) Consideration*”. The project was co-funded by BC Oil and Gas Research and Innovation Society (BC OGRIS) and Mitacs for funding this project. The objective for the proposed work is to develop a decision-making tool based on Bayesian belief network (BBN) to assess the vulnerability of pipeline subjected to the corrosion and earthquake-induced ground displacement hazards. Result indicated that the developed tool could derive the reliability of a pipeline operating under various conditions. Sensitivity analyses were also used to show the most sensitive parameters in the model. The developed tool comprises of the following specific tasks:

- Perform experimental test to measure the external corrosion rate (CR) of bare and fusion bonded epoxy (FBE)-coated X60 steel.
- Develop a BBN model for external general corrosion. This model is developed using the experimental corrosion rate data.
- Develop BBN model for external pitting corrosion. This model is developed using a publicly available pitting corrosion database.
- Develop BBN model for stress corrosion cracking. This model is developed based on literature, where the model details are obtained from the code developed by American Society of Mechanical Engineers (ASME) and SCC recommended practices prepared by the Canadian Energy Pipeline Association (CEPA).
- Development of datasets connected with geohazards as input for training the BBN model.
- Develop BBN model for incorporating seismic liquefaction-induced permanent ground displacements. This model is developed using the geohazards dataset.

The BBN model is coupled with an open-source Geographic Information System (GIS) system for visualization and effective decision making. The overall tool can be used by pipeline

operators to prioritize inspection and mitigation actions by quantifying failure probability of single pipeline or pipeline networks under external corrosion only, earthquake-induced ground displacement hazards, and coupled corrosion-earthquake multi-hazard.

Table of Contents

Table of Contents	vii
List of Figures	xi
Chapter 1 Introduction	20
1.1 Background.....	20
1.2 Scope of the report.....	24
Chapter 2 External General Corrosion: Experimental Test	25
2.1 Introduction	25
2.1.1 Overview of External Corrosion on Pipeline Steels	25
2.1.2 Technical Approaches.....	27
2.2 CR of X60 pipe steel in simulated field conditions.....	29
2.2.1 Experimental	29
2.2.2 Results and Discussion	32
2.3 Conclusions	49
Chapter 3 External General Corrosion – BBN Model	51
3.1 Introduction	51
3.2 Motivation for BBN Application.....	52
3.3 Bayesian belief network (BBN)	55
3.4 BBN Model development for corrosion	56
3.4.1 Corrosion rate: Experiments and BBN model	58
3.4.2 Burst pressure capacity	60
3.4.3 Probability of failure	63
3.5 Sensitivity analysis of the BBN model.....	64
3.6 Parametric study	65

3.7 Conclusions	71
Chapter 4 External Pitting Corrosion – BBN Model	73
4.1 Corrosion Mechanism and Factors Affecting its Rate	73
4.1.1 Soil Resistivity	74
4.1.2 Soil pH	74
4.1.3 Redox Potential	74
4.1.4 Chlorides and Sulfates	74
4.1.5 Moisture Content	75
4.2 BBN External Corrosion Model Development	75
4.2.1 Knowledge Based BBN for Coating Failure	76
4.2.2 Corrosion Defect Depth	81
4.2.3 Corrosion Defect Length	85
4.2.4 Results and Discussions	86
4.3 Sensitivity analysis	91
4.4 Conclusions	93
Chapter 5 Stress Corrosion Cracking.....	94
5.1 Introduction	94
5.1.1 Conditions for SCC.....	96
5.2 Factors affecting SCC.....	97
5.2.1 Cracking environment.....	97
5.2.2 Electrochemical potential and temperature.....	98
5.2.3 Coating and surface condition	99
5.2.4 Stress	100
5.2.5 Impact of distance to compressor or pump station	101

5.2.6 Impact of pipeline age.....	102
5.3 Integrity assessment.....	103
5.4 BBN model development for SCC.....	104
5.5 Results and discussions	110
5.6 Conclusions	111
Chapter 6 Seismic Liquefaction-Induced Permanent Ground Displacement	113
6.1 Introduction	113
6.2 Scope of Study.....	113
6.3 Background.....	114
6.4 Task 1 - Estimation of site-specific liquefaction-induced permanent ground displacements hazard as demand on buried pipelines	119
6.4.1 Youd et al. (2002) MLR Model and Usage in PSHA	120
6.4.2 PSHA in OpenQuake.....	121
6.4.3 Attenuation model for calculating lateral spread displacement hazard as the intensity measure type.....	124
6.4.4 Comparisons with Previous Similar PGD Hazard Predictions.....	125
6.4.5 Proposed base-line PGD hazard curves for South-west British Columbia.....	126
6.4.6 Estimation of site-specific PGD Hazard.....	129
6.5 Task 2 - Conduct a literature review specifically on the structural capacity of corroded pipelines.....	130
6.6 Estimation of Preliminary PGD Capacities of Buried Pipelines	131
6.6.1 Task 3 - Estimation of Preliminary PGD Capacities of intact Buried Pipelines	131
6.6.2 Task 4 - Estimation of Preliminary PGD Capacities of Corroded Buried Pipelines	136

6.7 Example calculation	141
6.8 BBN model development for PGD.....	143
6.9 Conclusions	145
Chapter 7 Summary	146

List of Figures

Figure 1-1: Total lengths of pipelines by type and status. Data obtained from BCOGC (2020).	20
Figure 1-2: Figures indicated: (a) Data on failure incidents due to corrosion from 2013 to 2020 and (b) Causes of Pipeline failures in BC.....	21
Figure 1-3: Pipeline failures due to corrosion in Alberta from 1990 to 2012.....	22
Figure 1-4: Causes of pipeline incidents, CEPA member 2014-2018.....	23
Figure 2-1: A schematic of (a) 1.5 cm ² bare electrodes for weight loss tests; (b) a 1 cm ² bare electrode for electrochemical tests; and (c) a coated X60 panel sample for corrosion immersion and electrochemical tests.	29
Figure 2-2: CR mapping of bare X60, small electrode samples, under different test conditions using the weight loss data (the data in the bracket is the electrolyte resistance estimated from EIS tests).	34
Figure 2-3: SEM morphology of corrosion products formed on sample surface after the 28-day tests in sodium sulfate solutions: (a) 40°C, pH 2, CP of -1.6 V; (b) 40°C, pH 7, no CP; and (c) 40°C, pH 12, CP of -1.6 V.....	35
Figure 2-4: XRD results of corrosion products formed on sample surface after the 28-day tests in sodium sulfate solutions: (a) 40°C, pH 2, CP of -1.6 V; (b) 40°C, pH 7, no CP; and (c) 40°C, pH 12, CP of -1.6 V.	35
Figure 2-5: SEM morphology of corrosion products formed on sample surface after the 28-day tests in sodium chloride solutions: (a) 10°C, pH 2, CP of -1.6 V; (b) 10°C, pH 7, CP of -0.8 V; and (c) 10°C, pH 12, no CP.	36
Figure 2-6: Surface morphology of sample tested at 10°C, pH 12, no CP using the 3D profilometer.....	36

Figure 2-7: CR mapping of coated X60 steel under different test conditions (the data in brackets is the volume of water absorbed by the coating after the 28-day test).	37
Figure 2-8: Holiday samples after immersion tests: (a) 65°C, pH7, no CP, NaCl, with a disbondment radius \approx 0 mm; and (b) 65°C, pH12, CP of -0.8 V, NaCl, with a disbondment radius = 12.5 mm.	38
Figure 2-9: FTIR spectrum of as-received FBE coating sample.	39
Figure 2-10: FTIR spectra of FBE coated sample tested at 10 °C.....	40
Figure 2-11: FTIR spectra of FBE coated sample tested at 40°C.....	41
Figure 2-12: FTIR spectra of FBE coated sample tested at 65 °C.....	42
Figure 2-13: (a) Normal probability plot of the studentized residuals to check for normality of residuals; and (b) studentized residuals versus predicted values to check for constant variation.	45
Figure 2-14: Predicted CR using the established mathematical model vs. actual measured CR (Designed points: runs 1-42; extra test points: runs X1-X6 in Table 2-3).....	46
Figure 2-15: CR as a function of both applied CP level and coating scenarios: (a) pH = 2; (b) pH = 7; and (c) pH = 12. The temperature is 40 °C and the salt composition effect was average over that of sodium chloride and sodium sulfate.	47
Figure 2-16: CR predicted by the model for the coated samples with different scenarios: (a) coating with a holiday; (b) coating with a dent; and (c) intact coating. The CP is fixed at -0.8 V, and the salt is the sodium chloride.	48
Figure 2-17: Predicted CR vs. Actual CR for coated samples tested at pH 7.....	49
Figure 3-1 Integration of the BBN model for generalized corrosion.....	58
Figure 3-2 A schematic of multi-parameters considered in the corrosion tests.....	59

Figure 3-3 BBN model for external corrosion rate with respect to a) experimental, and b) analytical model corrosion rates	60
Figure 3-4 Pairwise correlation for burst failure pressure	61
Figure 3-5 BBN model and experimental test failure pressure.....	63
Figure 3-6 BBN node distribution for varying mean values of operating pressure.....	65
Figure 3-7 BBN model for probability of failure and failure pressure variation over a) 1 year, b) 5 years, and c) 10 years.	66
Figure 3-8 Fragility curves for variation in pH (T=40°C, CP=N, coating condition=N, salt composition=SO ₄ , OPMn = 12 MPa)	67
Figure 3-9 Fragility curves for variation in temperature (pH = 7, CP=N, coating condition=N, salt composition=SO ₄ , OPMn = 12 MPa).....	67
Figure 3-10 Fragility curves for consideration of cathodic protection (pH = 7, T=40°C, coating condition=N, salt composition=SO ₄ , OPMn = 12 MPa)	68
Figure 3-11 Fragility curves for coating condition (pH = 7, T=40°C, CP=N, salt composition=SO ₄ , OPMn = 12 MPa)	70
Figure 3-12 Fragility curves for salt composition (pH = 7, T=40°C, CP=N, coating condition=N, OPMn = 12 MPa)	70
Figure 3-13 Fragility curves for variation in operating pressure (pH = 7, T=40°C, CP=N, coating condition=N, salt composition=SO ₄).....	71
Figure 4-1: Schematic representation of the BBN model for failure prediction due to external corrosion	75
Figure 4-2: BBN model for pipeline failure due to external corrosion.....	76
Figure 4-3: Knowledge-based BBN for corrosion initiation time	77
Figure 4-4: Examples of coating failure probability predicted by knowledge-based BBN....	81

Figure 4-5: BBN model for corrosion defect depth	84
Figure 4-6: Average maximum pit depth growth by soil categories	85
Figure 4-7: Evolution of pipeline failure probability and failure pressure capacity due to pitting corrosion	87
Figure 4-8: Predicted relative defect depth distribution for: (a) scenario 1, (b) scenario 2 and (c) scenario 3.....	89
Figure 4-9: Evolution of pipeline failure probability due to leakage.....	90
Figure 4-10: Pipeline failure probability due to burst.....	91
Figure 4-11: Pipeline failure probability due to leakage	91
Figure 4-12: Sensitivity analysis of: (a) coating failure time; (b) defect depth and (c) burst pressure limit state nodes based on variation in the input nodes	92
Figure 5-1: Metallographic section through: (a) high pH SCC (b) near-neutral pH SCC. Taken from (NEB, 1996)	94
Figure 5-2: Life model of stress-corrosion crack that would grow to failure. Taken from (NEB, 1996)	96
Figure 5-3: Conditions necessary for SCC on pipelines (NEB 1996)	97
Figure 5-4: Layout of the model for SCC in pipelines. Taken from (Jain et al., 2013).....	104
Figure 5-5: Hydrostatic test assessment factors. Obtained from Al-Amin et al. (2018)	107
Figure 5-6: Likelihood of failure due to SCC.....	111
Figure 6-1: Case histories reported pipeline failures during (a) 1971 San Fernando Earthquake, (b) 1994 Northridge Earthquake, (c) 1992 Landers and Big Bear Earthquakes, and (d) 2011 Japan Earthquake (Ariman et al., 1987; Lund, 1994, 1996; Mori et al., 2012)	115

Figure 6-2: Different types of liquefaction-induced ground displacements, viz., (a) sand boils, (b) Flow Slides, (c) lateral spreading and (d) bearing capacity	116
Figure 6-3: An example of fragility curve (O'Rourke, T. D et al. 1991)	117
Figure 6-4: Overview of the proposed basic framework	117
Figure 6-5: Conceptual BBN to incorporate seismic liquefaction-induced permanent ground displacements	118
Figure 6-6: Cities in southwestern component of Canada used for the present project	122
Figure 6-7: Comparison of UHS obtained from PSHA in OpenQuake with those from NBCC 2015 of selected cities, viz., (a) Vancouver (b) Victoria (c) Kamloops from South-west Canada	123
Figure 6-8: Lateral spread hazard curves obtained from PSHA in OpenQuake for selected cities for (a) Sloping ground, and (b) free-face conditions (T15=15 m, F15=5%, D5015=0.3 mm, S=6 %, W=20%)	125
Figure 6-9: Comparison of lateral spread hazard curves obtained from PSHA in OpenQuake with those from Honegger et al. (2010) for selected cities for (a) Sloping ground, and (b) free-face conditions (T15=15 m, F15=5%, D5015=0.3 mm, S=6 %, W=20%)	126
Figure 6-10: Cities in southwestern component of Canada with BCOGC sites	127
Figure 6-11: Lateral spread hazard curves obtained from PSHA in OpenQuake for BCOGC sites for (a) Sloping ground, and (b) free-face conditions (T15=15 m, F15=5%, D5015=0.3 mm, S=6 %, W=20%)	128
Figure 6-12: Figure showing negligible difference between lateral spread displacements obtained from PSHA and that by factoring of base-line curves	130
Figure 6-13: Pipeline subjected to (a) transverse ground movement and (b) longitudinal ground movement	131

Figure 6-14: Load distribution on pipe subjected to axial ground movement.....	132
Figure 6-15: Comparison of longitudinal lateral spread dimensions from review of historical data and closed-form approximation	133
Figure 6-16: Details of FE model of pipe developed in ABAQUS and the obtained results from analyses	135
Figure 6-17: Physical model of pipeline and soil deformation (after T. O'Rourke) and the obtained results (after Liu and O' Rourke 1997)	137
Figure 6-18: Variation of longitudinal strains with permanent ground displacements for NPS 12 pipe for different levels of corrosion using analytical model	139
Figure 6-19: Variation of longitudinal strains with permanent ground displacements for NPS 12 pipe for different levels of corrosion using FE model	140
Figure 6-20: Flow diagrams explaining the example for the calculation of PGD demand and two cases of PGD capacities (a) longitudinal, and (b) transverse.....	142
Figure 6-21: Layout of the BBN model for liquefaction induced permanent ground displacement	144
Figure 6-22: BBN model for the longitudinal PGD capacity	144
Figure 6-23: BBN model for the transverse PGD capacity	144

List of Tables

Table 2-1: CR of different pipe steels with and without a coating	26
Table 2-2: Independent parameters studied (either numerical or categorical type).....	27
Table 2-3: Levels and description of variables in actual form.....	28
Table 2-4: Levels and description of variables in coded form and the CR response.....	43
Table 2-5: The coefficients in the established mathematical equation	44
Table 2-6: ANOVA test for modified quadratic model	45
Table 3-1: Comparison of various network-based techniques (adapted from Kabir et al. 2014)	54
Table 3-2: Contributing factors to the CR of pipelines (CAPP 2018).....	57
Table 3-3: The coefficients in the established mathematical equation (Xu <i>et al.</i> 2021)	59
Table 3-4: Discretization details of the uniform corrosion BBN model nodes	59
Table 3-5: Discretization details of the burst pressure BBN model nodes	62
Table 3-6: Discretization details of the burst pressure failure probability.....	63
Table 4-1: Types of coating and its expected service time	77
Table 4-2: Parameters and their discretization for coating failure model.....	80
Table 4-3: Equation coefficients for the pitting exponent and the coefficient of proportionality for different soil types	82
Table 4-4: Discretization details of the external BBN model nodes	83
Table 4-5: Average value of the model parameters for pit growth. Adapted from Velázquez et al., (2009)	85
Table 4-6: Random variables and their parameters used in the example	86

Table 4-7: Probabilistic data of input parameters	88
Table 4-8: CTE and RME for defect depth and PoF of three scenarios	89
Table 5-1: Comparison of Near-neutral-pH and High-pH SCC (NEB 1996)	95
Table 5-2: Number of reported high-pH SCC failures of gas transmission pipelines as a function of operating stress (ASME 2008)	101
Table 5-3: High pH SCC failures as a function of proximity to compressor discharge stations (ASME 2008).....	102
Table 5-4: Near-neutral pH SCC failures as a function of proximity to compressor or pump station stations (ASME 2008).....	102
Table 5-5: Near-neutral pH SCC failures as a function of age (ASME 2008)	103
Table 5-6: General Reliability and General Reliance Factor.....	106
Table 5-7: ILI Assessment Factor.....	106
Table 5-8: General Reliability and General Reliance Factor.....	108
Table 5-9: Scores for Pipe Age.....	109
Table 5-10: Scores for Operating Stress	109
Table 5-11: Scores for HPC.....	109
Table 5-12: Example of Scores for Coating-Soil-Drainage.....	110
Table 5-13: Example of Scores for Coating, Pipe Manufacturer and Construction Year Combinations	110
Table 5-14: Scores for Distance from Upstream Compressor Station.....	110
Table 5-15: Scores for Landform/Topography.....	110
Table 5-16: Scores for CP.....	110
Table 5-17: Input parameters for SCC.....	111

Table 6-1: Pipeline Failure Probability and Bending Tension Strain	134
Table 6-2: Pipeline Perpendicular Displacement Capacities for Straight Pipe.....	134
Table 6-3: Comparison of PGDs corresponding to different strain levels from the FE model with those reported in Terasen (2010)	136
Table 6-4: Modification factors to account for corrosion for different pipe sizes using analytical model.....	139
Table 6-5: Transverse PGD capacities for corroded pipelines for different NPS sizes.....	141

Chapter 1

Introduction

1.1 Background

The oil & gas industry is vital to the economy and prosperity of a country. The industry products (e.g., natural gas and oil) are distributed through pipes because they are safe and efficient mode of transportation. The nature of the product transported and the aggressivity of the environment in which the pipelines are buried pose a significant threat to the safety of pipe operations. Hence, secure operation of pipelines is essential for the population safety and protection of the environment (BCOGC 2020).

In British Columbia (BC), the BC Oil and Gas Commission (BCOGC) protects public safety and safeguards the environment through sound regulation of oil, gas, and geothermal activities in B.C. The recent annual report disclosed that the commission regulates around 50,800 km of pipelines that transport refined and unrefined products including natural gas, sour natural gas, and liquid hydrocarbons (such as crude oil and high vapor pressure hydrocarbons), water and other miscellaneous gases (BCOGC 2020). Figure 1-1 indicates the total length of pipes by type and status, in which over 78% of the total pipelines transport natural gas and approximately 11% carry liquid hydrocarbons.

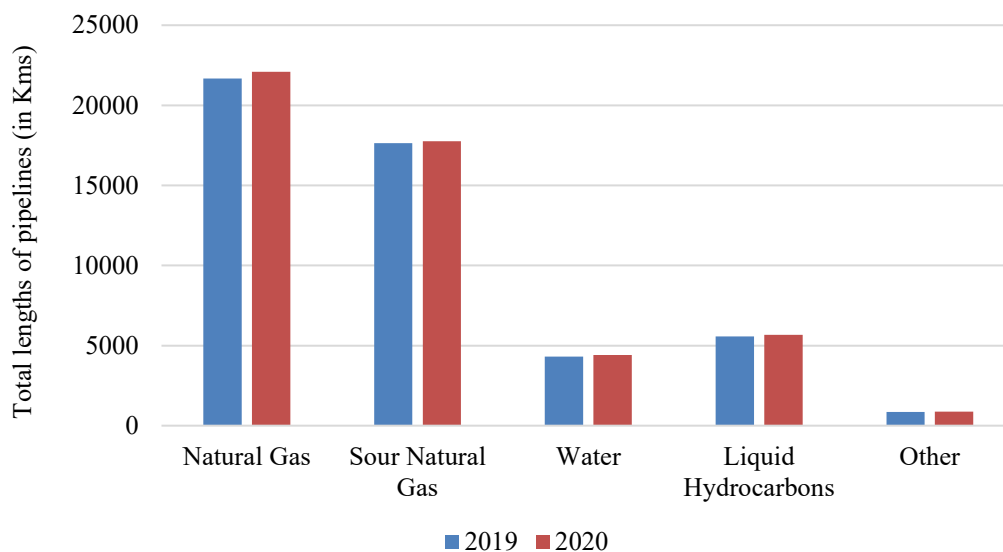
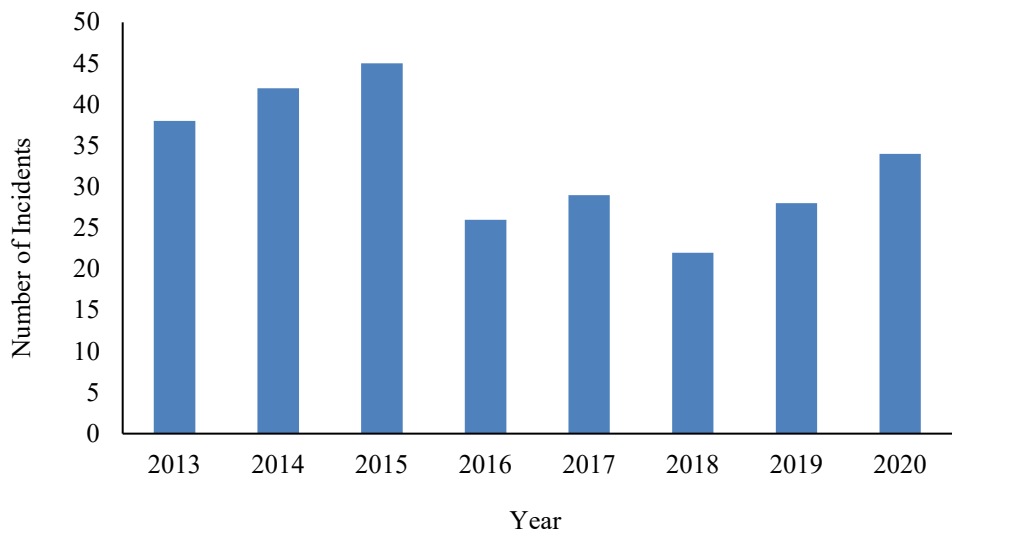


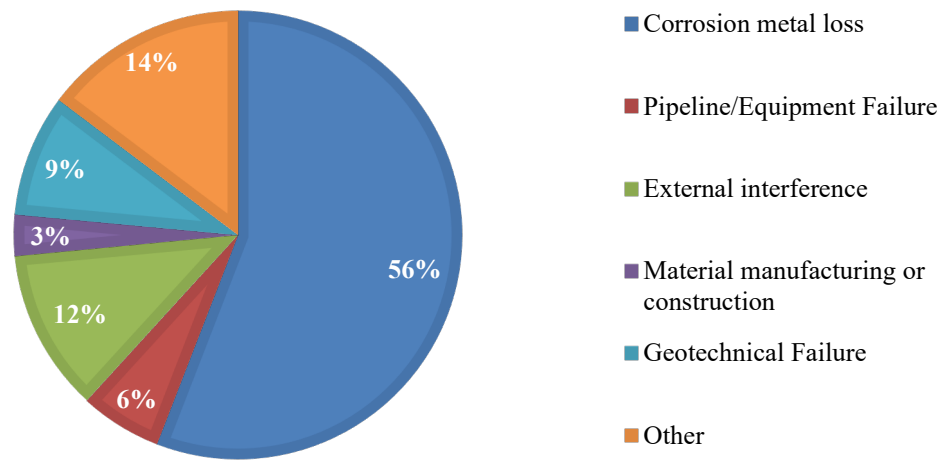
Figure 1-1: Total lengths of pipelines by type and status. Data obtained from BCOGC (2020).

The reliability of oil and gas pipelines is compromised due to deterioration processes, coupled with exposure to natural hazards (e.g. earthquake, geotechnical failure, climate change) and human

induced hazards (e.g. accidental hits, vandalism). The Transportation Safety Board of Canada (TSB) has published an annual statistical summary of pipeline accidents for the federally regulated pipelines. Among the 48 pipeline transportation occurrences occurred in 2019, the largest occurrences took place in Alberta (19) followed by British Columbia (12). The remain occurrences occurred in Ontario (6), Quebec (4), Northwest Territories (3), Manitoba (2) and Saskatchewan (2). The BCOGC has indicated the following causes of pipeline failures: corrosion metal loss, pipeline/equipment failure, external interference (e.g., third party interference and vandalism), material manufacturing or construction defects, geotechnical failure and improper operations (Figure 1-2). Furthermore, the BCOGC annual reports added that most failures were caused by corrosion, accounting for more than 50% of all failures (BCOGC 2020) (Figure 1-2).



(a)



(b)

Figure 1-2: Figures indicated: (a) Data on failure incidents due to corrosion from 2013 to 2020 and (b) Causes of Pipeline failures in BC.

In general, for each oil and gas infrastructure type (e.g., production, transmission, and distribution) there are several predominant factors, which may cause failure. At the initial stage of oil and gas production, one of the major threats to the integrity of pipelines is internal corrosion. The crude mixture extracted from the geological formation, composed of associated water, organic acids, and various dissolved gases such as carbon dioxide (CO₂) and hydrogen sulfide (H₂S), creates a corrosive environment for steel (Nešić, 2007).

Despite the growing understanding of corrosion mechanisms and improved corrosion detection techniques, the industry reports still show that corrosion plays a significant role in pipeline failure. For example, according to an Alberta Energy Regulator (AER) report, from 1990 to 2012, more than 9,000 failures occurred due to internal corrosion (Figure 1-3), which accounts for 54.8% of all spills (AER, 2013). The oil and gas companies in the US spend 1.052 billion dollars yearly to mitigate internal corrosion (Papavinasam, 2013).

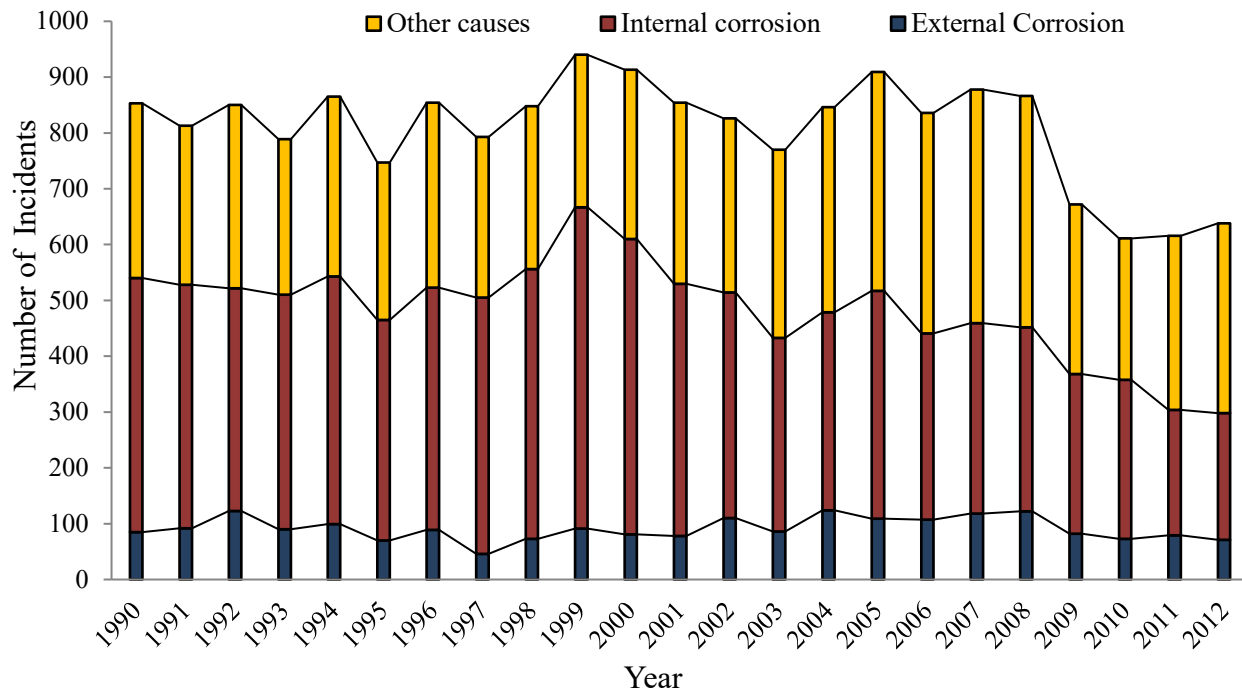


Figure 1-3: Pipeline failures due to corrosion in Alberta from 1990 to 2012.

External corrosion is also a significant cause of oil and gas pipeline failures. As indicated in the AER report, external corrosion in Alberta is the second leading cause of pipeline failures, accounting for 12.7% of the total number of failures (AER, 2013). It is important to note that despite the operators' effort, the number of external corrosion failures do not decline in contrast to the number of internal corrosion failures, which operators managed to reduce. This is explained by the fact that internal corrosion hazard can be mitigated by inhibitors or mechanical cleaning, whereas external corrosion hazard can only be ceased by excavation followed by rehabilitation,

which is very costly.

Furthermore a stress-corrosion cracking (SCC) has been recognized as a cause of pipeline failures in many countries including Canada, United States, Australia and others (NEB, 1996). SCC is defined as a cracking of a material produced by the joint action of corrosion and tensile stress (Beavers et al., 2006). This form of cracking begins when small cracks develop on the surface of a buried pipeline. Over a period, the individual cracks may increase in length and depth, and cracks within a colony join to form longer cracks. If the crack become large enough, the pipeline can lead to failure either due to leak or rupture (NEB, 1996). For example, a 36-inch natural gas pipeline operated by Westcoast Energy Inc. ruptured about 13 km northeast of Prince George, BC in October 2018. This led to release of the natural gas being transported and ignition resulted in fire. The Canadian Energy Pipeline Association (CEPA) has brought together experts in pipeline operation, pipeline integrity and risk assessment to develop and recommend practices designed to help prevent SCC. The published SCC recommended practices standard have dramatically reduced the risks related to SCC (CEPA 2015).

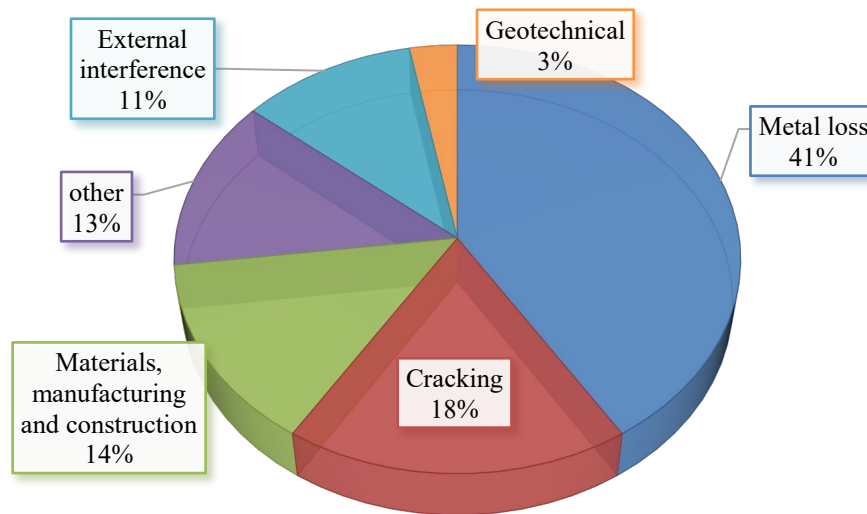


Figure 1-4: Causes of pipeline incidents, CEPA member 2014-2018.

The CEPA 2019 annual performance report indicated the leading causes of incidents for transmission pipelines are metal loss, cracking, materials, manufacturing, and construction defects (Figure 1-4). The majority of the significant incidents reported as a rupture were caused by third-party interference and crack, respectively (CEPA 2019). Likewise, the Pipeline and Hazardous Material Safety Administration (PHMSA) of the United States Department of Transportation (DOT) database for transmission pipelines indicated that internal and external corrosion causes constitute 8.4% and 23.7% of all pipe-related incidents between 2002 and 2013. More than 50% of the external and internal corrosion caused incidents resulted in ruptures (Lam and Zhou, 2016).

The rupture rate of significant incidents on Canadian gas transmission pipelines ($1.6 \times 10^{-5}/km - year$) between 2010 and 2014 were lower than the average rupture rate of the gas transmission pipeline ($3.1 \times 10^{-5}/km - year$) in the US between 2002 and 2013 (Lam and Zhou, 2016).

Understanding performance of the different pipelines and their interaction with the environment is important to support decisions about risk mitigation, future development, investments and maintenance policies – all of which are important so that pipeline operations can be made more efficient and reliable. Given the aforementioned challenges, coupled with companies' limited budgets and strengthening pipeline integrity regulations, there is a need for informed decisions to facilitate an effective resource allocation for pipeline rehabilitation and maintenance strategies.

1.2 Scope of the report

The objective of this project is to develop a vulnerability assessment tool for managing the system. A Bayesian Belief Network (BBN) is used to model the causal relations between the reported causes of failure and their effects, as identified in BCOGC reports and other studies. Developing a vulnerability assessment model for this problem is challenging as the different parameters are dependent and uncertain. Subsequently, a causal relation between the different causes of failure and their effects will be developed using a knowledge-based BBN framework. The ensuing vulnerability management framework will incorporate different mitigation technologies (e.g. cathodic protection or coatings). Different enabling and monitoring technologies will be incorporated into the BBN model. The specific objectives of this project include:

- Develop a BBN to model the failure probability of pipelines due to external corrosion by using corrosion rate data obtained from experimental test results and analytical burst failure models.
- Develop a BBN-based external corrosion model, considering different soil properties and pipeline coating types to evaluate external corrosion defects and associated probability of failure (PoF).
- Develop a BBN to model external SCC of pipelines.

This research proposes to develop a vulnerability assessment tool that accounts for external corrosion (uniform and pitting corrosion) and stress corrosion cracking. The proposed research topic is in line with the BC OGRIS priority, to address the knowledge gaps in engineering and safety in the areas of pipelines.

Chapter 2

External General Corrosion: Experimental Test

2.1 Introduction

2.1.1 Overview of External Corrosion on Pipeline Steels

For buried oil & gas steel pipelines cathodic protection (CP) and protective coatings are used to mitigate external corrosion. However, when an adequate balance between the condition of the coating and the CP level cannot be established, external corrosion usually occurs, exposing the steel surface at coating holidays or under disbonded sections (Kowalski and Sánchez, 2016). The rate of external metal loss is mainly controlled by the soil environment that the steel surface is in contact with. For this reason, soil corrosivity, which is determined by many physicochemical parameters such as soil resistivity, pH, temperature, sulphate and chloride concentrations, is a crucial factor in evaluating the pipeline's external corrosion process and the significance of the hazard. The correlation of external corrosion with the condition of the coating and CP level, as well as the soil corrosivity is key to predicting the pipeline steel CR in the field.

Table 2-1 lists some representative corrosion studies on steels (X52, X60, X65, X70 and X80) that have been widely used for underground pipelines. As expected, an intact coating together with a CP application provides good protection of pipe steel (X52) for corrosion ($CR \approx 0$ mm/y), whereas the existence of a holiday in the coating contributes to an increased corrosion risk at pH 8.2 at room temperature (RT), even though the CR is still negligible due to CP protection (Li and Castaneda, 2014). For bare X52 without CP protection in a similar electrolyte environment, CR increases to 0.023 mm/y (Lins et al., 2012). Differences in microstructure (percentage of pearlite and ferrite phases) in various pipe steels, e.g. X60, X65 and X70, leads to difference in the corrosion products formed, which can affect the corrosion processes and the CRs. X65 steel, which has the highest percentage of pearlite phase shows the highest CR among the three steels (Quej-Ake et al., 2018). Given a specific pipe grade, its corrosion resistance to the soil pH is debatable in the literature. Two review papers published lately represented two opposite opinions. One considers pH as one of the most important key factors influencing corrosion of buried pipes (Cole and Marney, 2012), while the other argued that even though an extremely low pH may be an indication of corrosion, there is no direct relationship between pH and CR since many other factors contribute to CR (Wasim et al., 2018). This argument implies the existence of complex interactions between pH and other factors, which is one of the aspects of the current study. CP is effective in lowering the CR. For example, when studying the CR of bare X70 in a clay-sand soil (pH 4.8~5.6),

it was found that CR decreased from around 0.2 mm/y to about 0.03 mm/y after applying CP for 2 days (Barbalat et al., 2012).

Table 2-1: CR of different pipe steels with and without a coating

Pipe steel	Coating type	CP application	Electrolyte	CR or corrosion current density	Ref.
X52	a 30- μ m thick layer of coal tar applied in the lab	-0.8 V vs. Ag/AgCl	Soil (RT, pH 8.2)	Corrosion current density (EIS estimation): $\sim 0 \mu\text{A}/\text{cm}^2$ (~ 0 mm/y)	(Li and Castaned a, 2014)
	Same as above but with a holiday			Corrosion current density (EIS estimation): 10^{-5} to $10^{-4} \mu\text{A}/\text{cm}^2$ ($\sim 7.6 \times 10^{-8}$ to 7.6×10^{-7} mm/y)	
X52	No	No	Synthetic soil solution ^a (RT, pH = 7.7, $1825 \Omega \cdot \text{cm}^2$)	CR (LPR test) = 0.023 mm/y	(Lins et al., 2012)
X60	No	No	Sand-clay soil (RT, pH 3; $499.5 \Omega \cdot \text{cm}^2$)	CR (5 hrs. after removed oxides, polarization test) = 0.56mm/y Possible pitting occurs	(Quej-Ake et al., 2018)
X65			Sand-clay soil (RT, pH 3; $183 \Omega \cdot \text{cm}^2$)	CR (5 hrs. after removed oxides, polarization test) = 1.29 mm/y Possible pitting occurs	
X70			Sand-clay soil (RT, pH 3; $213 \Omega \cdot \text{cm}^2$)	CR (5hr after removed oxides, polarization test) = 1.08mm/y Possible pitting occurs	
X70	No	No	Sand-clay soil added with water (RT, pH 4.8~5.6)	CR (7-day, polarization test) = 0.085 mm/y	(Barbalat et al., 2012)
		-0.9 V vs. Ag/AgCl		CR (7-day, polarization test) = 0.025 mm/y	
X80	No	No	Acidic red soil (buried underground, pH ~ 4.7)	CR (38-week, electric resistance test) = 0.0902 mm/y CR (5-year, electric resistance test) = 0.0226 mm/y	(Wang et al., 2015)

^a Synthetic soil solution: NaHCO_3 (0.483 g/L); KCl (0.122 g/L); $\text{CaCl}_2 \cdot 2\text{H}_2\text{O}$ (0.181 g/L); $\text{MgSO}_4 \cdot 7\text{H}_2\text{O}$ (0.131 g/L)

In addition to the effect of pH and CP, temperature also plays an important role. In a study of X60 steel, the corrosion current density increased nearly 3 times when the temperature increased from 20 to 60°C (Benmoussa et al., 2006). It is also worth mentioning that long-term corrosion behavior of pipe steel would differ from that observed in relatively short-term tests due to the formation of semi-protective corrosion products over time. One corrosion study of X80 steel compared its CR at 38 weeks and that after 5 years: CR decreased from 0.0902 mm/y to 0.0226 mm/y after 5 years buried in the soil. The corrosion products formed at 24 weeks consisted of two loose layers (the outer corrosion product was a mixture of $\text{FeO}(\text{OH})$ and FeCO_3 , and the inner product was composed mainly of FeCO_3), while those formed after 5 years had only a single denser layer that was composed of FeOOH , $\gamma\text{-Fe}_2\text{O}_3$, FeCO_3 , and a small amount of Fe_3O_4 .

Literature corrosion data are mostly for bare steel samples, with very few studies focusing on coated samples with or without a holiday. This is because (a) the techniques for detecting the CR (such as polarization tests) for bare steels are relatively more established and widely accepted, and

(b) the CR of coated samples is very low and quite often negligible when CP is applied. However, as coating defects including holidays, dents, gouges, etc. are unavoidably formed during pipe manufacturing, transportation and construction processes, corrosion at and/or under the coating of these defects would take place. Increased corrosion may also occur in these defect areas when CP is inadequate, e.g., interruption of CP, over protection or under protection.

Elucidating the correlation between the corrosion of pipe steel and its coating conditions, CP levels and surrounding soil conditions is important for service life prediction and risk mitigation. Such information is lacking in the literature, which motivates the work of this report. Bare and fusion bonded epoxy (FBE) coated X60 pipeline steels (CSA Z245.1 Cat. 2) provided by FortisBC were used. The effect of individual factors including soil corrosivity represented by salt composition, solution pH and temperature, coating scenarios (intact or containing a defect) and CP levels (under-optimized, and over-protection) on the CR of both bare and coated steel was investigated. Further, the interactions among these factors were analyzed with a mathematical model to predict CR as a function of these variables.

2.1.2 Technical Approaches

The Response Surface method using an I-optimal design from Design Expert was used to plan the experiments. The independent variables selected in this study include 1) solution corrosivity factor, related to solution temperature, solution pH, and salt composition; 2) treatment factor, related to the absence or presence of various levels of CP; and 3) pipe steel condition factor, related to coated (different coating scenarios) or non-coated (i.e. bare steel) condition. Table 2-2 describes each independent variable. A total of 42 experiments were generated by using a quadratic model, which is listed in Table 2-3. The testing period was four-weeks (28 days). The CRs were collected by conducting the experiments in a random order of run numbers. A mathematical model was established to describe the relationship of CR with all of the factors that were studied. 6 more tests (X1-X6 in Table 2-3), including applying an under-protection CP potential of -0.4 V vs. Ag/AgCl as well as a temperature that is periodically on and off, were conducted to validate the established model.

Table 2-2: Independent parameters studied (either numerical or categorical type)

Independent variables		Description	Type
Solution corrosivity	Solution temperature	10, 40, 65°C	Numerical
	Solution pH	2, 7, 12	Numerical
	Salt composition	NaCl or Na ₂ SO ₄	Categorical
CP		Without or with (-0.8 V and -1.6 V vs. Ag/AgCl)	Categorical
Coating		Without or with (intact, dented, or with a holiday)	Categorical

Table 2-3: Levels and description of variables in actual form

	Factor A	Factor B	Factor C	Factor D	Factor E
Run	Solution temperature (°C)	Solution pH	Salt composition	CP (V vs. Ag/AgCl)	Coating condition
1	10	12	SO4	Y-0.8	N
2	40	12	SO4	N	Y
3	65	7	Cl	Y-0.8	Y-D
4	10	2	Cl	Y-1.6	N
5	40	7	SO4	N	N
6	10	12	Cl	Y-1.6	Y-H
7	10	2	SO4	Y-1.6	Y-H
8	10	12	Cl	Y-0.8	Y-D
9	40	7	Cl	Y-0.8	N
10	65	2	SO4	N	Y-D
11	65	12	Cl	Y-0.8	Y
12	10	2	SO4	N	Y-H
13	40	12	SO4	N	Y-H
14	65	2	SO4	Y-1.6	Y
15	65	2	SO4	Y-0.8	N
16	40	12	SO4	Y-1.6	N
17	10	7	SO4	Y-1.6	N
18	40	2	Cl	N	Y
19	65	12	SO4	Y-0.8	N
20	65	12	Cl	Y-0.8	Y-H
21	40	7	SO4	N	N
22	65	7	SO4	Y-0.8	Y-H
23	10	12	SO4	Y-1.6	Y-D
24	10	2	Cl	Y-0.8	Y-H
25	40	2	Cl	Y-1.6	Y-D
26	10	2	Cl	Y-0.8	Y-D
27	65	12	Cl	Y-1.6	Y-D
28	10	12	Cl	N	N
29	10	12	Cl	Y-1.6	Y
30	40	2	SO4	Y-1.6	N
31	10	7	Cl	Y-0.8	N
32	65	2	Cl	Y-1.6	Y-H
33	10	7	Cl	N	Y-D
34	10	2	Cl	N	Y
35	40	2	Cl	N	N
36	10	2	SO4	Y-0.8	N
37	65	7	Cl	Y-1.6	N
38	40	7	SO4	Y-0.8	Y-D
39	65	7	SO4	Y-1.6	Y-D
40	65	7	Cl	N	Y-H
41	10	7	Cl	N	Y-D
42	10	7	SO4	Y-0.8	Y
X1	10	7	Na ₂ SO ₄	-0.4 V	Y
X2	10	7	Na ₂ SO ₄	-1.6 V	Y
X3	65	7	NaCl	N	N
X4	65	7	NaCl	-0.4 V	YD
X5	65 (on and off)	7	Na ₂ SO ₄	-1.6 V	YD
X6	65 (on and off)	7	NaCl	-1.6 V	YD

Factor 3: "SO4" refers to sodium sulfate; "Cl" refers to sodium chloride; salt concentration is 0.01 M.

Factor 4: "N" means no CP applied. "Y-0.8" and "Y-1.6" means with an applied CP of -0.8 V and -1.6 V vs. Ag/AgCl, respectively.; Factor 5: "N" means no coating, i.e., bare steel; "Y" means intact coating; "Y-D" means coating with an indent (around 1.2 mm in depth); "Y-H" means coating with a holiday (6 mm in diameter).

X1-X6: extra tests; X5, X6: "on and off" means the temperature is alternatively on for one week and off for another week, the total testing period is four-week.

2.2 CR of X60 pipe steel in simulated field conditions

2.2.1 Experimental

2.2.1.1 Weight loss tests and electrochemical tests for bare steel

For bare steel samples, weight loss tests based on ASTM G31 (ASTM 2004) were performed to obtain the CR. All the bare steels were ground to 1200 grit emery paper and washed using deionized water. A jacketed glass cell connected to a water bath was used to conduct the tests at different experimental temperatures. In each test solution, three samples (each with an exposed area of 1.5 cm^2) were simultaneously immersed and tested for four-weeks to obtain an average CR (Figure 2-1 (a)). One exception was for run #35, in which the CR was so high that four-week testing led to a complete dissolution of the sample. Therefore, a 4-day test was applied to obtain its CR. For samples with CP, a power supply was used to provide a constant negative current to the samples. During the tests, CP was checked/adjusted daily or every other day to ensure it is $\pm 50 \text{ mV}$ around its set values (either -0.8 V or -1.6 V vs. Ag/AgCl reference electrode ($+0.199 \text{ V}$ vs. NHE)). This is because the changes in steel surface composition/morphology and/or the electrolyte resistance during the tests can alter the applied potential to the sample. A graphite rod was used as an anode.

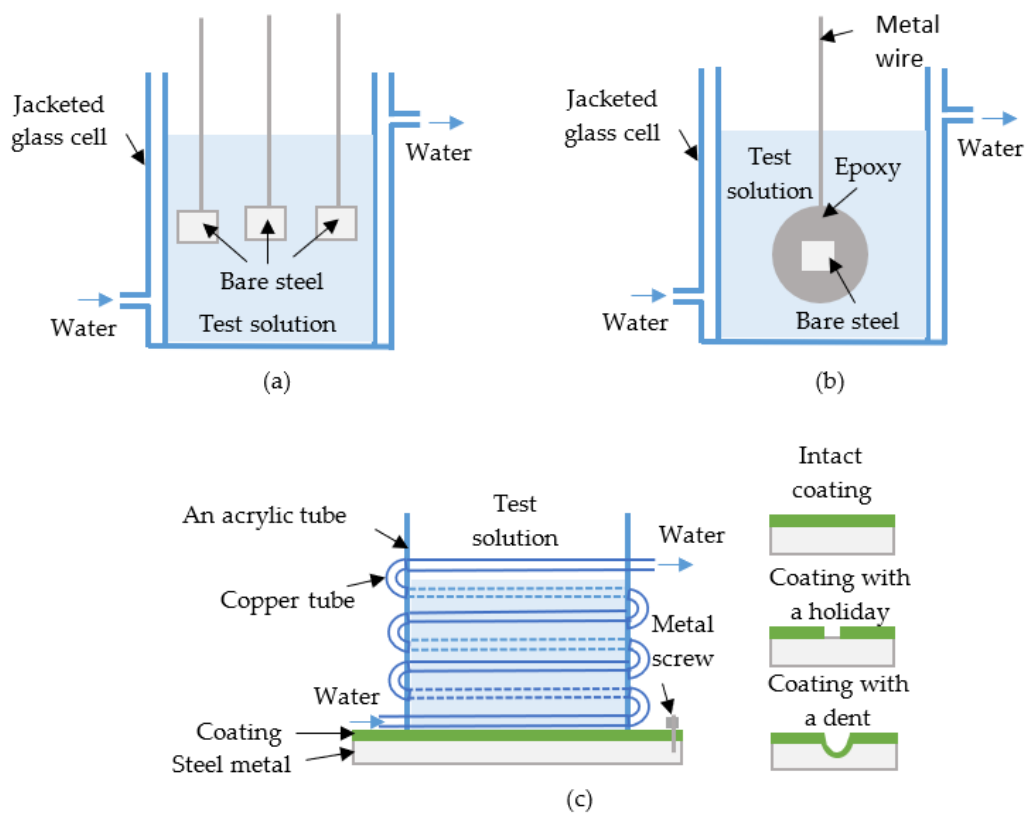


Figure 2-1: A schematic of (a) 1.5 cm^2 bare electrodes for weight loss tests; (b) a 1 cm^2 bare electrode for electrochemical tests; and (c) a coated X60 panel sample for corrosion immersion and electrochemical tests.

Another group of immersion tests with electrochemical impedance spectroscopy (EIS) was carried out separately from the weight loss tests and was done on bare samples with 1 cm² surface area that were mounted in epoxy (Figure 2-1 (b)). EIS was performed periodically by applying an AC ± 10 mV peak to peak signal in the frequency range of 100 kHz to 100 mHz. A three-electrode set-up was used, i.e., the bare steel as the working electrode, a graphite rod as the counter electrode, and a double junction Ag/AgCl reference electrode. A constant potential was applied during the EIS tests. For samples without CP protection, this constant potential was the open circuit potential. For samples with CP, the constant potential was the CP potential applied. All electrochemical experiments were carried out using a potentiostat (VersaSTAT 3, Princeton Applied Research). It should be noted that samples tested at CP potentials were disconnected from the power supply during the EIS tests, but the potentiostat then served as the power source.

For both the weight loss and immersion/electrochemical tests, the base solution was 0.01 M NaCl or 0.01 M Na₂SO₄, with its pH initially adjusted by either 0.03 ~ 0.3 M HClO₄ or 0.1 ~ 1 M NaOH solution. pH 2, 7 and 12 were studied to cover a wide spectrum of pH conditions that pipeline steel might encounter in the field. For bare samples as well as coated samples with a holiday, CP application results in proton consumption through hydrogen evolution in acidic electrolytes while hydroxyl ions are continually produced through water electrolysis in neutral and alkaline electrolytes. Both reactions lead to an increase of pH. For some of the bare steel samples tested, solution acidification was observed during the immersion tests, leading to a decrease of pH. In order to maintain the initial pH, it was adjusted either manually or by a pH controller. In this way, the electrolyte pH was adjusted around its initial value (+0.7/-0.4 to pH 2; +0.7/-2 to pH 7 and +0.5/-2 to pH 12).

2.2.1.2 Electrochemical tests for coated steel

For FBE coated X60 steel panel samples (10 cm × 10 cm), the coating surface was wiped with alcohol and then deionized water to remove any grease and dirt. An acrylic tube was attached on the cleaned coating surface to contain the solution for conducting electrochemical tests. The coated samples were in three different conditions, i.e., intact coating, coating with a holiday (6 mm in diameter), or coating with an indent (about 1.2 mm in depth). Figure 2-1 (c) shows a schematic of coated (panel) samples undergoing immersion and electrochemical tests. A coiled copper tube attached on the outside of the acrylic tube was connected to a water bath for testing of coated samples at 10°C. Hot plates were used for coated samples having experiments running at temperatures of 40 and 65°C. Rubber stoppers were used as lids on the top of the electrochemical

cells to minimize water evaporation at high temperatures. The base solution preparation and pH adjustment was done in the same way as that used for the bare samples.

The corrosion behavior of coated X60 were monitored and studied using electrochemical noise measurement (ENM) and EIS. ENM with a single cell arrangement as introduced in (Jamali et al., 2014) was applied to assess the corrosion resistance. During the tests, a two-electrode set-up was used, which comprises the working electrode (coated pipe steel panel sample) and a double junction Ag/AgCl reference electrode serving as both reference and counter electrode. The electrochemical noise potential (ENP) was measured by recording the sample potential against the reference electrode under the open circuit condition. The noise resistance R_n was calculated in accordance with Ohm's law by Equation 2-1, where $\sigma(V)$ and $\sigma(I)$ are the standard deviations of potential and current fluctuations.

$$R_n = \frac{\sigma(V)}{\sigma(I)} \quad 2-1$$

The current density i_{corr} was estimated by using Equation 2-2, the Stern-Geary coefficient B for most cases, was assumed to be 0.026 V for active and 0.052 V for passive corrosion of galvanized rebar in concrete (Gonzalez and Andrade, 1982). For the coated samples, B was taken as 0.052 V. The CR was then calculated by Equation 2-3 and was taken as an average value of that measured at the initial, the middle and the last day of the four-week testing. A_w is the atomic weight, z is electrons transferred, F is the Faraday constant, ρ is the density. It should be noted that since R_n is the resistance of the coating instead of the steel substrate directly, i_{corr} calculated can reflect the corrosion resistance of the coated samples, but may not accurately represent the true CR. Thus, these measurements should be considered qualitative and indicative rather than absolute.

$$i_{corr} = \frac{B}{R_n} \quad 2-2$$

$$Corrosion\ rate \left(\frac{mm}{year} \right) = \frac{i_{corr} A_w}{zF\rho} \quad 2-3$$

EIS measurement was also done on the coated panel samples, similar to that for bare steel samples (i.e. measured either at open circuit potential or CP potential that is consistent with the immersion testing conditions), except that the frequency range was from 100 kHz to 10 mHz.

2.2.1.3 Materials Characterization

The corrosion product morphology of the bare X60 samples exposed to different conditions was imaged by a field emission scanning electron microscope (SEM, Zeiss Sigma). During the SEM measurements, the acceleration voltage was 20 kV. The SEM imaging was repeated at three different areas of each specimen. The composition of the corrosion products was also determined

by X-ray diffraction (XRD), which was conducted on a Rigaku MultiFlex† machine with a 2 kW X-ray generator. During the measurements, the scan speed was 1°/min. The X-ray tube Cu K α settings were 40 kV and 20 mA. After the immersion tests, to study the surface chemistry change of these FBE coatings, mid-infrared spectroscopy of the coatings (4000-675 cm⁻¹, 150 scans with a resolution of 4 cm⁻¹) was collected using a Thermo Scientific Nicolet iS50 FT-IR Spectrophotometer.

2.2.2 Results and Discussion

2.2.2.1 Corrosion study of bare X60 steel samples (small electrodes)

2.2.2.1.1 CR of bare steel samples from weight loss data

Figure 2-2 shows a CR mapping of bare X60 samples under different test conditions using the weight loss data. In the figure, besides each tested point shown in blue, the testing temperature, CP value, type of salt and the electrolyte resistance are presented in brackets. This CR mapping is divided into three regions: region I in red where the CR is above 1 mm/y; region II in yellow where the CR is from 0.1 mm/y to 1 mm/y; region III is in green color where the CR is below 0.1 mm/y; 0.1 mm/y is generally accepted as an allowable CR for carbon steel pipes (Groisman, 2009). pH, temperature, and CP play important roles in determining the CR as per the following:

- At pH 2, the highest CR (30.87 mm/y) is found in sample A, which was tested without CP, and at a temperature of 40°C. At the same temperature of 40°C (sample B), with a high CP of -1.6 V, there is still an unacceptably high CR of 3.69 mm/y. Comparing to sample B: 1) sample C, which has a higher testing temperature of 65°C, a higher solution conductivity, but with a lower CP level of -0.8 V, shows a much lower CR of 0.09 mm/y; and 2) sample D, which has the same CP of -1.6 V, but has a lower temperature of 10°C, also shows an acceptable CR of 0.02 mm/y. One indication from the result is that the presence of both a high CP of -1.6 V and a temperature higher than 10°C led to the high CR observed in sample B. A high CP of -1.6 V, i.e., an overprotection results in a large amount of hydrogen produced from the acidic solution and from the cathodic reaction ($2H^+ + 2e^- = H_2$). CP that is more negative than -1.1 V vs. Cu/CuSO₄ (-1.0 V vs. Ag/AgCl) can cause problems including hydrogen induced cracking (HIC), hydrogen embrittlement (HE) and stress corrosion cracking (SCC) (Leeds, 1995). Though it is normally acknowledged that hydrogen related attack does not cause significant material loss, rather it makes the material more susceptible to mechanical failure (Song, 2003), there seems to be a correlation between the large amount of hydrogen produced at a high temperature and the observed high CR based on the tested results. The

reasons for this are not yet clear and need more detailed research. At pH 7, that which is most representative of “normal” pipeline soil, it is interesting to observe that the CR data fell into the three regions based on the level of CP. All three samples (F, G, and F’) without CP protection appeared in region I ($CR > 1$ mm/y); two samples H and I having a CP of -0.8 V were located in region II (1 mm/y $> CR > 0.1$ mm/y); and the other two samples (J and K) were in region III with a negligible CR due to CP of -1.6 V.

- At pH 12, without CP protection, sample M has a CR of 0.124 mm/y at a low temperature of 10°C . However, the highest CR of 2.86 mm/y was measured for sample L, which had a CP of -0.8 V and a high temperature of 65°C . The test solution also had the lowest electrolyte resistance/highest electrolyte conductivity. When the testing temperature was 10°C , at the same CP level of -0.8 V, the CR of sample N was reduced (0.004 mm/y). An increase of the CP level to -1.6 V also appeared to be very effective on depressing the CR to a negligible value, as seen for sample O, for which the testing temperature was 40°C . The comparison among sample L, N and O implies that in a hot alkaline environment, a moderate CP level of -0.8 V is not sufficient to protect steel from corrosion. Also, if considering coated samples with a holiday (exposed steel substrate area), it is well known that an application of CP causes an alkaline environment at the coating/substrate interface, leading to a loss of adhesion at the interface and causing cathodic disbondment. The high pH environment is supposed to protect the exposed substrate from corrosion. However, based on the present result on bare steel samples, if the coated sample is tested at a high temperature of 65°C with a CP of -0.8 V, both the exposed holiday area and the substrate underneath the disbonded coating may still experience corrosion.

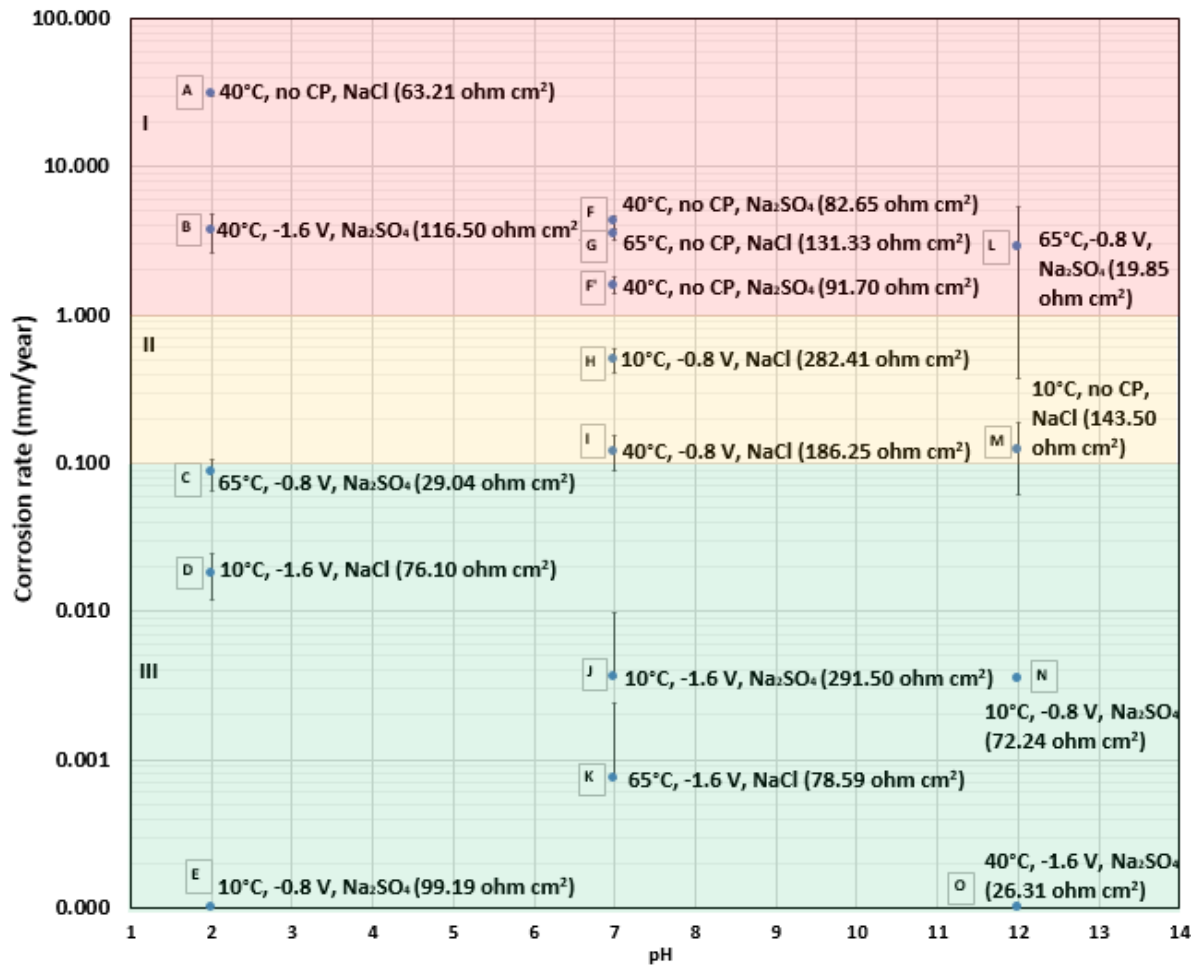


Figure 2-2: CR mapping of bare X60, small electrode samples, under different test conditions using the weight loss data (the data in the bracket is the electrolyte resistance estimated from EIS tests).

2.2.2.1.2 Corrosion products formed on the bare steel surface

Figure 2-3 shows representative samples tested in sodium sulfate solutions at a temperature of 40°C, with pH varied from 2 to 12 and with different CP levels. Figure 2-3 a, b and c represent CRs in order from highest to lowest. From the SEM images, for a and b samples tested at pH 2 and 7, the corrosion products completely covered the bare sample surface; in pH 12 solutions (c), a thin corrosion product layer was also observed. By investigating at a higher SEM magnification, as well as from the XRD results (Figure 2-4), it becomes clear that lepidocrocite, and maghemite or hematite are the major corrosion products formed in pH 2 and 7 solutions. Lepidocrocite, rozenite and ferrihydrite appear in the corrosion products formed at pH 12. The minor difference in phase type likely has little effect on the CR measured. While the more compact the corrosion products is, the better the prevention of any further corrosion is to expect. This has implications for long term corrosion as corrosion products impede mass transfer.

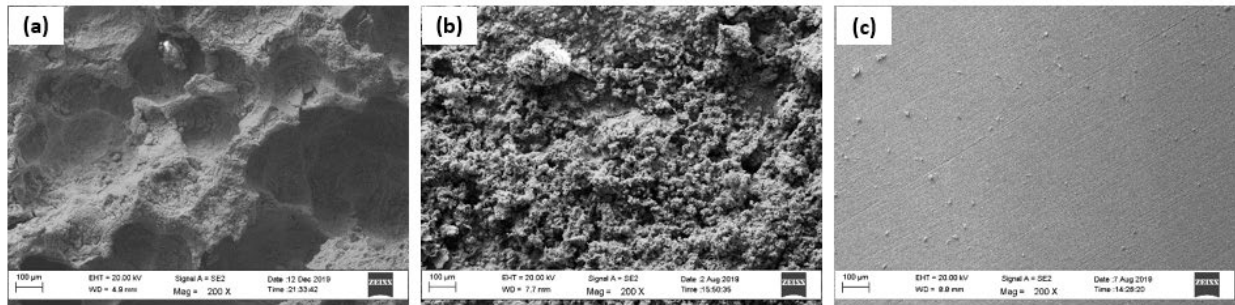


Figure 2-3: SEM morphology of corrosion products formed on sample surface after the 28-day tests in sodium sulfate solutions: (a) 40°C, pH 2, CP of -1.6 V; (b) 40°C, pH 7, no CP; and (c) 40°C, pH 12, CP of -1.6 V.

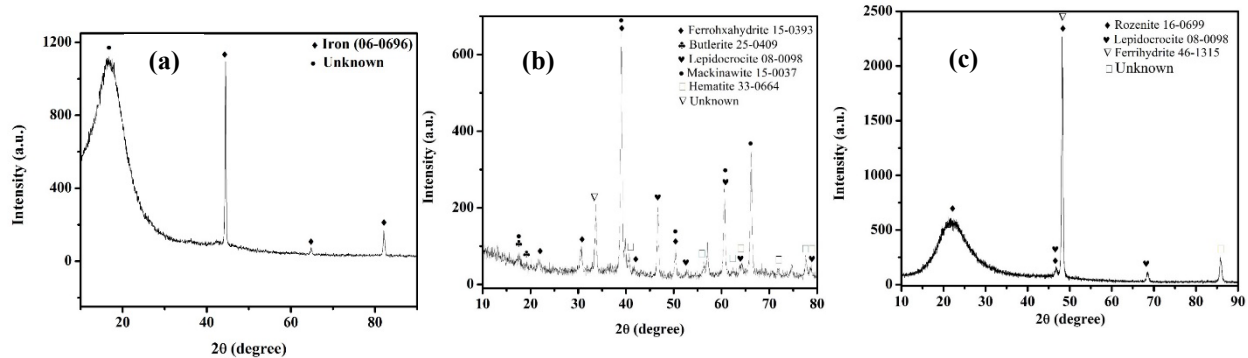


Figure 2-4: XRD results of corrosion products formed on sample surface after the 28-day tests in sodium sulfate solutions: (a) 40°C, pH 2, CP of -1.6 V; (b) 40°C, pH 7, no CP; and (c) 40°C, pH 12, CP of -1.6 V.

After exposure to sodium chloride solutions, the morphology of corrosion products formed on the three samples tested at a low temperature of 10°C is shown in Figure 2-5. It is clear to see that pitting corrosion occurs in the chloride containing solutions at pH 7 and 12. It is well known that chloride ions promote local aggressive chemistry. Using 3D profilometer, the depth of each pit was measured. As seen in Figure 2-6, the maximum depth of each pit in sample c, appearing in the center, is around 3 μm after a 28-day test. The CR estimated from this maximum depth is about 0.04 mm/y, which is lower than the uniform corrosion rate, i.e., 0.124 mm/y measured from the weight loss test. Therefore, for this sample tested at 10°C, pH 12, and with CP, pitting corrosion is not a primary concern. It should also be noted that these pits tend to form near the scratches, i.e., preferential dissolution of the metal surface around a micro-defect.

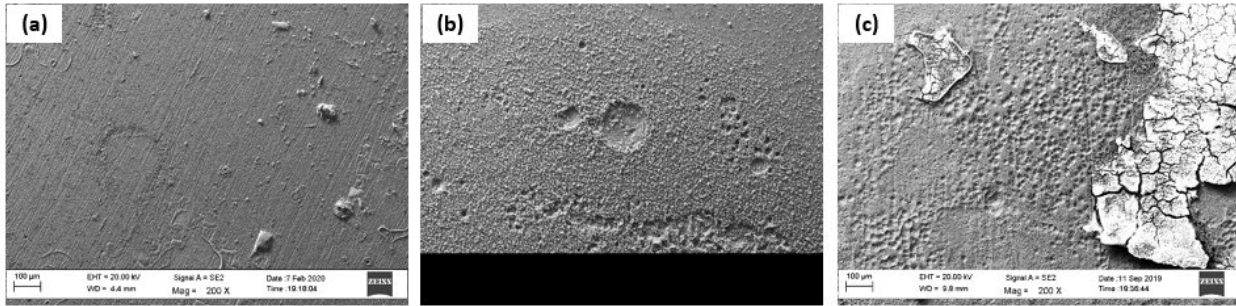


Figure 2-5: SEM morphology of corrosion products formed on sample surface after the 28-day tests in sodium chloride solutions: (a) 10°C, pH 2, CP of -1.6 V; (b) 10°C, pH 7, CP of -0.8 V; and (c) 10°C, pH 12, no CP.

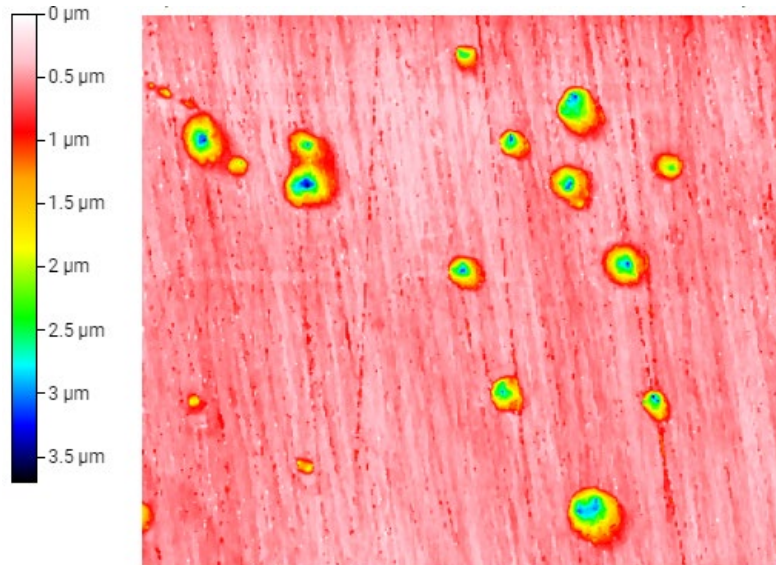


Figure 2-6: Surface morphology of sample tested at 10°C, pH 12, no CP using the 3D profilometer.

2.2.2.2 Corrosion of FBE-coated X60 steel panel samples

2.2.2.2.1 CR of coated steel samples

Similar to the bare steels, CR mapping was also used for the coated samples as seen in Figure 2-7. It is not surprising to find that the type of coating defect influences the CR the most, so CR of the coated samples is presented below as a function of the coating scenarios. The coated samples all had acceptable CRs for the studied conditions.

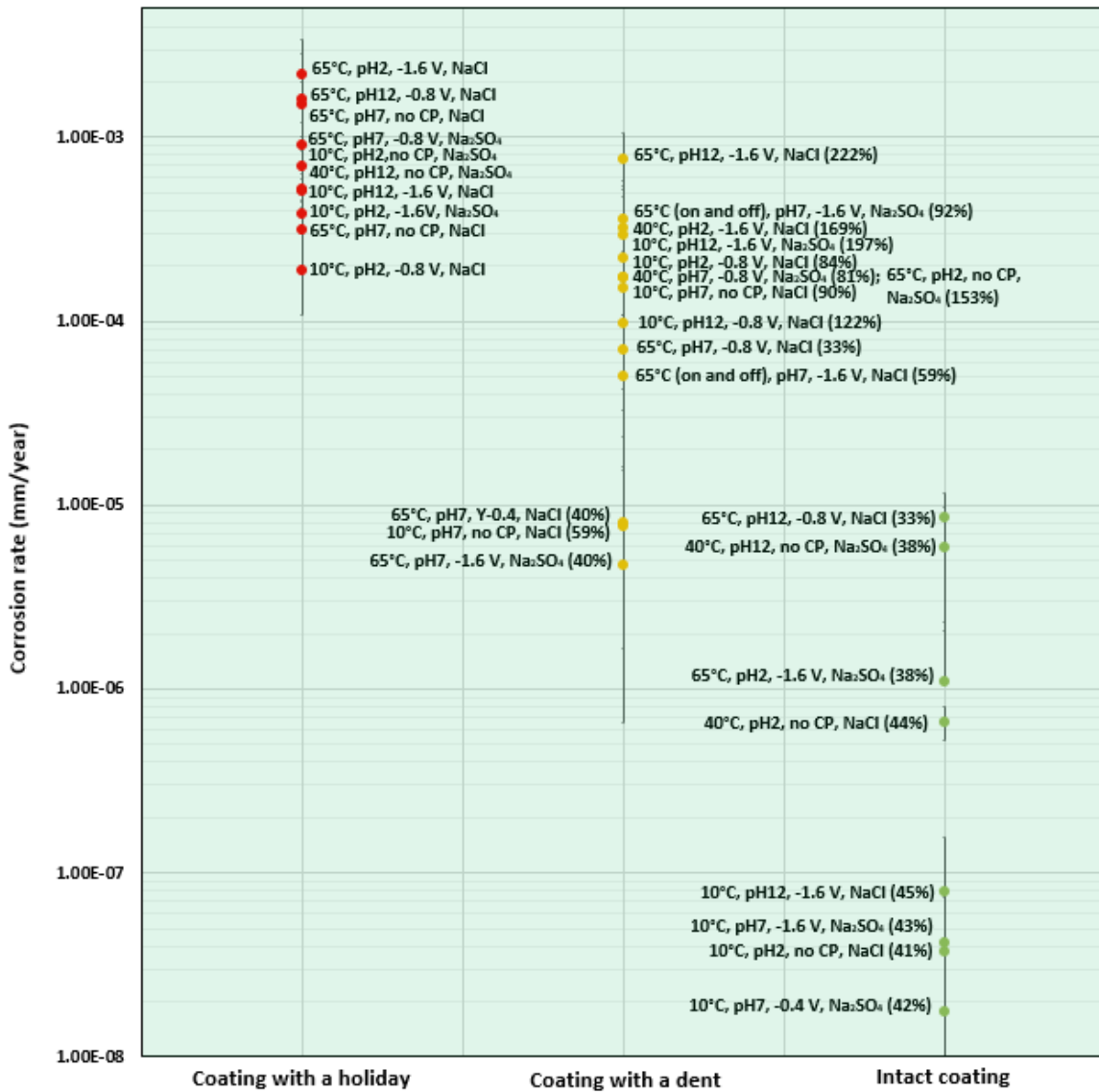


Figure 2-7: CR mapping of coated X60 steel under different test conditions (the data in brackets is the volume of water absorbed by the coating after the 28-day test).

Coating with a holiday

The holiday samples (red circles) show the highest CRs due to the exposed metal surface, which is similar to the bare steel samples. In addition, such samples may suffer from cathodic disbondment when exposed to an alkaline environment (e.g. caused by applying CP), which could contribute to an increased CR. As seen in Figure 2-8 (a), the holiday sample tested at 65°C, pH 7, no CP, showed nearly no cathodic disbondment, and its CR from ENM test was 3.1×10^{-4} mm/y. However, the sample tested at 65°C, pH 12, -0.8 V, showed a large disbondment of 12.5 mm, with a higher CR of 1.6×10^{-3} mm/y. This result is consistent with what was observed in bare steel samples, i.e., higher CR in hot alkaline environment with a moderate CP of -0.8 V. The CR range for these holiday samples was from 1×10^{-4} to 2.5×10^{-3} mm/y.

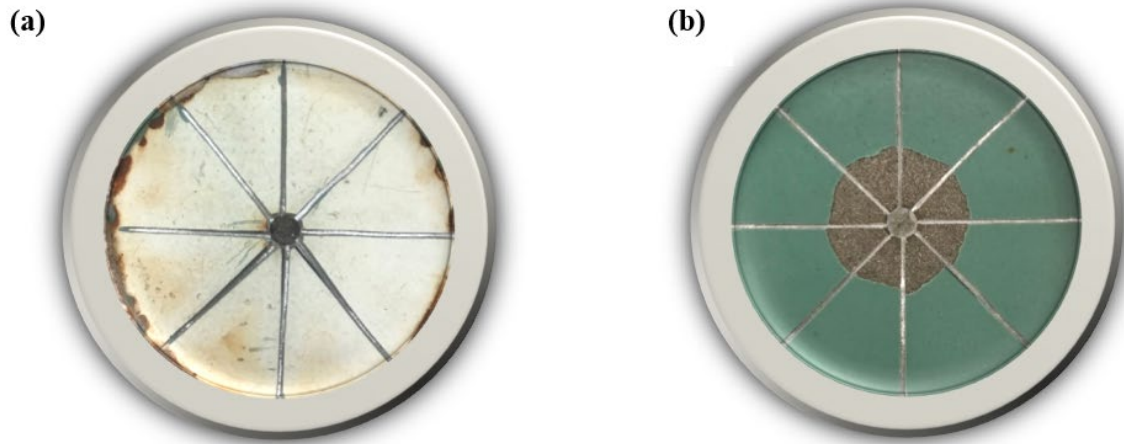


Figure 2-8: Holiday samples after immersion tests: (a) 65°C, pH7, no CP, NaCl, with a disbondment radius ≈ 0 mm; and (b) 65°C, pH12, CP of -0.8 V, NaCl, with a disbondment radius = 12.5 mm.

Coating with a dent

Most of the studied samples with a dent (yellow circles) are in the region where $5 \times 10^{-5} < CR < 1 \times 10^{-3}$ mm/y, having comparable CRs to the holiday samples, indicating a similar corrosion resistance of the coating with these two kinds of defect. No particular trend in CR can be found in the dented samples with respect to temperature, pH and CP. On the other hand, if looking at the volume of water (ϕ) being absorbed in the coating (the data in the brackets), it is found in general, when ϕ is higher than 60%, CR is above 1×10^{-5} mm/y; when ϕ is below 60%, CR is less than 1×10^{-5} mm/y.

Intact coating

Due to a good protection from the coating, CRs for all intact coating samples (green circles) are extremely low and less than 1×10^{-5} mm/y. ϕ for these samples are all below 60%. Among all the factors, the temperature seems to be the most critical. Negligible CRs on the order of 10^{-8} were found for the four samples tested at 10°C. Increasing the temperature accelerates the CR by one to two orders of magnitude. This is related to temperature-induced coating degradation, which is reflected by studying the chemical structure change of the coating surface as shown in the next section.

2.2.2.2.2 Chemical structure change of the coating surface

Figure 2-9 shows the FTIR spectrum/fingerprint of the as-received FBE coating before experiments. All the chemical bonds (e.g., O-H stretching, C=C of aromatic rings etc.) that can be identified are indicated in the spectra. The pipe where the tested samples were cut from was manufactured in 2017, so the sample has been exposed to the air for over 2 years before the tests.

A broad and strong band with wavenumbers ranging from 3700-3200 cm^{-1} indicates the existence of free liquid water in these as-received coating samples.

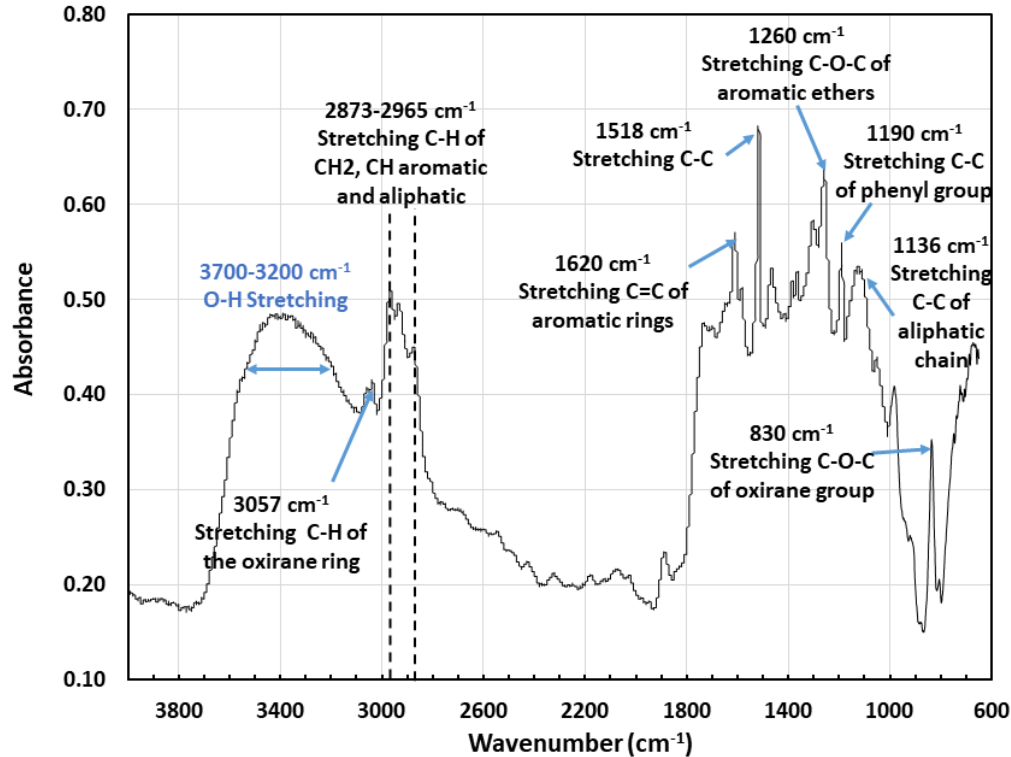


Figure 2-9: FTIR spectrum of as-received FBE coating sample.

According to the testing temperature (10, 40, 65°C), the FTIR spectra of dented and intact samples are grouped and presented in Fig. 10-11. The spectra are split into two regions: one has the wavenumbers from 4000-2500 cm^{-1} ; the other from 1850-750 cm^{-1} . The bottom row of the spectra (shown in black color) and sample image is from the reference FBE sample (that is without testing of any sort). The top four are the samples obtained after exposure to the testing environments.

At 10°C (Figure 2-10): From the left column of spectra (4000-2500 cm⁻¹), the O-H alcohol band becomes slightly sharper in all samples, indicating water absorption. Stronger C-H aromatic and aliphatic bands are also observed. In the right column spectra (1850-750 cm⁻¹), the position of the band peaks are indicated by the dotted lines. It can be seen that except for the C-C phenyl/aliphatic bands, all the band peaks shift to larger wavenumbers (about 50 cm⁻¹). Unlike that in the high wavenumber regions, the peak intensity of these bands does not show significant change.

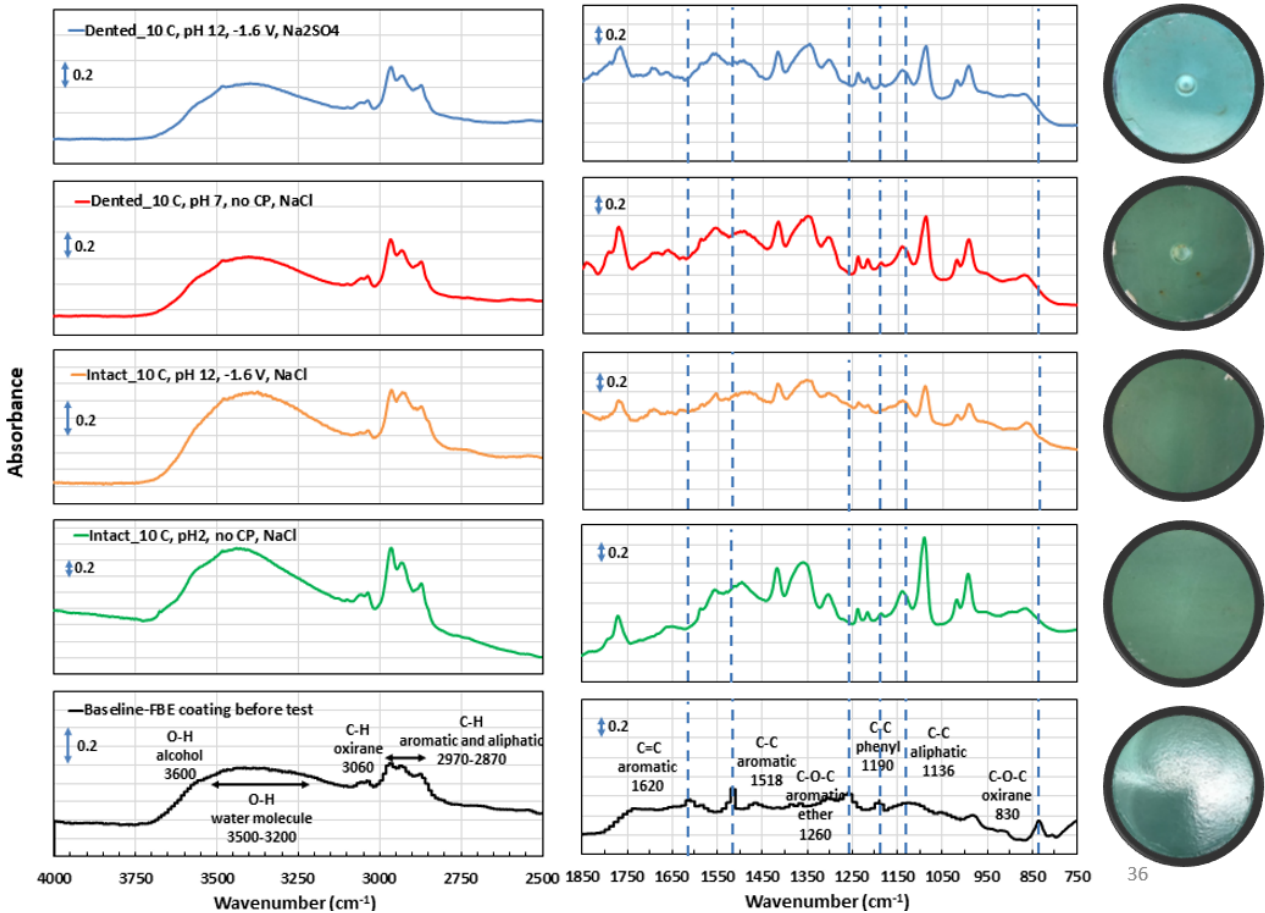


Figure 2-10: FTIR spectra of FBE coated sample tested at 10 °C.

At 40°C (Figure 2-11): When temperature is 40°C, the O-H band becomes much sharper (especially in the dented samples), indicating increased water absorption. The C-H band also becomes stronger, especially in the dented samples. In the low wavenumber region, a similar band peak shift to that at 10°C occurs and there is a slight increase of absorption intensities for the C-O-C aromatic ether and C-C aliphatic bands.

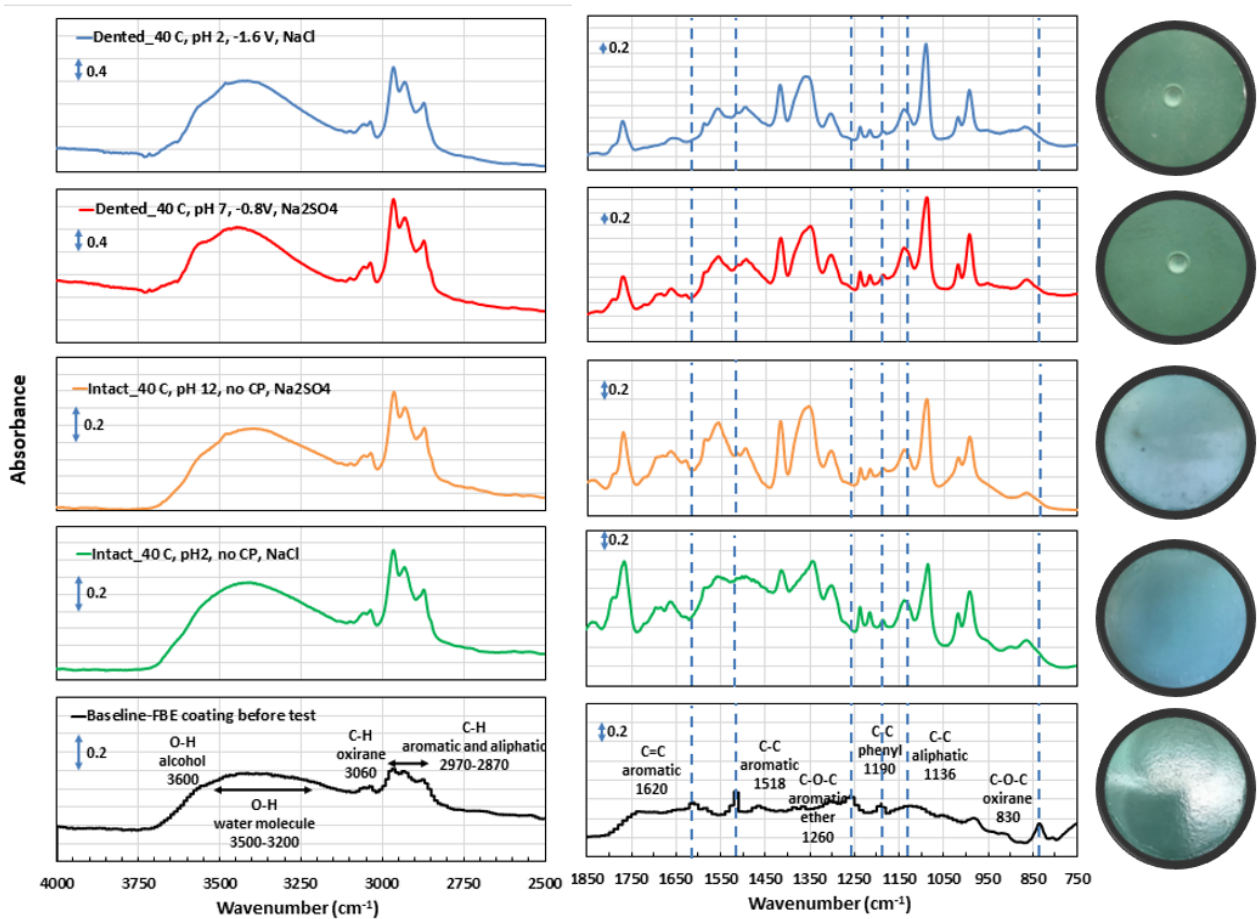


Figure 2-11: FTIR spectra of FBE coated sample tested at 40°C.

At 60°C (Figure 2-12): At 65°C, stronger O-H and C-H bands are seen, while no apparent difference between dented and intact coating samples is found. Band peak shifts were also observed, together with increased band peak intensity for the C-O-C and C-C aliphatic bands.

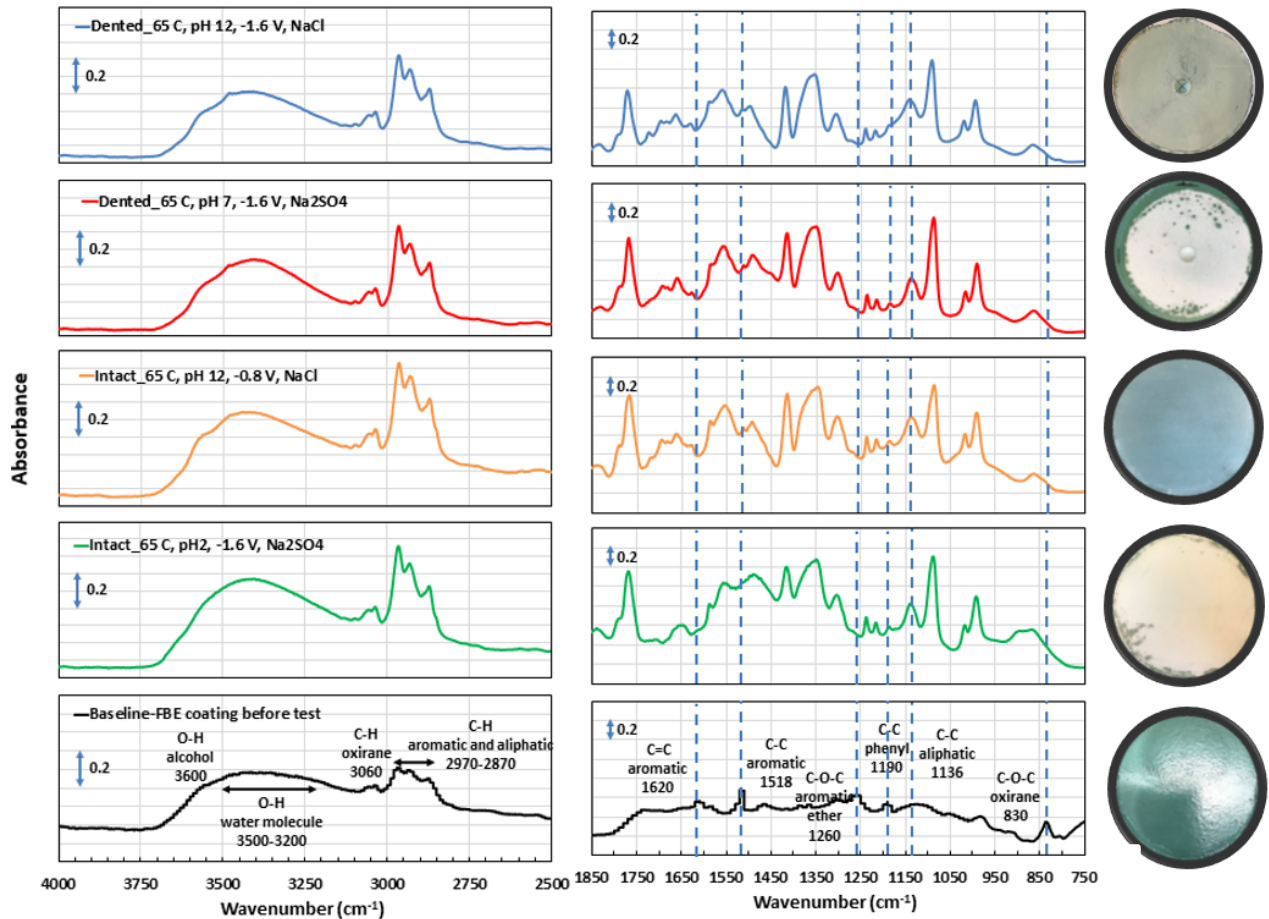


Figure 2-12: FTIR spectra of FBE coated sample tested at 65 °C.

2.2.2.3 Mathematical model

2.2.2.3.1 Model establishment

The CRs of both bare and coated samples were summarized in Table 2-4. Due to the wide range of CR (10^{-8} to 10^2 mm/y), a power transformation of CR was applied. By using a modified quadratic model, a general mathematical equation was fitted to the data and is presented in Equation 2-4. As listed in Table 2-5, the value of coefficients a , b , and c in the equation depends on the coating condition, salt type, and CP levels, respectively.

$$CR^{0.01} = a + b \times T + c \times pH + 0.00034 \times pH^2$$

2-4

Table 2-4: Levels and description of variables in coded form and the CR response

Run	Factor A Solution temperature (°C)	Factor B Solution pH	Factor C Salt composition	Factor D CP (V vs. Ag/AgCl)	Factor E Coating condition	Response CR mm/y
1	10	12	SO4	Y-0.8	N	3.57E-03
2	40	12	SO4	N	Y	5.85E-06
3	65	7	Cl	Y-0.8	Y-D	7.02E-05
4	10	2	Cl	Y-1.6	N	1.81E-02
5	40	7	SO4	N	N	1.58E+00
6	10	12	Cl	Y-1.6	Y-H	5.11E-04
7	10	2	SO4	Y-1.6	Y-H	3.83E-04
8	10	12	Cl	Y-0.8	Y-D	9.76E-05
9	40	7	Cl	Y-0.8	N	1.20E-01
10	65	2	SO4	N	Y-D	1.73E-04
11	65	12	Cl	Y-0.8	Y	8.64E-06
12	10	2	SO4	N	Y-H	6.91E-04
13	40	12	SO4	N	Y-H	5.17E-04
14	65	2	SO4	Y-1.6	Y	1.09E-06
15	65	2	SO4	Y-0.8	N	8.53E-02
16	40	12	SO4	Y-1.6	N	1.00E-04
17	10	7	SO4	Y-1.6	N	3.69E-03
18	40	2	Cl	N	Y	6.60E-07
19	65	12	SO4	Y-0.8	N	2.86E+00
20	65	12	Cl	Y-0.8	Y-H	1.62E-03
21	40	7	SO4	N	N	4.25E+00
22	65	7	SO4	Y-0.8	Y-H	9.12E-04
23	10	12	SO4	Y-1.6	Y-D	2.93E-04
24	10	2	Cl	Y-0.8	Y-H	1.86E-04
25	40	2	Cl	Y-1.6	Y-D	3.19E-04
26	10	2	Cl	Y-0.8	Y-D	2.22E-04
27	65	12	Cl	Y-1.6	Y-D	7.60E-04
28	10	12	Cl	N	N	1.24E-01
29	10	12	Cl	Y-1.6	Y	8.01E-08
30	40	2	SO4	Y-1.6	N	3.69E+00
31	10	7	Cl	Y-0.8	N	4.96E-01
32	65	2	Cl	Y-1.6	Y-H	2.18E-03
33	10	7	Cl	N	Y-D	1.52E-04
34	10	2	Cl	N	Y	3.78E-08
35	40	2	Cl	N	N	3.09E+01
36	10	2	SO4	Y-0.8	N	1.00E-04
37	65	7	Cl	Y-1.6	N	7.33E-04
38	40	7	SO4	Y-0.8	Y-D	1.76E-04
39	65	7	SO4	Y-1.6	Y-D	4.78E-06
40	65	7	Cl	N	Y-H	1.50E-03
41	10	7	Cl	N	Y-D	7.79E-06
42	10	7	SO4	Y-0.8	Y	1.81E-08

Table 2-5: The coefficients in the established mathematical equation

Coating condition	<i>a</i>	Salt composition	<i>b</i>	CP level	<i>c</i>
bare steel	0.97±0.014	NaCl	0.00020	no CP	-0.0047
Holiday sample	0.93±0.014			-0.8 V	-0.0028
Dented sample	0.91±0.014	Na ₂ SO ₄	0.00043	-1.6 V	-0.0065
Intact coating	0.86±0.014				

The corresponding ANOVA for this model is shown in Table 2-6. The Model F-value of 9.27 implies the model is significant. There is only a 0.01% chance that an F-value this large could occur due to noise. P-values less than 0.05 indicate model terms are significant. In this case only E-coating is considered as a significant model term. This result is not surprising as E-coating is apparently the most critical and determinant factor. The two endpoints of the broad CR range presented in Table 2-4, i.e., 1.81×10^{-8} and 30.87 mm/y, are corresponding to a sample with an intact coating versus one of bare steel. When statistically evaluating other factors along with the E-coating factor, the calculated p-values of factors other than E-coating hardly meet the 0.05 rule of thumb. On the other hand, from the p-values, the relative significance of individual affecting factors as well as their complexing interactions can be indicated. From Table 2-6, other than E-coating, factor A-Temp with a p-value of 0.08 is the most influencing factor, followed by factor D-CP (p-value of 0.15). There are two principles for choosing these model items: 1) all the five individual factors were included in the model. From the discussion in sections 2.2.1 and 2.2.2, it is obvious that these factors all play roles in CR determination; 2) model items in the quadratic model were reduced to ensure that the generated model is significant, and the lack-of-fit is not significant, and there is a good correlation between the CR predicted by the model and obtained by experiments. The final model interaction terms include:

- 1) AC – interaction between temperature and salt composition, which affects the solution conductivity;
- 2) BD – interaction between pH and CP, which determines the cathodic reaction process and influences the overall CR;
- 3) B² – a quadratic term of pH, which models/predicts the curvature on a response surface.

The adequacy of the regression model was checked using the normal probability plot of the studentized residual to confirm the normal error distribution (Figure 2-13 (a)), and the studentized residuals versus predicted values to check for constant variance (Figure 2-13 (b)). Figure 2-14 shows the predicted response values versus the actual response values for designed runs 1-42 (displayed in black dots). Using the mathematical model established from the results of these 42

runs, the predicted CR values of extra tests points (X1-X6) were plotted in these orange dots, which present a consistent trend with the model.

Table 2-6: ANOVA test for modified quadratic model

Source	Sum of Squares	Degree of Freedom	Mean Square	F-value	p-value	
Model	0.0709	12	0.0059	9.27	< 0.0001	significant
A-Temp	0.0020	1	0.0020	3.18	0.0849	
B-pH	2.059E-08	1	2.059E-08	0.0000	0.9955	
C-Salt comp	0.0003	1	0.0003	0.4486	0.5083	
D-CP	0.0026	2	0.0013	2.03	0.1491	
E-Coating	0.0650	3	0.0217	33.99	< 0.0001	significant
AC	0.0003	1	0.0003	0.4283	0.5180	
BD	0.0016	2	0.0008	1.23	0.3059	
B ²	0.0006	1	0.0006	0.9415	0.3399	
Residual	0.0185	29	0.0006			
Lack of Fit	0.0181	27	0.0007	3.27	0.2611	not significant
Pure Error	0.0004	2	0.0002			
Cor Total	0.0894	41				

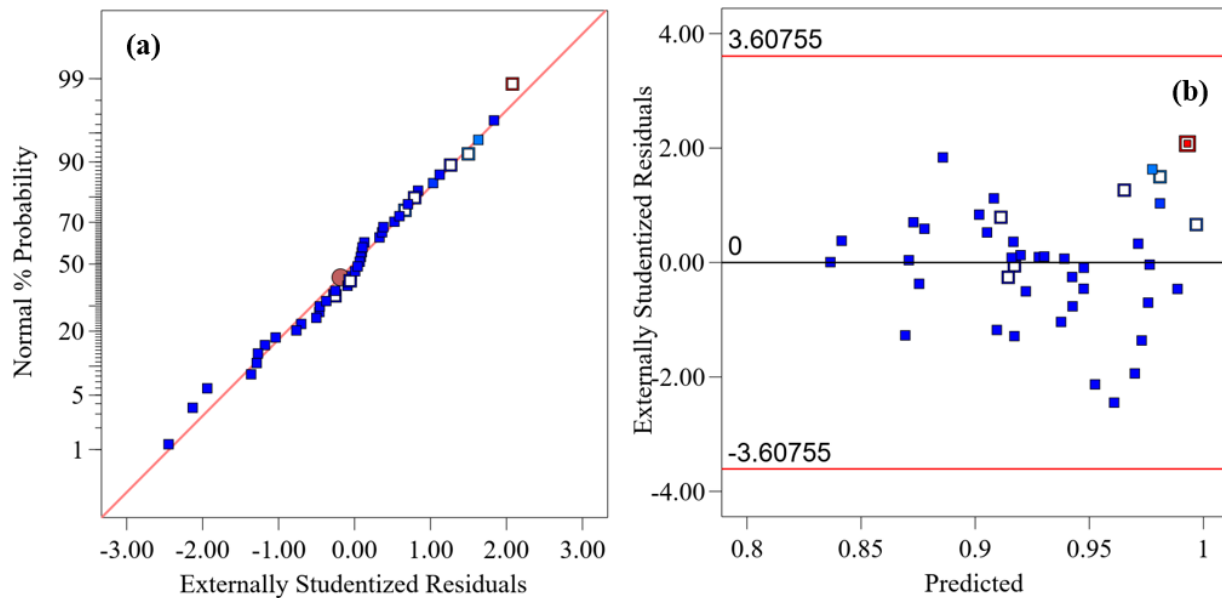


Figure 2-13: (a) Normal probability plot of the studentized residuals to check for normality of residuals; and (b) studentized residuals versus predicted values to check for constant variation.

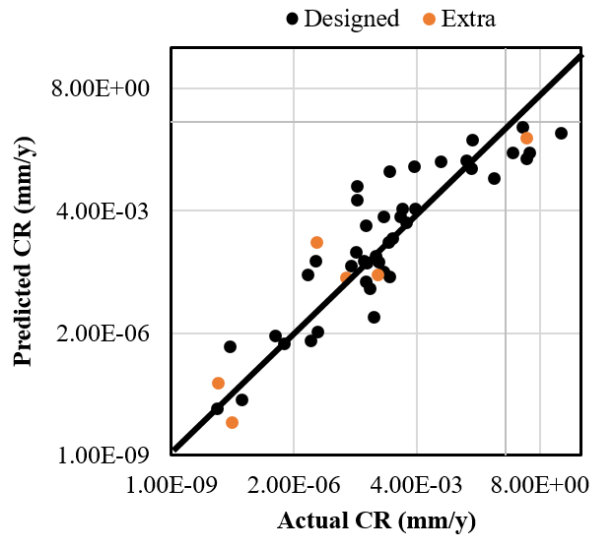


Figure 2-14: Predicted CR using the established mathematical model vs. actual measured CR (Designed points: runs 1-42; extra test points: runs X1-X6 in Table 2-3).

2.2.2.3.2 Model application/prediction

Since coatings and CP are commonly applied for in-service pipelines to protect them from corrosion, a prediction of the combined effect of coating and CP using this model is therefore of primary interests. In Figure 2-15, CR as a function of both coating and CP at different pH conditions is shown.

- The effect of coating

As expected, CR decreases in the order: bare steel > dented sample > holiday sample > intact coating. It is noteworthy that the CR of dented and holiday samples are in a similar order of magnitude (the following Figure 2-16 will show more details on this).

- The effect of CP

It is shown that the effect of CP relates to the pH level. This is primarily relevant to the bare steel samples. In Figure 2-15 (a), when pH is 2, a higher/more negative CP level of -1.6 V does not provide extra protection, but instead leads to a higher CR as compared to a CP level of -0.8 V . This is evidenced by comparing sample B and sample C shown in Figure 2-2. Hydrogen damage could be a reason, which indeed requires more in-depth study. At pH 7 and pH 12, the major cathodic reaction is oxygen reduction. Increased CP level results in an improved corrosion protection. For example, at pH 7 (Figure 2-15 (b)), a CP of -1.6 V brings down the CR to an acceptable level, i.e., less than 0.1 mm/y . At pH 12, increased temperature requires enhanced CP level to ensure corrosion protection. Especially when temperature is higher than 40°C , a CP level of -1.6 V is needed to maintain an acceptable CR (Figure 2-15 (c)). For bare steels with an application of CP, the predicted value is overall higher than the measured value.

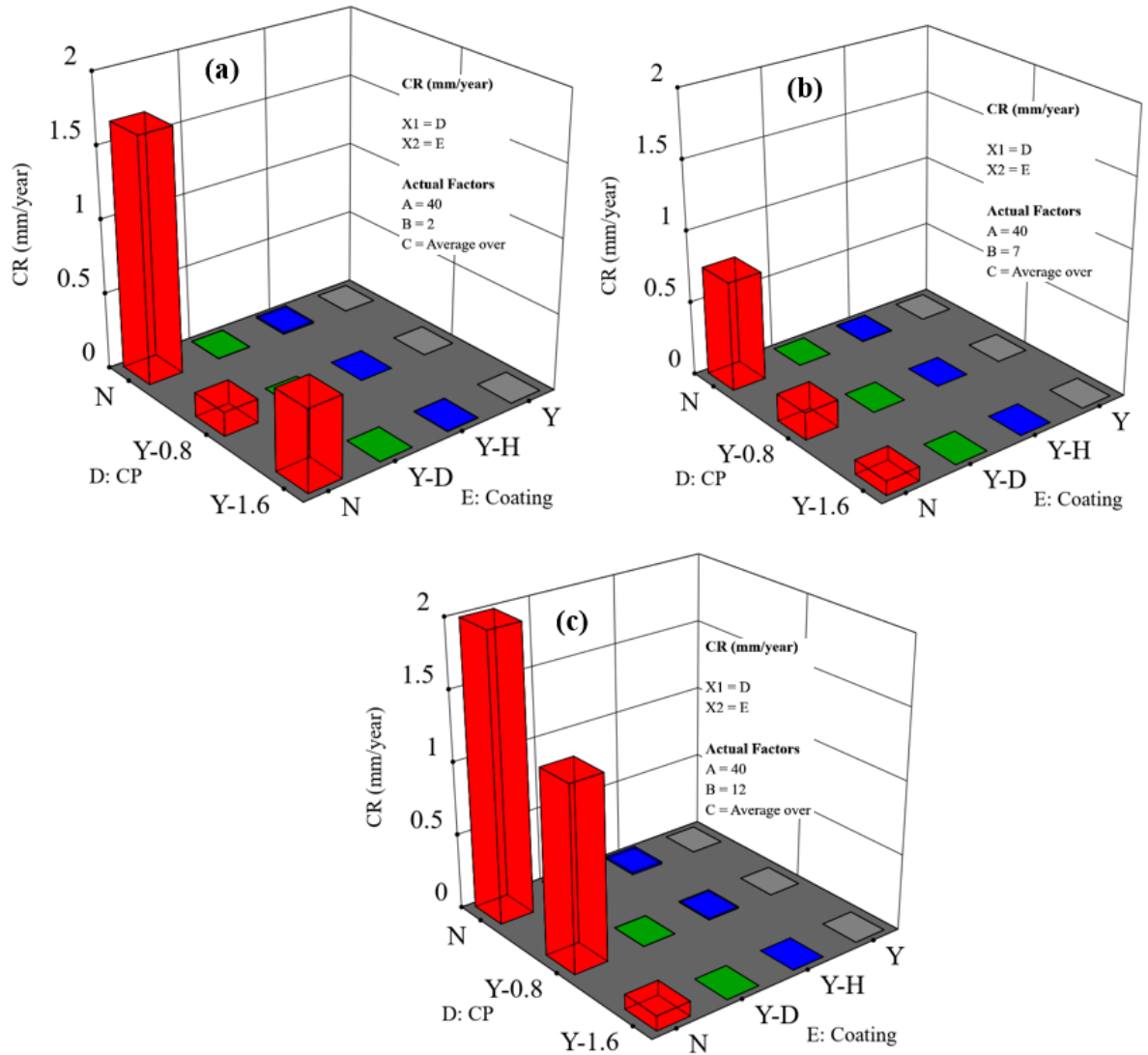


Figure 2-15: CR as a function of both applied CP level and coating scenarios: (a) pH = 2; (b) pH = 7; and (c) pH = 12. The temperature is 40 °C and the salt composition effect was average over that of sodium chloride and sodium sulfate.

Considering coated pipelines that are protected by a CP of -0.8 V (i.e., widely adopted in the field), based on the coating scenarios, the established mathematical model offers a prediction of their CRs as a function of the temperature, pH in a given salt composition environment. Figure 2-16 shows the details. It is obvious that all the coated samples protected at -0.8 V exhibit the same surface response pattern, i.e., at a given temperature, the highest CR appears at pH 12 as predicted by the BD (pH-CP) interaction model item. At pH 12, CR increases more rapidly with increased temperature, resulting in the highest CR located at 65 °C. The CR range for the dented samples is similar to that of the holiday samples, which is consistent with the experimental results (Figure 2-7). The model result further implies that these two types of coating defect should be treated with the same level of attention. It should also be noted that CR predicted by the model for both the

holiday and dented samples protected at -0.8 V is higher than what is observed. For example, the highest CR for the holiday sample in Figure 2-16 (a) is shown as $\sim 0.02\text{ mm/y}$ at 65°C , pH 12, while the actual measured value is 0.0002 mm/y , two orders of magnitude lower. For samples with intact coating, the predicted highest value is close to the actual one, i.e., $0.000011\text{ vs. }0.000009\text{ mm/y}$. For pipelines operated at a low temperature of 10°C , both the experimental and model results show acceptable/negligible CR over a wide range of pH conditions.

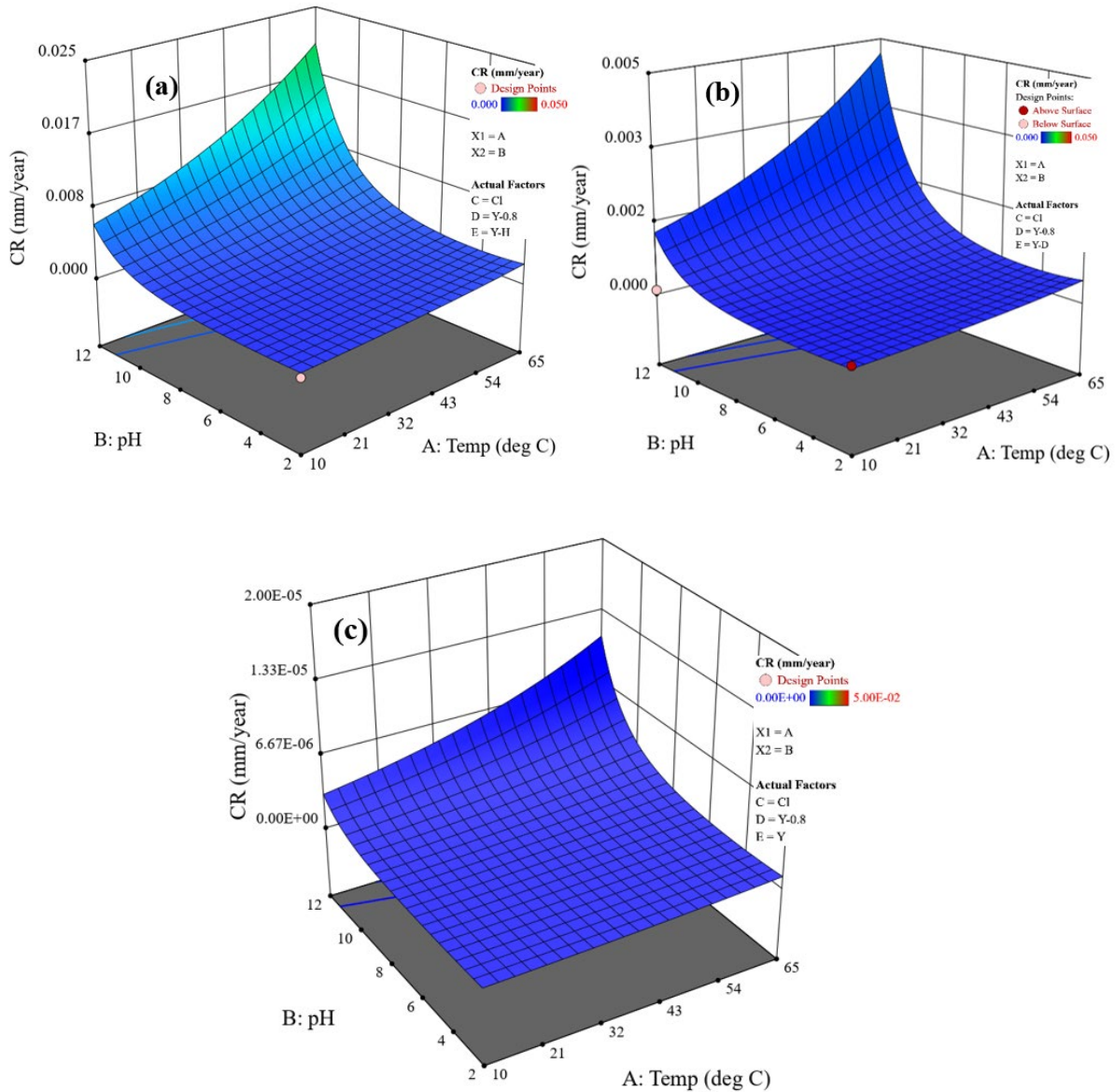


Figure 2-16: CR predicted by the model for the coated samples with different scenarios: (a) coating with a holiday; (b) coating with a dent; and (c) intact coating. The CP is fixed at -0.8 V , and the salt is the sodium chloride.

For the 8 coated samples tested at pH 7, i.e., the most relevant pH in the field, the difference between the predicted and measured CR is shown in Figure 2-17. For the one intact coating sample and two holiday samples, the predicted CR values were in the same order of magnitude with the

measured CR values, i.e., the model provides a very good prediction. For the coating samples with a dent, the difference between the predicted and measured CR was within one order of magnitude for three tested samples, which is not significant considering the CR range for these dented samples was from 0.0001 to 0.00001 mm/y. A larger difference (1 to 1.4 orders of magnitude higher in predicted CR) was observed in the other two dented samples, suggesting that the model provides a relatively conservative CR prediction for coating samples with a dent.

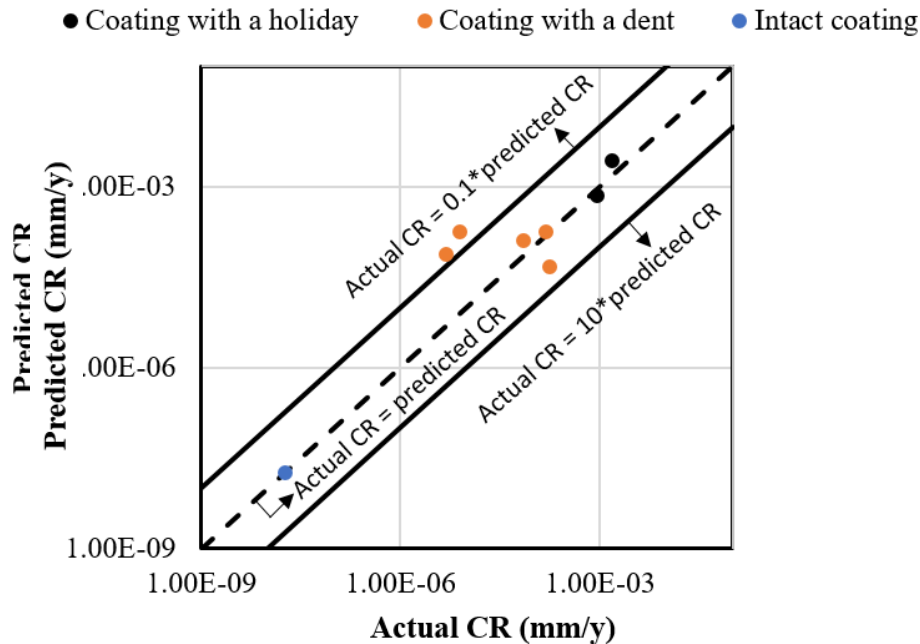


Figure 2-17: Predicted CR vs. Actual CR for coated samples tested at pH 7.

2.3 Conclusions

From the external corrosion of X60 pipe steel research, the main achievements are summarized below:

- 1) Established a test platform for conducting corrosion measurement on bare and FBE coated X60 steel samples by investigating different combinations of solution pH, temperature, salt composition as well as the application of CP.
- 2) Based on the weight loss data, the bare steel samples were categorized into three groups from their measured CRs. Samples having CRs below 0.1 mm/y are considered in a safe zone, while those having CRs above 0.1 mm/y, especially above 1 mm/y are on alert. Particular attention should be paid to two scenarios at high temperatures (40 °C and 65 °C), i.e., acidic environment (pH 2) associated with a high CP level of $-1.6 V$ and alkaline environment (pH 12) together with a moderate CP level of $-0.8 V$. It is assumed that the former is related to hydrogen attack, and the latter is due to hot alkaline corrosion, both of which are interesting research topics worthy of further studies.

- 3) For coated steel samples, their corrosion behavior was studied by electrochemical noise measurement, with coating condition being monitored by FTIR tests. The type of coating defect influences CR (mm/y) the most: CR of holiday sample > CR of dented samples > CR of intact samples. FTIR results show the changes in the coating surface chemistry after these immersion tests and also indicate water absorption in the coatings especially at high temperatures.
- 4) The Response Surface method using an I-optimal design was introduced as a practical method to study and model the influence of five affecting factors (temperature, pH, salt composition, CP and coating scenarios) as well as their complicated interactions on the CR of both bare and coated samples. Mathematical equations were established to predict the CR under different conditions. The experimental data and predicted data generated by this model can be integrated into the final BBN model.

Chapter 3

External General Corrosion – BBN Model

3.1 Introduction

The oil & gas industry is vital to the economy and prosperity of a country (Khan *et al.* 2021; Shahriar *et al.* 2012). In British Columbia (BC), the BC Oil and Gas Commission (BCOGC) regulates more than 37,000 km of pipelines that transport refined and unrefined products. Reliability of the pipelines may be compromised due to aging and deterioration, coupled with exposure to natural (e.g. earthquake, geotechnical failure, climate change) and human induced (e.g. accidental hits, vandalism) hazards (e.g. Xiang and Zhou 2021; Zhang and Weng 2020; Wu *et al.* 2017; Shabarchin and Tesfamariam 2016). The failure incidents reported in BC are (BCOGC 2016): metal loss (corrosion, erosion), cracking (pipe fittings/joint failure), external interference (accidental, vandalism), material manufacturing/construction, geotechnical failure (slope movement, weather) and other causes (operational). Quantifying corrosion progress and failure risk assessment is subject to significant uncertainties (Chakraborty and Tesfamariam 2021; Kanes *et al.* 2018; Yu *et al.* 2018; Li *et al.* 2016). The information required for such a quantification can be obtained from the literature, expert knowledge and experimental data. In this paper, a Bayesian belief network (BBN) framework is used to quantify external corrosion deterioration rate and develop a burst failure probability. A BBN model can efficiently be applied to make informed decisions when the available data is imprecise, ambiguous or incomplete (Kabir *et al.*, 2015).

Both external and internal corrosion are the leading cause of pipe failure (Shabarchin and Tesfamariam 2016; BCOGC 2016; Ayello *et al.* 2014). External corrosion of buried pipelines is observed as a general wall loss (e.g., Xu *et al.* 2021) or localized corrosion (e.g. Velázquez *et al.* 2009). External corrosion is prevalent due to the presence of defects (holidays, wrinkling, disbanding) in the protective coating or insufficient cathodic protection (CP), both of which result in unprotected bare metal being in contact with wet soil. CP and protective coatings are two proven ways to mitigate external corrosion of buried oil & gas steel pipelines. However, when adequate balance between the condition of the coating and the CP level are not established, external corrosion usually occurs (Kowalski and Sánchez 2016). The rate of external metal loss is mainly controlled by the soil environment that the steel surface is in contact with. For this reason, predicting soil corrosivity as well as correlating it with the metal deterioration rate is crucial to evaluating the pipeline's remaining service life. Considering that soil is a complex material consisting of an organic solid phase, liquid water phase, air and other gas phases, many parameters

including, but not limited to, soil resistivity, pH, redox potential, moisture content, chloride concentration would determine its corrosivity (Nakhaie *et al.*, 2020; Xu *et al.* 2021).

Increasing applications of BBN for corrosion risk assessment are reported in the literature. Zhang and Weng (2020) applied BBN for buried gas pipeline failure analysis caused by corrosion and external interference. Xiang and Zhou (2020) integrated a corrosion growth model and reliability analysis using dynamic BBN. Koch *et al.* (2015) and Ayello *et al.* (2014) developed a BBN-based quantitative risk assessment of oil and gas pipeline corrosion. Kowalski and Sánchez (2016) developed a soil corrosivity index in buried onshore pipelines using a BBN model. Demissie *et al.* (2016) developed a soil corrosivity index and remaining service life for metallic potable water pipelines. The BBN is particularly suitable for such processes because of its ability to establish a cause-effect network through integration of the various types of available information, such as analytical models, expert knowledge, published literature and historical data into a single flexible framework (Kabir and Papadopoulos 2019). In this paper, a BBN model is developed using the experimental corrosion rate data reported in Xu *et al.* (2021).

The remainder of this paper is structured as follows. A brief discussion on BBN is presented in the next section. The subsequent section discusses the development of the BBN model for corrosion. After that, the proposed model is applied to case studies and results are discussed in detail. Finally, conclusions and recommendations for future work are discussed.

3.2 Motivation for BBN Application

Many quantitative and qualitative methods have been proposed to investigate the impact of various hazards on the oil and gas pipeline infrastructure (El-Abbasy *et al.* 2015; Lahiri and Ghanta 2008; Marhavilas *et al.* 2011; Nataraj 2005; Shahriar *et al.* 2012). Qualitative methods are frequently based on an index system, whereas quantitative methods are usually based on numerical simulations (Han and Weng 2011). When substantial historical data is available, rigorous statistical or data mining techniques can be used to develop predictive tools (e.g. Artificial Neural Networks). However, in the case of sparse, ambiguous or imprecise data, soft computing techniques, such as decision tree models, fuzzy rule-based models and Bayesian belief networks (BBN) models can be used to quantify cause-effect relationships and handle uncertainties (Ismail *et al.* 2011). A detailed comparative analysis of commonly applied soft computing techniques is reported elsewhere (Kabir *et al.* 2015).

One of the quantitative methods is Failure Mode and Effect Analysis (FMEA). This is a widely applied analytical technique to define potential failure modes and estimate the risk related with each failure mode. FMEA results are used to rank the issues based on their significance and to

perform corrective actions to address the most severe concerns. FMEA is an efficient fault analysis framework; however, the ability of inference is limited and FMEA technique is not suitable for incorporation of the multiple fault related factors to carry out posterior inference (Yang et al. 2009). Additionally, FMEA method is difficult to integrate with new information and expert judgment. Conversely, BBN can be easily updated and refined as soon as new information becomes available (Chen et al., 2012). Furthermore, BBN can be developed based on the existing FMEA model; multiple factors, which cannot modelled with FMEA, can also be integrated with the help of BBN (Yang et al. 2009).

Another frequently used quantitative approach is Fault Tree (FT). This is a systematic and quantitative technique for dependability analysis, which is graphically represented, in order to model different combinations of fault events that may be described in parallel or sequential way, which leads the occurrence of the undesired event. The individual faults can be events that are associated with human errors or component failure, which may cause undesired outcome. Such outcome is the top event of the FT, which corresponds to a particular failure mode of the system. According to Bobbio et al. (1999), FT does not take into consideration probability distributions for component's failure as well as multiple factor interactions, which may affect the probability of failure. The outcome of the FT analysis explicitly quantifies the probability of failure of a system or a system's component. However, FT is not efficient when dealing with many failure components, which may lead to different consequences. Such cases are frequently encountered in risk and dependability analyses. In such scenarios, modelling needs to be done considering random variables with multiple states. Because FT applies only Boolean logic, FT is not a preferable option for such analyses. Another issue with FT models is its limitation to only one top event. BBN models have the similar capabilities as compared to FT models. However, a significant advantage of BBN that it permits multistate variable modelling and allows assessing many outputs in the same model. FT models can easily be mapped in a BBN model, but the reciprocity is not always possible.

Table 3-1 reflects a qualitative analysis between different quantitative computing techniques, which are frequently used in risk and hazard assessments. The major difference between these techniques is an approach to treat inherent uncertainties as well as an ability to handle interaction between various factors that encompass issues specific to failure of oil and gas pipelines.

Table 3-1: Comparison of various network-based techniques (adapted from Kabir et al. 2014)

Attributes	Network based techniques					
	ANN	ANP	BBN	CM/FCM	CN	FRBM
Network capability	L	VH	H ¹	VH ²	H ¹	L ³
Ability to express causality	N	H	VH	VH	H	M
Formulation transparency	N ⁴	VH	H	VH	H	H
Ease in model development	M	H	M	VH	M	M
Ability to model complex systems	VH	M	H	VH	H	H
Ability to handle qualitative inputs	N	VH	H	VH	H	H
Scalability and modularity	VL ⁵	VH ⁶	H	VH ⁶	H	L
Data requirements	VH	L ⁷	M ⁸	L ⁹	L ¹⁰	L
Difficulty in modification	M	N	L	N	L	H
Interpretability of results	VH	VH	VH	H	VH	VH
Learning/ training capability	VH ¹¹	H ¹²	H ¹³	H ¹⁴	H ¹³	M ¹⁵
Time required for simulation	H	L	L	L	M	L
Maturity of science	H	H	VH	M	M	H
Ability to handle dynamic data	H	M	H	M	H	H
Ability to combine with other approaches	VH ¹⁶	H ¹⁶	H	H ¹⁷	H	VH ¹⁶

Ratings: N = No or Negligible; VL = very low; L = low; M = medium; H = high; VH = very high Network based techniques: ANN = Artificial Neural Networks; ANP = Analytic Network Process; BBN = Bayesian Belief Networks; CM/FCM = Cognitive Maps/Fuzzy Cognitive Maps; CN = Credal Network and FRBM = Fuzzy Rule-Based Models

1. Can manage networks but cannot handle feedback loops, therefore referred to as directed acyclic graphs
2. Can handle feedback loops
3. Dimensionality is a major problem and formulation becomes complicated for network systems
4. Generally referred to as black box models
5. ANN needs to be retrained for new set of conditions
6. Very easy to expand, because algorithm is in the form of matrix algebra
7. Minimal data requirement, because causal relationships are given by decision makers
8. Medium data requirement for using precise probability
9. Minimal data requirement, because causal relationships are generally soft in nature
10. Minimal data requirement for using imprecise probability
11. Algorithms, e.g., Hebbian learning
12. Algorithms, e.g., minimizing the error function
13. Algorithms, e.g., evolutionary algorithms and Markov chain Monte Carlo
14. Training algorithms are available which have been successful in training ANNs
15. Clustering techniques, e.g., Fuzzy C-means
16. Examples are available in the literature to develop models using hybrid techniques, e.g., neuro-fuzzy models, fuzzy analytic network process
17. Has a potential to be used with other soft techniques.

In this project, BBN is used to address corrosion hazards because corrosion is a time-dependent random process (Nešić, 2007; Papavinasam, 2013). Any measurement or estimation of the corrosion rate will inevitably contain a degree of uncertainty, as it is influenced by a number of factors subject to aleatory and epistemic uncertainties (Ayello et al., 2012). BBN is particularly suitable to deal with such processes because of its ability to establish a cause-effect network through integration of the various types of available information, such as analytical models, expert

knowledge, published literature and historical data into a single flexible framework (Chen and Pollino 2012; Cockburn and Tesfamariam 2012). This combination is beneficial when dealing with processes that analytical modelling alone fails to describe (e.g. microbiologically influenced corrosion).

BBN is referred to as an analytical framework that permits the visual representation of causal dependencies among given variables in a probabilistic manner (Pearl, 2014). The BBN approach has been applied in the analysis of various complex engineering problems, such as structural reliability analysis, deterioration modelling, and has proven to be particularly effective in the area of risk analysis and decision making under uncertainties (Cheng et al. 2002; Tesfamariam et al. 2010). A BBN model can be efficiently applied to make informed decisions when the available data is imprecise, ambiguous or incomplete (Kabir et al. 2015).

3.3 Bayesian belief network (BBN)

The BBN, also known as Bayesian net, causal probabilistic network, Bayesian network or simply belief network, is a graphical model that permits a probabilistic relationship among a set of variables (Pearl 1988). A BBN is represented with a directed acyclic graph (DAG), where the nodes represent variables of interest (e.g., population, seismic code indicator, peak ground acceleration, etc.), and the links between them indicate informational or causal dependencies among the variables. The absence of a link between two variables is an indication of conditional independence between the corresponding variables. The variables can have any number of discrete states or a continuous sample space; however, they can only attain one realization at a time, which is associated with a degree of uncertainty. The uncertainties in a BBN model are reflected through subjective probability (Pearl 1988).

The relations between the variables in a BBN are expressed in terms of family relationships, wherein a variable A is said to be the parent of B and B the child of A if the link goes from A to B . A BBN is therefore composed of: (i) a set of variables and a set of directed links between the variables; (ii) a set of mutually exclusive states for each variable; and, (iii) an assigned conditional probability for each variable with parents. In the case of a variable with no parents, the conditional probability structure reduces to the unconditional probability of that variable. The efficacy of a BBN is realized in its flexibility to capture top-down inference, observing the cause (or parent) and inferring the possible effect (or child) and bottom-up inference, observing the effect (child) and inferring the possible cause (parent).

The main concept of a BBN is rooted in the use of Bayes' theorem, in which the relation between two nodes, hypothesis H (parent) and evidence E (child), is represented as:

$$P(H_j|E) = \frac{p(E|H_j)p(H_j)}{\sum_{i=1}^n p(E|H_i)p(H_i)} \quad 3-1$$

where $p(H/E)$ = one's belief for hypothesis H upon observing evidence E , $p(H/E)$ = the likelihood that E is observed if H is true, $p(H)$ = the probability that the hypothesis holds true, and $p(E)$ = the probability that the evidence takes place. $p(H/E)$ is known as *posterior* probability and $p(H)$ is called *prior* probability (Pearl 1988). The denominator $p(E)$ of Equation 3-1 is a normalizing constant and is taken as a unity.

Fundamentally, a BBN is used to update probabilities as new information is obtained. The dependencies are quantified by conditional probabilities for each node given its parents in the network. The network supports the computation of the probabilities of any subset of variables given evidence about any other subset. These dependencies are quantified through a set of conditional probability tables (CPTs); each variable is assigned a CPT of the variable given its parents. For variables without parents, this is an unconditional (also called a marginal) distribution. In this study, Bayesian network development software Netica has been used to develop the proposed BBN model (Norsys Software Corp., 2015).

3.4 BBN Model development for corrosion

External corrosion is a complex physico-chemical process that is affected by different and uncertain factors. A knowledge-based BBN framework is developed for vulnerability assessment of generalized corrosion of oil and gas pipelines. The cause-and-effect factors that contribute to corrosion and corrosion rate (CR) are summarized in Table 3-2.

Corrosion initiation time is of importance for any reliability assessment. The pipe coating serves as a physical barrier between the corrosive environment and the pipe steel surface. Corrosion initiates after disbondment of the coating or at other coating defects (Velázquez et al., 2009). Over time, even initially-intact coatings degrade and eventually fail, allowing moisture, oxygen, carbon dioxide and salts to be in contact with the steel surface. The coating can fail in numerous ways depending on the coating type, initial condition, and environmental factors.

The BBN corrosion rate was coupled with a time marching simulation to obtain thickness loss and quantify burst failure. The CR model was developed using corrosion rate data obtained from experimental results (Xu *et al.* 2021) and analytical burst failure models. Finally, in a reliability framework, the failure pressure capacity was coupled with uncertain pressure demand to obtain the probability of failure. The proposed BBN model is depicted in Figure 3-1. In the following subsections, the details are further discussed.

Table 3-2: Contributing factors to the CR of pipelines (CAPP 2018)

Contributor	Cause/sources	Effects
Excess operating temperature	<ul style="list-style-type: none"> Coating failure Coating disbondment 	<ul style="list-style-type: none"> Water ingress Cathodic shielding
Pipes movement/soil stress	<ul style="list-style-type: none"> Excess operating temperature Operating temperature variation Improper support 	<ul style="list-style-type: none"> Coating damage Water ingress Cathodic shielding
Ground movement/soil stress	<ul style="list-style-type: none"> Unstable soil Freeze/thaw cycles 	<ul style="list-style-type: none"> Coating damage Water ingress Cathodic shielding
Soil particle size	<ul style="list-style-type: none"> Aeration Permeability variation 	<ul style="list-style-type: none"> Increased CR
Groundwater level	<ul style="list-style-type: none"> Buried pipelines immersed Coating disbondment Soil wash out 	<ul style="list-style-type: none"> Water ingress Coating damage Cathodic shielding
Improper handling and backfill	<ul style="list-style-type: none"> Rock damage 	<ul style="list-style-type: none"> Coating damage Water ingress Cathodic shielding
Poor joint coating	<ul style="list-style-type: none"> Poor joint coating selection/incompatible pipe and joint coating Improper application of joint coating due to inadequate training/supervision/inspection 	<ul style="list-style-type: none"> Disbonded coating Water ingress Cathodic shielding
Improper insulation	<ul style="list-style-type: none"> Pipelines without a corrosion barrier between pipe and insulation Poor joint coating quality that allows water ingress 	<ul style="list-style-type: none"> Water can enter at holidays and follow the pipe wall Water can enter joint area Outer coating and insulation will shield cathodic protection
Concrete weights and anchor blocks	<ul style="list-style-type: none"> Pipelines without adequate coating within the concrete portion Damaged coating 	<ul style="list-style-type: none"> Water ingress Cathodic shielding by the concrete
Externally weight coating pipe and rock shielding	<ul style="list-style-type: none"> These are not corrosion barrier 	<ul style="list-style-type: none"> Water ingress Cathodic shielding
Cased crossing	<ul style="list-style-type: none"> Casing in contact with the carrier pipes Damaged coating 	<ul style="list-style-type: none"> Cathodic shielding by casing Insufficient CP
Trenchless crossing-no casing	<ul style="list-style-type: none"> Coating damaged during installation 	<ul style="list-style-type: none"> Water ingress Cathodic shielding by protection coating used as rock shields
Soil to air interface (Risers)	<ul style="list-style-type: none"> Damaged coating Lack of coating 	<ul style="list-style-type: none"> Coating UV degradation Coating mechanical damage Water ingress Unreliable CP due to intermittent electrolyte
Insufficient CP	<ul style="list-style-type: none"> CP operating below the NACE SP0169 criteria 	<ul style="list-style-type: none"> External corrosion at coating defects
Cathodic interference	<ul style="list-style-type: none"> Foreign CPs systems AC power lines 	<ul style="list-style-type: none"> Improper CP
Excess CP	<ul style="list-style-type: none"> Improper operating system 	<ul style="list-style-type: none"> Possible coating damage

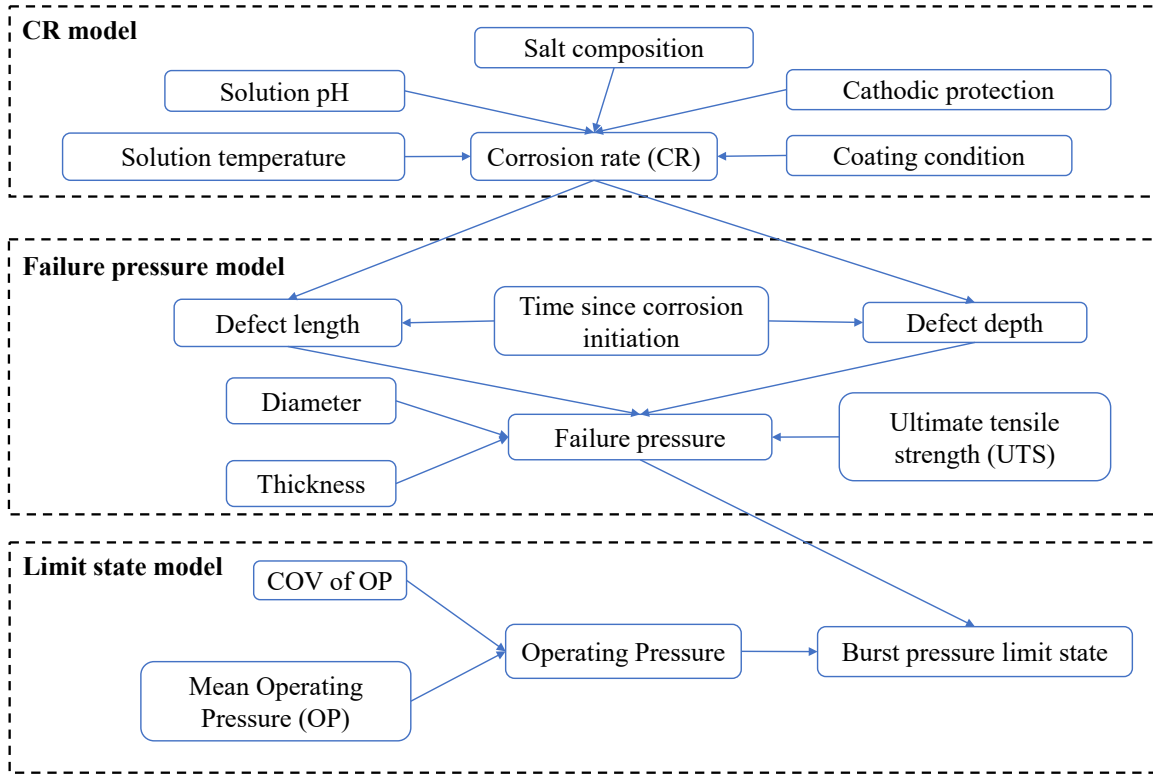


Figure 3-1 Integration of the BBN model for generalized corrosion

3.4.1 Corrosion rate: Experiments and BBN model

Xu *et al.* (2021) discussed the experimental details and results of CR measurements of X60 steel pipe in various simulated soil environments. Here a brief outline of the experimental details used to obtain the data for the current modeling effort is presented. A response surface method (RSM) using Design Expert software was applied to design the multi-variable corrosion tests, i.e., with consideration of various pipe steel conditions (bare steel or fusion bonded epoxy (FBE) coated samples with different coating defect scenarios), different CP levels (no-, optimized- and over-protection), and soil solution corrosivity that is reflected by combination of various solution temperature (T), pH and salt composition. As shown in Figure 3-2, a wide variety of conditions to support the modeling goal were considered. The weight loss method and electrochemical noise measurements were used to obtain the CR data of bare and coated steel samples, respectively. A mathematical model shown in Equation 3-2 was established and validated to provide predictions of CR for both bare and coated steel samples (Xu *et al.* 2021). The mathematical model was used in this work to generate more CR data points as inputs for establishing the BBN model.

$$CR^{0.01} = a + b \times T + c \times pH + 0.00034 \times pH^2 \quad 3-2$$

where CR = the corrosion rate in mm/y, a = a coating dependent parameter; b = a salt type dependent parameter; and c is a CP level dependent parameter. The value of coefficients a , b and c are determined by the coating condition, salt composition, and CP levels, respectively (Table 3-3).

Table 3-3: The coefficients in the established mathematical equation (Xu *et al.* 2021)

Coating Conditions	a	Salt Composition	b	CP Level	c
Bare steel	0.97 ± 0.014	NaCl	0.00020	No CP	-0.0047
Holiday sample	0.93 ± 0.014			-0.8 V	-0.0028
Dented sample	0.91 ± 0.014	Na ₂ SO ₄	0.00043	-1.6 V	-0.0065
Intact sample	0.86 ± 0.014				

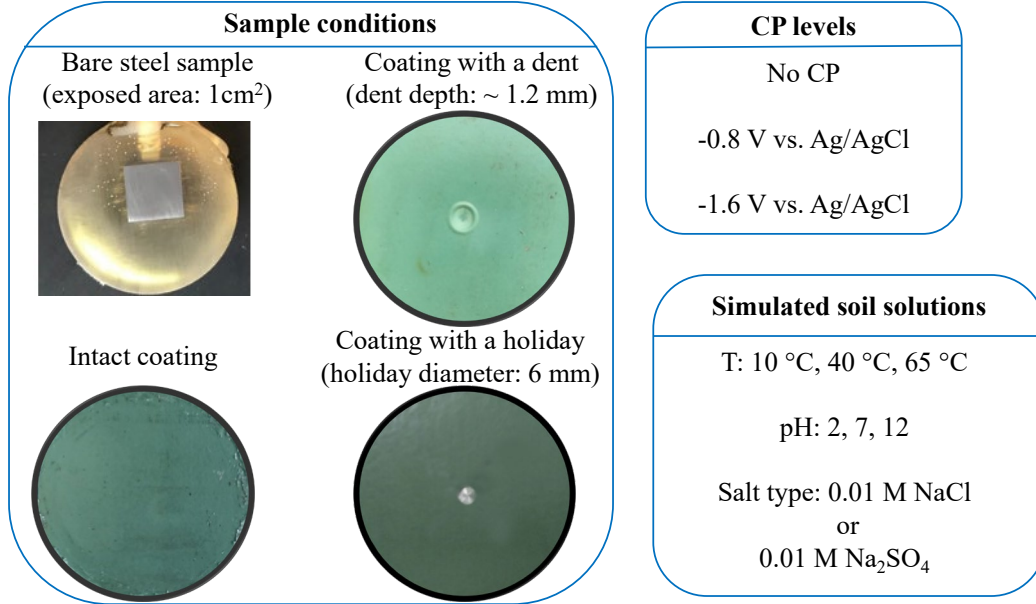


Figure 3-2 A schematic of multi-parameters considered in the corrosion tests

Table 3-4: Discretization details of the uniform corrosion BBN model nodes

Variables	Sub criteria	States	
Corrosion Rate	Temperature (°C)	Extremely Low	$0 \leq T < 15$
		Low	$15 \leq T < 30$
		Medium	$30 \leq T < 45$
		High	$45 \leq T < 60$
		Very High	$60 \leq T < 70$
pH (pH)	pH (pH)	Extremely Low	$0 \leq \text{pH} < 3$
		Low	$3 \leq \text{pH} < 6$
		Medium	$6 \leq \text{pH} < 8$
		High	$8 \leq \text{pH} < 10$
		Very High	$10 \leq \text{pH} < 12$
Salt Composition	Salt Composition	Sodium Sulfate	SO ₄
		Sodium Chloride	Cl
Cathodic Protection	Cathodic Protection	No CP	N
		CP of -1.6V	Y_16
		CP of -0.8V	Y_8
Coating Condition	Coating Condition	No coating	N
		Intact coating	Y
		Coating with an indent	Y_D
		Coating with a holiday	Y_H

The BBN model for the CR is shown in Figure 3-1, where each node represents the basic variables outlined in the experimental test. The states considered for each parameter are summarized in Table 3-4. Temperature (T , °C) is discretized into *extremely low* [0-15], *low* [15-30], *medium* [30-45], *high* [45-60] and *very high* [60-70]. The pH is discretized into *extremely low* [0-3], *low* [3-6],

medium [6-8], *high* [8-10] and *very high* [10-12]. The salt composition is a categorical variable with either $NaCl$ or Na_2SO_4 solution. The CP is classified into *no CP*, and applied CP of $-1.6V$ and $-0.8V$. The coating condition was discretized into *no coating*, *intact coating*, *coating with an indent* and *coating with a holiday*.

The experimental results of Xu *et al.* (2021) were used to develop the CPT of BBN model for CR (Figure 3-1). Figure 3-3a shows the result of the BBN and experimental corrosion rate. The high coefficient of determination ($R^2 = 0.82$) indicated accuracy of the model to predict corrosion rate. To validate the proposed model, 980 additional data points were generated for T [10, 65] using Equation 3-2 for comparison between the BBN and analytical model CR predictions. The result of this comparison is presented in Figure 3-3b and a similar coefficient of determination ($R^2 = 0.83$) was obtained. The model predicted CR was integrated with a coating failure time node in the BBN model to obtain the time dependent corrosion defect size and eventually to quantify failure pressure capacity.

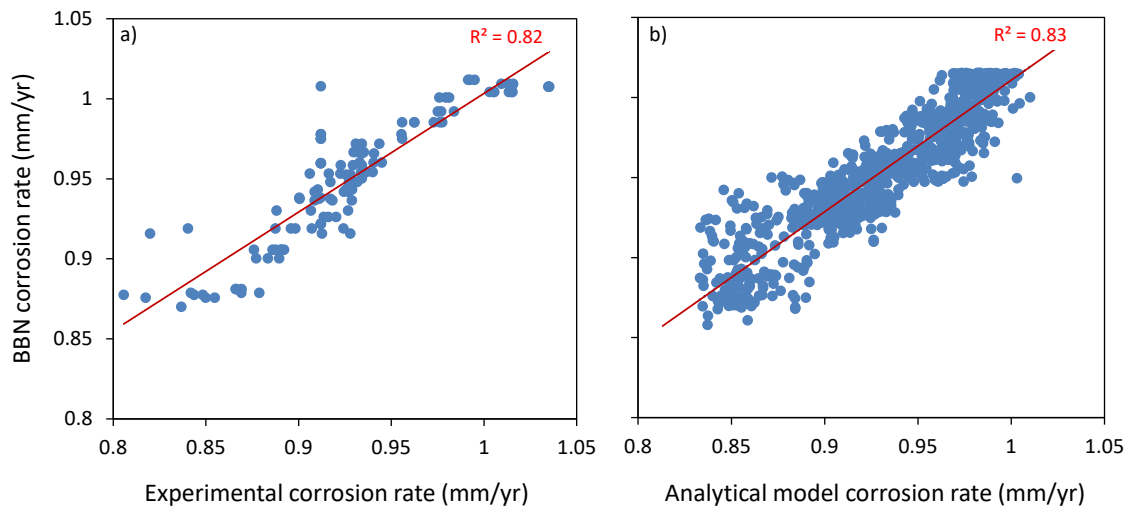


Figure 3-3 BBN model for external corrosion rate with respect to a) experimental, and b) analytical model corrosion rates

3.4.2 Burst pressure capacity

Different failure pressure (FP) models have been developed to assess corrosion defects in pipelines, e.g. ASME B31G (1991) and DNV-RP-F101 (DNV 2004). The different models consider corroded area geometry and pipe internal pressure. Mazumder *et al.* (2020) compiled a set of 92 experimental test results for oil and gas pipelines with corrosion defects. The database of burst failure tests is extracted from available previous studies. A pairwise correlation and histogram of the parameters in burst failure pressure provided in Mazumder *et al.* (2020) is shown in Figure 3-4. The experimental burst FP were compared with various models and the DNV-RP-F101 (DNV 2004) (Equation 3-3) was found to provide the best prediction.

$$FP = \frac{2t \times UTS}{D-t} \left(\frac{1 - \frac{d(T)}{t}}{1 - \frac{d(T)}{t} M^{-1}} \right) \quad M = \sqrt{1 + 0.31 \frac{L(T)^2}{Dt}} \quad \text{3-3}$$

where UTS = ultimate tensile strength, D = diameter, t = thickness, M = folias factor, d(T) and L(T) are depth and length of defects, respectively.

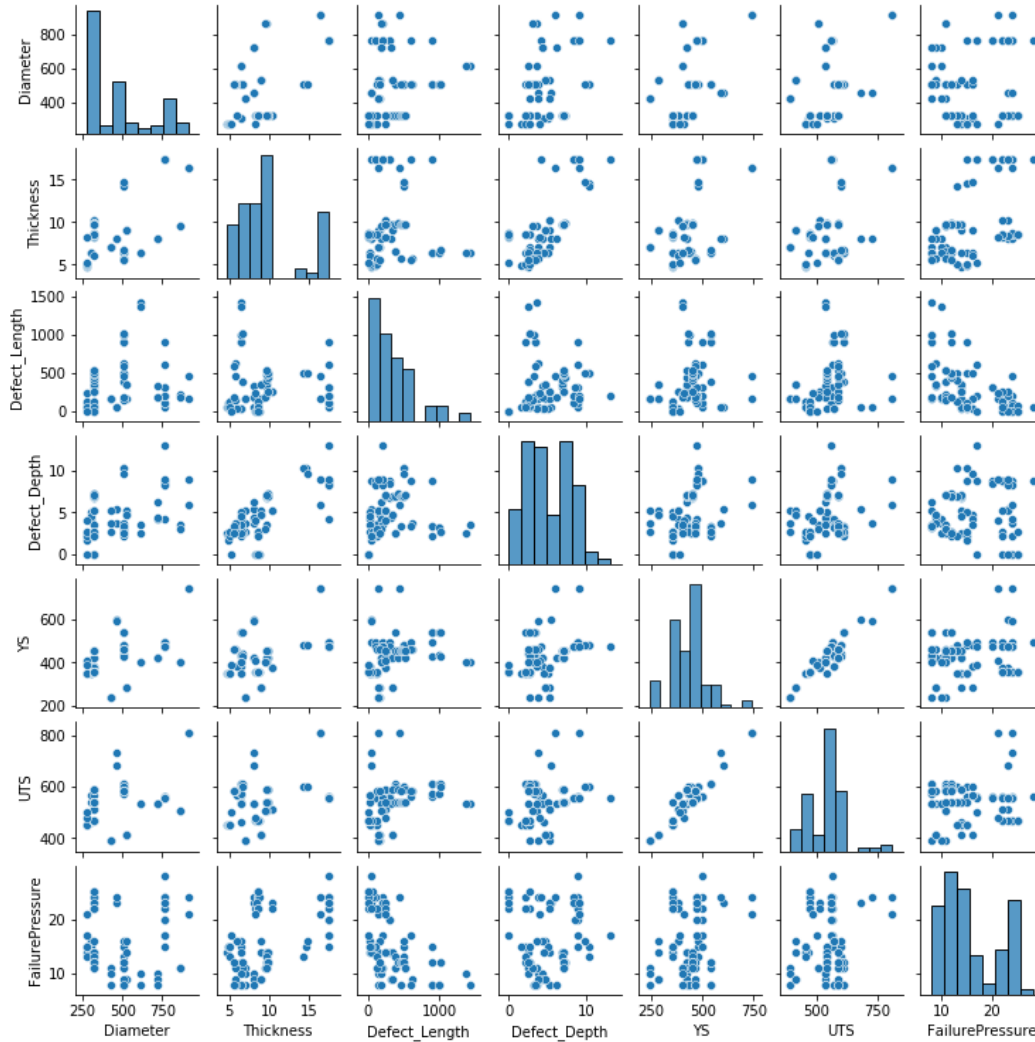


Figure 3-4 Pairwise correlation for burst failure pressure

The BBN model for the failure pressure is shown in Figure 3-1, where each node represents the basic variables outlined in the in the DNV-RP-F101 formula (Equation 3-3). The states considered for each parameter are summarized in Table 3-5, where units are also given. The CR was discretized into *extremely low* [0-0.35], *low* [0.35-0.5], *medium* [0.5-0.6], *high* [0.6-0.75] and *very high* [0.75-1.01]. The exposure period (EP) was discretized into *extremely low* [0-1], *low* [1-2.5], ----, *high* [35-40] and *very high* [40-45]. The defect length (DL) was discretized into *extremely low* [0-20], *low* [20-40], ----, *high* [1200-1500] and *very high* [1500-4400]. The defect depth (DD) was discretized into *extremely low* [0-2], *low* [2-4], ----, *high* [16-18] and *very high* [18-40]. The thickness was discretized into *extremely low* [2-4], *low* [4-5], ----, *high* [18-19] and *very high* [19-20]. Diameter was discretized into *extremely low* [200-350], *low* [350-500], ----, *high* [950-1100]

and *very high* [1100-1150]. The ultimate tensile strength (UTS) was discretized into *extremely low* [200-300], *low* [300-400], ----, *high* [600-700] and *very high* [700-900].

Table 3-5: Discretization details of the burst pressure BBN model nodes

Parameters	Sub criteria	States	
Defect Length	Corrosion rate (CR) (mm/yr)	Extremely Low Low Medium High Very High	$0 \leq CR < 0.35$ $0.35 \leq CR < 0.5$ $0.5 \leq CR < 0.6$ $0.6 \leq CR < 0.75$ $0.75 \leq CR < 1.01$
	Exposure period (EP) (year)	Extremely Low Low ---- High Very High	$0 \leq EP < 1$ $1 \leq EP < 2.5$ ---- $35 \leq EP < 40$ $40 \leq EP < 45$
Defect Depth	CR (mm/yr)	Similar as above	
	EP (year)	Similar as above	
Failure Pressure	Defect length (DL) (mm)	Extremely Low Low ---- High Very High	$0 \leq DL < 20$ $20 \leq DL < 40$ ---- $1200 \leq DL < 1500$ $1500 \leq DL < 4400$
	Defect depth (DD) (mm)	Extremely Low Low ---- High Very High	$0 \leq DD < 2$ $2 \leq DD < 4$ ---- $16 \leq DD < 18$ $18 \leq DD < 40$
	Thickness (mm)	Extremely Low Low ---- High Very High	$2 \leq \text{Thickness} < 4$ $4 \leq \text{Thickness} < 5$ ---- $18 \leq \text{Thickness} < 19$ $19 \leq \text{Thickness} < 20$
	Diameter (mm)	Extremely Low Low ---- High Very High	$200 \leq \text{Diameter} < 350$ $350 \leq \text{Diameter} < 500$ ---- $950 \leq \text{Diameter} < 1100$ $1100 \leq \text{Diameter} < 1150$
	Ultimate tensile strength (UTS) (MPa)	Extremely Low Low ---- High Very High	$200 \leq \text{UTS} < 300$ $300 \leq \text{UTS} < 400$ ---- $600 \leq \text{UTS} < 700$ $700 \leq \text{UTS} < 900$

The DNV model (Equation 3-3) was used to develop the CPT. The database of burst failure tests compiled by Mazumder *et al.* (2020) was used to validate the failure pressure BBN model. Comparison of the predicted BBN failure pressure and experimental failure pressure is shown in Figure 3-5. The high coefficient of determination ($R^2 = 0.91$) indicated that the BBN can model the burst failure pressure. The predicted failure pressure capacity was coupled with the operating pressure in a reliability framework to obtain the probability of failure of the pipeline due to burst pressure.

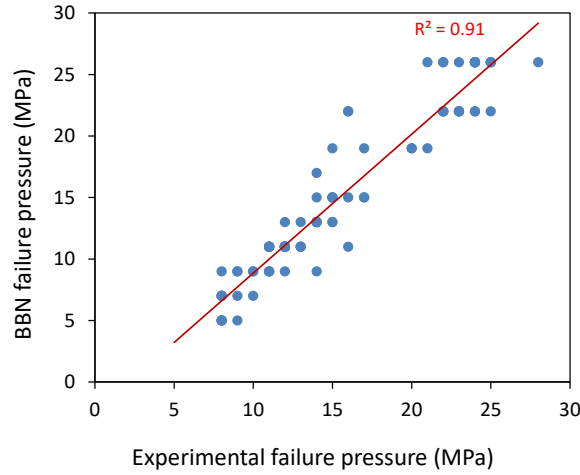


Figure 3-5 BBN model and experimental test failure pressure

3.4.3 Probability of failure

A limit state function (LSF) is defined by the Canadian Standard Association (CSA) Z662 (CSA 2015) as function of a set of basic random variables $x = x_1, x_2, \dots, x_n$, that assumes negative values when the limit state is exceeded (i.e., the pipeline fails). A burst LSF has been formulated as the difference between the pipeline failure pressure (FP) and operating pressure (OP). Mathematically, the LSF and pipeline failure probability due to an individual corrosion defect are expressed as:

$$LSF = FP - OP \tag{3-4}$$

Table 3-6: Discretization details of the burst pressure failure probability

Parameters	Sub criteria	States	
Operating Pressure	Mean operating pressure (OPMn) (MPa)	Extremely Low Low ---- High Very High	$0 \leq OPMn < 4$ $4 \leq OPMn < 6$ ---- $28 \leq OPMn < 32$ $32 \leq OPMn < 100$
	Coefficient of variation (COV) of OPMn	Fixed	0.05
Burst Pressure Limit State	Operating pressure (OP) (MPa)	Extremely Low Low ---- High Very High	$0 \leq OP < 4$ $4 \leq OP < 6$ ---- $28 \leq OP < 32$ $32 \leq OP < 100$
	Failure pressure (FP) (MPa)	Extremely Low Low ---- High Very High	$0 \leq FP < 4$ $4 \leq FP < 6$ ---- $28 \leq FP < 32$ $32 \leq FP < 100$

The BBN model for the failure pressure is shown in Figure 3-1, where each node represents the operating and failure pressure as outlined in the LSF (Equation 3-4). The OP (MPa) is modelled as a normal distribution defined with mean and coefficient of variation (COV). Discretization of the BBN nodes is summarized in Table 3-6. The operating pressure (OP, MPa) is discretized into *extremely low* [0-4], *low* [4-6], *----*, *high* [28-32] and *very high* [32-100]. The mean operating pressure (OPMn) has similar states as the operating pressure with a COV = 0.05. Failure pressure

(FP) is also discretized into *extremely low* [0-4], *low* [4-6], *----*, *high* [28-32] and *very high* [32-100].

3.5 Sensitivity analysis of the BBN model

BBN analysis utilizes prior conditional probabilities to estimate model output in the presence of new evidence. Since the final output is dependent on a priori assigned probabilities, there is a need to carry out sensitivity analysis to identify critical input parameters that have a significant impact on the output results. BBN sensitivity analysis also serves as an aid to identifying the important uncertainties for the purpose of prioritizing additional data collection (Laskey 1995).

Various methods have been proposed for carrying out sensitivity analysis in a BBN (e.g. Pearl 1988; Laskey 1995; Castillo *et al.* 1997). Since the input parameters required to evaluate the failure pressure have discrete and continuous values, the variance reduction method (Cheng 1986; Pearl 1988; Norsys Software Corp. 2015) is used here to determine the sensitivity of the BBN model's output to variation in a particular input parameter. The variance reduction method works by computing the variance reduction of the expected real value of a query node Q (e.g., *probability of failure*) due to a finding at varying variable node F (e.g., *pH*). Thus, the variance of the real value of Q given evidence F , $V(q/f)$, is computed as (Norsys Software Corp. 2015):

$$V(q/f) = \sum_q p(q/f)[X_q - E(Q/f)]^2 \quad 3-5$$

where q = the state of the query node Q , f = the state of the varying variable node F , $p(q/f)$ = the conditional probability of q given f , X_q = the numeric value corresponding to state q , and $E(Q/f)$ = the expected real value of Q after the new finding f for node F .

The first sensitivity analysis to burst pressure limit states by varying the unconditional input parameters was undertaken. The sensitivity with order of importance are: time since the initiation of corrosion (13.3%), OPMn (12%), Thickness (9.42%), Diameter (5.19%), UTS (3.56%), and to a very small degree factors related to CR. It is expected that the coating failure time is strongly associated with CR since corrosion occurs when the first line of coating protection, the coating, fails. This is especially true when there is no or inadequate CP. Indeed, with BBN model, factors closer to the parameter of interest show higher sensitivity (Shabarchin and Tesfamariam 2016). Another sensitivity analysis is carried out only with factors related to CR. From this analysis, Coating Condition (49.6%), CP (14.3%), and Salt Composition (1.01%) showed highest sensitivity. This sensitivity analysis result of the BBN model is, in general, consistent with the ANOVA analysis for the CR model shown in Equation 3-2 in which the Coating Condition (no coating, coating with a holiday or a dent, intact coating) is the most critical factor in determining CR, followed by Temperature, CP, Salt Composition and pH (Xu *et al.* 2021).

3.6 Parametric study

To identify critical parameters for the burst failure pressure, a parametric study is performed. The pipe material properties considered are: pipe material (X60), product specification level (PSL2), diameter (457 mm), thickness (8.2 mm) and UTS (517 MPa). A total of six cases are considered; five accounting for the soil corrosivity and one for operating pressure, respectively. The discrete values used for the six cases are: Case 1 $pH = \{3, 7, 11\}$; Case 2 $T = \{10, 40, 60\}$; Case 3 $CP = \{N, Y_8, Y_16\}$; Case 4 Coating condition = $\{Y, Y_D, Y_H, N\}$; Case 5 Salt composition = $\{Cl, SO_4\}$; Case 6 mean operating pressure = $\{7, 14, 21\}$. For the X60 pipe material, values for each case are varied by keeping Cases 1 and 2 at their median values, coating condition = N, CP = N, and salt composition = SO_4 . For Case 6, the mean operating pressures, with COV = 0.05, were discretized (Figure 3-6) with the OPMIn ranges shown in Table 3-5.

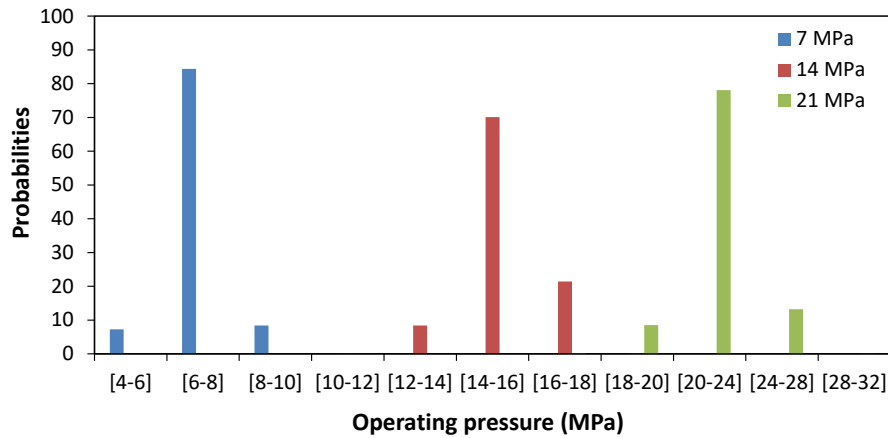


Figure 3-6 BBN node distribution for varying mean values of operating pressure.

The burst limit state is calculated from the probabilistic distribution of operating and failure pressures (Figure 3-7). Failure pressure, remaining capacity of a pipeline, decrease with elapsed time and hence increase the failure probability (Figure 3-7). For each scenario, the *exposure period* was varied from 0 to 45 years, and corresponding probability of failure, i.e. exceedance of the burst limit state is computed (e.g. Figure 3-7). Lognormal distribution fragility curves are fitted to the probability of failure, and the results are plotted in Figure 3-8 - Figure 3-13.

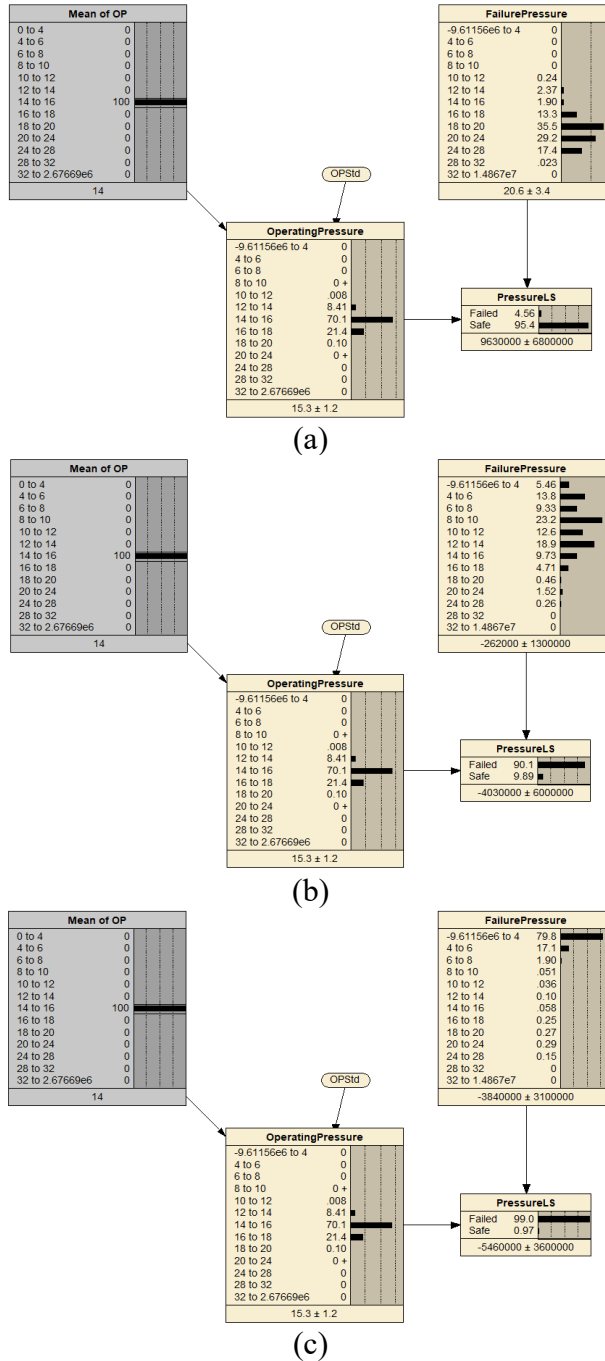


Figure 3-7 BBN model for probability of failure and failure pressure variation over a) 1 year, b) 5 years, and c) 10 years.

For Case 1, the fragility curves demonstrate that, for all duration of the exposure time, the failure probability at pH = 11 is lower than at pH = 3 and 7 (Figure 3-8). The 10th and 90th percentile of failure for the 3, 7 and 11 pH states are [2.26, 9.80], [2.01, 10.65] and [3.22, 21.20], respectively. The pH 11 has a higher uncertainty. Pipeline operating at pH 3 and 7 reaches 50% of the failure probability in 4.71 and 4.63 years, respectively. The median failure probability increases to 8.24 years at pH 11. This implies that the risk of CR rate increases with a decrease in pH and hence lower pH values can greatly increase the failure probability due to CR. It should be noted that the

pipe is assumed to have no coating and no CP under the conditions studied for this case. As a result, the BBN predictions can be compared to bare metal corrosion experiments. The weight loss tests on bare X60 steel without CP protection show similar results, i.e., the highest CR (30.87 mm/yr) was observed for a sample tested at pH 2, 40 °C in NaCl solution, followed by that tested at pH 7, 40 °C in Na₂SO₄ solution (4.25 mm/yr). Without CP protection, bare steel exposed to high pH environment (pH = 12) showed a relatively low CR that is less than 1 mm/yr (Xu *et al.* 2021).

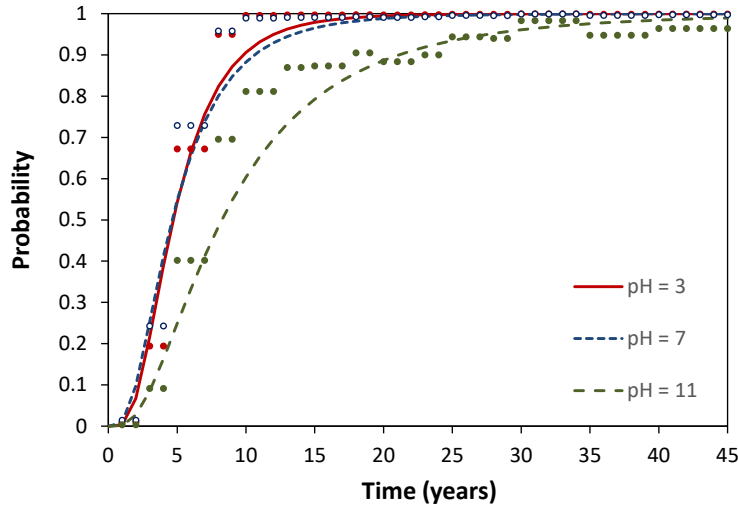


Figure 3-8 Fragility curves for variation in pH (T=40°C, CP=N, coating condition=N, salt composition=SO₄, OPMn = 12 MPa)

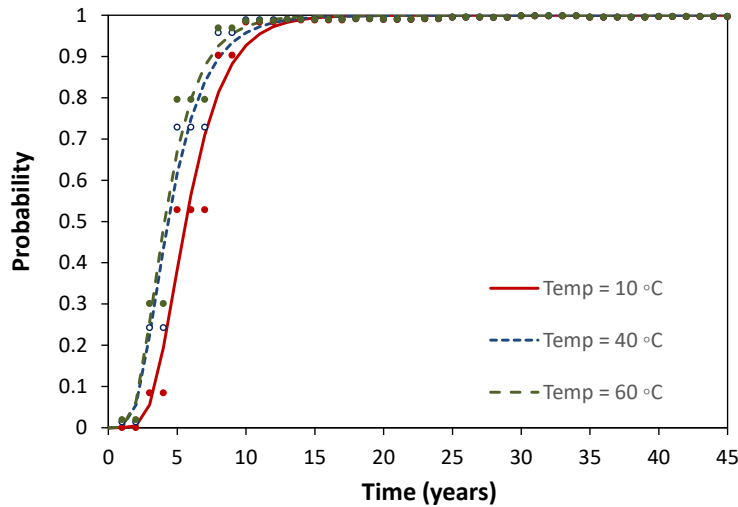


Figure 3-9 Fragility curves for variation in temperature (pH = 7, CP=N, coating condition=N, salt composition=SO₄, OPMn = 12 MPa)

The parametric study of Case 2 indicates that a pipeline has less failure probability at lower temperatures (Figure 3-9). As corrosion is an electrochemical reaction, change in temperature can affect its development. The 10th and 90th percentile of failure for the 10, 40 and 60°C temperature are [3.39, 9.30], [2.34, 8.08] and [2.25, 7.39], respectively. There is no significant difference on the spread of the time uncertainty. However, the failure duration has increased with a decrease in temperature (e.g., a pipeline operating at 10 °C can reach 90% of its limit state at 3.39 years, which

is one year after than at 40°C and 60°C). Pipeline operating at 40°C and 60°C reaches 50% of the failure probability in 4.35 and 4.10 years, respectively. The median failure probability increases to 5.64 years at 10°C. This is justified by the fact that, at lower temperatures, the chemical reactions are slow and this was also proved by the CR tests conducted in (Xu *et al.* 2021). Indeed, the probability and kinetics of chemical reactions increase with an increase in temperature (Balekelayi and Tesfamariam, 2020).

For Case 3, Figure 3-10 shows the fragility curves of a pipeline with and without CP. There is a noticeable difference among the three fragility curves. The 10th and 90th percentile of failure for the CP = N, Y_18 and Y_16 are [2.34, 8.08], [2.08, 6.62] and [3.32, 8.50], respectively. The Y_16 has the largest spread among the three states. The 10th and 90th percentile failure duration is observed to be higher for bare pipe than applied CP (Y_8). This can be due to insufficient applied CP. A pipeline with an applied CP (Y_16) reaches 50% of its failure probability in 6.1 years, which is higher than No (4.63 years) and Y_8 (3.80 years). This indicates, as expected, that CP is helpful in mitigating the hazard of external corrosion. From the experimental results, the effect of CP at pH 7, i.e., the case studied in Figure 3-9, was shown to be directly linked to the CP levels. The increase of CP (more negative) leads to better corrosion protection. However, in acidic or alkaline environments, other factors including cathodic reaction induced hydrogen evolution and temperature would influence the effectiveness of applied CP (Xu *et al.* 2021).

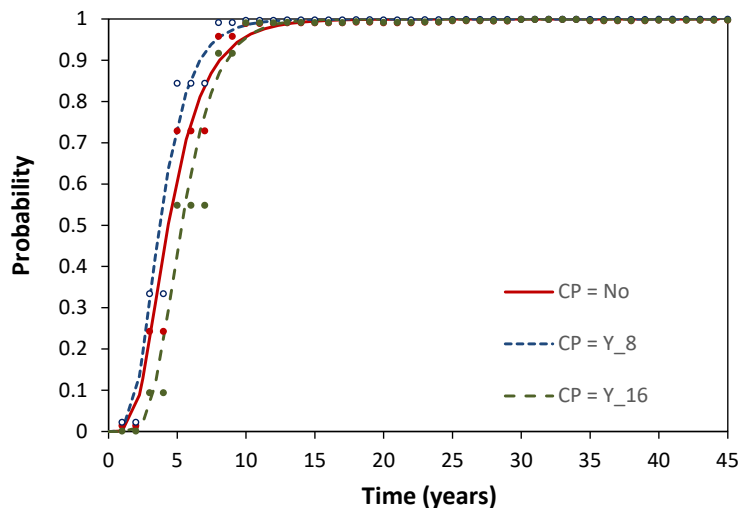


Figure 3-10 Fragility curves for consideration of cathodic protection (pH = 7, T=40°C, coating condition=N, salt composition=SO₄, OPMn = 12 MPa)

For Case 4, the fragility curves show that an intact coating provides good protection for pipeline steel (Figure 3-11). The fragility curves of a pipeline with a dented coating or holidays show a similar trend, and both have higher corrosion risk compared to an intact coating, which is reflected by the experimental results from the electrochemical noise measurements of coated samples (Xu

et al. 2021). Failure of a pipeline due to external corrosion is high in the absence of a coating, i.e. when the coating is so defective as to provide little barrier to transport of water, salts and gases to the pipe surface. The 10th and 90th percentile of failure for coating condition are: *Intact* [7.45, 45], *Dented* [4.21, 17.5], *Holiday* [4.06, 14.59], and *N* [2.02, 10.62]. The uncertainty of coating conditions are ranked in decreasing order as *Intact*, *Dented*, *Holiday* and *N*. As expected, it takes a longer time for a pipeline with an intact coating to fail due to external corrosion compared with other coating conditions. In the case shown here, there is no CP protection, and an intact coating pipeline takes 18.61 years to reach median percentile of failure, while it takes 8.57, 7.69 and 4.63 years for *Dented*, *Holiday* and *N*, respectively. It should be noted that for *intact* FBE coatings, gradual degradation does occur over time and the primary failure modes include both disbondment and blistering (water uptake) (Zargarneshad *et al.* 2021). When there is no CP considered, the blisters in FBE lead to the formation of microcracks in the coating (TR21447 NACE Standards 2020), which act as pathways for water and other species to penetrate into the coating/steel interface and cause corrosion. The formation of corrosion products can further disbond the coating, resulting in continuous pipeline metal loss and eventual failure of the pipeline (Kim *et al.* 2021). Based on the experimental results used for this BBN model, CRs for intact coatings are extremely low, i.e. 10^{-8} to 10^{-6} mm/yr (Xu *et al.* 2021). While these corrosion rates are very low it should be noted that the FBE-coated steel samples used in Xu *et al.* (2021) were manufactured in 2017 and used for testing in 2019. Due to time-dependent interaction with the atmosphere, these samples did contain free liquid water in the FBE coating based on Fourier Transform InfraRed spectroscopy measurements. For further information on the time-dependent degradation of FBE coatings in various environments please refer to Zargarneshad *et al.* (2021). Thus, the intact coating failure predictions presented here might be a little conservative when compared to those one would obtain based on measurements done on fresh coatings, where the measured CRs could be even lower, approaching zero, for intact coatings. However, it is not uncommon for pipes to be exposed to the atmosphere for several years before being installed for service so these results are not out of line or irrelevant to industrial practice. This indicates that coating condition is a critical component and integrity of the pipeline can be significantly improved by maintaining an intact coating condition.

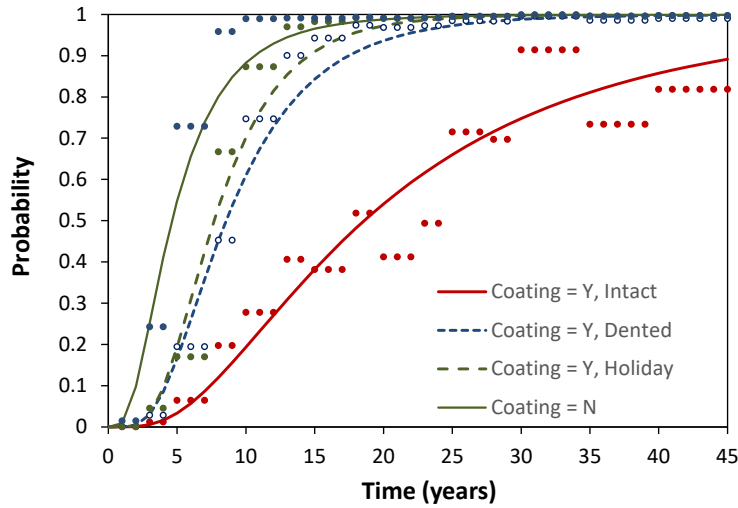


Figure 3-11 Fragility curves for coating condition (pH = 7, T=40°C, CP=N, salt composition=SO₄, OPMn = 12 MPa)

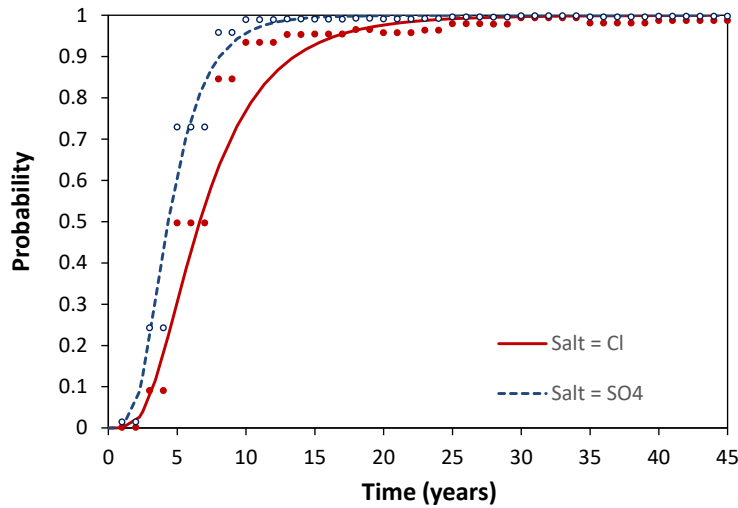


Figure 3-12 Fragility curves for salt composition (pH = 7, T=40°C, CP=N, coating condition=N, OPMn = 12 MPa)

The parametric study of Case 5 shows the fragility curves of two salt states (Figure 3-12). Among the two states, the SO_4 solution has a higher risk of failure due to CR. The 10th and 90th percentile of failure for solution = Cl and SO_4 are [3.25, 13.46] and [2.34, 8.08], respectively. The uncertainty for Cl is higher. A Cl solution reaches 50% of its failure probability in 6.62 years, which is higher than SO_4 (4.35 years). This indicates that SO_4 may contribute more towards corrosivity. The corrosivity of these two salt states cannot be revealed from the designed experiments shown in (Xu *et al.* 2021). For bare samples, the CR is decreased when the corrosion product is found more compact in a certain salt solution.

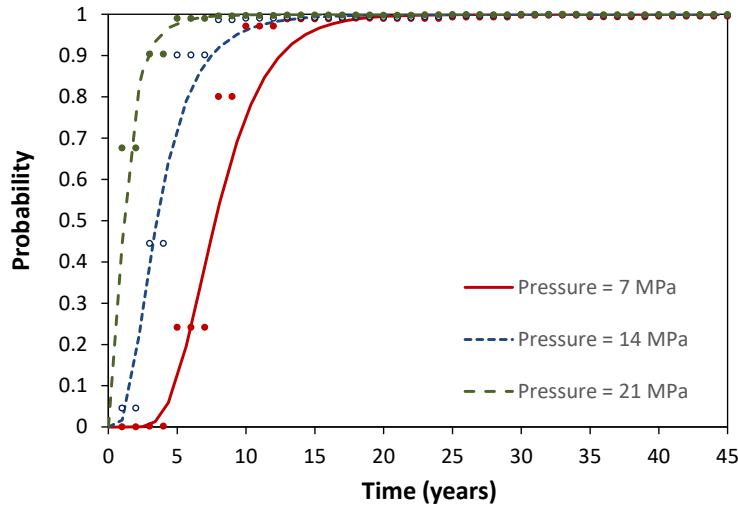


Figure 3-13 Fragility curves for variation in operating pressure (pH = 7, T=40°C, CP=N, coating condition=N, salt composition=SO₄)

For Case 6, the fragility curves indicated that a pipeline has less failure probability at lower operating pressure (Figure 3-13). As expected, the risk of external corrosion increases with an increase in operating pressure. The 10th and 90th percentile of failure for operating pressure of 7, 14 and 21 MPa are [4.81, 12.43], [1.65, 7.46] and [0.43, 2.89], respectively. The uncertainty for operating are ranked in decreasing order as 7, 14 and 21 MPa. Pipeline operating at 14 and 21 MPa reaches their 50th percentile in 3.53 and 1.11 years, respectively. The failure duration at median percentile increases to 7.77 years at 7 MPa. The significant difference in the failure durations of each state of the operating pressure indicates that the risk of CR rate increases, as expected, with an increase in operating pressure.

3.7 Conclusions

In this chapter, a BBN model has been developed using CR data obtained from experimental test results (Xu *et al.* 2021) and analytical burst failure models. The BBN CR was coupled with a time marching simulation to obtain corrosion defects and quantify failure pressure capacity. Finally, in a reliability framework, the failure pressure capacity was coupled with operating pressure to obtain the probability of failure.

The BBN model for CR was validated using 980 data points generated using Equation 3-2 for comparison between the BBN and analytical model CR predictions. A high coefficient of determination ($R^2 = 0.83$) was obtained and hence indicate accuracy of the model to predict CR. The BBN model for failure pressure was validated using a burst failure tests database that was compiled by Mazumder *et al.* (2020). A high coefficient of determination ($R^2 = 0.91$) was obtained and this indicates that BBN can model the burst failure pressure with high accuracy.

The developed BBN model was used to perform a parametric study to identify the critical

parameters for the CR of X60 pipe material. The predicted results are consistent with the input experimental test results to a large extent. The parameters considered are pH, temperature, CP, coating condition, salt composition and operating pressure. Values for each case are varied by keeping pH = 7, temperature at 40°C, coating condition = N, CP = N, and salt composition = SO₄. The overall results of the parametric study indicated that pipeline failure probability increases with a decrease in soil solution pH level. The duration for the median failure probability is high at higher pH level. It was seen that pipeline operating at lower temperature also has a lower failure probability. The failure duration for all percentiles increased with a decrease of temperature. Availability of intact coating condition and applied CP also reduces the risk of failure probability. In addition, among the two states of salt composition, the SO₄ solution observed to have higher risk of failure due to external corrosion. The increase in operating pressure is observed to simultaneously increase the failure probability.

This paper can be extended in the future to incorporate reliability assessment of pipelines due to leakage, where a leakage failure is based on the corrosion defect depth and wall thickness of a pipeline. In addition, the developed BBN model can be integrated with consequence assessment to develop a comprehensive risk assessment tool.

Chapter 4

External Pitting Corrosion – BBN Model

4.1 Corrosion Mechanism and Factors Affecting its Rate

In the oil and gas industry, it is a common practice to bury pipelines underground. This exposes them to an environment that is potentially corrosive to steel. To protect from this detrimental exposure, a two-layer protection system is applied, such as external coating and cathodic protection (CP). The protective coating acts as a first layer of defence, while cathodic protection serves as a backup system. In the case of coating failure, CP should mitigate corrosive exposure. When both protective systems fail or work incorrectly, external corrosion occurs. This process frequently propagates in four stages:

- i. At the initial stage, corrosion species (e.g. chlorides) are transported on the pipeline coating surface. After some time, these elements reach the steel surface by penetration through the coating surface or damaged areas on the coating surface (due to soil stress or manufacturing defects).
- ii. At stage 2, a corrosion product forms, which is bigger in volume than its initial elements. This mechanically affects coating, causing its disbonding.
- iii. Gradually, coating damage increases from a microscopic size to a holiday, which is a visible discontinuity in the coating surface. Consequently, the pipe's steel surface becomes directly exposed to the corrosive environment.
- iv. At the final stage, metal dissolution propagates, causing the formation of corrosion flaws, which ultimately may compromise the pipeline integrity.

Cathodic protection supplies electrons to the pipeline, which decreases its natural electromotive force, leading to the reduction of the corrosion rate (Castaneda and Rosas, 2015). However, CP and protective coating systems themselves are susceptible to malfunction or failure. As indicated by Muhlbauer, any coating can fail and there is no defect free coating (Muhlbauer, 2004). Coating systems can fail due to several causes, including mechanical damage, incorrect application (e.g. excessive operating temperatures), cathodic disbondment, and so on. In addition, a poorly designed or malfunctioning CP system can be a cause of corrosion damage. For instance, CP may provide insufficient current, which is not able to stop the corrosion process, whereas high current may damage the protective coating. Furthermore, the normal work of CP can be interrupted by the presence of another CP protected object. The aforementioned failures of the external corrosion protection systems allow the corrosion process to initiate. The rate of this corrosion process and, therefore, the time of pipeline failure is strongly dependent on soil corrosivity, which, in turn, is affected by the mechanical and chemical properties of soil (Demissie et al., 2015; Sadiq et al.,

2004a). Soil is a complex material, constituted by solid, liquid and gas phases. Liquid and gas phases can comprise up to 50% of the total soil volume. One part of this liquid phase is bound to the mineral surfaces; the other part can freely flow through the soil pores. This flow is governed by soil permeability, which is determined by the size of particles in the solid phase. Such complexity creates many parameters, affecting soil corrosivity. The most important ones among them include soil resistivity, soil pH, chloride concentration, redox potential, water content, etc. (Castaneda and Rosas, 2015). These parameters are mostly seasonal, and their values correspond to precipitation amounts and atmospheric temperatures. Some of these parameters and their influence on the corrosion rate are briefly described in the following paragraphs.

4.1.1 Soil Resistivity

Electrical resistivity or conductivity of soil primarily affects the electron transport mechanism in the corrosion process. Low soil conductivity decreases transport kinetics, which slows down corrosion reactions. Soil resistivity is reported to be a function of the soil moisture content, temperature, and porosity (Demissie et al., 2015). Resistivity is the most commonly applied prediction parameter of soil corrosivity. Many researchers observed a strong correlation between soil resistivity and the corrosion rate (Demissie et al., 2015; Sadiq et al., 2004b).

4.1.2 Soil pH

A pH value indicates ion concentration in the soil environment. It was reported that soil pH has a strong influence on corrosion processes (Arzola et al., 2003). In certain conditions pipelines, which are exposed to a subsurface environment with high pH may produce alkali formations, causing coating delamination followed by the initiation of localized corrosion. In general, soils with low pH (acidic) promote corrosion reactions.

4.1.3 Redox Potential

Redox potential corresponds to a degree of the soil aeration; the higher the redox potential, the higher the oxygen content in the soil. Redox potential also serves as an indicator of the sulfate reducing bacteria (SRB), which has been proven to accelerate the corrosion process (Javaherdashti et al., 2016; Muthukumar et al., 2003). It was observed that SRB can actively proliferate when the values of the redox potential are in the low range (Sooknah et al., 2008).

4.1.4 Chlorides and Sulfates

Chlorides and sulfates are potent agents that may significantly intensify external corrosion. This fact can be attributed to the high conductivity of the chloride and sulfate ions. Furthermore, chlorides may not only reduce the soil resistivity, but also can cause damage to the protective passive films, which may initiate localized corrosion (Castaneda and Rosas, 2015; Papavinasam, 2013).

4.1.5 Moisture Content

As it is known from corrosion science, there is no corrosion reaction possible without a conductive electrolyte. Moisture in the soil acts as the conducting electrolyte, promoting faster transport of ions from the pipe surface. Many studies indicate that moisture content may be a predominant factor, which affects soil corrosivity (Demissie et al., 2015). Soil moisture content also influences soil resistivity; low moisture content correlates with high resistivity and vice versa. The moisture content depends on soil texture, groundwater movements, annual precipitation level, etc.

4.2 BBN External Corrosion Model Development

To quantify the external corrosion hazard, the proposed BBN model determines a pipeline PoF based on the predicted failure pressure (capacity) of the segment weakened by the corrosion defect and operating pressure (loading). Similarly, the leakage failure is based on the corrosion defect depth and wall thickness of the pipeline. Experts knowledge, statistical models and experimental results are used to estimate the above parameters in the BBN model. The proposed BBN model is schematically depicted in Figure 4-1.

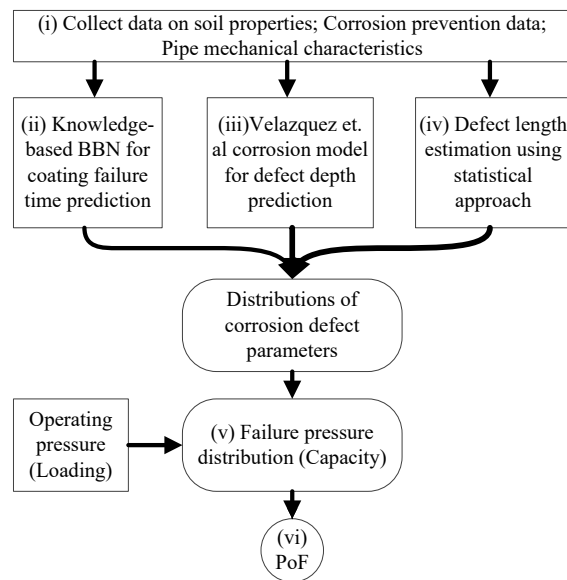


Figure 4-1: Schematic representation of the BBN model for failure prediction due to external corrosion

As is shown in Figure 4-1, the analysis is performed in the following steps:

- i. Gather data on soil properties, pipe mechanical parameters, and corrosion prevention measures.
- ii. Predict coating failure applying the knowledge-based BBN.
- iii. Calculate defect depth using the Velazquez et al. (2009) corrosion model.
- iv. Determine defect length applying the statistical approach proposed by (Zimmerman et al., 1998).
- v. Predict failure pressure based on pipeline mechanical characteristics and defect parameters.
- vi. Calculate PoF using a limit state function (LSF).

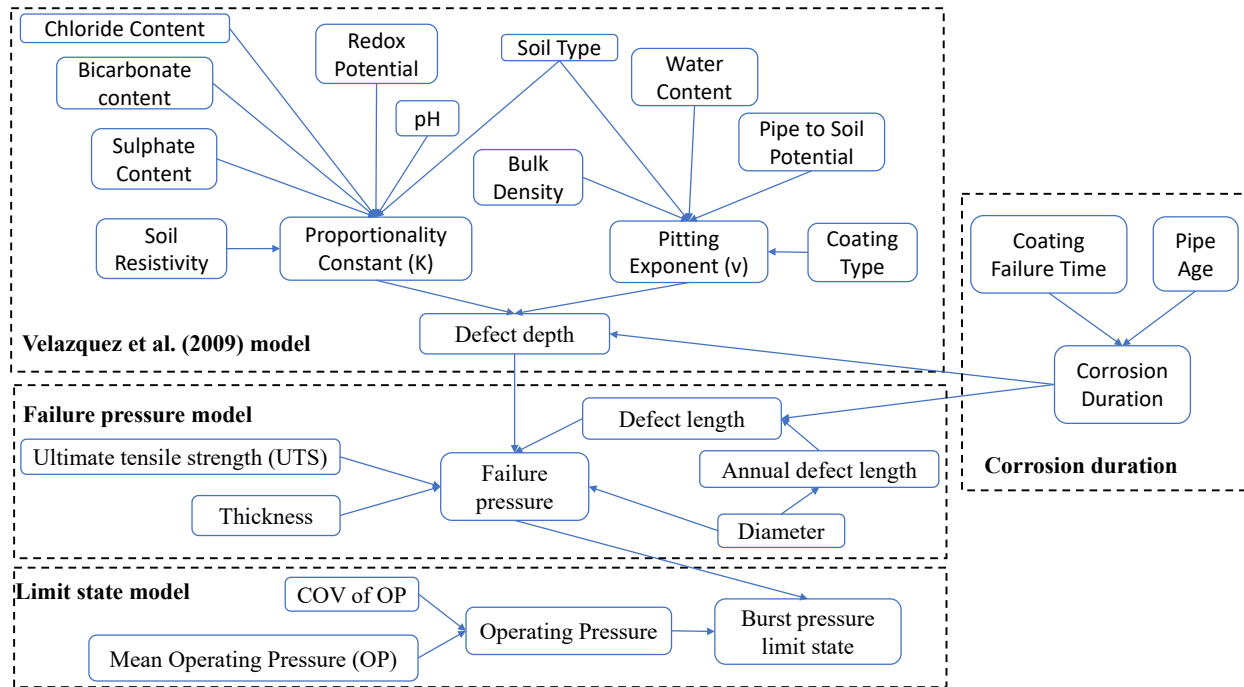


Figure 4-2: BBN model for pipeline failure due to external corrosion

Figure 4-2 depicts details of the proposed BBN model. In the illustrated model, nodes represent stochastic variables, which affects PoF, whereas arrows show causal connections between them. Many of the random variables are assigned to have continuous states (e.g., soil resistivity, chloride content, etc.), whereas some others have been modelled with discrete states (coating type, soil type, etc). CPT are filled using expert opinion and previously established models, which are discussed in the following sections.

4.2.1 Knowledge Based BBN for Coating Failure

External corrosion preventive measures have proved to be effective in protecting the pipe steel surface from a detrimental corrosive environment. However, the majority of pipelines still fail due to corrosion problems (Ayello et al., 2014). The corrosion initiation time is of crucial importance for any integrity assessment. In many studies, for simplicity, corrosion is conservatively assumed to initiate right after the pipeline has been commissioned, whereas in reality, corrosion initiates after some time. In the proposed framework, corrosion initiation is determined using knowledge-based BBN.

In this study, the corrosion model, which is used to predict corrosion defects, already accounts for the potential imposed by cathodic protection; thus, to reflect the action of pipeline protective measures, the analysis boils down to the prediction of the coating failure time. The developed knowledge-based BBN model for coating failure time prediction is depicted in Figure 4-3. Nodes represent significant variables affecting coating integrity. Condition probabilities were assigned

based on expert opinion and the extensive literature review of factors that may compromise coating integrity. After determining coating failure time t_0 (i.e. corrosion initiation time), a distribution of the corrosion defect depth can be predicted using pitting corrosion model proposed by (Velázquez et al., 2009).

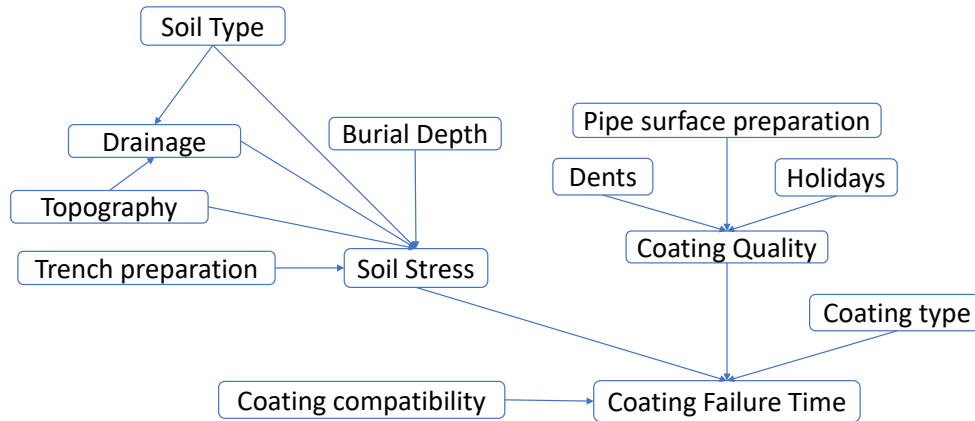


Figure 4-3: Knowledge-based BBN for corrosion initiation time

Table 4-1: Types of coating and its expected service time

Coting type	Service time in idealized conditions as outlined in (Papavinasam, 2013)	Assumed distribution Stdev
FBE	40 years	Normal, 20
Alkyd enamel	10 years	Lognormal, 5
Wrap tape	15 years	Lognormal, 7.5
Coal tar	20 years	Normal, 10
Bare pipe	Corrosion initiates right after pipeline commissioning	N/A

The coating serves as a physical barrier between the corrosive environment and pipe steel surface. Every protective coating has a finite service time. Over time, the coating degrades and eventually fails, allowing moisture, oxygen and other chemicals to be in contact with the steel surface. In general, any change in coating protective properties is deemed a coating failure (Norsworthy, 2009). Coating can fail in numerous ways depending on the coating type, its initial condition and environmental factors. In addition, certain types of coating, when it fails, can shield the CP current, leaving the pipe unprotected. In this study, the following types of coating are considered: fusion bonded epoxy (FBE), alkyd enamel, wrap tape (single and double wrapped), and coal tar. The mean value of coating service time (in idealized conditions) proposed by Papavinasam (2013) were adopted and then adjusted considering the following factors: severity of the exerted soil stress, coating condition and operating temperature. Table 4-1 provides the values of the expected coating service time and assumed distributions.

4.2.1.1 Coating Condition

When the coating has some initial imperfections, its protective properties will progressively diminish over time and its service time without failure will be limited (Papavinasam et al., 2006). In this study, the coating quality indicator reflects the pre-commissioning coating condition, which is determined by such criteria as *pipe surface preparation* (for the coating application) and coating defects. Coating defects, such as *holidays* and *dents* can be caused by improper transportation, storage or positioning of the pipeline. The BBN node *coating quality* has been introduced with three qualitative performance levels, which indicate coating condition: *good*, *fair* and *poor*.

The *pipe surface preparation* significantly affects the coating performance; as pointed out by Papavinasam, pipe surface preparation is a predominant factor, which is often responsible for premature coating failure (Papavinasam, 2013). The steel surface can be prepared for coating application by using one of the following methods: sandblasting, wire brushing and scraping. Since these methods predetermine coating service time, they are used as discrete states in the pipe surface preparation BBN node. In addition, no surface preparation state is introduced to account for the case when the pipe was coated without any preliminary surface preparation.

Sandblasting is factory-made and this is the most efficient method, which substantially enhances coating adhesion. On the contrary, wire brushing and scraping are primarily applied in situ and, therefore, more prone to have coating quality imperfections, which can be a cause of early coating disbonding. Extensive field investigations have shown that coal tar coatings applied over the surface with wire-brush preparation failed after being in service for one year. Conversely, coal tar coatings applied to sandblasted pipes operating in the same environment were in excellent condition after five years of service (Papavinasam, 2013).

Girth weld coating should be checked for compatibility with the mainline coating. Because this type of coating is applied in-situ, due attention should be paid to the quality of its application. Poorly applied or incompatible girth weld coating can be a cause of early initiated corrosion, which is localized in the weld zone proximity (Norsworthy, 2009). If the evidence of incompatibility is observed, poor performance level is assigned to overall coating condition.

Coating defects can occur due to improper manufacturing or can result from damage during pipeline transportation and construction. Numerous coating defects may exist, but in this study the discussion is limited by pipe dents and holidays. Pipe dents create concentrated stress regions and coating in them is more susceptible to the soil stress damage or disbonding. Any discontinuity in the coating surface (e.g. voids, uncoated regions, cracks, etc.) is referred as a holiday; these

localized spots (especially in wrap tape and coal tar coatings) may prevent the CP current to reach pipe surface facilitating initiation of corrosion. Over time, coating degrades, and holidays may grow in size, requiring more CP current to be supplied. To reflect the presence of these coating defects, the BBN nodes: dents and holidays were introduced in the network. The discretization details of these nodes as well as other nodes affecting coating quality are provided in the Table 4-2.

4.2.1.2 Soil Stress

This criterion is used to describe a detrimental physical exposure exerted on the coating by the subsurface environment. A coating damage may result from mechanical stress caused by repeated volumetric fluctuations of the surrounding soil. This exposure is particularly strong in clay soils with the frequently changing moisture content. Field experience shows that such coatings as alkyd enamel and wrap tape are particularly susceptible to soil stress (Papavinasam, 2013). In this work, soil stress is a qualitative factor, which is determined based on sub-factors: soil type, burial depth, water content, and trench preparation. The BBN node soil stress has been introduced to the model, considering three performance levels, namely low, medium, and high.

The same soil types as in the (Velázquez et al., 2009) corrosion model have been used to discretize the soil type BBN node. These soil types include clay, clay loam, sandy and mixed soils. Soil type governs the soil specific gravity, which, in turn, affects the soil overburden pressure. As reported in the literature, the highest stress is exerted by the clay soil, whereas low stress is observed in sandy soils (Andrenacci and Wong, 2012).

Burial depth significantly influences soil vertical pressure, exerted on the pipe. This confirms by the laboratory studies of the coating performance under the soil stress. The studies conclude that the higher the burial depth, the higher the exerted soil stress (Andrenacci and Wong, 2012). Conversely, small diameter pipes with low burial depth are subjected to low stress, which does not exceed the cohesion capacity; thus, coating is less likely to fail (Andrenacci and Wong, 2012).

Table 4-2:Parameters and their discretization for coating failure model

Parameters	Sub criteria	States
Coating Quality	Pipe surface preparation	Sandblasting Wire-brushing Scraping No preparation
	Holidays	Yes No
	Dents	Yes No
Soil stress	Soil type	Clay Clay Loam Sandy Mixed Soil
	Burial depth	Low Medium High
	Topography	Level Inclined Ridged
	Trench preparation	Yes No
	Drainage	Good Fair Poor
Coating failure, years	Soil stress	Low Medium High
	Coating quality	Low Medium High
	Maximum coating life services	FBE Alkyd enamel Coal tar Wrap tape No coating
	Coating compatibility	Compatible No

Water content shows the amount of water is in the soil represented as a percentage of total volume. Moisture content and its variations have a substantial effect on the swelling and shrinkage tendency of the soil. Such repetitive movements may induce localized stress on the pipe and damage pipe coating. The higher the moisture, the higher the soil stresses, especially in the clay and clay-loam soils (Muhlbauer, 2004). To minimize this exposure, a good construction practice commonly includes a preliminary trench preparation. This preparation is carried out by using a fine bedding material or complete replacement of the offending material with higher quality soil. These measures reduce soil stress and eliminate coating damage due to rock impingement (Muhlbauer, 2004). To reflect the aforementioned discussion, child node (soil stress) and its parent nodes (soil type, burial depth, water content and trench preparation) have been created in the BBN; the discretization details are summarized in Table 4-2.

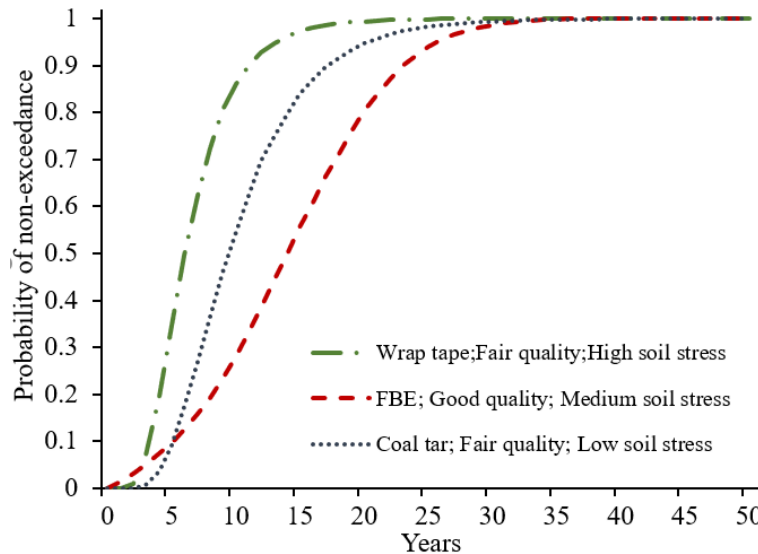


Figure 4-4: Examples of coating failure probability predicted by knowledge-based BBN

The pipe surface preparation was discretized into *sandblasting*, *wire-brushing*, *scraping* and *no preparation*. Coating defects are holidays and dents, each with a state *Yes*, *No*. The soil type (ST) is classified into clay, clay loam, sandy clay loam and mixed soil. Burial depth (bd, m) is discretized into *low* [0-1], *medium* [1-3], *high* [3-5]. Topography is discretized into *level*, *inclined*, *ridged*. Trench preparation has two discrete states: *Yes*, *No*. Drainage is discretized into *good*, *fair*, *poor*. Soil stress and coating quality nodes have discrete states: *low*, *medium*, *high*. The maximum coating life services is discretized into *FBE*, *Alkyd enamel*, *coal tar*, *wrap tape*, *no coating*. Coating compatibility is discretized into *compatible*, *No*.

4.2.2 Corrosion Defect Depth

The estimation of the external corrosion defect depth is one of the most important steps in the analysis. The distribution of the maximum defect depth has been calculated using in the BBN a pitting corrosion model proposed by (Velázquez et al., 2009). The justification of the selected model is outlined in the following paragraph.

In the literature, there are analytical corrosion models which aim to predict corrosion defect depth. Since external corrosion is a complex process to model using electrochemical principals, statistical approaches are commonly used to predict corrosion defect evolution (Sadiq et al., 2004a). The majority of corrosion models predict evolution of the corrosion defect as a function of the exposure time and soil properties. These predictive models primarily have a form of a power law model, linear model or two-phase model. Although many models were developed, only a few of them consider protective coating properties and the presence of cathodic protection. Because the Velázquez et al., (2009) corrosion model is capable of addressing these shortcomings; this model has been adopted in this study.

The Velázquez et al., (2009) is a power law corrosion model for the onshore oil and gas pipelines. The model has been developed using data obtained from 259 field investigations of coated pipelines and soil properties. The authors used multiple regression analysis to derive corrosion exponent (v) and coefficient of proportionality (k) for a variety of soils to predict maximum defect depth (d_{max}) at any time in the future. The corrosion defect depth at any time in the future (t) can be predicted using Velázquez et al., (2009) model as:

$$d_{max} = k(t - t_0)^v \tag{4-1}$$

$$k = k_0 + k_1rp + k_2ph + k_3re + k_4cc + k_5bc + k_6sc \tag{4-2}$$

$$v = n_0 + n_1pp + n_2wc + n_3bd + n_4ct \tag{4-3}$$

$$d_{max} = \left(k_0 + \sum_{i=1}^n k_i X_i \right) (t - t_0)^{n_0 + \sum_{j=1}^m (n_j X_j)} \tag{4-4}$$

where d_{max} = maximum corrosion defect depth (mm); k = coefficient of proportionality; v = pitting exponent; rp = redox potential (mV); ph = soil pH; pp = pipe to soil potential (mV); re = soil resistivity (Om); wc is water content (wc); bd is soil bulk density (g/ml); cc = chloride content (ppm); bc = bicarbonate content (ppm); sc = sulfate content (ppm); ct = coating type; t = exposure time (years); t_0 is corrosion initiation time (years); $k_{0..i}$ and $n_{0..j}$ are multiple regression correlation coefficients. Numerical values of these coefficients are provided in Table 4-3.

Table 4-3: Equation coefficients for the pitting exponent and the coefficient of proportionality for different soil types

Equation coefficients (Velázquez et al.,2009)	Soil Type			
	Mixed Soil	Clay Soil	Sandy-Clay Loam Soil	Clay Loam Soil
k₀	6.08×10 ⁻¹	5.41×10 ⁻¹	5.99×10 ⁻¹	9.85*10 ⁻¹
k₁	-1.80×10 ⁻⁴	-8.99×10 ⁻⁵	-1.82×10 ⁻⁴	-1.06×10 ⁻⁴
k₂	-6.54×10 ⁻²	-5.91×10 ⁻²	-6.42×10 ⁻²	-1.17×10 ⁻¹
k₃	-2.60×10 ⁻⁴	-2.15×10 ⁻⁴	-2.11×10 ⁻⁴	-2.99×10 ⁻⁴
k₄	8.74×10 ⁻⁴	8.38×10 ⁻⁴	8.62×10 ⁻⁴	1.80×10 ⁻³
k₅	-6.39×10 ⁻⁴	-1.29×10 ⁻³	-6.78×10 ⁻⁴	-4.85×10 ⁻⁴
k₆	-1.40×10 ⁻⁴	-5.31×10 ⁻⁵	-1.14×10 ⁻⁴	-2.09×10 ⁻⁴
n₀	8.96×10 ⁻¹	8.85×10 ⁻¹	9.65×10 ⁻¹	2.82×10 ⁻¹
n₁	5.19×10 ⁻¹	4.83×10 ⁻¹	5.12×10 ⁻¹	4.61×10 ⁻¹
n₂	4.65×10 ⁻³	3.72×10 ⁻⁵	4.51×10 ⁻³	1.69×10 ⁻²
n₃	-9.91×10 ⁻²	-1.01×10 ⁻¹	-1.58×10 ⁻²	-9.82×10 ⁻²
n₄	4.31×10 ⁻¹	4.61×10 ⁻¹	4.34×10 ⁻¹	5.67×10 ⁻¹

Table 4-4: Discretization details of the external BBN model nodes

Variables	Sub criteria	States	
Pitting exponent	Coating type (ct)	FBE Alkyd enamel Wrap tape Coal tar Bare pipe	No measured parameter is applied
	Soil type (ST)	Clay Clay loam Sandy clay loam Mixed soil	No measured parameter is applied
	Pipe to soil potential (pp), mV	Low Medium High Very High	$-2 \leq pp < -1.4$ $-1.4 \leq pp < -1$ $-1 \leq pp < -0.8$ $-0.8 \leq pp < -0.4$
	Water content (wc), %	Low Medium High	$0 \leq wc < 20$ $20 \leq wc < 50$ $50 \leq wc < 70$
	Soil bulk density (bd), g/ml	Low Medium High	$1.1 \leq bd < 1.2$ $1.2 \leq bd < 1.4$ $1.4 \leq bd < 2$
Coefficient of proportionality of	Redox potential (rp), mV	Low Medium High	$0 \leq rp < 100$ $100 \leq rp < 200$ $rp > 200$
	Soil pH (SpH), pH	Low Medium High	$5 \leq SpH < 7$ $7 \leq SpH < 8$ $8 \leq SpH < 9$
	Soil resistivity (sr), Ohm	Low Medium High	$0 \leq sr < 400$ $400 \leq sr < 800$ $sr > 800$
	Chloride content (cc), ppm	Low Medium High	$100 \leq cc < 200$ $200 \leq cc < 300$ $cc > 300$
	Bicarbonate content (bc), ppm	Low Medium High	$0 \leq bc < 100$ $100 \leq bc < 400$ $bc > 400$
	Sulfate content (sc), ppm	Low Medium High	$0 \leq sc < 400$ $400 \leq sc < 600$ $sc > 600$
	Soil type (ST)	The same as above	
Defect depth	Pitting exponent (v)	Extremely Low Low ---- High Extremely High	$0 \leq v < 0.01$ $0.01 \leq v < 0.1$ ---- $5 \leq v < 10$ $10 \leq v$
	Coefficient of proportionality (k)	Extremely Low Low ---- High Extremely High	$0 \leq k < 0.01$ $0.01 \leq k < 0.1$ ---- $5 \leq k < 10$ $10 \leq k$

The BBN model for the defect depth is shown in Figure 4-2, where each node represents the basic variables outlined in the Velázquez et al., (2009) model. The states considered for each parameter are summarized in Table 4-4. The coating condition (ct) was discretized into *FBE*, *alkyd enamel*, *wrap tape*, *coal tar* and *bare pipe*. The soil type (ST) is classified into clay, clay loam, sandy clay loam and mixed soil. Pipe to soil potential (pp, mV) is discretized into *low* [-2 - -1.4], *medium* [-

1.4 - -1], *high* [-1 - -0.8] and *very high* [-0.8 - -0.4]. The water content (wc, %) is discretized into *low* [0-20], *medium* [20-50], *high* [50-70]. The soil bulk density (bd, g/ml) is discretized into *low* [1.1-1.2], *medium* [1.2-1.4], *high* [1.4-2]. Redox potential (rp, mV) is discretized into *low* [0-100], *medium* [100-200], *high* [>200]. Soil pH (SpH) is discretized into *low* [5-7], *medium* [7-8], *high* [8-9]. Soil resistivity (sr, Ohm) is discretized into *low* [0-400], *medium* [400-800], *high* [>800]. The chloride content (cc, ppm) is discretized into *low* [100-200], *medium* [200-300], *high* [>300]. Bicarbonate content (bc, ppm) is discretized into *low* [0-100], *medium* [100-400], *high* [>400]. Sulfate content (sc, ppm) is discretized into *low* [0-400], *medium* [400-600], *high* [>600]. Proportionality constant (k) is discretized into *extremely low* [0-0.01], *low* [0.01-0.1], --- [5-10], *high* [>10]. Pitting exponent (v) is discretized into *extremely low* [0-0.01], *low* [0.01-0.1], --- [5-10], *high* [>10].

The Velázquez et al., (2009) model (Equations 4-1 to 4-4) was used to develop the CPT. The database of burst failure tests compiled by Velázquez et al., (2009) was used to validate the corrosion defect depth BBN model. Comparison of the predicted BBN pit depth and observed pit depth is shown in Figure 4-5. The high coefficient of determination ($R^2 = 0.88$) indicated that the BBN can model the corrosion pit depth. The model predicted pit depth was used to obtain the corrosion defect length and eventually to quantify failure pressure capacity.

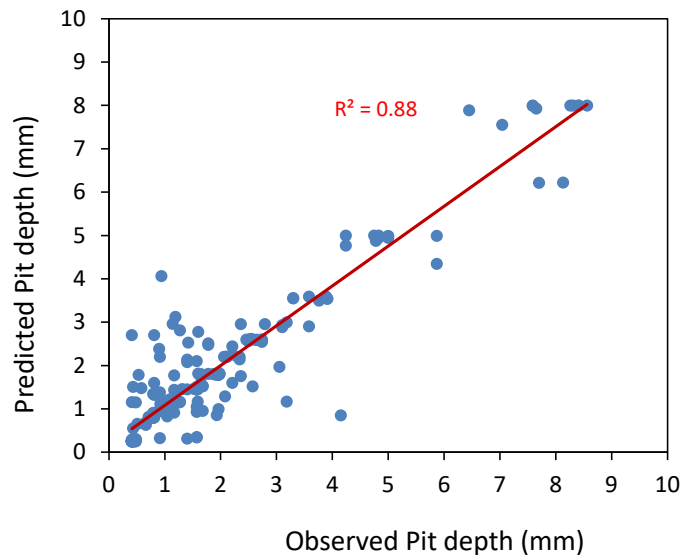


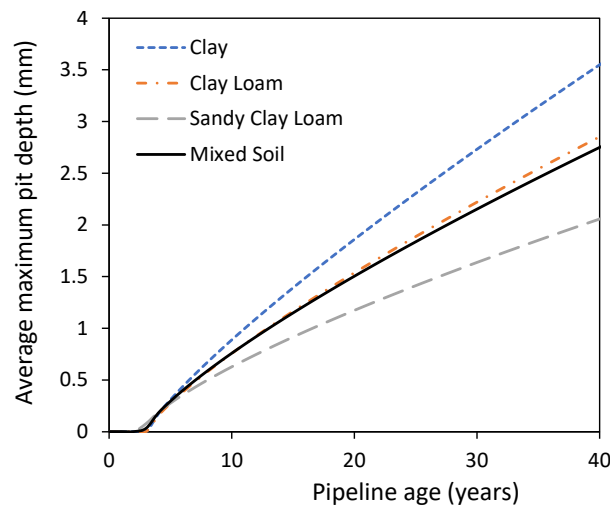
Figure 4-5: BBN model for corrosion defect depth

The time evolution of the average maximum pit depth in a soil category is predicted using Equation 4-1. Velázquez et al., (2009) have obtained the average value of the model parameters (v and k) using a Monte Carlo simulation, where random values drawn from the distributions of the independent variables in Equations 4-2 and 4-3 were used as an input. The unbiased estimates of v and k for each soil category are given in Table 4-5.

Table 4-5: Average value of the model parameters for pit growth. Adapted from Velázquez et al., (2009)

Parameters	Soil Category			
	Clay	Clay Loam	Sandy Clay Loam	All
K (mm/y)	0.178	0.163	0.144	0.164
ν	0.829	0.793	0.734	0.780

Figure 4-6 shows the time evolution of the average maximum pit depth by soil category. The average maximum pit depth for each soil type in increasing order of corrosiveness is sandy clay loam, clay loam and clay. The mixed soil type has similar trend with clay loam, but it overestimates and underestimates the pitting depth in sandy clay loam and clay soil types, respectively. The impact of soil environment on the pitting can be clearly seen after around 15 years of operation.

**Figure 4-6:** Average maximum pit depth growth by soil categories

4.2.3 Corrosion Defect Length

To quantify external corrosion hazard, corrosion defect length must be specified. Despite the availability of comprehensive models to predict the external corrosion defect depth, in the case of external defect length, there are no analytical means to predict this parameter. Furthermore, many studies show that corrosion depth and length are independent parameters (Papavinasam, 2013). However, Amirat et al. (2009) indicated that to a given corrosion flaw depth there is a range of the associated flaw lengths. For instance, if defect depth reaches 20% of the wall thickness, then the observed defect length varies between 8 and 608mm (Amirat et al., 2009). The other way to determine defect length is to use the approach proposed by Zimmerman et al. (1998). This approach assumes that the defect length parameter follows Weibull distribution function with a coefficient of variation $COV = 50\%$ (Zimmerman, Cosham, & Sanderson, 1998). The probability of defect length (l) greater or equal than its characteristic value (l_c) can be calculated using the following expression:

$$P(l \geq l_c) = 1 - F(l) = e^{-\left(\frac{l}{\theta}\right)^{\beta'}} = \int_{l_c}^{\infty} f(l) dl \quad 4-5$$

where $F(l)$ = cumulative distribution of the defect length (l); (β') = shape parameter of the Weibull distribution; (θ) = scale parameter of this distribution.

The annual defect length node has been introduced in the BBN network, following the Zimmerman et al., (1998) approach to model defect length. Characteristics of the Weibull distribution for this parameter have been determined for each pipe diameter using assumptions outlined in (Khan et al., 2006). Khan et al. (2006), assumed that characteristic defect length equals $l_c = 4\%$ of the outside diameter, considering that $F(l) = 0.9$ (Khan et al., 2006). Since covariance is $COV = 50\%$, then the shape parameter (β') = 2.1. Then the Equation 4-5 is used to determine the scale parameter (θ). Thus, for pipeline, for example, with diameter of 88.9 mm, the mean value of the annual defect length equals to 2.12 mm with standard deviation of 1.06 mm. Consequently, defect length at the given time in the future is computed using the following expression (Caleyo et al., 2002; Opeyemi et al., 2015):

$$DL(t) = IDL + ADL \times t \quad 4-6$$

where $DL(t)$ = corrosion defect length at a given time t ; ADL is the annual defect length. IDL is the initial defect length, which can be known from the latest in-line inspection (ILI). When ILI data is available, t represents an elapsed time since the latest inspection. Conversely, if no ILI was performed, time t equals to the corrosion duration (years).

4.2.4 Results and Discussions

To demonstrate the applicability and usefulness of the proposed BBN model, a pipeline case study is obtained from the study of Caleyo et al. (2002). The pipeline pertaining information is given in Table 4-6, where all the random variables have a normal distribution.

Table 4-6: Random variables and their parameters used in the example

Symbol	Description	Type	Mean	Cov
d_0	Defect depth	Normal	8.24 mm	0.1
D	Pipe diameter	Normal	914.4 mm	0.02
L_0	Defect length	Normal	200 mm	0.1
P_{op}	Operating Pressure	Normal	7.8 MPa	0.1
t	Pipe wall thickness	Normal	20.6 mm	0.02

A vector of the basic random variables in Table 4-7 is generated by sampling each variable from their own distribution. The generated values are used to compute the failure pressure (Equation 3-3) and this is compared with the operating pressure to check if the limit state condition is violated ($LSF \leq 0$). This step is repeated several times for duration up to 40 years, where each time the vector of the basic variables is randomly generated from the distribution, and the probability of failure for a single defect and period is calculated as follows:

$$PF_{defect} = n(LSF \leq 0)/N \tag{4-7}$$

where $n(LSF \leq 0)$ is the number of trials for which the operating pressure surpass the failure pressure; N is the total number of trials conducted for each year. The evolution of pipeline failure probability with time is given in Figure 4-7a. The burst failure probability of the pipeline was very low during the first ten years of operation, and this increased rapidly after ten years. The 10th and 90th percentile of failure is [11, 17]. This means that if a pipeline is not maintained or replaced from an active defect, it can reach 50% of the failure probability during the first 15 years. The evolution of the failure pressure capacity of the pipe with time is shown in Figure 4-7b, where the pipe capacity decreased with time. A pipeline failure probability started to increase when the operating pressure surpassed the failure pressure capacity.

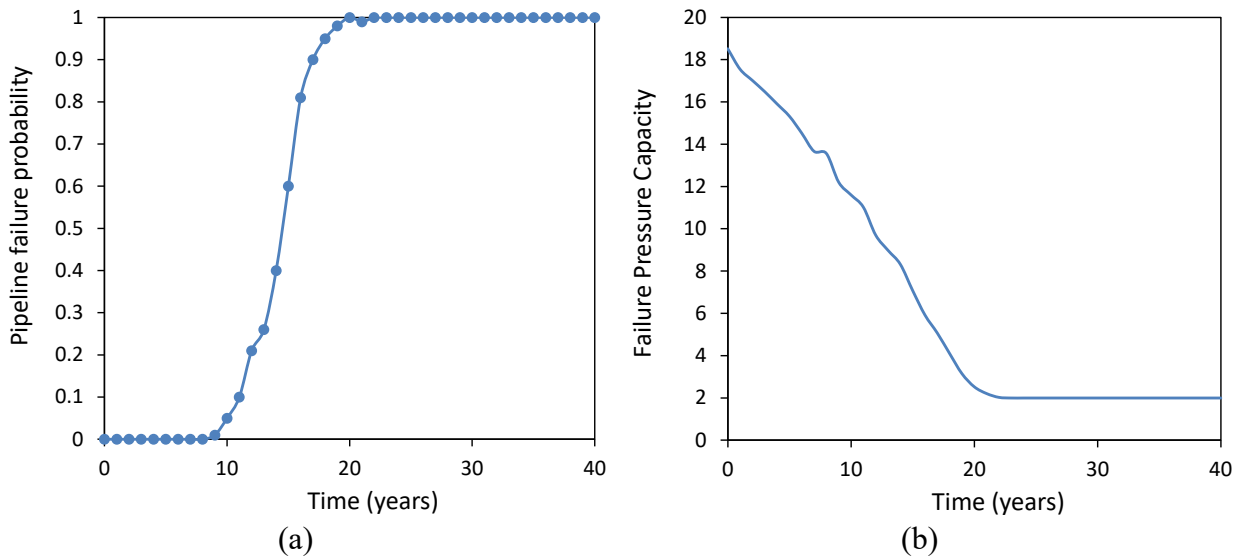


Figure 4-7: Evolution of pipeline failure probability and failure pressure capacity due to pitting corrosion

Furthermore, the application of the developed approach has been applied in three hypothetical scenarios as well. Parameters of the BBN model as well as statistical characteristics of the subjectively defined distributions are provided in Table 4-7. These random variables are applied in Monte Carlo simulation for 4000 iterations. The number of iterations is deemed sufficient due to the stabilization of covariance in the output distribution.

Table 4-7: Probabilistic data of input parameters

Parameter		Pipeline 1			Pipeline 2			Pipeline 3		
		PDF	Mean	Stdev	PDF	Mean	Stdev	PDF	Mean	Stdev
1	Redox potential (mV)	Unknown			LN	300	95	LN	55	50
2	Soil pH level	N	5.13	0.92	N	5.2	1.5	N	8.31	0.5
3	Soil resistivity (Om)	U	[50...150]		N	300	90	LN	800	70
4	Chloride content (ppm)	LN	55	71	LN	800	120	U	[0...30]	
5	Bicarbonate content (ppm)	LN	20	29	Unknown			U	[0...400]	
6	Sulfate content (ppm)	LN	150	100	Unknown			Unknown		
7	Soil density (g/ml)	N	1.35	0.2	U	[1.3...1.5]		N	1.25	0.1
8	Water content (%)	LN	27	6.5	LN	35	9.3	Unknown		
9	Pipe to soil potential (mV)	LN	-0.89	-0.21	LN	-0.6	-0.3	LN	-1.5	-0.3
10	Soil type	Sandy			Clay loam			Mixed		
11	Trench preparation	No			Yes			No		
12	Burial depth (m)	N	2	0.1	N	1.5	0.4	N	1	0.2
13	Coating type	Wrap tape			FBE			Wrap tape		
14	Pipe surface preparation	Brushing			Blasting			Brushing		
15	Holidays	No			Unknown			No		
16	Dents	No			Yes			Yes		
17	Operating temperature	Excessive			Unknown			Not excessive		
18	Pipe age (years)	fixed	2		fixed	9		fixed	15	
19	Wall Thickness (mm)	fixed	3.2		fixed	4.8		fixed	3.2	
20	Outside Diameter (mm)	fixed	88.9		fixed	168.3		fixed	88.9	
21	Toughness (Low/High)	High			High			Unknown		
22	SMYS (MPa)	LN	395	27.65	LN	395	27.65	LN	395	27.65
23	OP (MPa)	LN	5.96	0.596	LN	3.97	0.397	LN	2.07	0.207

where N – normal distribution; LN – Lognormal distribution; U- uniform distribution
 In the first scenario, the recently commissioned pipe is shown. It is assumed that the pipeline has the wrap tape coating, which is in a good condition. The pipe is buried in soil with moderately corrosive properties (low soil resistivity and low pH). Scenario two depicts a pipeline that is buried in a highly corrosive soil (high chloride content). The coating of this pipeline is FBE with some defects due to transportation. Scenario three represents the high age pipeline with wrap tape coating, which has minor defects. The simulation output reflecting corrosion situation is presented in Figure 4-8.

Table 4-9 shows the 50th and 90th percentile values, which represent central tendency estimate (CTE) and reasonable maximum estimate (RME). In scenario 1, the proposed model predicts high probability of failure irrespective the pipe is recently commissioned, and the wrap tape coating is in a good condition. This is due to high operating pressure, which has a significant impact on the failure probability. In scenario two, the BBN model predicts that CTE and RME of the defect depth are 26.182 and 31.038 respectively. The associated probability of failure due to this defect has

been predicted to be 0.007 (CTE) and 0.012 (RME). The probability of failure predicted for scenario 3, accounting for 0.065 (CTE) and 0.097 (RME).

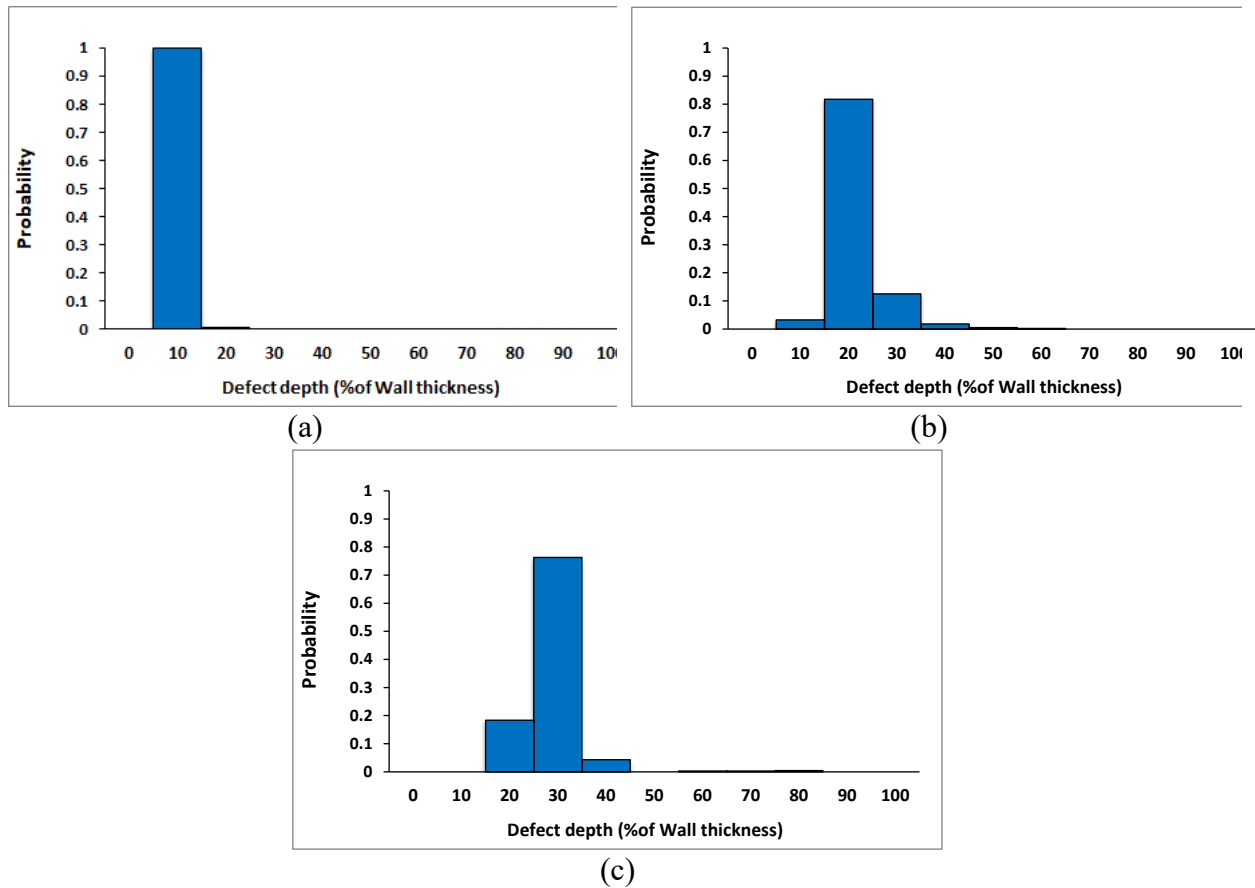


Figure 4-8: Predicted relative defect depth distribution for: (a) scenario 1, (b) scenario 2 and (c) scenario 3

Table 4-8: CTE and RME for defect depth and PoF of three scenarios

Parameter	Pipeline 1	Pipeline 2	Pipeline 3
Defect depth (CTE)	10.776	26.182	30.568
Defect depth (RME)	14.283	31.038	38.082
PoF (CTE)	0.041	0.007	0.065
PoF (RME)	0.317	0.012	0.097

As is shown in the sensitivity analysis section, operating pressure is the most influential parameter in the model affecting probability of failure. This is confirmed in scenario one and two, when despite the wall thickness loss is higher in pipeline 2, the PoF was lower than pipeline 1. In third scenario, the pipeline has the highest corrosion defect depth. This can be explained by the high age of the pipeline and the initially low wall thickness.

A leakage LSF has been defined as the difference between the maximum allowable defect depth (0.8 t) and corrosion defect depth. This LSF indicates that a defect of size 80% of the pipe wall thickness can lead to a state of failure. Mathematically, the leakage LSF is expressed as:

$$LSF = 0.8t - DD$$

4-8

Similar to burst failure pressure, a vector of the basic random variables in Table 4-6 is generated by sampling each variable from their own distribution. The generated values are used to check if the limit state condition defined in Equation 4-8 is violated ($LSF \leq 0$). This step is repeated several times for duration up to 40 years, where each time the vector of the basic variables is randomly generated from the distribution, and the probability of failure for a single defect and period is calculated as shown in Equation 4-7.

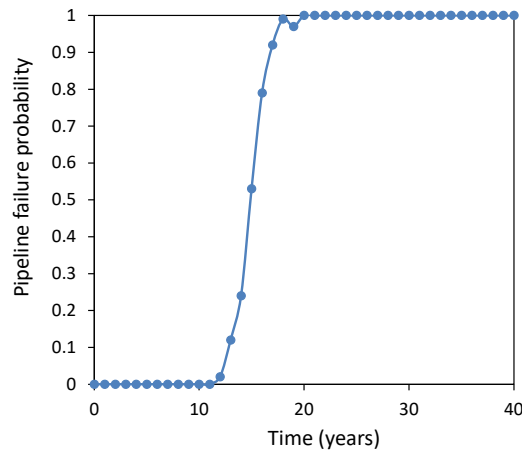


Figure 4-9: Evolution of pipeline failure probability due to leakage

The evolution of pipeline failure probability with time is given in Figure 4-9. The leakage probability of the pipeline was very low during the first 12 years of operation and increased rapidly after this period. The 10th and 90th percentile of failure is [13, 17]. This means that if a pipeline is not maintained or replaced from an active defect, it can reach 50% of the failure probability during the first 15 years.

The developed models applied to public dataset of pipeline segments obtained from BC Oil and Gas Commission Open Data Portal. The dataset doesn't have any pipe and environment related information and hence, random values are used for visualization purpose. The figures showing probability of failure due to burst and leakage are showing in Figure 4-10 and Figure 4-11, respectively.

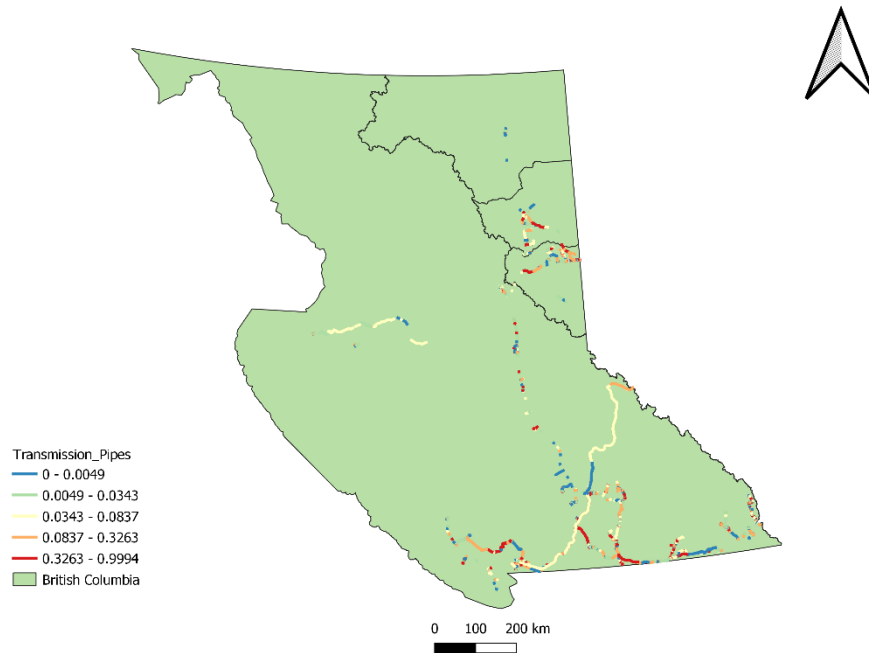


Figure 4-10: Pipeline failure probability due to burst

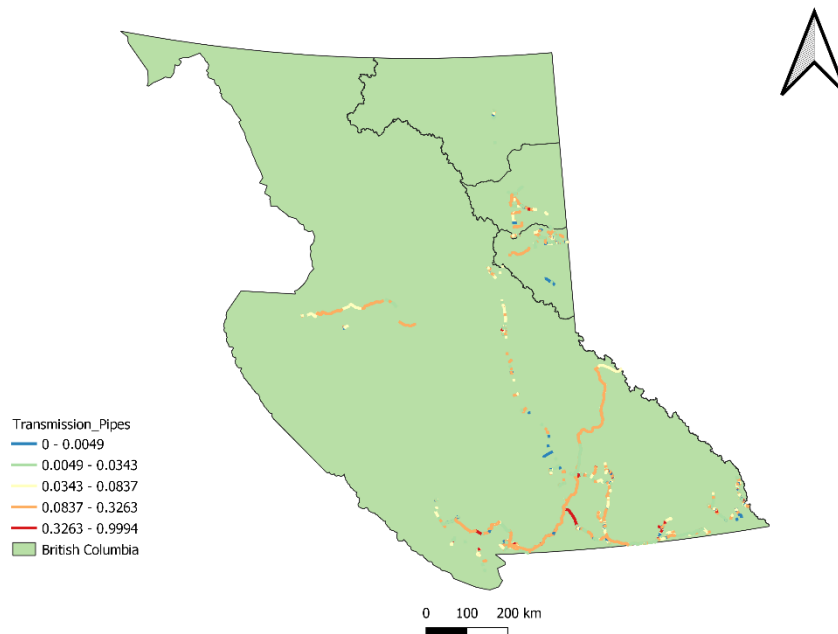


Figure 4-11: Pipeline failure probability due to leakage

4.3 Sensitivity analysis

Sensitivity analysis was carried out for coating failure time, defect depth and burst pressure limit state nodes by varying the input parameters (Figure 4-12). The sensitive parameters for the coating failure time node (Figure 4-12a) are: joint coating compatibility (36.1%), maximum coating life service (30.1%), coating quality (4.79%), soil stress (3.59%), and pipe surface preparation (2.41%). The coating failure time decreases when there is no compatible joint coating. The

maximum coating life service also varies depending on the coating type. In addition, the coating quality has an impact, and this depends on the presence of holidays, dents and pipe to surface preparation. The sensitive parameters for the defect depth node (Figure 4-12b) are: exposure time (17.9%), proportionality parameter (12.7%), and pitting exponent (8.55%). The proportionality parameter is a function of redox potential, pH, resistivity and dissolved ion concentrations. The pitting exponent is a function of pipe-to-soil potential, water content, bulk density and coating type. The sensitive parameters for the burst pressure limit state node (Figure 4-12c) are: failure pressure (34%), operating pressure (15.2%), thickness (8.81%), diameter (6.86%), UTS (5.09%), defect depth (2.35%) and defect length (0.4%). It is expected that failure pressure is strongly associated with the burst pressure limit state because failure pressure, remaining capacity of a pipeline, decrease with elapsed time and hence increase the failure probability.

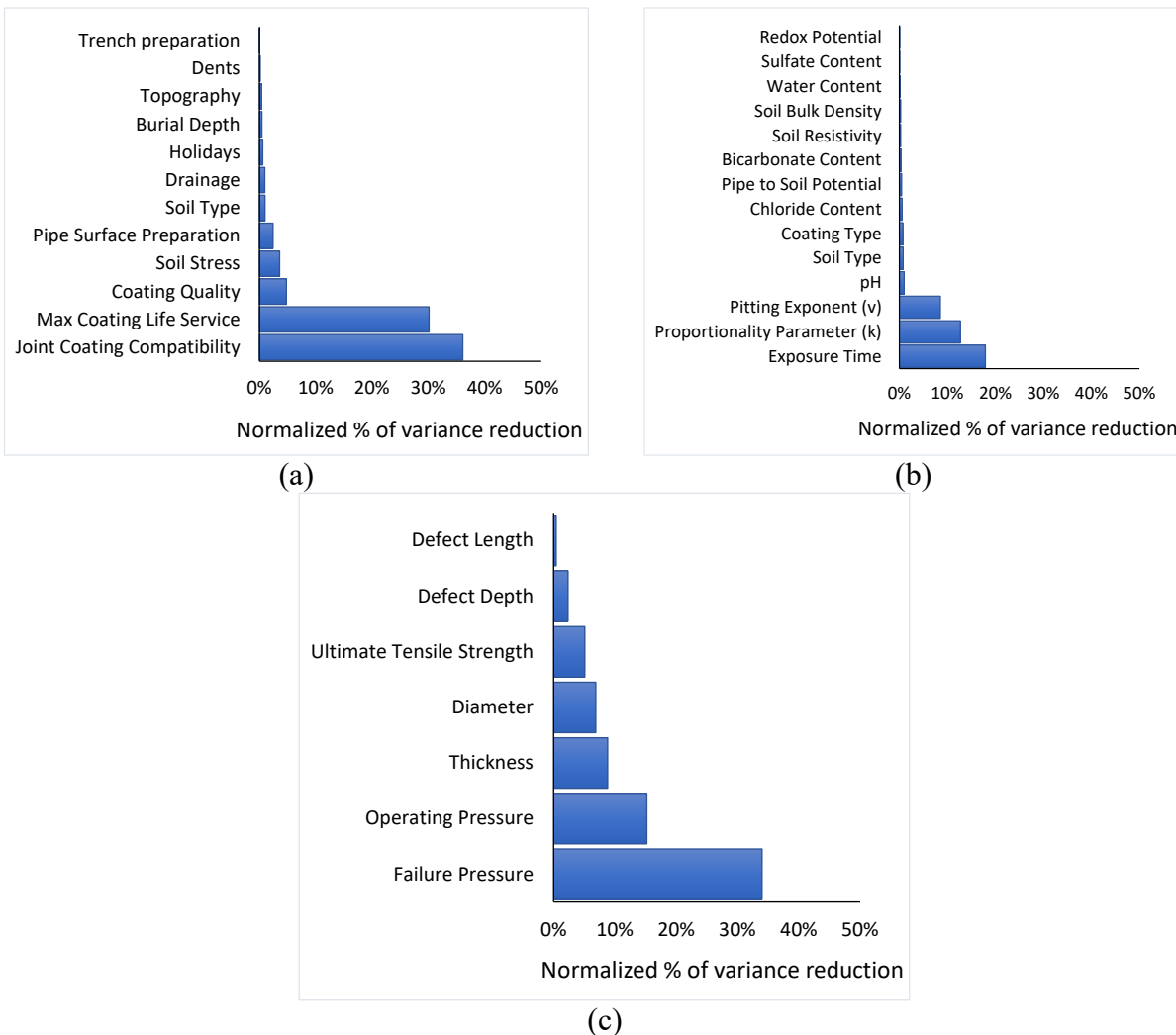


Figure 4-12: Sensitivity analysis of: (a) coating failure time; (b) defect depth and (c) burst pressure limit state nodes based on variation in the input nodes

4.4 Conclusions

In the external pitting corrosion study, a BBN model was developed using Velazquez et al. (2009) corrosion data and analytical burst failure models. The model consists of various parameters, including soil type, coating type and operating pressure. The overall analysis indicated that pipeline failure probability increases with an increase in soil corrosivity. Soil corrosivity is ranked in increased order as sandy clay loam, clay loam, and clay. In addition, availability of intact coating condition reduces the risk of failure probability and FBE has the lowest risk of failure due to pitting corrosion. Like uniform corrosion, the increase in operating pressure is observed to simultaneously increase the failure probability due to pitting corrosion. This study can be extended in the future by integrating the developed BBN model with consequence assessment to develop a comprehensive risk assessment tool.

Chapter 5

Stress Corrosion Cracking

5.1 Introduction

Cracking is a common type of material failure, which can be caused by several factors. The various mechanisms of cracking are known as environmentally assisted cracking (EAC), which includes stress corrosion cracking (SCC), corrosion fatigue (CF) and hydrogen-induced cracking (HIC) (Cheng, 2013). The previous chapter's discuss on probability of pipeline failure due to general and pitting corrosion, and this chapter will discuss on the probability of pipeline failure due to SCC. SCC is defined as cracking that's caused by a process combining both corrosion and straining of metal due to residual or applied stress (Cheng, 2013). A SCC from the external surface of a buried pipeline has a serious impact and can lead the pipe to leakage or rupture. There are two forms of SCC on underground pipelines: high-pH SCC (intergranular) and near-neutral-pH SCC (transgranular).

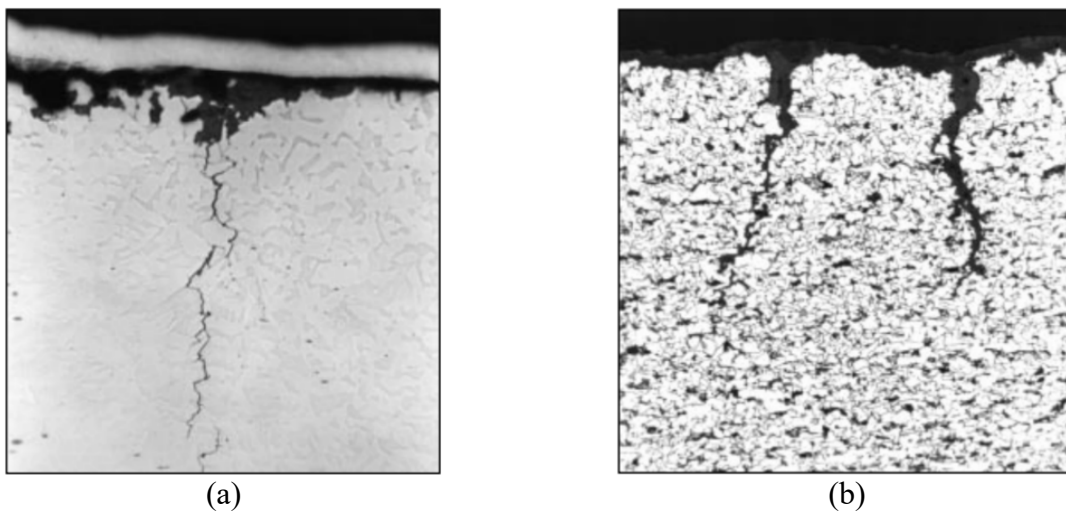


Figure 5-1: Metallographic section through: (a) high pH SCC (b) near-neutral pH SCC. Taken from (NEB, 1996)

The near-neutral-pH and high-pH SCC refers to the degree at which the environment in contact with the pipe surface is either alkaline or neutral (NEB, 1996). The high-pH SCC is intergranular, where the cracks propagate between the grains in the metal (Figure 5-1a). The near-neutral-pH SCC is transgranular, where the cracks propagate through the grains in the metal (Figure 5-1b). There are many similarities between high-pH SCC and near-neutral-pH SCC, in which both occur as colonies of multiple parallel cracks that are perpendicular to the direction of highest stress on the external pipe surface. The cracks vary in depth and length, and they increase in dimension and tend to coalesce to form longer cracks. At some point the cracks may reach a critical depth and

length that can result in rupture. In order for rupture to occur, the crack depth doesn't have to fully penetrate through the wall, i.e., a shallow crack may reach a length that becomes critical (Zheng et al., 2011). Contrary, the difference between the two forms of cracks is the temperature sensitivity of the high-pH SCC, fracture morphology and pH of the pipe environment. Table 5-1 summarizes the characteristics of both high-pH and near-neutral-pH SCC.

Table 5-1: Comparison of Near-neutral-pH and High-pH SCC (NEB 1996)

Factor	Near-neutral pH SCC	High pH SCC
Location	<ul style="list-style-type: none"> Associated with specific terrain conditions, often alternate wet-dry soils, and soils that tend to disbond or damage coatings 	<ul style="list-style-type: none"> Downstream of pump or compressor station (within 20 km) Number of failures falls markedly with increased distance from compressor/pump and lower pipe temperature
Temperature	<ul style="list-style-type: none"> No obvious correlation with temperature of pipe May occur more frequently in the colder climates where CO₂ concentration in groundwater is higher 	<ul style="list-style-type: none"> Temperature increase leads to an exponential increase of the growth rate
Associated Electrolyte	<ul style="list-style-type: none"> Dilute bicarbonate solution (pH between 5.5 and 7.5) 	<ul style="list-style-type: none"> Concentrated carbonate-bicarbonate solution (pH greater than 9.3)
Electrochemical Potential	<ul style="list-style-type: none"> -760 to -790 mV (Cu/CuSO₄) Cathodic protection does not reach pipe surface at SCC sites 	<ul style="list-style-type: none"> -600 to -750 mV (Cu/CuSO₄) Cathodic protection contributes to achieving these potentials
Crack Path and Morphology	<ul style="list-style-type: none"> Primarily transgranular Wide cracks with evidence of substantial corrosion of crack side wall 	<ul style="list-style-type: none"> Primarily intergranular Narrow tight cracks with almost no evidence of secondary corrosion of crack wall.

The SCC crack growth consists of four stages of process as shown in Figure 5-2 (NEB 1996). In stage 1, the conditions necessarily for SCC initiation develop at the pipe surface. This includes coating disbondment and development of cracking electrolyte at the pipe surface. After the coating disbondment, electrolytes reach the pipe surface and cracks begin to initiate in stage 2 as a result of surface residual stresses, metallic imperfections, stress concentrations or a combination of these. As shown in Figure 5-2, the relatively high crack growth rate of the initiation of SCC has been observed to decrease rapidly after initiation is complete. The subsequent stage (stage 3) is characterized by continuous initiation, growth, and crack coalescence. The coalescence of large

cracks leads to failure in stage 4. Beyond stage 4, the cracks close to one another combine and forms colony of cracks that put at risk the integrity of pipeline (Beavers et al., 2006).

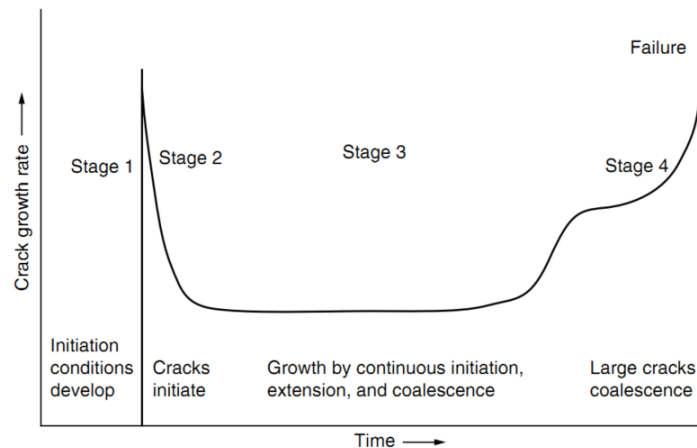


Figure 5-2: Life model of stress-corrosion crack that would grow to failure. Taken from (NEB, 1996)

5.1.1 Conditions for SCC

Three conditions must be met in order SCC to occur on an engineering structure: potent environment must develop at the pipe surface, a susceptible material and tensile stresses must be above a certain threshold limit (Figure 5-3) (Beavers and Harle, 2001).

In potent environment, the high-pH and near-neutral-pH SCC are associated with two distinct environments that develop at the surface of pipelines. The cracking environment responsible for high-pH SCC has been created by generation of concentrated carbonate-bicarbonate ($CO_3^{2-} - HCO_3^-$) electrolyte. This is created by applied cathodic protection (CP) that causes the pH of an electrolyte trapped under disbonded coating to increase, and carbon dioxide readily dissolves in the elevated pH electrolyte (Yunovich et al., 1998). Carbon dioxide is present in most soils from the decay of organic matter. This type of environment leads to the generation of a concentrated carbonate-bicarbonate solution with a pH between 8 and 10 (Cheng, 2013). In a near-neutral-pH, the cracking environment appears to be dilute groundwater containing dissolved carbon dioxide and pH value ranges between 6 and 8. The CP current doesn't reach, or little if any, the pipe surface because of the presence of a shielding coating, ineffective CP or highly resistive soil (Cheng, 2013). Overall, the condition for either of these potent environments to happen depends on four factors: coating type, soil, CP and temperature.

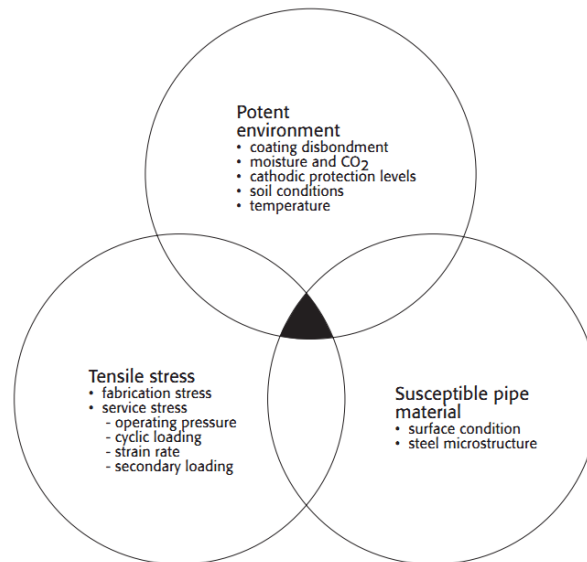


Figure 5-3: Conditions necessary for SCC on pipelines (NEB 1996)

The susceptibility of material is a necessary condition in the development of SCC. Susceptibility of material includes several factors, including pipe manufacturing process, type of steel, grade of steel, cleanliness of steel, steel composition, plastic deformation characteristics of the steel, steel temperature and pipe surface condition (NEB 1996). The stress component indicates for the load per unit area within the pipe wall. There are several stresses in pipelines, including operating pressure, pressure fluctuations and residual stress (Beavers and Garrity, 2001).

5.2 Factors affecting SCC

The environmental and stress-related factors that affect SCC are discussed in the below section.

5.2.1 Cracking environment

The electrolytes trapped in between the pipeline steel and disbonded coating determines the type of environment that results in pipeline SCC. This corrosive environment may not be the same as the soil environment and is created as a combination of coating failure, soil conditions and CP penetration level. Soil environment may also result in pipeline SCC when a pipe coating is damaged and the pipe is exposed directly to the soil (Cheng, 2013).

The early field investigations for high-pH SCC indicated that small quantities of liquids were found beneath disbonded coatings, including carbonate and bicarbonate ions along with traces of nitrates. For high-pH SCC to occur, the coating should allow for the CP and oxygen to pass through. The high-pH SCC has occurred most frequently on coal-tar-coated pipelines and coatings such as polyethylene tape are unlikely to allow the formation of high-pH solutions because they shield the CP current when disbonded. The cathodic protection system is one of the major contributing factor in the high-pH cracking process. A combination of CP current collected on the pipe surface at disbondment and dissolved CO₂ in the ground water leads to generation of high-

pH SCC environment (Beavers et al., 2006). The CP influence the pipe-to-soil potential to be in the potential range for cracking. This form of SCC occurs over a narrow potential range [-600 to -750 mV (Cu/CuSO₄)] (Fang et al., 2003). In addition, seasonal fluctuation may play a role in the generation of cracking environment. The potent environment might be generated when CP levels are high and cracking occurs when adequate protection is lost, such as in summer months when the soil dries out (Beavers and Harle, 2001). The condition of the soil has also a major role in permeation of CP. Soil resistivity and moisture content of the soil are primary soil-related factors that influence the effectiveness of CP. Some research results indicated that sufficient carbon species and soluble cations (sodium or potassium) must be present for high-pH SCC to occur (Beavers et al., 2002).

The investigations for near-neutral pH SCC indicated that the electrolytes found beneath disbonded coatings have lower pH with very dilute solutions of bicarbonate ions and carbonic acid. Additionally, there was no significant trend with respect to the soluble cation concentrations of the soils at the SCC sites. Thus, for near-neutral pH SCC to occur, with lower pH values and soluble cation concentration within the disbonded regions, the pipe surface must not have received adequate cathodic protection (Beavers and Bubenik, 2017).

5.2.2 Electrochemical potential and temperature

The high pH SCC is occurred over a limited potential range that has about 100 mV wide. This range lies between the native potential of most pipelines with no cathodic protection, which is typically more positive than -650 mV (Cu/CuSO₄), and adequate cathodic protection, which is typically more negative than -850 mV (Cu/CuSO₄) (Beavers and Harle, 2001). The potential range for SCC also varies depending on the temperature and solution concentration, where decreasing in temperature leads to a decrease in the potential range for high pH SCC and crack velocity (Parkins and Zhou, 1997). Temperature affects the SCC growth kinetics, coating deterioration, potential range for active cracking, concentration of the environment in contact with the pipe, and moisture content of the soil near the pipeline.

For the high-pH environment to develop, a significant current has to flow to the pipe surface to generate an elevated pH environment that can absorb the carbon dioxide. The cathodic protection potentials has to be more negative than -850 mV off potential (Cu/CuSO₄) to have a high pH environment (above pH of 9) and adequate cathodic protection. Although the potential range for SCC lies between the native potential of most pipelines and adequate protection, SCC still occurs in pipes during periods of the year where adequate CP is not achieved. This indicate that seasonal fluctuations are significant in cracking process (Beavers and Harle, 2001). Hence, the current

depends on the overlap between the potential range for SCC and effective potential during a dry weather.

The current for a near-neutral pH SCC shows a monotonic increase with potential and it's assumed to be a function of effective potential and solution concentration (Jain et al., 2013). Contrary to the high-pH SCC, the near-neutral pH SCC behaviour is relatively independent of temperature. The elevated temperature can lead to degradation of pipeline coating and indirectly creating an environment where near-neutral pH SCC occurs. However, this cracking doesn't follow the same temperature trends as a high-pH SCC. The near-neutral pH SCC occurs where the cathodic protection fails to penetrate the coating and reach the steel surface. The potential ranges between -670 and -790 mV (Cu/CuSO₄), which is more negative (slightly cathodic) than the native potential of steel with no cathodic protection (Beavers and Bubenik, 2017).

5.2.3 Coating and surface condition

Surface coating and cathodic protection are used to protect new pipelines from corrosion. However, after a period of pipeline operation, the pipeline coating may be deteriorated and can lead to formation of holidays and diffusion of water, carbon dioxide and other species through the coating (Fang et al., 2003). The coating related requirements for an effective prevention of SCC initiation in pipelines include the following conditions: 1) resistance to disbonding by preventing the environment or electrolyte that causes SCC from contacting the pipeline steel surface 2) the coating should be able to allow current to pass through the coating, or under disbonded tents, in order to protect the disbonded regions from SCC 3) The surface preparation prior to coating application should alter the pipe surface condition to render it less susceptible to SCC initiation (CEPA 2015). Coating types (e.g., Fusion bonded epoxy, urethanes and liquid epoxy coatings) that meet all three criteria are effective in preventing SCC. There are several factors that contribute to the deterioration and disbondment of coating, including age of the coating, external stress, temperature and CP potential.

External forces include soil stress, proximity to seam welds or girth welds and surface preparation. Soil stress is one of the major causes of coating failure problems (Papavinasam et al., 2006). The type of soil affects performance of the coating, e.g., clay type soil can hold moisture and create soil stresses that cause disbondment of polyethylene tape coatings. Rocky type of soil can also create holiday in coatings, allowing groundwater to seep and come in contact with the pipe surface. An earthquake-prone areas or slopes may incur pipeline a significant longitudinal stress due to ground movement. The amount of moisture in the soil also has an effect on the formation of a near-neutral pH SCC environment. Surface preparations improve the adhesive qualities of the coating

by cleaning the surface from contaminants (e.g., dirt, greasy, moist, or rusting) to make it rough, which is necessary for optimum coating performance. In addition, the high temperature near a compressor can cause a coating disbondment.

A disbonded coating impacts a pipe surface by exposing to a ground water dissolution. The composition of the ground water solution changes depending on the amount of cathodic current reaching the pipe surface. The composition will remain unaltered for the following reasons: 1) if the cathodic protection current cannot pass through the coating 2) if there is high electrical resistance within the soil 3) if there is no significant cathodic protection current reaching the exposed pipe surface (Fang et al., 2003). Hence, if the cathodic protection current fails to reach the surface of the pipe due to either of the reasons, then the natural ground water solution can cause a transgranular cracking SCC. Majority of the near-neutral pH SCC used to be seen in tape coating and asphalt coating, consecutively (Beavers and Bubenik, 2017). On the other side, a substantial cathodic protection current at the surface can also lead to increase of pH due to the generation and accumulation of hydroxyl ions. This leads to increase concentration of carbonate, which can further lead to a formation of intergranular cracking. The common industry guidelines consider coatings other than fusion bond epoxy to be susceptible to near-neutral pH SCC.

5.2.4 Stress

A buried pipeline is subjected to several types of stresses, in which all of them have some contribution to SCC. The stresses can be either tensile (e.g., axial and circumferential stress) or compressive. The cracks formed have a perpendicular orientation to the direction of stresses. Therefore, axial cracks are found in areas of high circumferential stress, and circumferential cracks are found in areas of high axial stress. The SCC in pipeline is initiated and propagated only if there is sufficient stress known as a threshold stress. Below this value, the crack may not be initiated. In the presence of mill scale or pits, the threshold stress for an actual pipe surface is markedly reduced.

The circumferential stress in the pipe has several sources, including hoop stress (due to internal operating pressure and has the highest stress component in the pipe), residual stress (due to pipe manufacturing such as welds, bends, dents), local stress (caused by any irregularities in the surface of the pipe), secondary stresses (stresses caused by soil settlement and landslides), temperature stress (caused by temperature difference through the thickness of the pipe wall) and others (NEB 1996). The axial stress also depends on the operating pressure, geo-technical issues (e.g., land movement) and temperature changes along the pipe axis (Cheng, 2013). Furthermore, there is a relation between the number of cracks and maximum stress, where there will be more cracks with

close spacing between them in a high stress (Fang et al., 2003). In addition, the comprehensive stress might be caused by surface preparation and manufacturing conditions.

Majority of the high pH SCC occurred on the bottom half of the pipelines. This can be the reason for the higher frequency of high pH SCC downstream of the compressor station at location where stress is high. In Table 5-2, the number of reported failures of gas transmission pipelines is given as a function of operating stress (ASME 2008). The failures for almost all the larger diameter pipelines occurred at a level greater than or equal to 60% of the specified minimum yield stress (SMYS). Contrary, failure for the smaller diameter pipelines is observed at lower stress levels. In general, a common industry guideline is that pipelines operating over 60% SMYS should be considered more susceptible to high-pH SCC. However, this doesn't mean that cracking and failures doesn't occur at stress level below 60% SMYS (e.g., smaller diameter pipelines in Table 5-2. For near-neutral pH, the industry guideline states that pipeline operating at stress levels above 60% SMYS should be considered more susceptible to near-neutral pH SCC.

Table 5-2: Number of reported high-pH SCC failures of gas transmission pipelines as a function of operating stress (ASME 2008)

% SMYS	Service failures		Hydrotest failures	
	<12" diameter	≥ 12" diameter	<12" diameter	≥ 12" diameter
<30	0	0	0	0
30-40	2	0	0	1
40-50	3	0	10	0
50-60	3	0	0	1
60-70	0	9	0	37
>70	4	33	0	250

5.2.5 Impact of distance to compressor or pump station

Majority of the high-pH SCC failures have occurred within 10-20 miles (16-32 km) of a compressor/pump station because temperature and stress are higher at this location. A common industry guideline is that the first 20 miles (32km) downstream of a station are considered more susceptible to high-pH SCC. However, this doesn't mean that cracking and failures doesn't occur at distances beyond 20 miles (32km). In Table 5-3, the number of high pH SCC failures as a function of proximity to compressor discharge stations is shown (ASME 2008). It can be observed from Table 5-3 that majority (almost 90%) of the pipeline failure occurred within 20 miles and others beyond 20 miles on both coal tar enamel and tape coated pipelines.

Table 5-3: High pH SCC failures as a function of proximity to compressor discharge stations (ASME 2008)

Distance (miles)	Service failures		Hydrotest failures	
	Coal tar enamel	Tape	Coal tar enamel	Tape
0-5	19	8	107	3
5-10	10	2	88	7
10-20	10	1	17	29
20-30	2	1	3	6
30-40	0	1	0	3
40-50	1	0	0	0
>50	1	0	2	1

Similar to high-pH SCC, majority of the near-neutral pH SCC failures on tape coated pipelines have occurred within 10-20 miles of a station. In addition, failures observed beyond 20 miles are seen in asphalt-coated pipelines. In Table 5-4, the number of near-neutral pH SCC in-service failures as a function of proximity to compressor or pump stations is shown (ASME 2008). From the table, it can be observed that 2/3 of the failures on tape coated pipelines were within 20 miles of a compressor station, but the failures on asphalt-coated lines were distributed along the entire pipeline length. Hence, there is no specific industry criterion related to distance to compressor station for near-neutral pH SCC (Beavers and Bubenik, 2017).

Table 5-4: Near-neutral pH SCC failures as a function of proximity to compressor or pump station stations (ASME 2008)

Distance (miles)	Coating type		
	Tape wrapped	Asphalt	Wax
0-5	2	1	0
5-10	2	0	1
10-20	1	3	0
20-30	1	0	0
30-40	0	1	0
40-50	0	0	0
>50	0	5	0

5.2.6 Impact of pipeline age

Age of pipeline has a contribution in failure of pipelines due to SCC. A common industry guideline is that lines more than 10 years old should be considered more susceptible to high-pH SCC. However, this doesn't mean that cracking and failures doesn't occur at distances beyond 20 miles (32km) (ASME 2008).

The relationship between pipeline age and near-neutral pH SCC failure have been analysed for in-service and hydrostatic test failures as shown in Table 5-5. The earliest reported age for in-service failure is 12 and 35 years on a tape and wax coated pipelines, respectively. As a result, a common industry guideline states that pipes more than 10 years old should be considered as susceptible.

Table 5-5: Near-neutral pH SCC failures as a function of age (ASME 2008)

Pipe age (years)	Near-neutral pH SCC failures as a function of age							
	Tape-wrapped		Asphalt		Wax		Coal tar	
	In-service	Hydrotest	In-service	Hydrotest	In-service	Hydrotest	In-service	Hydrotest
0-10	0	0	0	0	0	0	0	0
10-20	4	4	1	0	0	0	0	0
20-30	3	6	3	1	0	0	0	0
30-40	0	4	5	21	1	0	0	0
40-50	0	0	2	15	0	0	0	0
>50	0	0	0	0	0	0	0	0

In summary, according to industry guidelines, high-pH SCC failures are most likely on pipe that is: within 20 miles of a compressor station, more than 10 years old, at temperature above 38-43 C, coated with coal tar or tape and operating stress above 60% SMYS. Similarly, near-neutral pH SCC failures are most likely on pipe that is: over 10 years old, coated with tape or asphalt and operating at stress level above 60% SMYS.

5.3 Integrity assessment

The three common techniques used for assessing integrity of pipelines subject to time dependent threats (e.g., corrosion) and SCC are in-line inspection, hydrostatic testing, and direct assessment. Each technique has its weakness and strengths, and a combination of all provides the most effective integrity management.

Hydrostatic testing is used to conduct strength tests on pipelines, which can be either in the manufacturing process or during installation in the field that is prior to place the pipe in service. This technique is a preferred integrity assessment method when the pipeline is incapable of inspected internally. In hydrostatic testing, the pipelines are pressure tested with water at pressure significantly greater than the operating pressure in order to identify and remove flaw that are near critical. The assumption is that any remaining flaws in the pipeline are smaller than the critical size. Hydrostatic testing has limitations, including: 1) Obtaining an adequate sources of water and freezing of water is an issue in dry climates and northern climates (during winter months), respectively 2) Addition of water can introduce the threat of internal corrosion in some pipelines 3) Water has to be treated to prevent contamination of the environment for liquid petroleum and gas pipelines 4) Cracks may grow during the test and lead to pressure reversal, where the failure pressure is lowered after the test (Revie, 2015).

In-line inspection technique (e.g., magnetic flux leakage and ultrasonic tools) is used to manage time-dependent integrity depend on operating pipelines. This technique has advantage over hydrostatic testing because they are capable of detecting cracks, smaller than the critical flaws, which could fail a hydrostatic test. Unlike hydrostatic testing, ILI generally doesn't require that the pipeline be taken out of service. Also, there isn't any problem associated with using large of

volumes of water. However, one of the drawbacks of ILI is that pipeline has to accommodate the tools (Revie, 2015).

The SCC direct assessment (SCCDA) is a four-step process that assist pipeline operators to assess the extent of SCC on buried pipelines. This improves integrity of the pipeline by reducing the impact of external SCC. The first step in SCCDA process is preassessment, which uses operational records of pipeline segment and knowledge of the immediate surface environments exposed to corrosive electrolytes to assess the likelihood the pipeline is susceptible to SCC. The main limitation of this technique is that not finding SCC at excavated locations does not indicate that the pipeline doesn't have SCC elsewhere (Revie, 2015; Beavers and Bubenik 2017).

5.4 BBN model development for SCC

The initiation and propagation of SCC is a complex process that depends on several interconnected factors. Jain et al., (2013) proposed a BBN to model the high pH SCC of pipelines by considering the effects of stresses, soil environment and electrolyte chemistry beneath a disbonded coatings (Figure 5-4). The failure probability of pipeline due to SCC starts with disbondment of pipeline coating. The disbonded coating combined with other factors such as environment, effective potential and stresses leads to initiation and growth of crack rate as shown in Figure 5-4. The proposed model has nodes for each of these factors (e.g., coating disbondment, carbonate or bicarbonate concentration estimation, potential or current estimation, stress estimation, crack initiation and growth, and failure) and some of the nodes have an independent process that was modelled using a BBN.

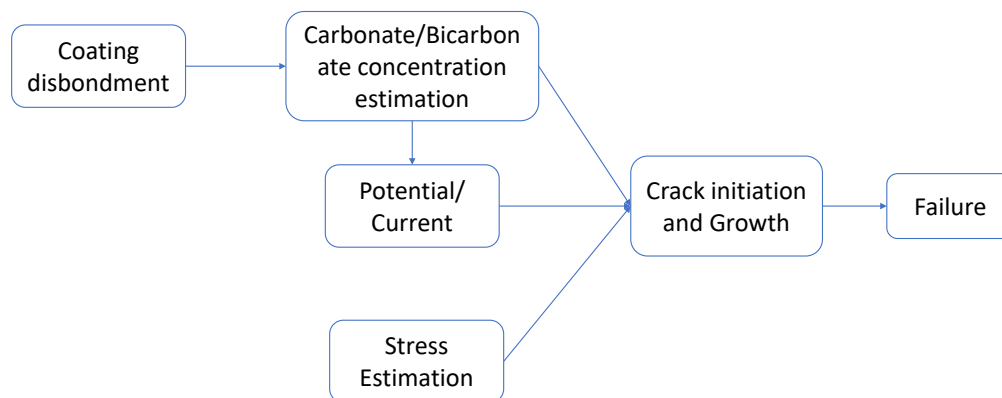


Figure 5-4: Layout of the model for SCC in pipelines. Taken from (Jain et al., 2013)

In this study, a BBN model is developed to model SCC failure assessment based on previous study of Al-Amin et al. (2018). The proposed model was developed by TransCanada for risk assessment of SCC threat. The BBN network for SCC is constructed based on the code developed by American Society of Mechanical Engineers (ASME) and SCC recommended practices prepared by the

Canadian Energy Pipeline Association (CEPA) (ASME 2008, CEPA 2015). The input parameters include operating stress and temperature, distance from compressor station, age, coating type and prior SCC history. The model combines observations from assessments (i.e., ILIs, pressure tests and digs), evidence available from failure history, and mechanistic understanding of SCC. The developed model and its components are explained in subsequent sections.

5.4.1.1 Likelihood of failure

The probability of failure is calculated based on a subsystem-specific. A subsystem differs from another based on its unique performance and empirical (evidence based) condition. Hence, the likelihood of failure due to SCC is calculated based on the following equation:

$$LOF_{SCC} = \alpha_{SCC} A_{SCC} + \beta_{SCC} H_{p_SCC} \quad 5-1$$

where LOF_{SCC} = Likelihood of failure due to SCC; α_{SCC} = reliability of the assessment results; A_{SCC} = previous evidence from assessment of SCC threat; β_{SCC} = Reliance factor for the predicted failure rate; H_{p_SCC} = Predicted failure rate of the pipe segment due to SCC.

The first and second term of Equation 5-1 represents the findings from integrity assessments, and learnings from historical failures and scientific evidence, respectively. The integrity assessment methods that are considered in the model to identify areas with SCC are ILI, hydrostatic testing and SCC direct assessment. Hence, Equation 5-1 is modified into Equation 5-2 to incorporate all these assessments.

$$LOF_{SCC} = \alpha_{general} (\alpha_{CD_ILI} A_{CD_ILI} + \alpha_{HT} A_{HT} + \alpha_{DA} A_{DA}) + \beta_{general} \beta_{MFL_ILI} H_{p_SCC} \quad 5-2$$

where $\alpha_{general}$ = General reliability factor for assessments; α_{CD_ILI} = Reliability factor of crack-detection ILI assessment; A_{CD_ILI} = Assessment factor based on crack-detection ILI result; α_{HT} = Reliability factor of hydrostatic test assessment; A_{HT} = Assessment factor based on hydrostatic test result; α_{DA} = Reliability factor of direct assessment; A_{DA} = Assessment factor based on direct assessment result; $\beta_{general}$ = General reliance factor for predicted failure rate; β_{MFL_ILI} = reliance factor based on finding from MFL ILI result; Details of these parameters are given in subsequent sections

The general reliability and reliance factors used in the assessment are shown in Table 5-6. The factors varies depending on the scenario. For example, if a segment was inspected by any of the crack detection methods in the last 5 years, then $\alpha_{general}$ and $\beta_{general}$ are taken as 1 and 0,

respectively. Contrary, if no assessment has been done for the segment, then then $\alpha_{general}$ and $\beta_{general}$ are taken as 0 and 1, respectively.

Table 5-6: General Reliability and General Reliance Factor

Scenario	$\alpha_{general}$	$\beta_{general}$
Segment was inspected by crack-detection ILI or hydrostatically tested within the hydrostatic test re-inspection interval or a DA was performed in last 5 years	1	0
Segment was hydrostatically tested only and the age of the test is between 5 to 10 years, but the pipeline age is less than 10 years or the pipeline is coated with high performance coating	0	1
Segment was hydrostatically tested only and the age of the test is between 5 to 10 years, the pipeline age is more than 10 years or the pipeline is coated with non-high-performance coating	1	1
Segment was assessed only by DA and the assessment was done more than 5 years ago	1	1
No assessment has been done for the segment	0	1

Table 5-7: ILI Assessment Factor

CEPA SCC Severity Category	Assumed ILI Assessment Factor, ACD_ILI (failures/km-year)
Category IV	1E-03
Category III	1E-04
Category II	1E-05
Category I	1E-06
No SCC found	1E-07

The crack detection tool (e.g., ILI) is useful to locate and estimate the size of cracks. The cracks obtained using this method are analyzed in a deterministic or probabilistic way to determine the predicted failure pressure. Accordingly, severity of cracks are categorized based on failure pressures according to CEPA Recommended Practice (CEPA 2015). The crack categories are assigned an assessment factor and used to compute the likelihood of failure in absence of probabilistic assessment. Assignment of the factor was based on the learning from fully validated and implemented similar probabilistic corrosion assessment as well as the historical failure rate in TransCanada’s system due to SCC. The ILI and SCC direct assessment (SCCDA) factors (A_{CD_ILI}) are shown in Table 5-7. The DA factor is applied to pipeline segments having similar properties with the excavated pipe in terms manufacturer, external coating, soil and drainage condition.

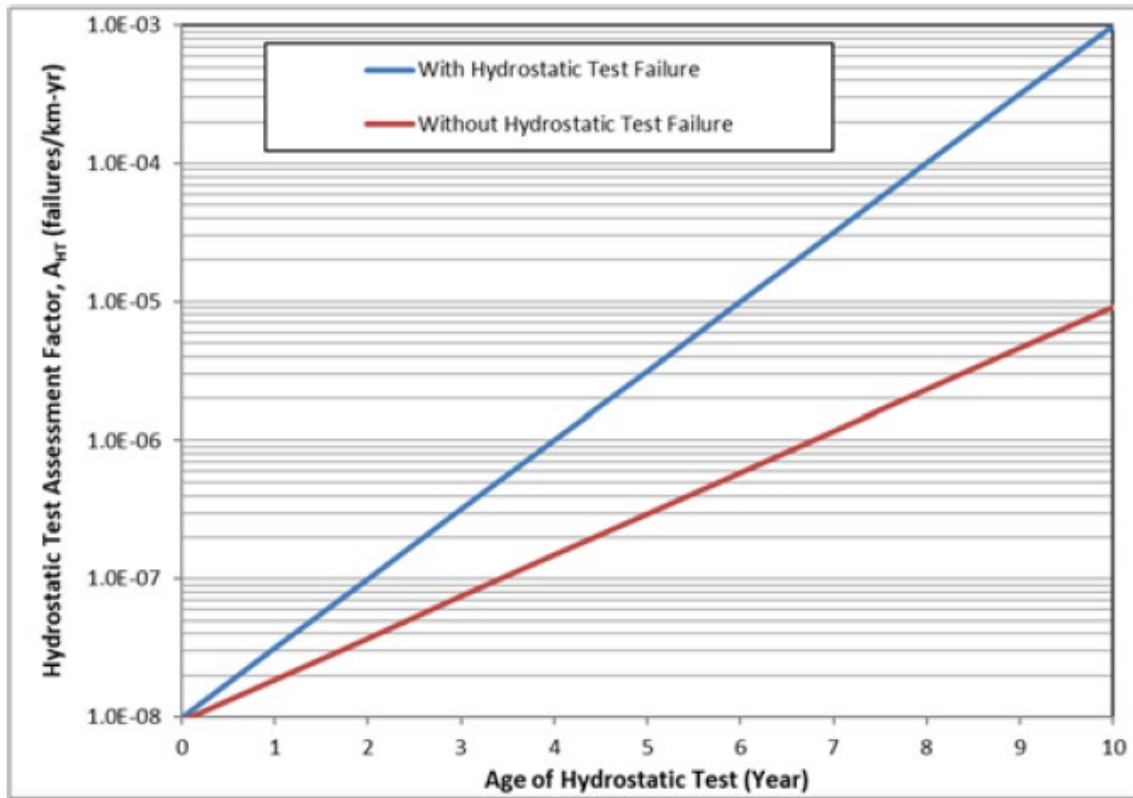


Figure 5-5: Hydrostatic test assessment factors. Obtained from Al-Amin et al. (2018)

The hydrostatic testing helps to find the SCC defects that are in critical and near critical stages, and doesn't provide information pertaining the remaining features of SCC. The hydrostatic test assessment factor (A_{HT}) was estimated based on the following assumptions: 1) Assume that the benefit of hydrostatic test decline linearly with time after the test 2) The risk of SCC for a pipeline segment that was tested within the re-inspection interval is considered low (less than 1E-06 per km-year) 3) Two different criteria were used to differentiate between the hydrostatic test without SCC failure and with SCC failure 4) No credit was taken for the hydrostatic test performed more than 10 years ago. The hydrostatic testing assessment factors were calculated based on the above assumptions and failure history of TransCanada. The hydrostatic testing assessment factors can be obtained from Figure 5-5. Finally, the assessment reliability factors that represent effectiveness of the assessment methods are given in Table 5-8. A higher α_{DA} values are assigned to pipeline segment that were assessed using DA method only before long time. This is to insure that the risk of SCC has increased over time as there is no other assessment used to estimate SCC in the pipeline.

Table 5-8: General Reliability and General Reliance Factor

Scenario	α_{CD_ILI}	α_{HT}	α_{DA}
Only ILI is available for the segment	1	0	0
Segment was hydrostatically tested within the re-inspection interval	0	1	0
ILI is available for the segment, and it was hydrostatically tested 5 to 10 years ago,	1	1	0
Segment was hydrostatically tested 5 to 10 years ago and DA was done in last 5 years	0	1	1
Segment was assessed only by DA method in last 5 years	0	0	1
Segment was assessed only by DA method between 6 to 15 years ago	0	0	5
Segment was assessed only by DA method in more than 15 years ago	0	0	10

The reliance factor β_{MFL_ILI} is applied to pipeline segments where no SCC assessment has been completed. For example, if results from MFL ILI indicated a low level of corrosion on the pipe segment, then the β_{MFL_ILI} factor is used to dial up the predicted failure frequency, and vice versa. The developed model uses historical and mechanistic factors to predict the likelihood of failure due to SCC in absence of assessment data. The model output is derived from the correlation of actual failure rate H_{p_SCC} and causal and resistance factors FR_{SCC} . Al-Amin et al. (2018) summarized the steps to calculate the actual failure rate as follows: 1) dynamically segmented pipelines based on the significant parameters for SCC threat 2) For each in-service failure, determine the combination of significant parameters of the pipe segment where failure occurred 3) For each pipeline system, determine the total exposure of pipe segments (in unit of km-year) that has the same combination of significant parameters as the failure segments 4) Calculate the actual failure rate dividing the number of failures by the total exposure of similar pipe segments. The FR_{SCC} estimates the SCC susceptibility based on pipe data, operational data, environmental data and preventative actions as shown in Equation 5-3.

$$FR_{SCC} = Ag \times S \times HPC \times [0.3 \times CSD + 0.3 \times CMY + 0.2 \times DCS + 0.05 \times L + 0.1 \times CP] \quad 5-3$$

where Ag = Score for pipe age; S = Score for operating stress level; HPC = Score for high performance coating; CSD = Score for interaction of parameters between pipe external coating type, soil type and drainage; CMY = Score for interaction of parameters between pipe external coating type, manufacturer and construction year; DCS = Score for distance from upstream compressor station; L = Score for landform or topography; CP = Score for CP level; Relative

weights of each of these parameters and their combinations are determined based on the mechanistic understanding of SCC susceptibility and expert's opinion on the subject matter. The scores of each parameters in Equation 5-3 ranges between 0 and 1 based on the relative effectiveness in causing and resisting the occurrence of SCC. Details of these parameters are discussed below.

The score for pipe age, operating stress, HPC, Coating-Soil-Drainage, Coating-Manufacturer-Construction Year, Distance from Upstream Compressor Station, Landform/Topography are given in Table 5-9 to Table 5-15. The criteria for age of the pipeline is determined based on ASME B31.8S, where a pipe with greater than 10 years old is seen as a possible threat of SCC. The criteria for operating stress level is determined based on the guideline of ASME B31.8S and historical excavations. Pipe segments that are operated at pressure greater than 60% SMYS have higher score and mid-level scores are assigned for pipeline with operating stress between 40% SMYS and 60% SMYS. The HPC score is based on the observation that high performance coatings are less susceptible to SCC initiation on pipelines and hence lower score. These coatings include: Fusion Bonded epoxy (FBE), Liquid epoxies, Urethanes, Multi-layer and Extruded polyethylene.

Table 5-9: Scores for Pipe Age

Pipe Age	Score
≥ 10 years	1
< 10 years	0.1

Table 5-10: Scores for Operating Stress

Operating Stress (%SMYS)	Score
≥ 60	1
< 60 and ≥ 55	0.6
< 55 and ≥ 40	0.3
< 40	0.1

The score for the interaction of coating, soil and drainage are determined based on TransCanada's in-service and hydro-test failure rate, as well as CEPA's SCC recommended practices and ASME guidelines. Additionally, non-mechanistic process such as pipe manufacturer is considered in Equation 5-3 because historically produced pipes are prone to SCC. The score for combination of coatings, manufacturers and construction year is determined based on TransCanada's experience of hydrostatic test and in-service SCC failures as well as findings from excavations.

Table 5-11: Scores for HPC

Presence of HPC	Score
HPC on pipe body and girth weld	0.1
HPC on pipe body, non-HPC on girth weld	0.5
Non-HPC on pipe body	1

Table 5-12: Example of Scores for Coating-Soil-Drainage

Coating-Soil-Drainage	Score
Tape-Clay-Very poorly drained	1
Asphalt-Sand-Well drained	0.85
Asphalt-Sand-Poorly drained	0.5
Tape-Sand-Very poorly drained	0.6

Table 5-13: Example of Scores for Coating, Pipe Manufacturer and Construction Year Combinations

Coating&Manufacturer&Construction Year	Score
Tape&Stelco&>=1970, <=1975	1
Asphalt&Stelco&>=1970, <=1975	0.85
Asphalt&Ipsco&>1985	0.3
Tape&Alberta Phoenix&<=1978	0.8

Table 5-14: Scores for Distance from Upstream Compressor Station

Distance from Upstream Compressor Station	Score
<= 32km	1
> 32km	0.1

Table 5-15: Scores for Landform/Topography

External Coating	Landform	Score
Tape	Depressed	1
Asphalt	Depressed	0.6
Asphalt	Side Slope	0.5
Asphalt	Level	0.9

The impact of distance from upstream compressor station on SCC is explained in the introduction section, where there is high risk of SCC near a compressor station because the temperature in the surrounding is higher than in other places (Fang et al., 2003). The score for distance from upstream compressor station is given in Table 5-14. The score for pipe coating and topography interaction is obtained from the SCC historical failures as shown in Table 5-15. The score for CP depends on the type of coating. For example, coating disbondment is commonly seen in Tape coatings, where the highest score of 1.0 is given to Tape coating. The score for the CP is summarized in Table 5-16.

Table 5-16: Scores for CP

Cathodic protection	Score
Ineffective, shielded	1
Partially effective, variable, some shielding	0.5
Always good	0.1

5.5 Results and discussions

To demonstrate the applicability and usefulness of the proposed BBN model, two hypothetical pipeline scenarios are assumed. Parameters of the BBN model are provided in Table 5-17. Both cases assume that no assessment has been done for the segment. The parameters for pipeline age,

coating, drainage, cathodic protection and others are kept constant. However, the first pipeline operates at operating stress level of ≥ 60 and the remaining at <40 . The obtained likelihood of failure is given in Figure 5-6. This indicates that the higher the operating stress, the higher will be the likelihood of failure.

Table 5-17: Input parameters for SCC

	Pipeline1	Pipeline2
General Reliability and General Reliance Factor	No assessment has been done for the segment	No assessment has been done for the segment
Assessment Reliability Factor	Segment was assessed only by DA method in more than 15 years ago	Segment was assessed only by DA method in more than 15 years ago
ILI Assessment Factor	Category II	Category II
Hydrostatic Test Assessment Factors-Age of Hydrostatic Test (Year)	6	6
Hydrostatic Test Failure	With Hydrostatic Test Failure	With Hydrostatic Test Failure
Dig Assessment Factor	Category II	Category II
Pipe Age	≥ 10 years	≥ 10 years
Operating Stress Level	≥ 60	<40
High Performance Coating (HPC)	Non-HPC on pipe body	Non-HPC on pipe body
Coating Soil Drainage	Tape-Sand-Very poorly drained	Tape-Sand-Very poorly drained
Coating Manufacturer Year	Tape & Alberta Phoenix & ≤ 1978	Tape & Alberta Phoenix & ≤ 1978
Distance from Upstream Compressor Station	> 32 km	> 32 km
Landform / Topography	Tape-Depressed	Tape-Depressed
Cathodic Protection	Partially effective, variable, some shielding	Partially effective, variable, some shielding
Reliance Factor Based on MFL_ILI	Low level corrosion	Low level corrosion

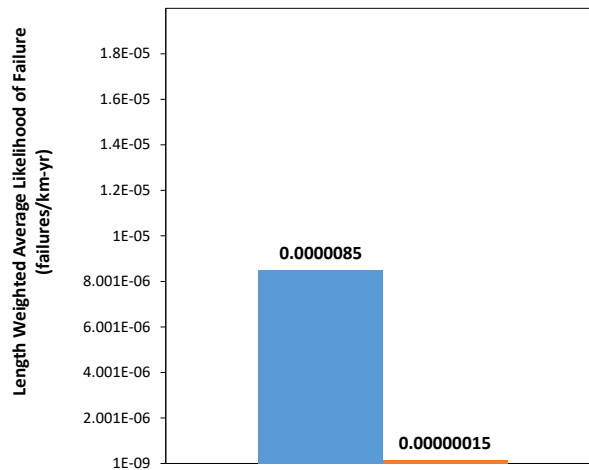


Figure 5-6: Likelihood of failure due to SCC

5.6 Conclusions

The SCC BBN model was developed based on the code developed by ASME and SCC recommended practices prepared by the CEPA. The model consists of various parameters, including operating stress, temperature, distance from compressor station, age, coating type and

prior SCC history. The model also incorporates observations obtained from integrity assessment techniques (e.g., ILIs, pressure tests and digs), evidence available from failure history and mechanistic understanding of SCC. The model can be used in an integrity assessment of a pipeline system. This study can be extended in the future by incorporating new scientific learnings and validating the model by finding of SCC from inspection.

Chapter 6

Seismic Liquefaction-Induced Permanent Ground Displacement

6.1 Introduction

The integrity of pipelines is affected by pipeline ageing and deterioration processes, coupled with exposure to natural hazards (e.g. earthquake, geotechnical failure, climate change) and human-induced hazards (e.g. accidental hits, vandalism). In this project, the primary aim is to develop a Bayesian Belief Network- based (BBN-based) decision making tool to assess the vulnerability of pipeline subjected to two key hazards, viz., the corrosion hazard and the earthquake-induced ground displacement hazards. The component of developing datasets due to geohazards required for training BBN model was undertaken by Dr. Wijewickreme's research group. The estimation of demand on buried pipelines due to liquefaction-induced permanent ground displacements (PGD) was a key objective under the geohazards component. It was recognized that the estimation of pipeline strain capacities due to PGDs (called PGD capacities) is a complex structural problem that involves structural and materials engineering. Considering the need to provide datasets for BBN model training of the pipeline response to PGDs, it was judged to include the PGD capacity estimations for intact and corroded buried pipelines within the geotechnical scope of work on a preliminary basis (i.e., these capacities need to be defined after further research). The approaches developed on this basis are discussed in detail in this report.

6.2 Scope of Study

In this project, Dr. Dharma Wijewickreme's geotechnical research group has been involved in implementing the following key tasks (confirmed as per progress review meeting on February 22, 2021). The primary objective involves performing pipeline vulnerability assessment due to liquefaction-induced lateral permanent ground displacements (PGDs) as input to multi-hazard BBN modelling:

1. Task 1 - Estimate site-specific lateral PGD hazard (at specific locations identified by BCOGC)
2. Task 2 - Conduct a literature review specifically on the structural capacity of corroded pipelines
3. Task 3 - Estimation of preliminary PGD capacities for intact pipelines
4. Task 4 - Develop a preliminary way to modify the above GD capacities to account for corrosion

6.3 Background

Pipelines are one of the safest ways of transporting fluids over long distances and thus, it is in everyone's best interest to ensure safe pipelines to safeguard our health and quality life, to protect communities and environment, to promote economic growth and value creation. Under seismic loading, several studies have reported these pipelines to have suffered damage and undergone failures. In 1971, San Fernando earthquake, 11 pipelines got damaged and 80 breaks have been reported. These pipes were primarily subjected to liquefaction-induced lateral spread displacements and landslides. Similar failure cases, as shown in Figure 6-1 have been reported in the literature, wherein the pipelines have undergone failures essentially due to permanent ground displacements.

Typically, under seismic loading, induced ground displacements can be of 2 types; transient ground displacements (TGD) and permanent ground displacements (PGD). TGDs are those displacements, which the ground undergoes during shaking as a result of wave propagation, whereas, PGDs are the irreversible permanent displacements that the ground develops and retains even after the shaking. It is of concern only when the induced strains result in the loss of pressure integrity of buried pipelines. The risk to pipeline damage due to TGDs is considered insignificant compared to PGDs as the TGD-induced strains can be accommodated by the ductile nature of these pipes (PRCI 2009a). Further, it was observed that the corroded pipes can undergo significant damage even under ground displacements of lesser magnitude. As documented in the BCOGC (2018) report, the documented pipeline failures in Canada without any human intervention and considering only natural hazards are due to: (a) corrosion and (b) geotechnical hazard. The performance of the pipeline under geotechnical hazard depends upon the pipeline condition. A suitable mitigation measure can be adopted if the contributions from both the hazards are quantified. It is understood that, the problem under consideration is a multi-hazard problem and is proposed to be addressed using Bayesian Belief Network, i.e., BBN model in the present framework.

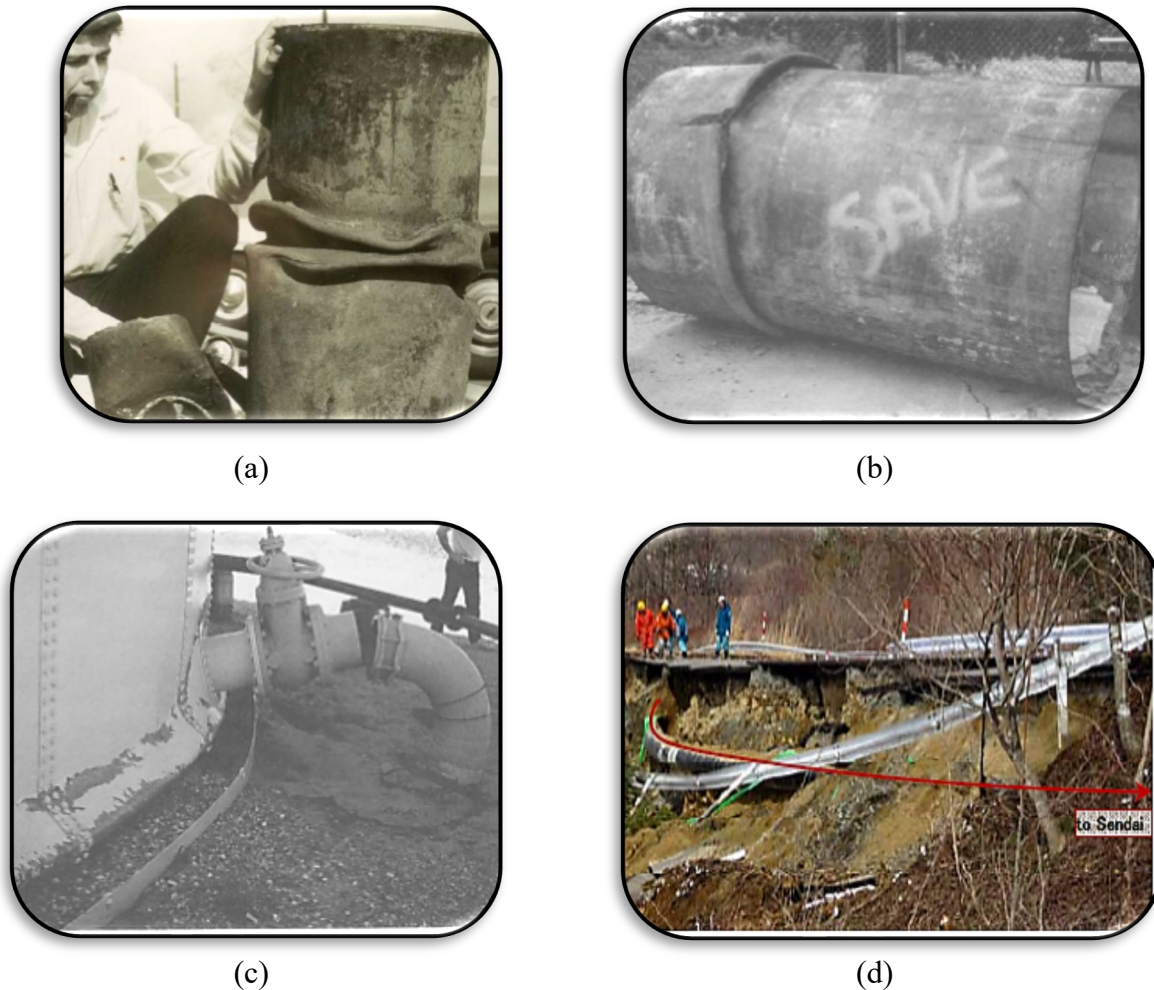


Figure 6-1: Case histories reported pipeline failures during (a) 1971 San Fernando Earthquake, (b) 1994 Northridge Earthquake, (c) 1992 Landers and Big Bear Earthquakes, and (d) 2011 Japan Earthquake (Ariman et al., 1987; Lund, 1994, 1996; Mori et al., 2012)

In this project, the research group led by Dr. Dharma Wijewickreme have dealt with the geotechnical component of the hazard problem. During earthquake loading, there are different types of possible ground displacement hazards as shown in the Figure 6-2, viz., sand boils, flow slides, lateral spreading and bearing capacity failures. In this project, focus has been on the estimation of lateral spread displacement hazard. Lateral spread displacements are the finite lateral displacements of gently sloping ground as a result of liquefaction in a shallow underlying deposit during an earthquake.

Different approaches are at present adopted to cater this hazard for pipelines. The usually adopted approach is the use of fragility curves framework for evaluating damage to the buried pipelines. Figure 6-3 shows typical example of the empirical curves used in practice to predict the repairs/km with the intensity of shaking. However, these curves have been developed primarily for water pipelines; the segments of such pipes are usually connected with the flexible connections like bell and spigot joints. As a result, these pipes tend to have more separations and hence, more potential

breaks/repairs unlike, oil and gas pipelines which are constructed of welded steel. Thus, framework based on fragility curves may be considered to have reduced applicability for oil and gas pipelines (Honegger and Wijewickreme, 2013)



(a)



(b)



(c)



(d)

Figure 6-2: Different types of liquefaction-induced ground displacements, viz., (a) sand boils, (b) Flow Slides, (c) lateral spreading and (d) bearing capacity

During past earthquakes, liquefaction-induced lateral spread displacements have resulted in failure of many buildings, bridges, transportation infrastructure and pipelines. Several studies have been performed to estimate the magnitude of lateral spread permanent ground displacements (PGDs) to be accounted for in the seismic design of engineering structures at a given site. Among these, the empirical predictive equations proposed by Youd et al. (2002) based on multiple linear regression (MLR) of data from past earthquakes have been widely adopted in practice owing to its accountability for the key governing seismic, geotechnical, and topographic parameters in a simplistic manner (Honegger et al. 2010). Specifically, the MLR equations by Youd et al. (2002) require the values of the earthquake magnitude (M) and distance from the source (R) to define the seismic hazard at a subject site. There are difficulties in representing the earthquake hazard at a

given site simply based on one pair of M-R input (i.e., deterministic approach), particularly when the site seismicity could arise from a multiplicity of earthquake sources; in turn, such a use of a single M-R pair could lead to significant uncertainty in the computed lateral spread PGDs from the MLR equations.

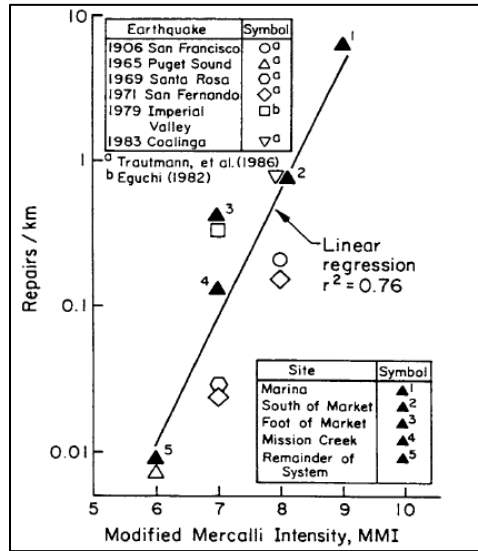


Figure 6-3: An example of fragility curve (O'Rourke, T. D et al. 1991)

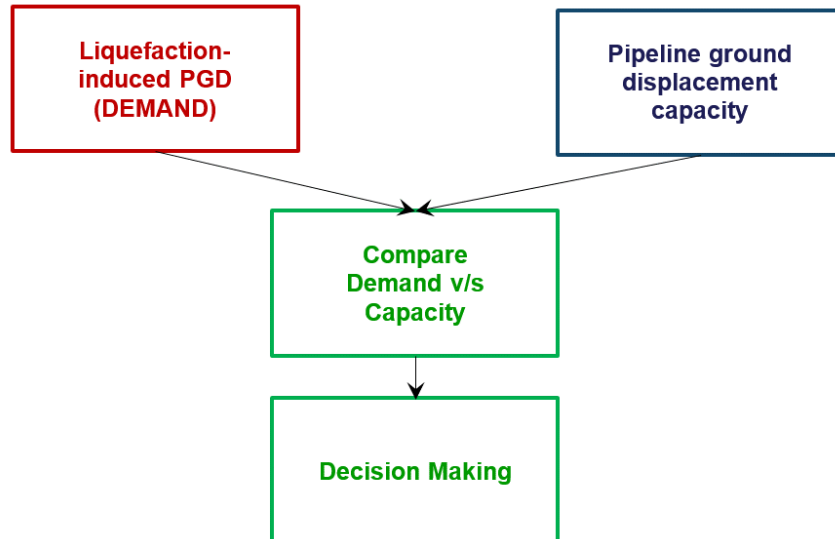


Figure 6-4: Overview of the proposed basic framework

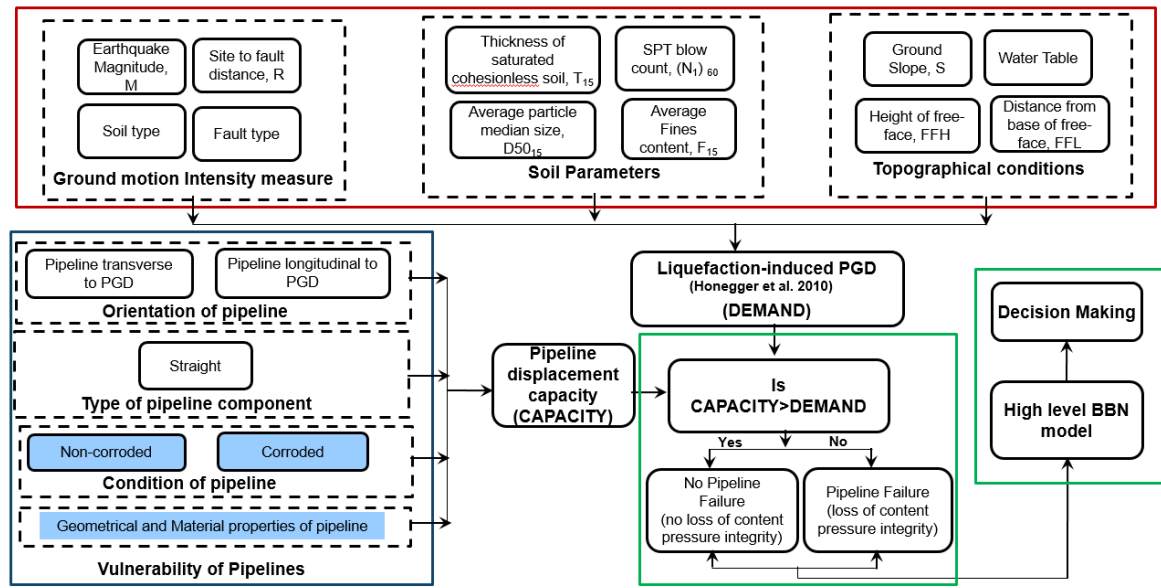


Figure 6-5: Conceptual BBN to incorporate seismic liquefaction-induced permanent ground displacements

The currently available probabilistic seismic hazard assessment (PSHA) approaches provide a well-established way to compute the seismic shaking hazard (e.g., peak ground acceleration) at a given site as a function of the probability of occurrence. Emulating this framework, a study was undertaken to estimate the lateral spread PGD hazard from the Youd et al. (2002) empirical model in probabilistic manner using the National Building Code of Canada (NBCC 2015) PSHA model; in this approach, the Youd et al. equations are embedded in place of the ground motion prediction equations (GMPEs) in the NBCC-PSHA ground motion estimation model that also accounts for the Cascadia Subduction earthquake event also as probabilistic scenario. Since the NBCC-PSHA ground motion model is currently available in the open source software engine by OpenQuake (Global Earthquake Model, Pavia, Italy), it was possible to undertake the work without resorting to expensive commercial software. Moreover, the contributions herein made through the PGD hazard curves for British Columbia would be available for use at various BCOGC sites for estimating site-specific lateral spread displacement demand as input to performance-based design of buried pipelines.

The capacity of buried pipelines to withstand these permanent ground displacements would depend upon several factors like geometrical and material properties of pipe, condition of pipe as in corroded or intact, type of pipeline component and orientation of pipeline with respect to the ground displacements. In order to obtain the pipeline strain and PGD capacities, as requested by the project team, a literature review has been undertaken to explore and identify different groups throughout the globe working on similar problem statement, but are using different techniques/approaches to tackle this problem. Further as discussed in group project meetings, it was agreed

that the PGD capacities for intact pipelines will be retrieved from the previous report available from FortisBC (Terasen 2010), in which Dr. Wijewickreme was one of the team members.

In addition to this, to address the project requirements, there is a need to adjust the PGD capacities of intact pipelines to account for the reduction in thickness due to corrosion. It is recognized that the solution to this problem involves both material engineering and geotechnical engineering expertise. In spite of this, during the progress review meeting on Feb 22, 2021, the geotechnical team was requested to examine the ability to arrive at potential modification factors to the intact-pipe PGD capacities to account for the corrosion effects; essentially, the idea is to explore a simplified method to account for the changes in PGD capacity due to the expected changes in equivalent pipe geometric properties such as pipeline cross-sectional area (A) and second-moment of area (I) due to corrosion.

The overall framework has been represented through the flow diagram given in Figure 6-4, which conveys that the demand due to liquefaction induced PGD to buried pipelines and the capacities of these pipelines to withstand this demand will be evaluated. Appropriate decision can be made by comparing demand with the capacity. This framework in detail has been represented in the form of conceptual BBN as shown in Figure 6-5.

6.4 Task 1 - Estimation of site-specific liquefaction-induced permanent ground displacements hazard as demand on buried pipelines

This section presents the approach adopted for the estimation of site-specific liquefaction-induced PGDs hazard curves (considering specific locations relevant to BCOGC sites) as per Task 1.

Several methodologies involving empirical, semi-empirical, and analytical/numerical approaches have been developed and implemented over the past few decades for predicting liquefaction-induced permanent ground displacements. Empirical predictive models (Hamada et al. 1987, Youd and Perkins 1987, Barlett and Youd 1992; 1995, Youd et al. 2002, Bardet and Tobita, 1999; Rauch and Martin 2000; Zhang and Zhao, 2005) are simple and based on data collected from a large number of sites that have undergone lateral spread displacements during past earthquake loading. Semi-empirical approaches essentially involve estimating maximum cyclic shear strains using field tests as a function of earthquake and soil parameters which are integrated over depth to obtain lateral spread displacements (Faris et al., 2006; Idriss and Boulanger, 2008; Zhang et al., 2004). In these, the effect of topography has been incorporated empirically through a parameter such that the obtained displacements are equated with those from real case studies. There are a few analytical approaches like the Newmark (1965) sliding block method proposed for calculating lateral spread displacements, wherein, the displacements would take place whenever the “yield acceleration” (Biondi et al., 2000; Leshchinsky et al., 2018; Matasovic et al., 1997; Rathje and Bray, 2000) is

exceeded by the input ground acceleration. Although mechanistically sound, the Newmark approach has a major limitation since it requires treating the liquefiable soil zones as rigid; hence, there is less confidence in the applicability of the model in practice.

Among these, the empirical predictive equations proposed by Youd et al. (2002) based on multiple linear regression (MLR) of data from past earthquakes have been widely adopted in practice owing to its accountability for the key governing seismic, geotechnical, and topographic parameters in a simplistic manner. The following sections provide a brief overview of Youd et al. (2002) method and the current use of PSHA to develop PGD hazard curves that provided the impetus to the work undertaken in the present study.

6.4.1 Youd et al. (2002) MLR Model and Usage in PSHA

The approach by Youd et al. (2002) has been widely adopted in practice for calibration of advanced numerical models and estimation of PGDs for selected projects. The model is based on multiple linear regression (MLR) analysis of US and Japanese case histories of lateral spread. It consists of two separate equations for representing two different possible boundary conditions, viz., lateral spread towards a free-face and that goes down the gentle ground slopes, as represented by Equations 6-1 and 6-2, respectively.

$$\begin{aligned} \text{Log}(PGD) = & -16.713 + 1.532M - 1.406\text{Log}R^* - 0.012R + 0.592\text{Log}W + 0.540\text{Log}T_{15} \\ & + 3.413\text{Log}(100 - F_{15}) - 0.795\text{Log}(D50_{15} + 0.1) \end{aligned} \quad \mathbf{6-1}$$

$$\begin{aligned} \text{Log}(PGD) = & -16.213 + 1.532M - 1.406\text{Log}R^* - 0.012R + 0.338\text{Log}S + 0.540\text{Log}T_{15} \\ & + 3.413\text{Log}(100 - F_{15}) - 0.795\text{Log}(D50_{15} + 0.1) \end{aligned} \quad \mathbf{6-2}$$

In these equations, PGD is horizontal lateral spread permanent ground displacement in m, M represents earthquake moment magnitude ($6.0 < M < 8.0$), R is the horizontal or mapped distance between site and source in km, $R^* = R + R_0$ where $R_0 = 10^{0.89M - 5.64}$, S is the ground slope ($0.1\% < S < 6.0\%$), W is the free face ratio = 100 (height of free face/ distance from base of free face) ($1\% < W < 20\%$), T_{15} is the thickness in m of the saturated cohesionless soils with $(N_1)_{60} < 15$ blows ($1 \text{ m} < T_{15} < 15 \text{ m}$) where $(N_1)_{60}$ is the normalized standard penetration resistance, F_{15} is average fines content in T_{15} ($0\% < F_{15} < 50\%$) and $D50_{15}$ is average median particle size in T_{15} ($0 \text{ mm} < D50_{15} < 50 \text{ mm}$). These equations are essentially functions of seismicity parameters through M and R , site soil parameters through T_{15} , F_{15} and $D50_{15}$ and topographical parameters through S and W .

Site soil and topographical parameters can be obtained using readily available approaches; however, it is difficult to estimate the seismic parameters for site under consideration. The values for M and R have been observed to have significant influence on the estimated lateral spread displacements and thus Youd (2018) has indicated the need to choose these values with minimum

uncertainty. The values for M and R would depend upon the understanding and quantification of influence of all the possible earthquake sources in vicinity on the site. Using PSHA, it is possible to obtain expected peak ground acceleration and spectral acceleration at a site, but it is not possible to obtain a deterministic value of M and R responsible for that particular hazard level. At present, pseudo-probabilistic approaches are adopted for estimating these M and R values. According to this approach, using deaggregation analysis corresponding to a particular return period, distribution for M and R can be obtained. Using mean or modal values of M and R , lateral spread displacements can be obtained deterministically. As this approach involves probabilistic approach of obtaining M and R but deterministic calculation of lateral spread displacements, it is considered as pseudo-probabilistic approach. Although this approach has been observed to reasonably estimate the lateral spread, yet there is lack of confidence in the predicted displacements owing to the uncertainty associated with the chosen M and R values.

In order to address this drawback, in this study, the Youd et al. equations are embedded in place of the ground motion prediction equations (GMPEs) in the NBCC-PSHA ground motion estimation model that also accounts for the Cascadia Subduction earthquake event also as probabilistic scenario using open source software engine by OpenQuake (Global Earthquake Model, Pavia, Italy). Similar work has been performed in the recent past by a few others (Ekstrom and Franke, 2016; Franke and Kramer, 2014; Honegger et al., 2010). However, these studies have been performed by doing rigorous PSHA or using proprietary codes for PSHA analysis, the approaches have not been readily available for adoptability and use among practitioners in a cost-effective manner. In recent years, the OpenQuake software engine has been widely adopted for performing PSHA owing to its flexibility to accommodate recent discoveries in hazard calculations. This platform can benefit users from different domains as it can be customized as per individual usage needs. Further, the source and ground motion models developed for NBCC 2015 have been implemented by Allen et al. (2020) in OpenQuake platform which was the motivation us for exploring this platform for estimating lateral spread hazard for the present study.

6.4.2 PSHA in OpenQuake

South-western Canada is vulnerable to three types of earthquakes - viz., crustal earthquakes, subduction intra-slab, and subduction interface earthquakes. The National Building Code of Canada (National Building Code of Canada, 2015), the 5th Generation Seismic Hazard Model for Canada (SHMC) published by the Natural Resources Canada (NRCan) sets out technical provisions for the design and construction of new buildings. This fully probabilistic 5th Generation SHMC model consists of four components for four quadrants of Canada, viz., South-western Canada (SWCan), South-eastern Canada (SECan), North-western Canada (WArtic) and North-

eastern Canada (EArtic). Each of these components may consist of single or multiple weighted sub-models giving the source information. SWCan component follows single sub-model. Accordingly, GSC input file, which is in Python programming language (.pkl) provides information like depth of source, inclination characteristics of fault source, moment magnitude, etc. for each of the areal and fault sources which may result in earthquakes in SWCan region of Canada (Halchuk et al., 2014). For analysis using OpenQuake, Allen et al. (2020) has converted these files into NRML - i.e., ‘Natural Hazard’ Risk Markup Language, which were readily available in Treviallen Git hub repository (Allen, 2021), and hence, have been retrieved for use in current study where the OpenQuake platform is used to predict the liquefaction-induced lateral PGDs. These sources belong to seven different types of tectonic regions. The ground motion prediction equation for earthquakes due to these sources have been given in the form of tables applicable to these seven different types of tectonic regions; in essence these provide variation of ground-motion amplitudes with distance for different values of magnitudes. GSC has provided the source model file in Python programming language (.pkl). For analysis using OpenQuake, it is important that these files are converted into NRML - i.e., ‘Natural Hazard’ Risk Markup Language - and Allen et al. (2020) has extensively contributed to this effort. The ground motion interpolator implemented by Allen et al. (2020) in OpenQuake has enabled using NBCC 2015 attenuation tables for performing PSHA in this platform.

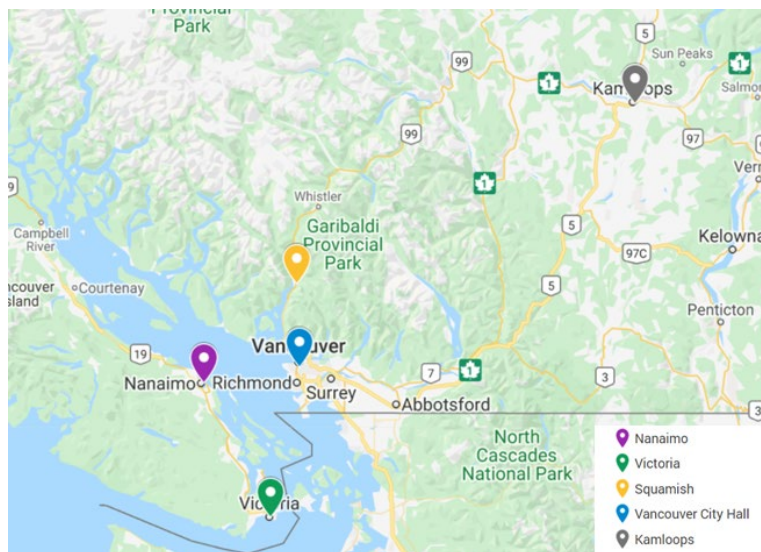


Figure 6-6: Cities in southwestern component of Canada used for the present project

Through the above work, the source model files in NRML format were readily available in Treviallen Git hub repository (Allen, 2021), and hence, have been retrieved for use in current study where the OpenQuake platform is used to predict the liquefaction-induced lateral PGDs. As a first step, it was considered prudent to cross-check and verify the ground motion Uniform Hazard

Spectra (UHS) predicted by OpenQuake code (using source model files from Treviallen Git hub repository) and compare the outcomes with those from NBCC 2015. The PSHA was specifically performed in this regard using OpenQuake to obtain UHS for two return periods, viz., 2500 (2% in 50 years) and 500 (10% in 50 years), for three different cities in British Columbia, viz., Victoria in Vancouver island, Vancouver, Kamloops from lower mainland of British Columbia as shown in Figure 6-6.

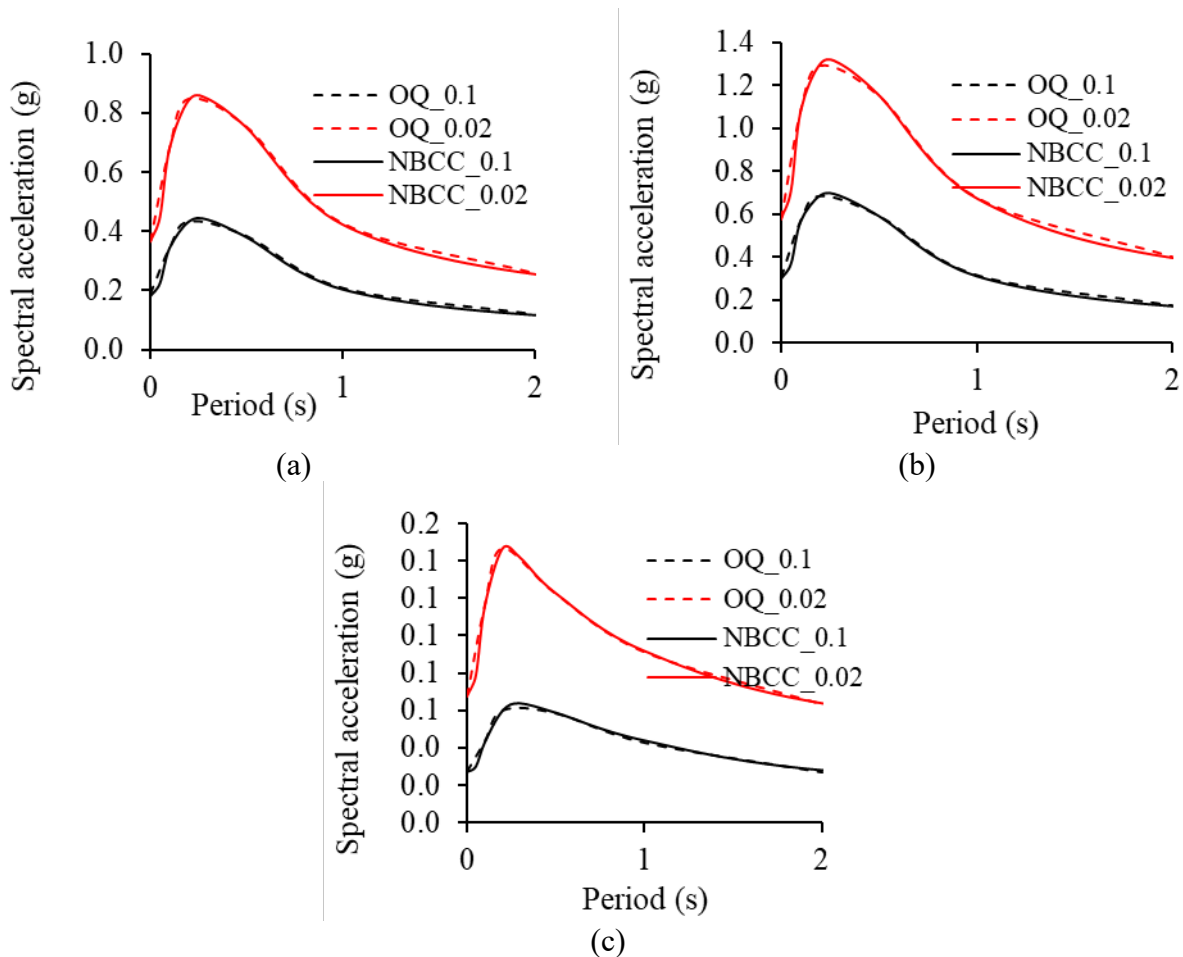


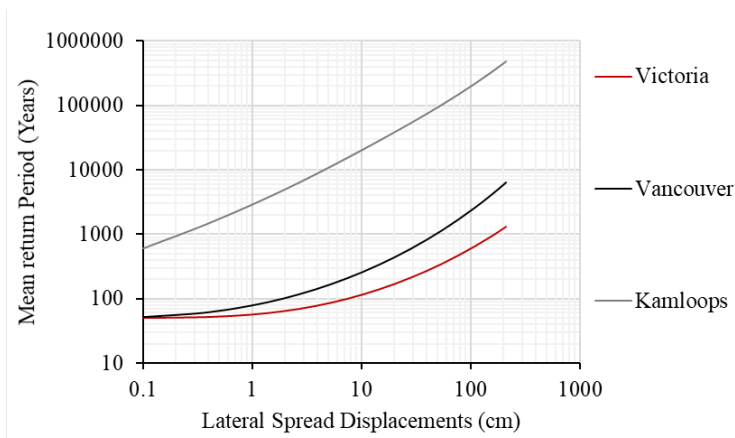
Figure 6-7: Comparison of UHS obtained from PSHA in OpenQuake with those from NBCC 2015 of selected cities, viz., (a) Vancouver (b) Victoria (c) Kamloops from South-west Canada

The results obtained from OpenQuake platform were compared with those obtained from NRCan earthquake hazard calculator in accordance with NBCC 2015; typical comparison for three of these cities are shown in Figure 6-7 (a), (b) and (c), respectively. In an overall sense, it can be observed that the calculated UHS for almost all cities showed a closer match with that obtained from NRCan earthquake hazard calculator as given in Figure 6-7. Thus, the source model codes retrieved from Treviallen Git hub repository (Allen, 2021) was considered suitable for confidently using in the present study for predicting PSHA-based permanent ground displacements deployed from an OQ platform.

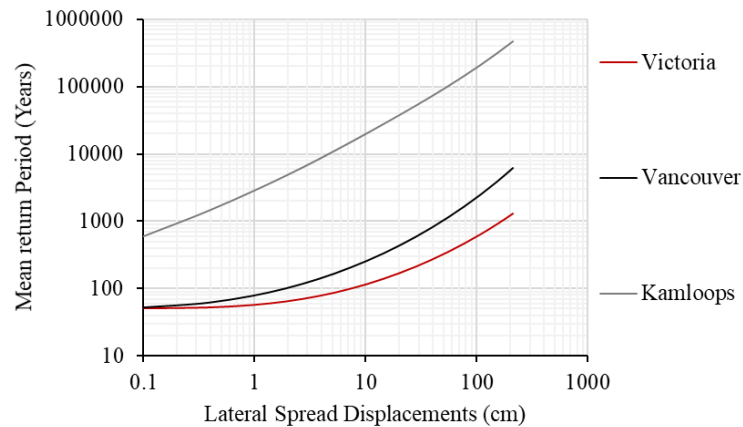
6.4.3 Attenuation model for calculating lateral spread displacement hazard as the intensity measure type

As described above, the primary aim herein is to develop lateral spread curves using Youd et al. (2002) MLR model for the SWCan component by performing PSHA analysis using OQ platform. As the first step, the Youd et al. (2002) MLR lateral spread displacement (PGD) equations were embedded in the OpenQuake platform – essentially as the “attenuation model” - for use in place of the GMPEs usually employed for prediction of the ground shaking intensity hazard. The equations for both “sloping ground” and “free-face” conditions as per the Youd et al. (2002) was embedded. In this process, using the developer version of OQ, the code for Youd et al. (2002) model was developed and included in the hazard library. For a given set of “reference” soil properties ($T_{15} = 15$ m, $F_{15} = 5\%$, $D_{50_{15}} = 0.3$ mm, $S = 6\%$, $W = 20\%$), analysis was performed and PGD curves were obtained for the same three cities considered for the verification of source model codes. It is also of relevance to note that, as per Youd et al. (2002), the lateral spread PGDs manifested in the field are expected to lie within a factor of 2 of the predicted displacements. The error contributions from different sources of uncertainties such as seismic loading, soil parameters, topographic parameters, etc., are quantified in one term – e.g., model error as reported by Franke and Kramer (2014) as $\sigma_{\log(\text{PGD})} = 0.197$.

The lateral spread displacement hazard curves obtained from this analysis (with specifically selected reference topographic and geotechnical parameters as per above) for sloping ground and free-face conditions are as shown in Figure 6-8 (a) and (b), respectively. It can be observed that the sites in coastal region have higher probability of occurrence of lateral spread hazard than sites in interior region. This can be attributed to the closer proximity of the coastal region to subduction interface and intra-slab earthquakes than the interior region that are primarily subjected to shallow crustal earthquakes. Thus, it is evident that the approach of performing PSHA analysis such that PGD is directly obtained as the measure of intensity [as per Figure 6-8 (a) and (b)] enables the user to have better clarity on the cause of level of hazard.



(a)



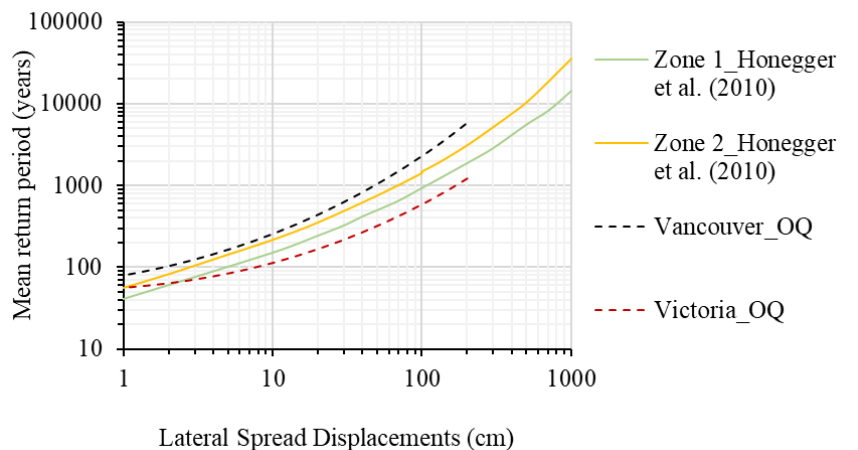
(b)

Figure 6-8: Lateral spread hazard curves obtained from PSHA in OpenQuake for selected cities for (a) Sloping ground, and (b) free-face conditions ($T_{15}=15$ m, $F_{15}=5\%$, $D_{5015}=0.3$ mm, $S=6\%$, $W=20\%$)

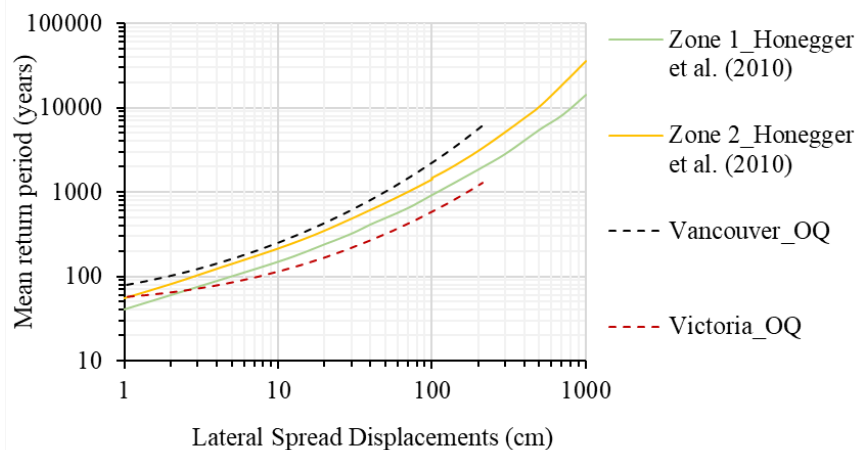
6.4.4 Comparisons with Previous Similar PGD Hazard Predictions

There is no already established bench-mark-type PGD hazard curves to conduct a direct validation of the proposed method. However, it was realized that it would be of relevance to compare the PGD hazard curves generated from the proposed framework above with similar predictions that have been made for the geographic area in the past. In this regard, the PGD predictions made by Honegger et al. (2010) for the BC Region, as a part of a study undertaken to assess the vulnerability of the local natural gas pipeline system, were considered suitable for comparisons while being mindful that the predictions by Honegger et al. (2010) were made using NBCC 2005 model (the 4th generation NBCC model). They provided a “reference” lateral spreading hazard versus probability for three selected geographic zones (called Zones 1 through 4) in the Greater Vancouver and Vancouver Island area – i.e., not for specific cities. It was observable that Victoria is located in the Zone 1 of Honegger et al. (2010); similarly, it was noted that Vancouver is in Zone 2. Based on this, it was judged reasonable to compare the hazard predictions made for Victoria and Vancouver in the present study with those from Honegger et al. for Zone 1 and Zone 2,

respectively, as depicted in Figure 6-9 - Note: Figure 6-9 (a) for the case of “sloping ground” and Figure 6-9 (b) for that corresponding to “free-face” condition. The curves obtained from the current analysis are slightly higher in terms of risk as that of Honegger et al. (2010). The slightly higher PGD prediction for a given risk level is considered meaningful since the ground shaking intensities in the newer NBCC 2015 model are more than those in the NBCC 2005 seismic model used by Honegger et al. (2010) predictions. However, in an overall sense, the PGD predictions made by the current model seems to be in good agreement with those from Honegger et al. (2010) for the same region.



(a)



(b)

Figure 6-9: Comparison of lateral spread hazard curves obtained from PSHA in OpenQuake with those from Honegger et al. (2010) for selected cities for (a) Sloping ground, and (b) free-face conditions ($T_{15}=15$ m, $F_{15}=5\%$, $D_{5015}=0.3$ mm, $S=6\%$, $W=20\%$)

6.4.5 Proposed base-line PGD hazard curves for South-west British Columbia

Based on the information available (Personal communications with Dr. Bhuyan Gouri, BCOGC), 14 cities/areas in BC for which the estimation of lateral spread hazard would be of relevance for BCOGC use. Therefore, Openquake analysis were performed to obtain lateral spread displacement

(PGD) curves for the following selected cities as shown in Figure 6-10, viz., Victoria, Nanaimo, Vancouver, Squamish, Hope, Merritt, Kamloops, Kelowna, Nelson, Prince George, Kitimat, Prince Rupert, Fort St. John's, Fort Nelson. The obtained PGD curves for these cities under sloping ground and free-face conditions are as shown in Figure 6-11 (a) and (b), respectively. It can be observed that, the level of hazard reduces as the location of interest moves from the coastal areas to the interior - e.g., from Victoria to Hope. As these curves have been obtained for specific set of base-line site soil and topographic parameters, they are referred as base-line curves which would be used for obtaining site-specific lateral spread displacements for general conditions as discussed in the later section.

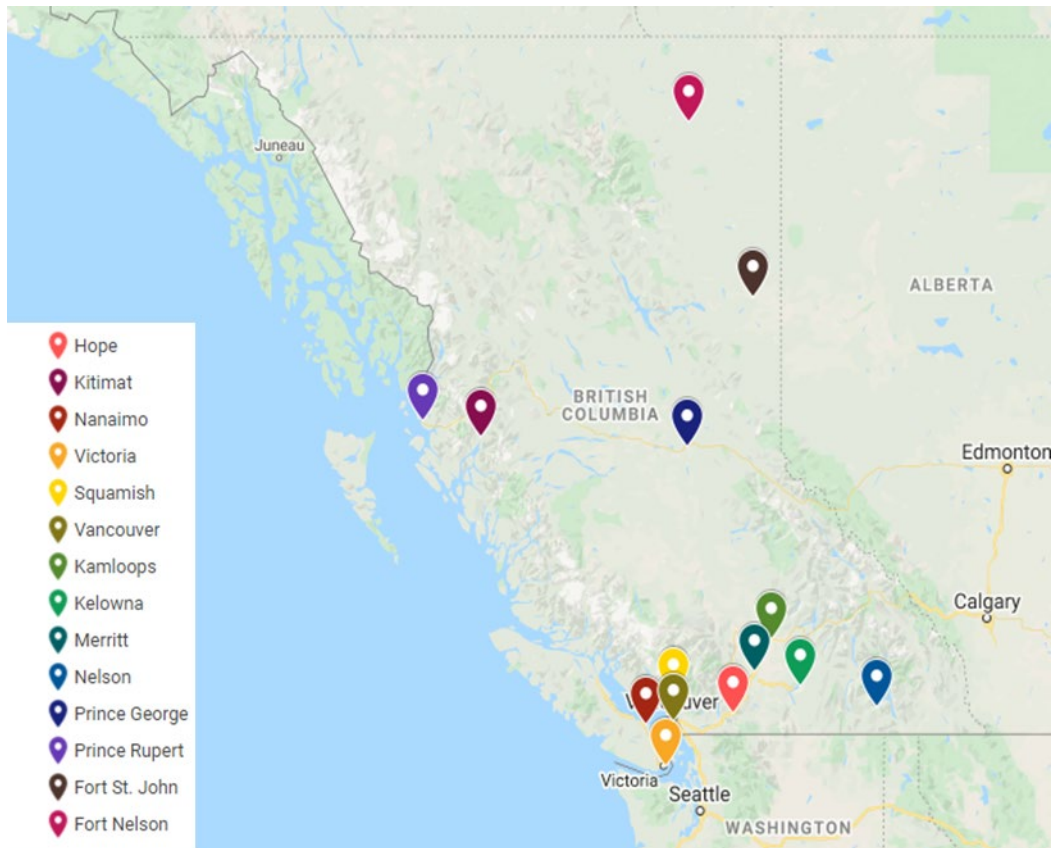


Figure 6-10: Cities in southwestern component of Canada with BCOGC sites

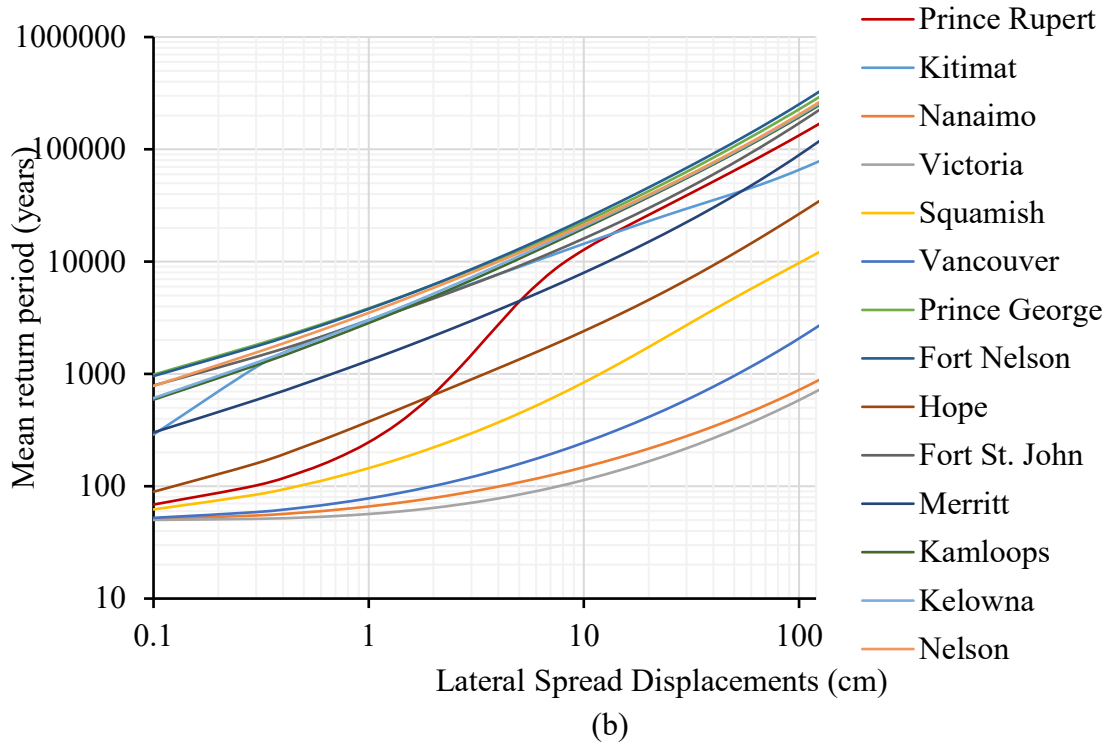
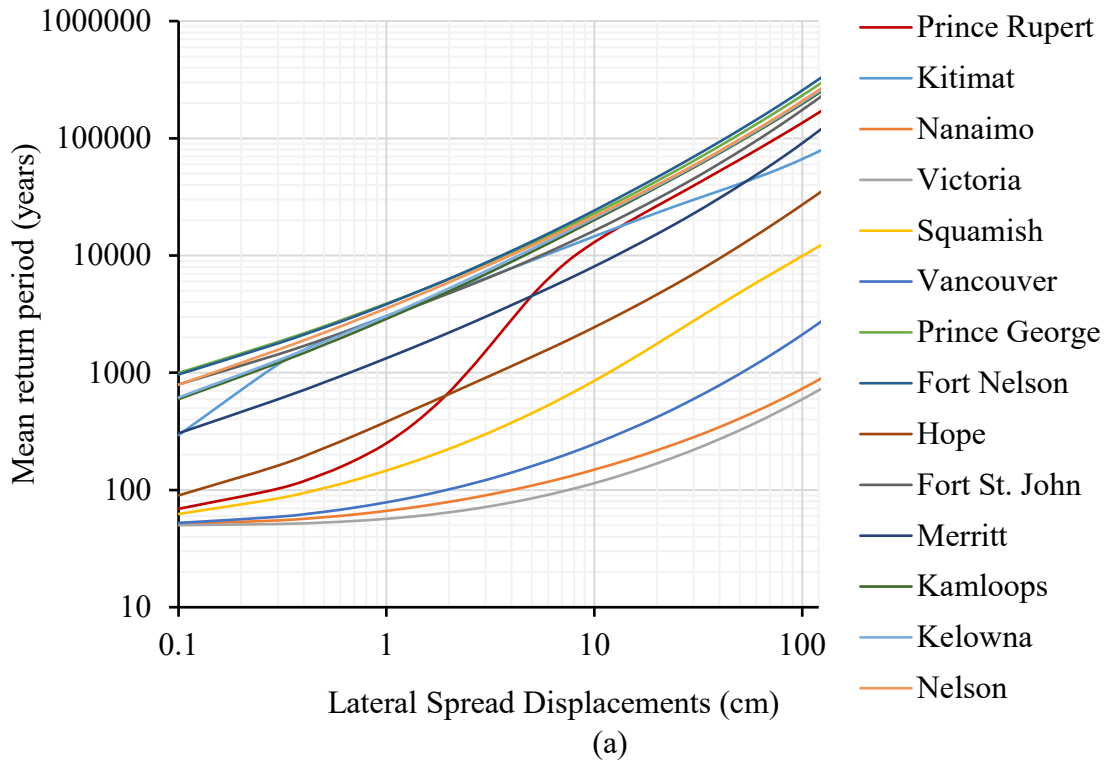


Figure 6-11: Lateral spread hazard curves obtained from PSHA in OpenQuake for BCOGC sites for (a) Sloping ground, and (b) free-face conditions (T15=15 m, F15=5%, D5015=0.3 mm, S=6 %, W=20%)

6.4.6 Estimation of site-specific PGD Hazard

As noted earlier, the predictions of ground displacements given in Figure 6-9, have been developed assuming a certain “reference” topographic and geotechnical parameters. At a particular site, for the same set of seismic sources, the relationships (Ekstrom and Franke, 2016; Honegger et al., 2010) given in Equations 6-3 and 6-4 can be used to obtain lateral spread displacements for free-face and ground slope configurations, respectively, when the topographic and geotechnical parameters corresponding to the site differ from the baseline parameters.

$$\frac{(PGD_{site})}{(PGD_{ref})} = \frac{10^{C+0.592LogW+0.540LogT_{15}+3.413Log(100-F_{15})-0.795Log(D50_{15}+0.1)}}{10^{C+0.592Log20+0.540Log15+3.413Log(100-5)-0.795Log(0.3+0.1)}} \quad 6-3$$

$$\frac{(PGD_{site})}{(PGD_{ref})} = \frac{10^{C+0.338LogS+0.540LogT_{15}+3.413Log(100-F_{15})-0.795Log(D50_{15}+0.1)}}{10^{C+0.338Log6+0.540Log15+3.413Log(100-5)-0.795Log(0.3+0.1)}} \quad 6-4$$

The idea was to obtain the PGD factor for the value of site parameter and then use it to calculate the lateral displacements corresponding to a particular hazard level. The present study proposes to use simplified procedure for calculating site-specific lateral spread displacements using the PGD curves developed using baseline parameters. The applicability of the simplified procedure would depend upon the uncertainties associated with the empirical predictive relationship [i.e., whether Youd et al. (2002) or other future method to be used]. Although seismic parameters would not change for the site under consideration, the change in site geotechnical and topographic parameters would alter the attenuation model. Hence, it is important to check if the hazard level for the base-line curve also stands applicable once the site parameters are altered. This would depend upon the type of sources and associated seismicity. Although, Ekstrom and Franke (2016) from their study have shown insignificant difference between displacements predicted using PSHA and simplified procedure, still it would vary for contribution from different sources. In view of this, for all the sites, by varying the site geotechnical and topographic parameters, displacements were obtained from both PSHA as well as simplified procedure using Equations 6-3 and 6-4 and are as shown in Figure 6-12. It can be observed that there is negligible variation and hence simplified procedure is proposed to be adopted. Following example would show the use of proposed curves for estimating site-specific lateral spread displacements.

Example: Lateral spread displacement hazard is expected for a site in Delta corresponding to hazard level return period of 500 years. If the soil and topographical parameters of the site are: $T_{15}=3$ m, $F_{15}=15$, $D50_{15}=0.5$ mm, $S=3$ %, calculate the corresponding lateral spread displacements expected on site.

PGD from base-line curve corresponding to return period as 500 years is 55 cm. The PGD factor is 0.1644 and the site-specific lateral spread displacements are 9 cm.

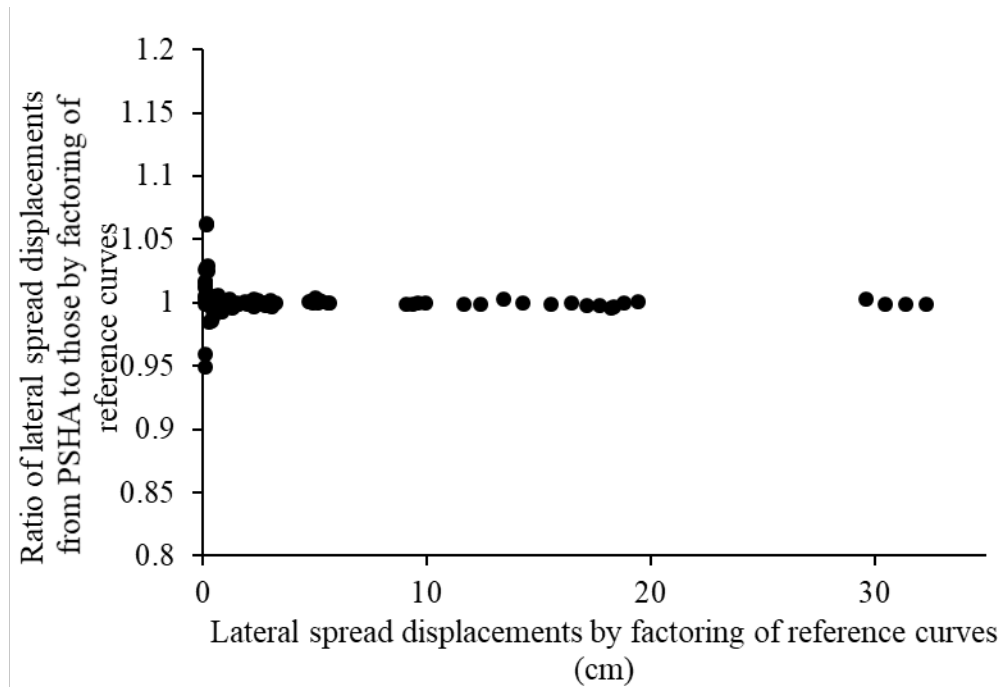


Figure 6-12: Figure showing negligible difference between lateral spread displacements obtained from PSHA and that by factoring of base-line curves

Using the base-line curves given in Figure 6-11 and varying the soil/ topographical parameters, the lateral spread displacements obtained corresponding to 75, 100, 200, 300, 500, 1000, 2500 and 5000 years have been provided for all the BCOGC sites as the input for training BBN model. It can be understood that instead of assuming the values of M-R values in the calculation of lateral spread displacements, the obtained displacement values from the performed PSHA analyses are more meaningful and reliable for the sites under consideration within the vicinity of sites considered in the present study. It is believed that the reliability of the BBN model would depend on the input datasets used for training it; and hence, the BBN model based on the provided datasets is expected to give meaningful predictions of PGDs for the BCOGC sites. Further, implementation of the developed code in OQ platform is presently under progress; which, then can be used for training the BBN model for a broader database.

6.5 Task 2 - Conduct a literature review specifically on the structural capacity of corroded pipelines

Appropriate datasets are the key inputs that govern the performance of BBN model. A detailed literature review was performed to explore different studies undertaken globally to understand the influence of corrosion on the performance of pipelines subjected to ground displacements, such that the pressure integrity of these buried pipelines are retained. The idea was to identify different research groups involved in working on this multi-hazard problem; so that the data/ results reported

can be evaluated for usage in better training the BBN model. The observations reported from different studies are given in the Table A1 in Appendix.

6.6 Estimation of Preliminary PGD Capacities of Buried Pipelines

When the buried pipeline experiences ground displacements, strains will be induced in the pipeline. The ground displacements can be characterized by the dimensions of the lateral spread zone and magnitude of the ground displacements. The orientation of this pipeline with respect to the direction of ground movement would govern the mode of failure in this pipeline. The longitudinal and transverse ground displacement capacities of the pipelines assessed based on the mechanisms shown in Figure 6-13 have been considered for this study. Buried pipelines will have different components, viz., straight pipe segments, T-section, elbow sections and so on. In this study, the focus is on straight pipe segments only. Further, the pipelines are susceptible to different types of pitting corrosion patterns, viz., single pit, multiple non-interacting pit clusters and multiple interacting pit clusters. In this project, as the corrosion group have developed model for estimating corrosion rates considering uniform reduction in the thickness of the buried pipelines, the PGD capacities have been estimated for equivalent reduced thickness only.

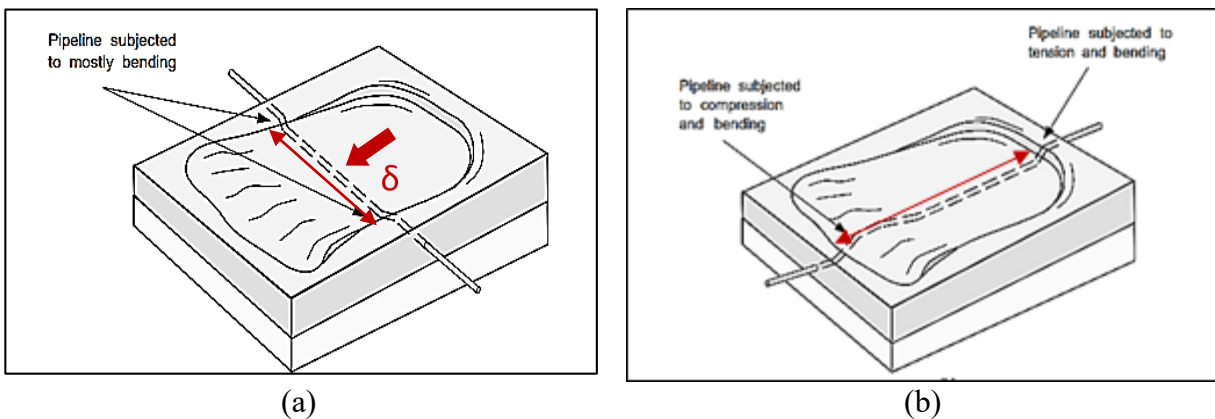


Figure 6-13: Pipeline subjected to (a) transverse ground movement and (b) longitudinal ground movement

6.6.1 Task 3 - Estimation of Preliminary PGD Capacities of intact Buried Pipelines

6.6.1.1 Estimation of longitudinal PGD capacities

When a buried pipeline is subjected to longitudinal ground displacements, the pipeline experiences tension on one end of the lateral spread zone and compression at the other end of this zone as shown in Figure 6-14. The buried pipeline offers resistance to the longitudinal/ axial ground displacements as a result of the frictional forces developed along the length of the pipeline to accommodate the ground displacements.

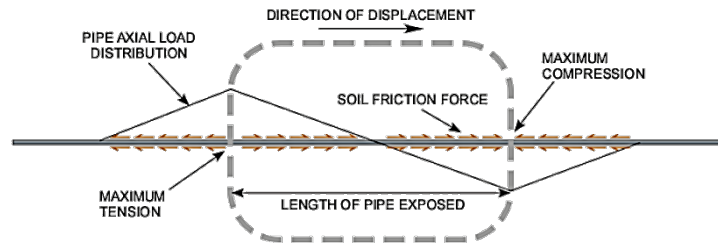


Figure 6-14: Load distribution on pipe subjected to axial ground movement

Although, this length of the pipeline would depend upon the pipeline alignment, it is important to ensure that the length of the pipeline is sufficient enough to accommodate the ground displacements as well as provide the required anchorage outside the zone of ground movement. This equivalent anchor length of the pipe, L_{EA} , can be obtained by equating the axial forces due to the axial soil restraint force acting along this length, L_{EA} , with the axial force corresponding to the axial stress of 110% of the minimum specified yield strength.

$$L_{EA} = \frac{1.1\pi Dt\sigma_y}{T_u} \quad 6-5$$

where D = outer diameter of pipe, t = pipe wall thickness, T_u = maximum axial soil restraint, and σ_y = minimum specified yield strength. The equivalent length, L_{EA} is the length required for the soil restraint force, T_u , to induce axial yield in the pipeline. Based on the length of PGD zone, relative to this L_{EA} , following cases are possible.

Case A: length of lateral spread zone $< 2 L_{EA}$

In this case, the probability of failure due to axial PGD is considered 0%.

Case B: length of lateral spread zone $> 2 L_{EA}$

This condition signifies that the soil restraint forces, T_u , acting along the length, L_{EA} , would result in yielding and that the pipe would have negligible additional capacity. Under such circumstances, the probability of failure would depend upon the likelihood that the length of PGD zone is actually greater than $2 L_{EA}$ and that the axial displacements induced are greater than the maximum displacements induced due to tension and compression at the ends of the PGD zone. The evaluations for probability of lateral spread displacements being greater than $2 L_{EA}$ are performed based upon the interpretations of historical lateral spread hazard given in Figure 6-15. Further, for yield strain of 0.5% assuming triangular distribution for axial soil restraint forces, the axial pipe displacement capacities, D_{Amax} , have been estimated using Equation 6-6.

$$D_{Amax} = 0.005L_{EA} \quad 6-6$$

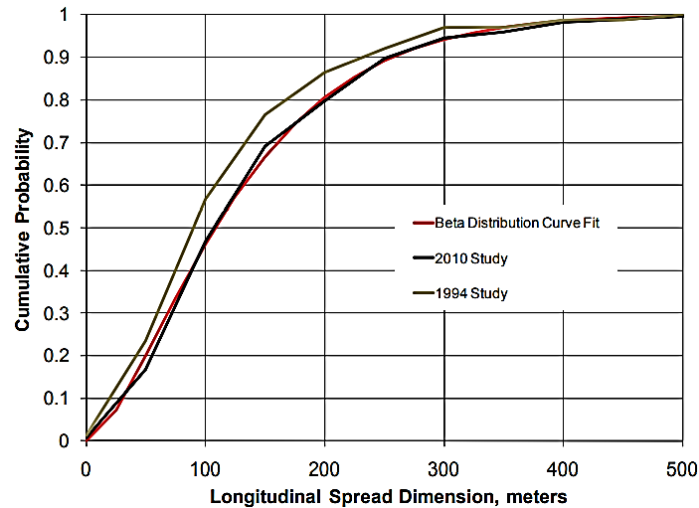


Figure 6-15: Comparison of longitudinal lateral spread dimensions from review of historical data and closed-form approximation

6.6.1.2 Estimation of transverse PGD capacities

A buried pipeline when subjected to transverse PGD would stretch and bend to accommodate the transverse ground displacements. Under this scenario, the failure mode will be governed by the relative amount of axial tension and flexural/bending strain. The pipeline would rupture due to the combined effects of the axial tension and flexure, if axial strains in pipe are considerable; whereas, if the axial strains are low, the pipeline may buckle in compression due to excessive bending.

For a project by FortisBC (Terasen 2010), Honneger et al. (2010) performed the FE analyses on the several cases of pipe configurations subjected to transverse abrupt PGD, and in order to obtain % strains corresponding to different magnitudes of PGDs for a project. Further, based on past experience and professional judgement, Table 6-1, showing correlation between the induced longitudinal strain and failure probability was also provided. For the present study, the PGD capacities for the intact pipelines were decided to be obtained from this report, as it is judged from the previous meetings with the project team (project progress meeting dated February 22, 2021) that this data would be suitable for initial training of the BBN model. It is also noted that Dr. Wijewickreme was a team member of the project that led to this report. As noted in the last progress meeting, since this report provides GD capacities for many pipe sizes, it is judged that this data shown in Table 6-2 would be appropriately suitable for initial training of the BBN model. However, before providing this data as an input to the BBN model, we decided to perform limited review of this data to confirm the suitability.

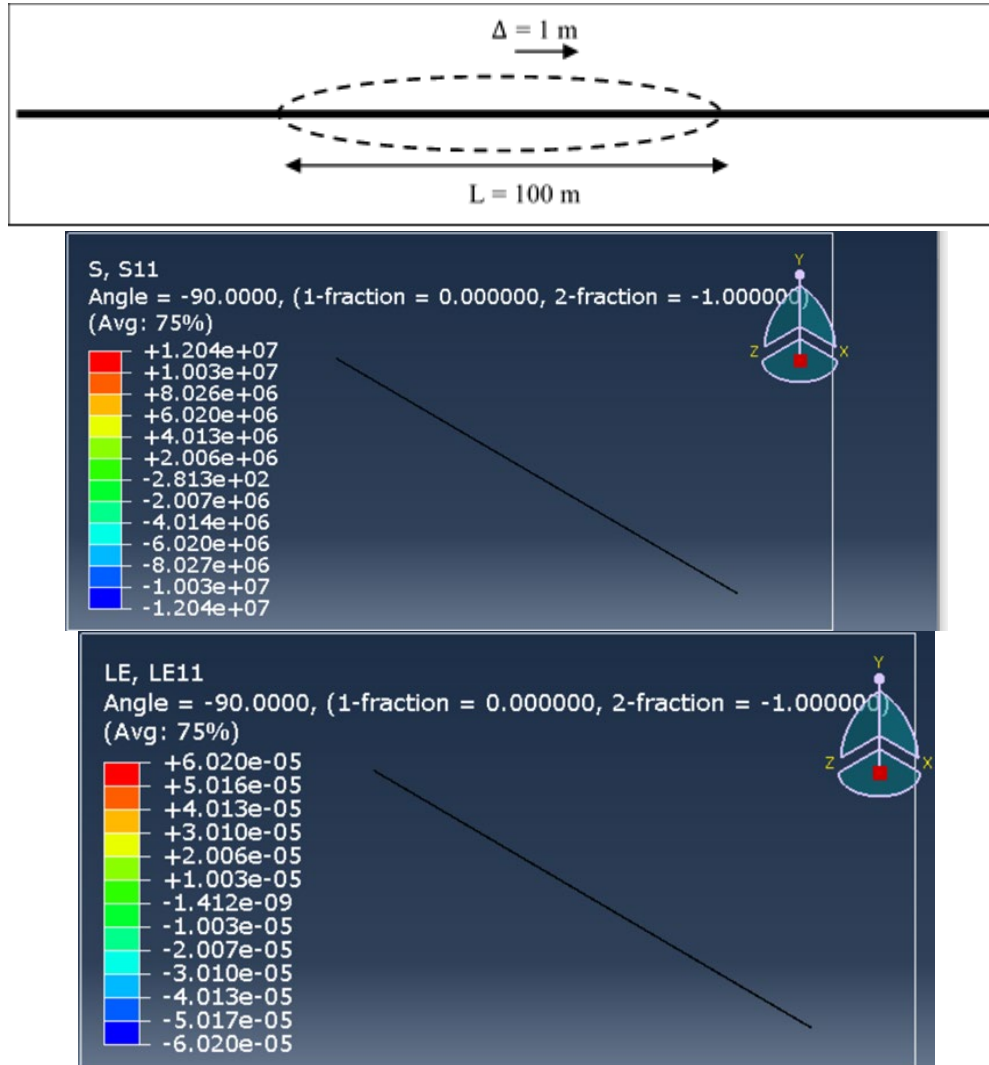
Table 6-1: Pipeline Failure Probability and Bending Tension Strain

Bending Tension Strain	Probability of Failure
Less than 0.5%	0%
0.5% to 1.5%	10%
1.5% to 3.5%	25%
3.5% to 5.5%	50%
Greater than 5.5%	100%

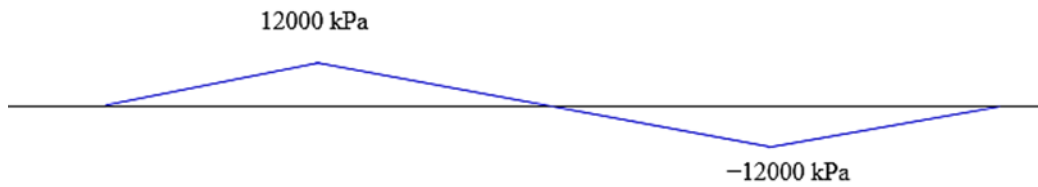
Table 6-2: Pipeline Perpendicular Displacement Capacities for Straight Pipe

NPS Size	Displacement to Exceed Listed Strain Level (m)				
	0.5%	1.0%	2.5%	4.5%	5.5%
4	0.2	1.4	4.2	4.2	4.2
6	0.2	0.9	2.8	2.8	2.8
8	0.4	3.9	4.9	4.9	4.9
12	0.8	5.5	7.0	7.0	7.0
16	0.4	0.9	6.2	7.0	7.0
18	0.4	0.5	6.3	6.3	6.3
20	0.5	1.0	7.0	7.0	7.0
24	0.6	1.2	7.0	7.0	7.0
30	0.7	1.4	7.0	7.0	7.0
36	0.8	1.5	5.9	7.0	7.0
42	1.0	1.8	7.0	7.0	7.0

The non-linear FE analyses using large deformation theory of buried pipeline were performed using ABAQUS software (Smith, 2018). The pipe was modeled using PIPE31 elements with 6 degrees of freedom that can account for the effect of stresses due to internal pressure of fluid. The pipe has been modeled using deformation plasticity model in ABAQUS with Ramberg-Osgood parameters (Walker and Williams, 1995). Soil in the vicinity of the pipe was modeled using equivalent discrete 3-D soil springs, and hence, the pipe-soil interaction can be represented by the force-displacement “soil springs” in the axial, horizontal (lateral), and vertical direction, connected to the nodes of the pipe elements. These soil spring representations are typically bi-linear and hence, are described by two parameters, viz., soil restraint forces in N/m and the relative displacement between pipe and soil necessary to mobilize these forces. The values for these soil springs are obtained either experimentally or from the guidelines viz., PRCI (2009b). These springs are modeled using PSI34 elements, which have only one degree of freedom of displacement. Two nodes of the PSI34 are same as that of pipe element and the other two nodes are on the other side representing far-field surface, on which the boundary conditions are imposed. The anchor points are modelled far from the edges of the PGD zone and were fixed. The bases of the soil springs outside of the PGD zone were fixed whereas those within the PGD zone were applied the ground displacements.



Axial stress distribution along the Pipe



Axial strain distribution along the Pipe

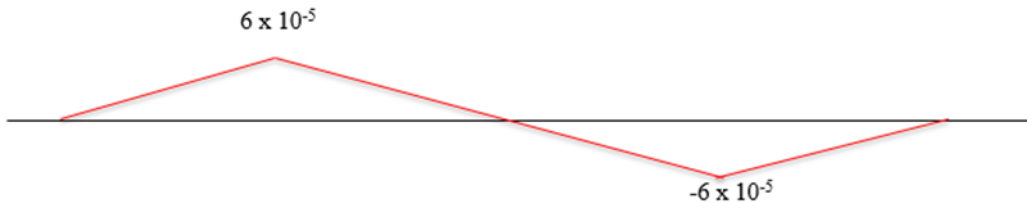


Figure 6-16: Details of FE model of pipe developed in ABAQUS and the obtained results from analyses

In view of validating the model, a 600 m long X42 steel pipe ($D = 0.762\text{ m}$, $t = 0.0105\text{ m}$, NPS 30 where NPS means Nominal Pipe Size) subjected to lateral spread displacements of 1 m in

longitudinal direction was simulated. The lateral spread zone width modeled was 100 m. Soil restraint forces were calculated for soil with parameters, $\phi' = 32^\circ$, $\gamma = 18 \text{ kN/m}^3$. The obtained stress-strain values were compared with the closed form analytical solutions as shown in Figure 6-16; the numerical outcomes matched well, thus, confirming the suitability of the model.

Using this model, the strains induced in the buried pipeline were obtained by exerting the pipeline to transverse displacements of 7 m as mentioned in the report. The variation in the strains with respect to the ground displacements were obtained for three NPS sizes viz., NPS 12, NPS 20 and NPS 30. The values obtained are reported in the Table 6-3. It can be observed that the obtained values are aligned with those mentioned in the report.

Table 6-3: Comparison of PGDs corresponding to different strain levels from the FE model with those reported in Terasen (2010)

		FE model (m)	Terasen (2010) (m)
NPS 30	0.50%	0.9	0.7
	1%	1.8	1.4
	>1%	7	7
NPS 12	0.50%	0.65	0.7
	1%	1m-5m	5.5
	>1.5%	7	7
NPS 20	0.50%	0.9	0.5
	1%	1.4	1
	>1.5%	7	7

6.6.2 Task 4 - Estimation of Preliminary PGD Capacities of Corroded Buried Pipelines

6.6.2.1 Estimation of Preliminary longitudinal PGD capacities of corroded pipelines

The steps/ procedure mentioned for intact pipelines was adopted for corroded pipelines. The LEA and the corresponding D_{Amax} have been calculated for the X60 pipeline for different pipe sections viz., NPS 4, 8, 12, 24, 30 and 42. The soil parameters considered for the estimation of the soil restraint forces, T_u , are $\gamma = 18 \text{ kN/m}^3$, $\phi = 32^\circ$, $K = 0.6$ (for pipe coated with FBE) and burial depth of 1 m. The longitudinal PGD capacities for intact pipelines for the considered case are given in the provide excel sheet. For each of these cases, considering 10%, 20%, 30%, 40% and 50% reduction in thickness due to the corrosion, the LEA and the D_{Amax} computed are given in the datasheet. It can be observed that, with the decrease in the thickness of the pipe due to corrosion, the anchor length required for resisting the PGDs require the PGD capacities to withstand the longitudinal ground movement. Thus, as a result of the reduction in the thickness due to the corrosion, there is increase in the probability of exceeding the reduced the anchored length and reduced longitudinal PGD capacities.

6.6.2.2 Estimation of Preliminary transverse PGD capacities of corroded pipelines

It was realized that performing FE analyses for several cases with reduced thickness due to corrosion is beyond the scope of this study. In view of this, it was decided to explore and examine existing analytical methodologies and their applicability for estimating PGD capacities of corroded pipelines. Further, based on the analyses using analytical models the idea was to develop modification factors which can be directly applied to the PGD capacities of the intact pipelines.

Liu and O’ Rourke (1997) have proposed analytical expressions for estimating strains in the pipe corresponding to different values of PGDs. According to this model, the pipe is modeled elastic and is subjected to PGD following cosine wave function over the lateral spread zone as shown in Figure 6-17. According to Liu and O’ Rourke (1997), during PGD, the pipe displaces by same magnitude as that of ground up to certain magnitude of PGD, known as critical displacements δ_{cr} , beyond which, the strains induced in the pipe are nearly constant and there is relatively lesser increase in the pipe displacements.

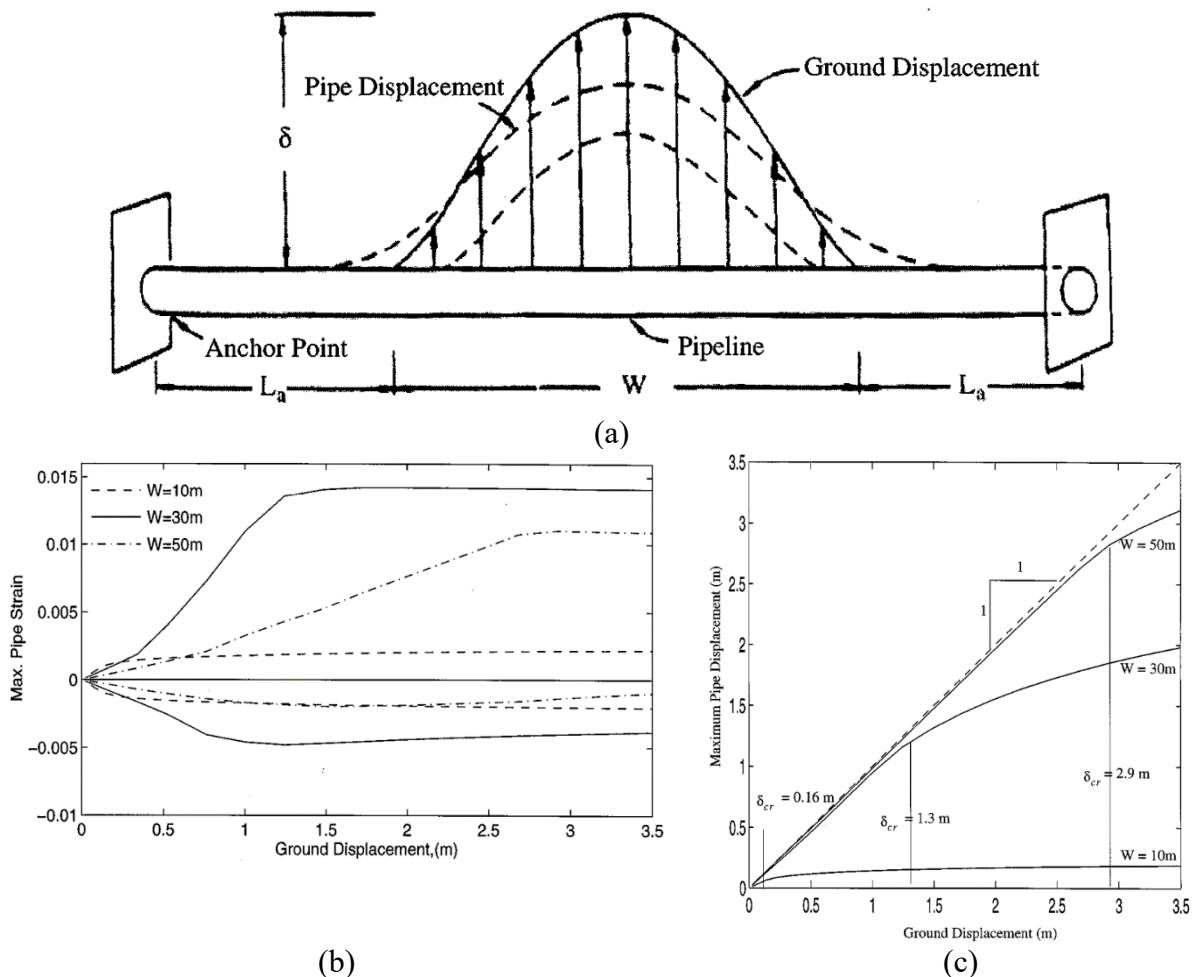


Figure 6-17: Physical model of pipeline and soil deformation (after T. O’Rourke) and the obtained results (after Liu and O’ Rourke 1997)

Based on this theory, Liu and O' Rourke (1997) proposed the following expressions to estimate the critical displacements, δ_{cr} , which accounts for the flexural (beam) as well as axial (cable) effects. As δ_{cr} represents ground displacements beyond which the pipe cannot match the ground displacements, these are also referred as PGD_T. Along the similar lines, they proposed the expressions for estimating maximum strains in the elastic pipe due to combined effects of axial tension and flexural bending. These equations were embedded in matlab code given in Appendix B to obtain longitudinal strain versus ground displacements for all the NPS sizes.

$$\delta_{cr} = \frac{1}{\frac{1}{\delta_{cr-bending}} + \frac{1}{\delta_{cr-axial}}} \quad 6-7$$

$$\delta_{cr-bending} = \frac{p_u W^4}{384 EI} \quad 6-8$$

The following two Equations 6-9 and 6-10 are solved to obtain, $\delta = \delta_{cr-axial}$,

$$T = \pi D t \sigma = \frac{p_u (W/2)^2}{8(\delta/2)} = \frac{p_u W^2}{16\delta} \quad 6-9$$

$$\frac{\pi^2 \delta^2}{4W} = \frac{\sigma W}{E} + 2 \frac{\pi D t \sigma^2}{2E t_u} \quad 6-10$$

Further, using Equation 6-11, the strains can be computed as a function of displacements,

$$\varepsilon_{elastic} = \begin{cases} \frac{\sigma}{E} \pm \frac{\pi^2 \delta D}{W^2} & \delta \leq \delta_{cr} \\ \frac{\sigma}{E} \pm \frac{\pi^2 \delta_{cr} D}{W^2} & \delta > \delta_{cr} \end{cases} \quad 6-11$$

$$\text{where, } \frac{\sigma}{E} = \begin{cases} \frac{\pi \delta}{2} \cdot \sqrt{\frac{t_u}{AEW}} & \delta \leq \delta_{cr} \\ \frac{\pi \delta_{cr}}{2} \cdot \sqrt{\frac{t_u}{AEW}} & \delta > \delta_{cr} \end{cases}$$

In these expressions, W represents the width of PGD zone as shown in Figure 6-17, which in this study was considered 100 m. D , t , A and I represent cross-sectional properties of the corresponding NPS pipe section, viz., diameter, thickness, area and area moment of inertia, respectively. E represents Young's modulus of steel pipe considered as 210 GPa. P_u and T_u represents lateral soil restraint forces and axial soil restraint forces, respectively. In the present study, the values for the soil restraint forces have been calculated using those from PRCI (2009) guidelines for soil with internal friction angle, 32° , unit weight of 18kN/m^3 and pipe burial depth of 1 m. It is to be noted that the soil parameters need to be updated to represent the site-specific conditions as required.

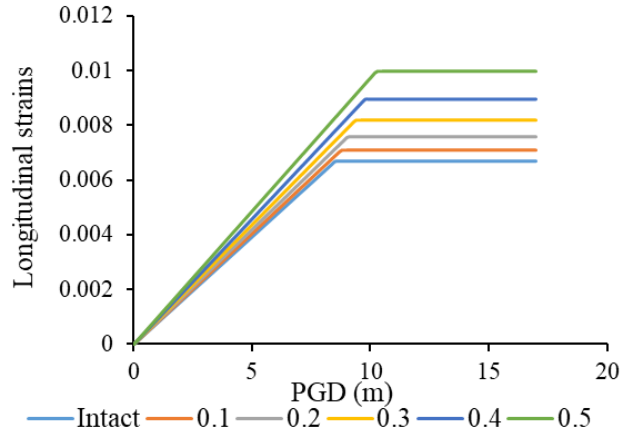


Figure 6-18: Variation of longitudinal strains with permanent ground displacements for NPS 12 pipe for different levels of corrosion using analytical model

Table 6-4: Modification factors to account for corrosion for different pipe sizes using analytical model

NPS 4					
% Corrosion	D (m)	t (m)	δ_{cr} (m)	Strain	Factor
0%	0.102	0.0054	11.6	0.007	1.000
10%	0.101	0.0049	12.0	0.008	0.960
20%	0.099	0.0043	12.4	0.008	0.916
30%	0.098	0.0038	12.8	0.009	0.867
40%	0.097	0.0032	13.3	0.010	0.813
50%	0.096	0.0027	14.0	0.011	0.753

NPS 24					
% Corrosion	D (m)	t (m)	δ_{cr} (m)	Strain	Factor
0%	0.610	0.0071	7.6	0.008	1.000
10%	0.608	0.0064	7.8	0.009	0.978
20%	0.607	0.0057	8.0	0.009	0.953
30%	0.605	0.0050	8.3	0.010	0.924
40%	0.604	0.0043	8.7	0.011	0.890
50%	0.603	0.0036	9.1	0.012	0.850

NPS 8					
% Corrosion	D (m)	t (m)	δ_{cr} (m)	Strain	Factor
0%	0.203	0.0055	9.6	0.007	1.000
10%	0.202	0.0050	9.9	0.007	0.965
20%	0.201	0.0044	10.2	0.008	0.926
30%	0.200	0.0039	10.6	0.009	0.882
40%	0.199	0.0033	11.0	0.009	0.834
50%	0.198	0.0028	11.6	0.011	0.778

NPS 30					
% Corrosion	D (m)	t (m)	δ_{cr} (m)	Strain	Factor
0%	0.762	0.0105	6.6	0.008	1.000
10%	0.760	0.0095	6.8	0.008	0.983
20%	0.758	0.0084	7.0	0.009	0.964
30%	0.756	0.0074	7.3	0.009	0.941
40%	0.754	0.0063	7.7	0.010	0.914
50%	0.752	0.0053	8.1	0.011	0.880

NPS 12					
% Corrosion	D (m)	t (m)	δ_{cr} (m)	Strain	Factor
0%	0.305	0.0064	8.5	0.007	1.000
10%	0.304	0.0058	8.8	0.007	0.970
20%	0.302	0.0051	9.0	0.008	0.936
30%	0.301	0.0045	9.4	0.008	0.898
40%	0.300	0.0038	9.8	0.009	0.854
50%	0.298	0.0032	10.3	0.010	0.804

NPS 42					
% Corrosion	D (m)	t (m)	δ_{cr} (m)	Strain	Factor
0%	1.067	0.0091	6.6	0.010	1.000
10%	1.065	0.0082	6.9	0.011	0.985
20%	1.063	0.0073	7.1	0.011	0.968
30%	1.061	0.0064	7.4	0.012	0.947
40%	1.060	0.0055	7.8	0.013	0.923
50%	1.058	0.0046	8.2	0.014	0.893

These curves were obtained for the reduced equivalent thickness of the pipe for each NPS size, to different levels of corrosion, viz., 10%, 20%, 30%, 40% and 50%. The typical curves obtained for NPS 12 are as shown in Figure 6-18. The magnitude of displacements resulting in same magnitude of strain can be observed to decrease with increase in corrosion. As the curve follows linear trend up to critical displacements, the modification factors were calculated as the ratio of displacement capacity for the corroded pipe to that of an intact pipe for a particular strain value. These modification factors for different levels of corrosion are given in Table 6-4.

Furthermore, in order to check if the factors can be applied to the PGD capacities for intact pipelines from Terasen (2010) report, for NPS 12, the ABAQUS analysis was performed for 20% and 40% reduction in thickness due to corrosion and the modification factors were obtained using the above-mentioned exercise. Figure 6-19 shows the variation of longitudinal strains with permanent ground displacements for NPS 12 pipe for different levels of corrosion from the FE analyses. The modification factors using the FE analyses were obtained. Slight deviation in the factors can be observed owing to the different set of boundary conditions than those considered in the analytical model. Liu and O'Rourke (1997) considered gradually applied transverse displacements following cosine wave pattern unlike Honneger et al. (2010), wherein abrupt displacements were applied. As a result, for Honneger (2010), the PGD capacity reduced further as the pipeline would show lower tendency to accommodate abrupt displacements. It was deduced that, the modification factor for abrupt displacements is ~ 0.86 times the factor obtained based on analytical model that considers gradual cosine wave displacement pattern. Further, the modification factors have been proposed for linear part of the curve only as prorating for higher displacements is beyond the scope as it will involve high non-linearity.

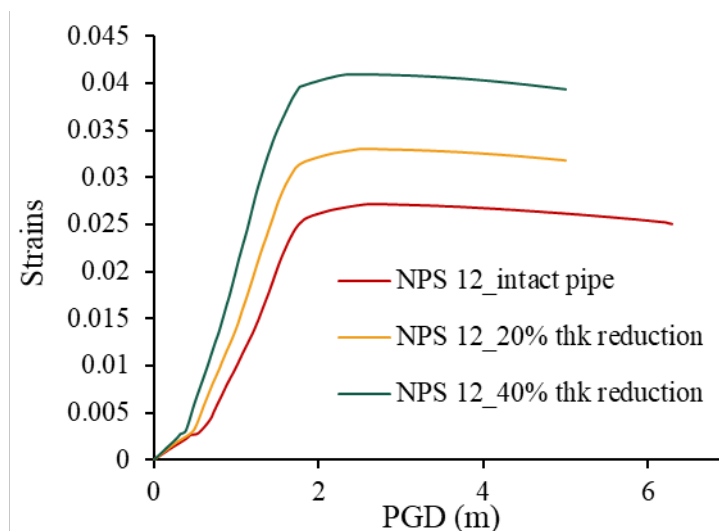


Figure 6-19: Variation of longitudinal strains with permanent ground displacements for NPS 12 pipe for different levels of corrosion using FE model

These modification factors, as given in given in Table 6-4, were applied to the PGD capacities for intact pipelines obtained from Terasen (2010) for different levels of corrosion. The resulting PGD capacities for corroded pipelines on this basis are given in the Table 6-5.

Table 6-5: Transverse PGD capacities for corroded pipelines for different NPS sizes

0% corrosion						30% corrosion					
NPS	PGDs corresponding to different strain levels					NPS	PGDs corresponding to different strain levels				
	0.50%	1.00%	2.50%	4.50%	5.50%		0.50%	1.00%	2.50%	4.50%	5.50%
4	0.2	1.4	4.2	4.2	4.2	4	0.1	1.0	3.1	3.1	3.1
6	0.2	0.9	2.8	2.8	2.8	6	0.2	0.7	2.1	2.1	2.1
8	0.4	3.9	4.9	4.9	4.9	8	0.3	3.0	3.7	3.7	3.7
12	0.8	5.5	7	7	7	12	0.6	4.2	5.4	5.4	5.4
16	0.4	0.9	6.2	7	7	16	0.3	0.7	4.8	5.4	5.4
18	0.4	0.9	6.3	6.3	6.3	18	0.3	0.7	4.9	4.9	4.9
20	0.5	1	7	7	7	20	0.4	0.8	5.5	5.5	5.5
24	0.6	1.2	7	7	7	24	0.5	1.0	5.6	5.6	5.6
30	0.7	1.4	7	7	7	30	0.6	1.1	5.7	5.7	5.7
36	0.8	1.5	5.9	7	7	36	0.6	1.2	4.8	5.7	5.7
42	1	1.8	7	7	7	42	0.8	1.5	5.7	5.7	5.7
10% corrosion						40% corrosion					
NPS	PGDs corresponding to different strain levels					NPS	PGDs corresponding to different strain levels				
	0.50%	1.00%	2.50%	4.50%	5.50%		0.50%	1.00%	2.50%	4.50%	5.50%
4	0.2	1.2	3.5	3.5	3.5	4	0.1	1.0	2.9	2.9	2.9
6	0.2	0.7	2.3	2.3	2.3	6	0.1	0.6	2.0	2.0	2.0
8	0.3	3.2	4.1	4.1	4.1	8	0.3	2.8	3.5	3.5	3.5
12	0.7	4.6	5.8	5.8	5.8	12	0.6	4.0	5.1	5.1	5.1
16	0.3	0.8	5.2	5.9	5.9	16	0.3	0.7	4.6	5.2	5.2
18	0.3	0.8	5.3	5.3	5.3	18	0.3	0.7	4.7	4.7	4.7
20	0.4	0.8	5.9	5.9	5.9	20	0.4	0.8	5.3	5.3	5.3
24	0.5	1.0	5.9	5.9	5.9	24	0.5	0.9	5.4	5.4	5.4
30	0.6	1.2	5.9	5.9	5.9	30	0.5	1.1	5.5	5.5	5.5
36	0.7	1.3	5.0	5.9	5.9	36	0.6	1.2	4.7	5.5	5.5
42	0.8	1.5	5.9	5.9	5.9	42	0.8	1.4	5.6	5.6	5.6
20% corrosion						50% corrosion					
NPS	PGDs corresponding to different strain levels					NPS	PGDs corresponding to different strain levels				
	0.50%	1.00%	2.50%	4.50%	5.50%		0.50%	1.00%	2.50%	4.50%	5.50%
4	0.2	1.1	3.3	3.3	3.3	4	0.1	0.9	2.7	2.7	2.7
6	0.2	0.7	2.2	2.2	2.2	6	0.1	0.6	1.8	1.8	1.8
8	0.3	3.1	3.9	3.9	3.9	8	0.3	2.6	3.3	3.3	3.3
12	0.6	4.4	5.6	5.6	5.6	12	0.6	3.8	4.8	4.8	4.8
16	0.3	0.7	5.0	5.7	5.7	16	0.3	0.6	4.3	4.9	4.9
18	0.3	0.7	5.1	5.1	5.1	18	0.3	0.6	4.5	4.5	4.5
20	0.4	0.8	5.7	5.7	5.7	20	0.4	0.7	5.0	5.0	5.0
24	0.5	1.0	5.7	5.7	5.7	24	0.4	0.9	5.1	5.1	5.1
30	0.6	1.2	5.8	5.8	5.8	30	0.5	1.1	5.3	5.3	5.3
36	0.7	1.2	4.9	5.8	5.8	36	0.6	1.1	4.5	5.3	5.3
42	0.8	1.5	5.8	5.8	5.8	42	0.8	1.4	5.4	5.4	5.4

6.7 Example calculation

An example has been presented in this section to estimate the lateral spread PGD demand, considering a selected site. The PGD has been computed and this demand is compared with the longitudinal and transverse displacement capacities of a pipeline NPS 12. This example has been

explained through the following two flow diagrams in Figure 6-20 for the two cases, wherein, the lateral spread displacement demand exceeds the longitudinal as well as transverse capacity of pipelines. The input parameters for the calculation of both demand and capacity are indicated in blue color whereas the output obtained following the steps mentioned in report (or referring to the data in shared datasheet) is given in green color.

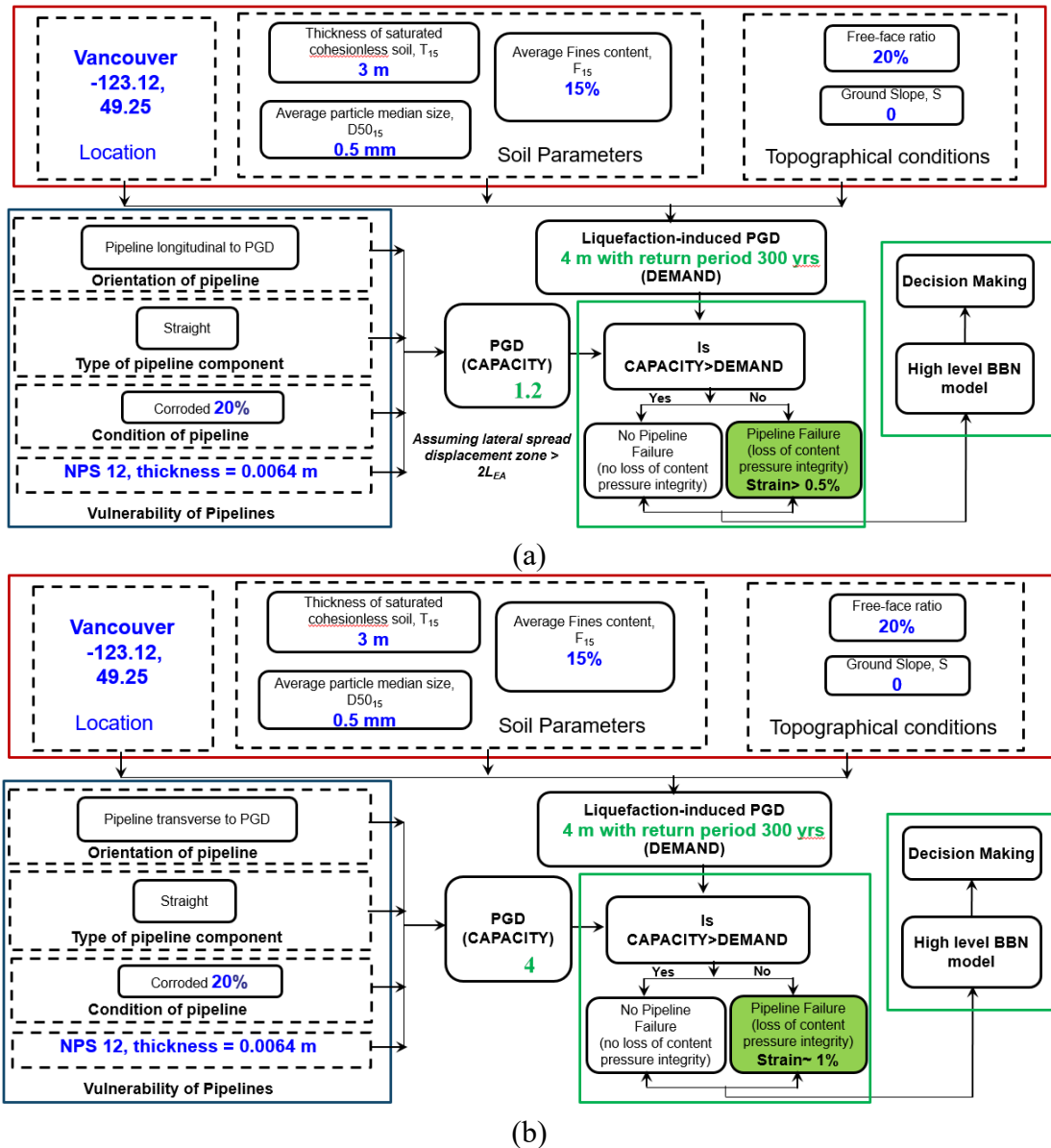


Figure 6-20: Flow diagrams explaining the example for the calculation of PGD demand and two cases of PGD capacities (a) longitudinal, and (b) transverse

The steps implemented for the calculated demand as well as capacity are discussed below:

Step 1: Estimation of lateral spread PGD demand

Input parameters:

Location: Vancouver (-123.12, 49.25)

Soil parameters: T15: 3 m, F15: 15%, D5015: 0.5mm

Topographical parameters: Free-face ratio: 20%

Return period: 300 years

Analyses: Using the curve for Vancouver for free-face conditions in Figure 6-11 (b) and using Equations 6-3 and 6-4, the site-specific lateral spread displacements can be calculated as 4 m.

Step 2: Estimation of preliminary PGD capacity of buried pipeline with corrosion

Input parameters:

Geometry: NPS 12 straight pipeline of thickness 0.0064 m and level of corrosion, 40%

Properties of soil surrounding the pipe: Unit weight 18kN/m³, Soil friction angle 38°, depth of cover 1m and soil-pipe interface friction angle =0.8 ϕ

Analyses:

Case 1- Estimation of longitudinal PGD: Using Equation 6-5 for the reduced thickness of pipe-section due to corrosion, the equivalent anchor-length, L_{EA} calculated is 278 m. Figure 6-15 can be referred to check if the size of lateral spread displacement zone is expected to be greater than $2L_{EA}$. As per section 6.1.1 and referring Figure 6-15, this belongs to case B, and the probability of lateral spread zone size exceeding $2L_{EA}$ is ~3%. Using Equation 6-6, the estimated PGD resulting in 0.5% yield strain is 1.2 m. Beyond yield strain, the pipeline would have negligible additional capacity [as assumed during Terasen (2010) study]. As the expected PGDs on site from step 1, i.e., 4 m, are greater than the longitudinal PGD 1.2 m, 0.5% yield strains would be induced in the pipe-section. Further, if desired for BBN modelling, the probability of failure can be considered 3% as the yield strains got induced as the size of lateral spread block exceeded $2L_{EA}$.

Case 2: Estimation of transverse PGD: For the considered pipe-section, the transverse PGD for the corroded pipeline can be obtained as 4.0 m, using Table 6-5, which is quite equal to the demand of 4 m and hence, would result in 1% strains in pipeline. If desired for BBN modelling, according to Table 1, these strains correspond to about 10% probability of failure.

6.8 BBN model development for PGD

A BBN model is developed based on this chapter report on earthquake hazard, permanent ground displacement and liquefaction, for vulnerability assessment of pipes. The model accounts the effects of permanent ground displacements with respect to pipeline damage. The high-level BBN network is shown in Figure 6-21, where the PGD demand and capacity are compared to estimate the failure probability of a pipeline in longitudinal and transverse direction. The PGD demand is obtained from the dataset developed for liquefaction-induced permanent ground displacement on

buried pipelines. The BBN models (Figure 6-22 and Figure 6-23) for the PGD capacities are obtained from Section 6.7.2.

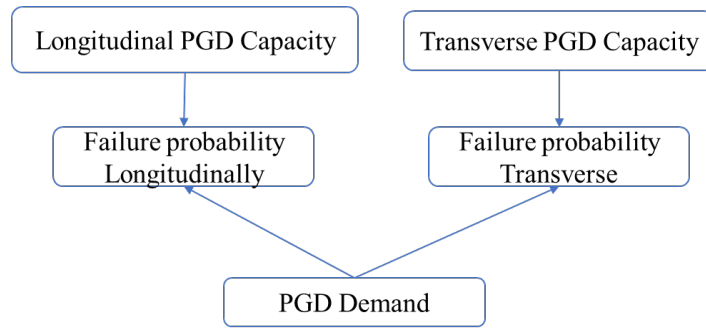


Figure 6-21: Layout of the BBN model for liquefaction induced permanent ground displacement

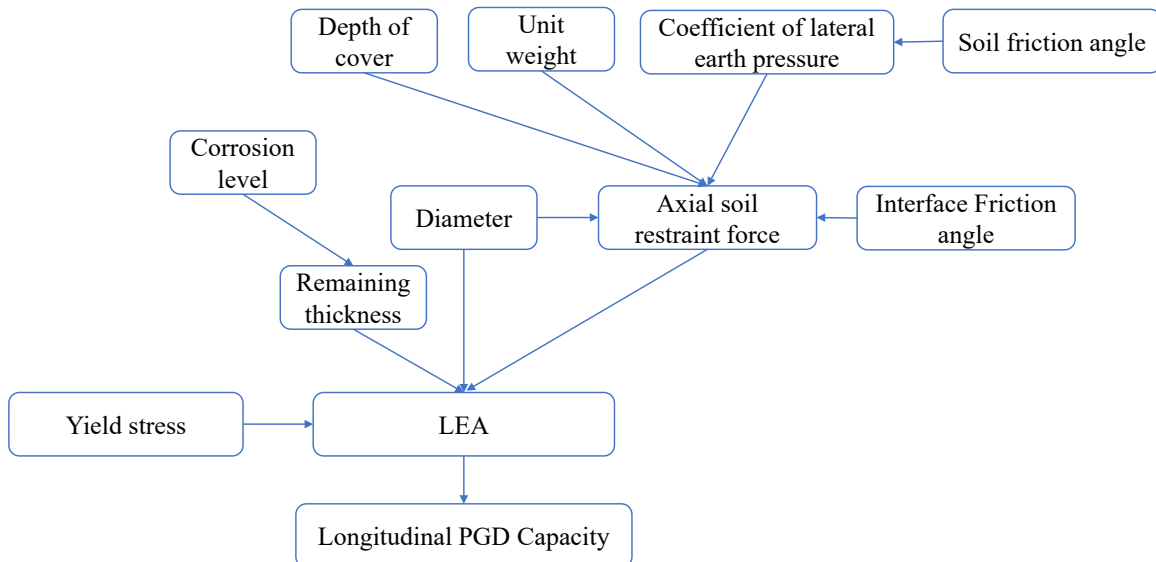


Figure 6-22: BBN model for the longitudinal PGD capacity

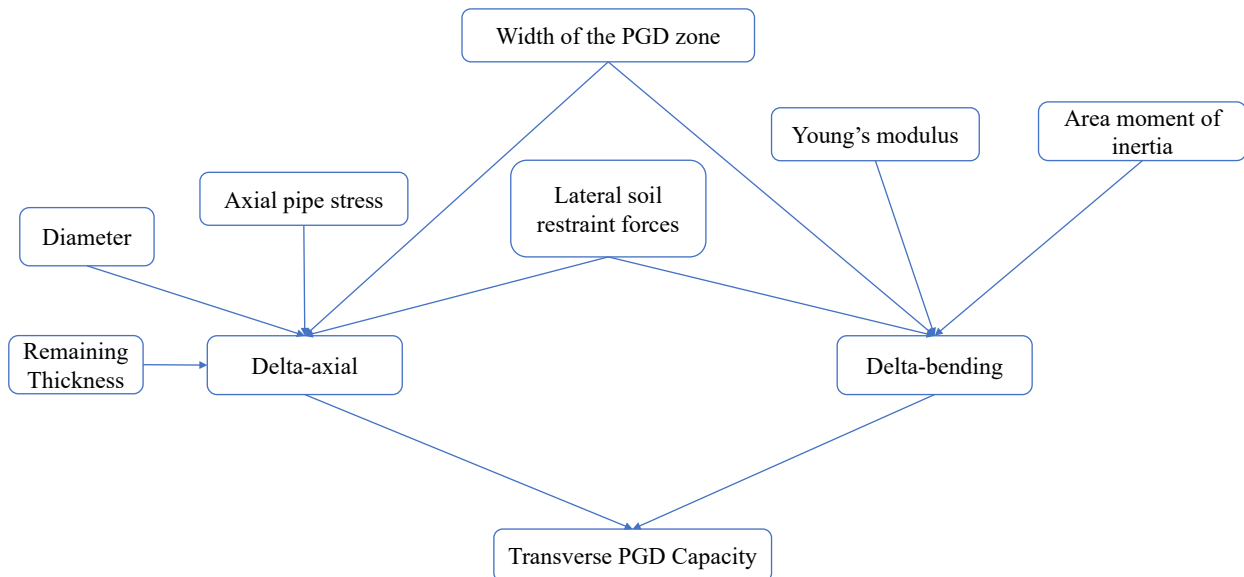


Figure 6-23: BBN model for the transverse PGD capacity

6.9 Conclusions

The primary aim of this chapter is to develop a BBN-based decision making tool to assess the vulnerability of pipeline subjected to two key hazards, viz., the corrosion hazard and the earthquake-induced ground displacement hazards. Herein, the component of developing datasets due to geohazards required for training BBN model was undertaken by Dr. Dharma Wijewickreme's research group.

For the multi-hazard (corrosion and geohazard) problem, datasets have been developed for liquefaction-induced permanent ground displacement demand on buried pipelines and the preliminary PGD capacity of corroded buried pipelines to be used for training the BBN model.

The key highlights from the study are as follows:

1. Liquefaction-induced probabilistic permanent ground displacement hazard (PGD) curves for selected sites (as suggested by BCOGC) have been obtained by implementing the classical Youd et al. (2002) model as GMPE equation in Openquake platform. The curves obtained are more reliable as compared to those obtained using conventional pseudo-probabilistic approaches based on the assumptions for the values for M and R.
2. Using this fully probabilistic approach, reference curves have been developed for the selected BCOGC sites. A simplified procedure has been mentioned to obtain PGD hazard values site-specific parameters using the reference curves.
3. Detailed literature review has been conducted to identify different research groups and the type of data (experimental, numerical, stochastic) available to be used for better training the BBN model.
4. On a preliminary basis, the PGD capacities for intact pipelines has been obtained from a previous project (Terasen 2010, wherein Dr. Dharma Wijewickreme was one of the team members) was reviewed using selected/limited soil-pipe interaction (SPI) finite element modelling using ABAQUS software. Upon confirmation of the suitability, the dataset was presented as input for BBN modeling.
5. After considering outcomes from SPI finite element analysis modeling and those from available closed-form SPI analysis, a simplified/preliminary technique was developed to extrapolate pipeline ground displacement capacities developed for intact pipes to those pipes with different levels of corrosion.
6. Example calculations have been shown; wherein, for the considered set of input parameters, demand as well as capacity is estimated and the decision on pipe failure is made by comparing demand with capacity.

Chapter 7

Summary

The output of this work is to develop a decision-making tool based on Bayesian belief network to assess the vulnerability of pipeline subjected to corrosion (uniform and pitting corrosion), stress corrosion cracking and earthquake-induced ground displacement hazards. The causes of these hazards were first identified, and Bayesian networks were developed based on the casual relationship to model the pipeline failure. The Bayesian network has been developed using different data sources, including corrosion rate data obtained from experimental test results, pitting corrosion data, recommended code of practices, observations obtained from integrity assessment techniques, evidence available from failure history, mechanistic understanding of SCC, and analytical burst failure models. The BBN tool is integrated with GIS to show network level condition of pipelines, which is effective for visualization and decision-making process. Result indicated that the developed tool could derive the reliability of a pipeline operating under various conditions. Sensitivity analyses were also used to show the most sensitive parameters in the model. This study can be extended in the future by strengthening the model with data to overcome any assumptions considered. Furthermore, the developed BBN failure assessment model can be integrated with consequence assessment model to develop a comprehensive risk assessment tool.

Bibliography

- Alberta Energy Regulator (AER) 2013. Report 2013-B: Pipeline performance in Alberta, 1990-2012. Calgary, AB, Canada.
- Ahamed, M., & Melchers, R. E., 1994. Reliability of underground pipelines subject to corrosion. *Journal of Transportation Engineering*, 120(6), 989-1002.
- Al-Amin, M., Kariyawasam, S., & Riverol, E. S., 2018. A Robust Risk Assessment Model for Stress Corrosion Cracking. In *International Pipeline Conference*, American Society of Mechanical Engineers. Vol. 51876, p. V002T07A026.
- Allen, T. I., 2021. Trevallien Git hub repository. https://github.com/treviallen/2015_gsc_nshm
- Allen, T. I., Halchuk, S., Adams, J., & Weatherill, G. A., 2020. Forensic PSHA: Benchmarking Canada's Fifth Generation seismic hazard model using the OpenQuake-engine. *Earthquake Spectra*, 36, 91–111.
- Amirat, A., Benmoussat, A., & Chaoui, K., 2009. Reliability assessment of underground pipelines under active corrosion defects. *Damage and Fracture Mechanics Springer*. pp. 83-92.
- Andrenacci, A., Wong, D., 2012. Evaluation of buried pipeline coatings under soil stress. In: *Corrosion 2012*.
- Arzola, S., Palomar-Pardavé, M.E., Genesca, J., 2003. Effect of resistivity on the corrosion mechanism of mild steel in sodium sulfate solutions. *Journal of Applied Electrochemistry*. 33, 1233–1237.
- Ariman, T., Lee, B. J., & Chen, Q., 1987. Failure of buried pipelines under large ground deformations. In *Developments in Geotechnical Engineering*, Elsevier. Vol. 49, pp. 63–75.
- ASME B31G, A., 1991. Manual for determining the remaining strength of corroded pipelines. ASME B31G-1991.
- ASTM G31-72, 2004. Standard Practice for Laboratory Immersion Corrosion Testing of Metals, ASTM International.
- Ayello, F., Alfano, T., Hill, D., Sridhar, N., others, 2012. A Bayesian network based pipeline risk management. In: *Corrosion 2012*.
- Ayello, F., Jain, S., Sridhar, N. and Koch, G.H. 2014. Quantitative assessment of corrosion probability—a Bayesian network approach. *Corrosion*, 70(11), 1128-1147.
- Balekelayi, N., and Tesfamariam, S., 2020. External corrosion pitting depth prediction using Bayesian spectral analysis on bare oil and gas pipelines. *International Journal of Pressure Vessels and Piping*, 104224.
- Bardet, J. P., Mace, N., and Tobita, T., 1999. Liquefaction-induced ground deformation and failure. Pacific Earthquake Engineering Research Center.
- Bartolini, L. M., Battistini, A., Marchionni, L., & Vitali, L., 2009. Strength and Deformation Capacity of Corroded Pipes. In *XIX Congress Italian Association for Theoretical and Applied Mechanics AIMETA*, Ancona.
- Bartlett, Steven F, and Youd, T. L., 1995. Empirical prediction of liquefaction-induced lateral spread. *Journal of Geotechnical Engineering*, 121(4), 316–329.
- Bartlett, Steven Floyd. ,1992. Empirical analysis of horizontal ground displacement generated by

- liquefaction-induced lateral spreads. Brigham Young University.
- Barbalat, M., Lanarde, L., Caron, D., Meyer, M., Vittonato, J., Castillon, F., Fontaine, S., Refait, P., 2012. Electrochemical study of the corrosion rate of carbon steel in soil: Evolution with time and determination of residual corrosion rates under cathodic protection. *Corrosion Science* 55, 246–253.
- BC Oil and Gas Commission (BCOGC), 2016. Pipeline Performance Summary 2016 Annual Report. Accessed on 09 June 2021 [<https://www.bco.gc.ca/node/14625/download>].
- BC Oil and Gas Commission (BCOGC) 2020. Pipeline Performance Summary 2020 Annual Report. Accessed on 07 September 2021 [<https://www.bco.gc.ca/files/reports/Technical-Reports/2020-Pipeline-Performance-Summary.pdf>].
- Beavers, J., Bubenik, T.A., 2017. Stress corrosion cracking. *Trends in Oil and Gas Corrosion Research and Technologies*, 295-314.
- Beavers, J.A., Garrity, K.C., 2001. 100 mV polarization criterion and external SCC of underground pipelines. In: *Corrosion 2001*.
- Beavers, J.A., Garrity, K.C., Durr, C.L., 2002. The influence of soil chemistry on SCC of pipelines and the applicability of the 100 mV polarization criterion. In: *Corrosion 2002*.
- Beavers, J.A., Harle, B.A., 2001. Mechanisms of high-pH and near-neutral-pH SCC of underground pipelines. *Journal of Offshore Mechanics and Arctic Engineering*. 123, 147–151.
- Beavers, J.A., Thompson, N.G., others, 2006. External corrosion of oil and natural gas pipelines. *ASM Handbook*. 13, 1015–1025.
- Benmoussa, A., Hadjel, M., Traisnel, M., 2006. Corrosion behavior of API 5L X-60 pipeline steel exposed to near-neutral pH soil simulating solution. *Materials and Corrosion*. 57, 771–777.
- Benjamin, A. C., & de Andrade, E. Q. 2003. Predicting the failure pressure of pipelines containing nonuniform depth corrosion defects using the finite element method. In *International Conference on Offshore Mechanics and Arctic Engineering*. Vol. 36827, pp. 557-564.
- Bobbio, A., Portinale, L., Minichino, M., Ciancamerla, E., 1999. Comparing fault trees and bayesian networks for dependability analysis. In: *International Conference on Computer Safety, Reliability, and Security*. pp. 310–322.
- Biondi, G., Cascone, E., Maugeri, M., & Motta, E., 2000. Seismic response of saturated cohesionless slopes. *Soil Dynamics and Earthquake Engineering*. 20(1–4), 209–215.
- Caleyo, F., González, J.L., Hallen, J.M., 2002. A study on the reliability assessment methodology for pipelines with active corrosion defects. *International Journal of Pressure Vessels and Piping*. 79, 77–86. [https://doi.org/10.1016/S0308-0161\(01\)00124-7](https://doi.org/10.1016/S0308-0161(01)00124-7)
- Canadian Energy Pipeline Association (CEPA), 2015. CEPA Recommended Practices for Managing Near-neutral pH SCC, Third Edition, Canadian Energy Pipeline Association, Calgary, AB, Canada.
- Canadian Association of Petroleum Producers (CAPP), 2018. Best management practice: Mitigation of External Corrosion on Buried Carbon Steel Pipeline Systems, Canadian Association of Petroleum Producers. [Accessed on 09 June 2021] [https://www.capp.ca/wp-content/uploads/2019/11/Mitigation_of_External_Corrosion_on_Buried_Carbon_Steel_Pipeline_Syst-322047.pdf].
- Castaneda, H., Rosas, O., 2015. External Corrosion of Pipelines in Soil. In: *Oil and Gas Pipelines*.

- John Wiley & Sons, Ltd, pp. 265–274. <https://doi.org/10.1002/9781119019213.ch20>
- Castillo, E., Gutiérrez, J.M., and Hadi, A.S., 1997. Sensitivity analysis in discrete Bayesian Networks. *IEEE Transactions on Systems, Man, and Cybernetics Part A: Systems and Humans*, 27(4), 412-423.
- Canadian Energy Pipeline Association (CEPA), 2015. The 2015 Pipeline Industry Performance Report. Calgary, AB, Canada.
- Canadian Energy Pipeline Association (CEPA), 2019. The 2019 Transmission Pipeline Industry Performance Report. Calgary, AB, Canada.
- Chakraborty, S. and Tesfamariam, S., 2021. Subset simulation based approach for space-time-dependent system reliability analysis of corroding pipelines. *Structural Safety*, 90, p.102073.
- Chen, S.H., Pollino, C.A., 2012. Good practice in Bayesian network modelling. *Environmental Modelling & Software*. 37, 134–145.
- Cheng, J., Greiner, R., Kelly, J., Bell, D., Liu, W., 2002. Learning Bayesian networks from data: An information-theory based approach. *Artificial Intelligence*. 137, 43–90.
- Cheng, R.C., 1986. Variance reduction methods. *Proceedings of the 18th conference on Winter simulation*. J. Wilson, J. Henriksen, and S. Rovers, eds. pp. 60-68
- Chegeni, B., Jayasuriya, S., & Das, S., 2019. Effect of corrosion on thin-walled pipes under combined internal pressure and bending. *Thin-Walled Structures*, 143, 106218.
- Cheng, Y.F., 2013. *Stress corrosion cracking of pipelines*. John Wiley & Sons.
- Cockburn, G., Tesfamariam, S., 2012. Earthquake disaster risk index for Canadian cities using Bayesian belief networks. *Georisk: Assessment and Management of Risk for Engineered Systems and Geohazards*, 6, 128–140.
- Cole, I.S., Marney, D., 2012. The science of pipe corrosion: A review of the literature on the corrosion of ferrous metals in soils. *Corrosion Science* 56, 5–16.
- C-CORE, & , D.G. Honegger Consulting SSD, I., 2009a. Guidelines for Constructing Natural Gas and Liquid Hydrocarbon Pipelines Through Areas Prone to Landslide and Subsidence Hazards. Design, Materials, and Construction Committee of Pipeline Research Council International, Inc., January. <http://citeseerx.ist.psu.edu/viewdoc/download?doi=10.1.1.250.5780&rep=rep1&type=pdf>
- C-CORE, & , D.G. Honegger Consulting SSD, I. , 2009b. Guidelines for Constructing Natural Gas and Liquid Hydrocarbon Pipelines Through Areas Prone to Landslide and Subsidence Hazards. In Design, Materials, and Construction Committee of Pipeline Research Council International, Inc. (Issue January). <http://citeseerx.ist.psu.edu/viewdoc/download?doi=10.1.1.250.5780&rep=rep1&type=pdf>
- Canadian Standards Association (CSA), 2015. CSA oil and gas pipeline systems. CSA Z662-15. Ontario, Canada: CSA.
- CSA-Z662-2019, 2019. Canadian standards association. Oil and gas pipeline systems. Rexdale, Ontario, Canada.
- Demissie, G. Tesfamariam, S. and Sadiq, R. 2016. Considering soil parameters in prediction of remaining service life of metallic pipes: Bayesian belief network model. *Journal of Pipeline Systems Engineering and Practice* 7(2), 04015028
- Demissie, G., Tesfamariam, S., Sadiq, R., 2015. Prediction of soil corrosivity index: A Bayesian belief network approach, in: 12th Int. Conf. on Applications of Statistics and Probability in

Civil Engineering, ICASP12, Digital Repository of the University of British Columbia, Vancouver, Canada.

- Det Norske Veritas (DNV), 2004. Corroded pipelines: Recommended practice DNV-RP-F101. Hovic, Norway.
- Ebenuwa, A. U., & Tee, K. F., 2017. Reliability analysis of buried pipes with corrosion and seismic impact. In *Geo-Risk 2017*. pp. 424-433
- Ebenuwa, A. U., & Tee, K. F., 2019. Reliability estimation of buried steel pipes subjected to seismic effect. *Transportation Geotechnics*, 20, 100242.
- El-Abbasy, M.S., Senouci, A., Zayed, T., Mosleh, F., 2015. A condition assessment model for oil and gas pipelines using integrated simulation and analytic network process. *Structure and Infrastructure Engineering*, 11, 263–281.
- Ekstrom, L. T., & Franke, K. W. , 2016. Simplified procedure for the performance-based prediction of lateral spread displacements. *Journal of Geotechnical and Geoenvironmental Engineering*, 142(7), 4016028.
- Fang, B.Y., Atrens, A., Wang, J.Q., Han, E.H., Zhu, Z.Y., Ke, W., 2003. Review of stress corrosion cracking of pipeline steels in “low” and “high” pH solutions. *Journal of Materials Science* 38, 127–132.
- Faris, A. T., Seed, R. B., Kayen, R. E., & Wu, J., 2006. A semi-empirical model for the estimation of maximum horizontal displacement due to liquefaction-induced lateral spreading. *Proc. 8th US Conference on Earthquake Engineering*, 3, 1584–1593.
- Hessler, R.R., Batte, A.D. and Hereth, M., 2008. Integrity management of stress corrosion cracking in gas pipeline high consequence areas. *ASME Standards Technology, LLC*.
- Franke, K. W., & Kramer, S. L., 2014. Procedure for the Empirical Evaluation of Lateral Spread Displacement Hazard Curves. *Journal of Geotechnical and Geoenvironmental Engineering*, 140(1), 110–120. [https://doi.org/10.1061/\(asce\)gt.1943-5606.0000969](https://doi.org/10.1061/(asce)gt.1943-5606.0000969)
- Gonzalez, J.A., Andrade, C., 1982. Effect of carbonation, chlorides and relative ambient humidity on the corrosion of galvanized rebars embedded in concrete. *British Corrosion Journal*. 17, 21–28.
- Groysman, A., 2009. *Corrosion for everybody*. Springer Science & Business Media.
- Guo-bing Chen, Zi-chun Yang, Ji-hong Sun, 2010. Safety analysis of complex systems based on Bayesian Networks In: 2010 The 2nd International Conference on Industrial Mechatronics and Automation. pp. 92–95. <https://doi.org/10.1109/ICINDMA.2010.5538083>
- Hamada, M., Towhata, I., Yasuda, S., & Isoyama, R., 1987. Study on permanent ground displacement induced by seismic liquefaction. *Computers and Geotechnics*, 4(4), 197–220.
- Han, Z.Y., Weng, W.G., 2011. Comparison study on qualitative and quantitative risk assessment methods for urban natural gas pipeline network. *Journal of Hazardous Materials* 189, 509–518.
- Halchuk, S., Allen, T. I., Adams, J., & Rogers, G. C., 2014. Fifth generation seismic hazard model input files as proposed to produce values for the 2015 National Building Code of Canada. *Geological Survey of Canada Open File, 7576*, 18.
- Hasegawa, K., Li, Y., Bezensek, B., & Hoang, P., 2011. Evaluation of torsion and bending collapse moments for pipes with local wall thinning. In *Pressure Vessels and Piping Conference (Vol. 44519, pp. 215-221)*.

- Harle, B.A., Beavers, J.A., Jaske, C.E., 1996. Effect of stress corrosion cracking on integrity and remaining life of natural gas pipelines. In: Corrosion 96.
- Hasan, S.M., Khan, F., Kenny, S., 2012. Probabilistic transgranular stress corrosion cracking analysis for oil and gas pipelines. *Journal of Pressure Vessel Technology* 134.
- Hasegawa, K., Li, Y., Bezensek, B. and Hoang, P., 2011. Evaluation of torsion and bending collapse moments for pipes with local wall thinning. In *Pressure Vessels and Piping Conference*, Vol. 44519, pp. 215-221.
- Hessler, R.R., Batte, A.D. and Hereth, M., 2008. Integrity Management of Stress Corrosion Cracking in Gas Pipeline High Consequence Areas, ASME STP-PT-011, ASME Standards Technology, LLC, New York, NY.
- Honegger, D.G. and Wijewickreme, D., 2013. Seismic Risk Assessment for Oil and Gas Pipelines. *Seismic Risk Analysis and Management of Civil Infrastructure Systems*. Woodhead Publishing Ltd.
- Honegger, D. G., Rahman, M., Puebla, H., Wijewickreme, D., & Augello, A. , 2010. Definition of Lateral Spread Displacement for Regional Risk Assessments of Pipeline Vulnerability. *International Pipeline Conference*, 44236, 583–592.
- Idriss, I. M., & Boulanger, R. W., 2008. Soil liquefaction during earthquakes. *Earthquake Engineering Research Institute*.
- Ismail, M.A., Sadiq, R., Soleymani, H.R., Tesfamariam, S., 2011. Developing a road performance index using a Bayesian belief network model. *Journal of the Franklin Institute* 348, 2539–2555.
- Jain, S., Ayello, F., Beavers, J.A., Sridhar, N., 2012. Development of a probabilistic model for stress corrosion cracking of underground pipelines using bayesian networks: a concept. In: *International Pipeline Conference*. pp. 615–625.
- Jain, S., Beavers, J.A., Ayello, F., Sridhar, N., 2013. Probabilistic model for stress corrosion cracking of underground pipelines using Bayesian networks. In: *Corrosion 2013*.
- Jamali, S.S., Mills, D.J., Sykes, J.M., 2014. Measuring electrochemical noise of a single working electrode for assessing corrosion resistance of polymer coated metals. *Progress in Organic Coatings* 77, 733–741.
- Javaherdashti, R., Nwaoha, C., Tan, H., 2016. *Corrosion and materials in the oil and gas industries*. CRC Press.
- Kabir, G., Tesfamariam, S., Francisque, A., Sadiq, R., 2015. Evaluating risk of water mains failure using a Bayesian belief network model. *European Journal of Operational Research*. 240, 220–234.
- Kabir, S. and Papadopoulos, Y., 2019. Applications of Bayesian networks and Petri nets in safety, reliability, and risk assessments: A review. *Safety Science*, 115, 154-175.
- Kanes, R., Marengo, M.C.R., Abdel-Moati, H., Cranefield, J. and Vechot, L. 2017. Developing a framework for dynamic risk assessment using Bayesian networks and reliability data. *Journal of Loss Prevention in the Process Industries*, 50, 142-153.
- Karamanos, S. A., Keil, B., & Card, R. J., 2014. Seismic design of buried steel water pipelines. In *Pipelines 2014: From Underground to the Forefront of Innovation and Sustainability* (pp. 1005-1019).
- Katano, Y., Miyata, K., Shimizu, H., Isogai, T., 2003. Predictive model for pit growth on

- underground pipes. *Corrosion* 59, 155–161.
- Khan, F., Yarveisy, R., and Abbassi, R., 2021. Risk-based pipeline integrity management: A road map for the resilient pipelines. *Journal of Pipeline Science and Engineering*, 1(1), 74-87.
- Khan, F.I., Haddara, M.M., Bhattacharya, S.K., 2006. Risk-based integrity and inspection modeling (RBIIM) of process components/system. *Risk Analysis: An International Journal*. 26, 203–221.
- Kim, W. S., Kim, Y. P., Kho, Y. T., & Choi, J. B., 2002. Full scale burst test and finite element analysis on corroded gas pipeline. In *International Pipeline Conference* (Vol. 36207, pp. 1501-1508).
- Kiefner, J., Maxey, W., Eiber, R., Duffy, A., 1973. Failure stress levels of flaws in pressurized cylinders. In: *Progress in Flaw Growth and Fracture Toughness Testing*. ASTM International.
- Kim, C., Chen, L., Wang, H. and Castaneda, H., 2021. Global and local parameters for characterizing and modeling external corrosion in underground coated steel pipelines: A review of critical factors. *Journal of Pipeline Science and Engineering*, 1(1), 17-35.
- Koch, G., Ayello, F., Khare, V., Sridhar, N. and Moosavi, A., 2015. Corrosion threat assessment of crude oil flow lines using Bayesian network model. *Corrosion Engineering, Science and Technology*, 50(3), 236-247.
- Kowalski, A.R., Sánchez, A.N., 2016. Soil Corrosivity in Buried Onshore Pipelines: A Bayesian Network Approach. In: *NACE International Corrosion Conference Proceedings*. p. 1.
- Lahiri, S.K., Ghanta, K.C., 2008. Development of an artificial neural network correlation for prediction of hold-up of slurry transport in pipelines. *Chemical Engineering Science*. 63, 1497–1509.
- Lam, C., Zhou, W., 2016. Statistical analyses of incidents on onshore gas transmission pipelines based on PHMSA database. *International Journal of Pressure Vessels and Piping*. 145, 29–40.
- Laskey, K.B. 1995. Sensitivity analysis for probability assessments in Bayesian Networks. *IEEE Transactions on Systems Man and Cybernetics*, 25(6), 901-909.
- Leshchinsky, B. A., Mason, H. B., Olsen, M. J., & Gillins, D. T., 2018. Lateral spreading within a limit equilibrium framework: Newmark sliding blocks with degrading yield accelerations. *Géotechnique*. 68(8), 699–712.
- Levold, E., Restelli, A., Marchionni, L., Molinari, C., & Vitali, L., 2013. Strength and deformation capacity of corroded pipes: The joint industry project. In *International Conference on Offshore Mechanics and Arctic Engineering*, American Society of Mechanical Engineers. Vol. 55362, p. V04AT04A029
- Leeds, J.M., 1995. Interaction between coatings and CP deserves basic review. *Pipe line & gas industry* 78.3 (1995): 21-25..
- Liu, X., & O'Rourke, M. J., 1997. Behaviour of continuous pipeline subject to transverse PGD. *Earthquake Engineering & Structural Dynamics*, 26(10), 989–1003.
- Liu, Y., Zhang, Z. and Liu, S., 2017, March. Research on analysis method for lateral displacement of buried pipeline. In *IOP Conference Series: Earth and Environmental Science* (Vol. 59, No. 1, p. 012056). IOP Publishing.
- Liu, W. and Li, J., 2008. Stochastic seismic response of pipelines with corrosion. *Journal of Earthquake Engineering*, 12(6), 914-931.

- Li, X., Castaneda, H., 2014. Influence of soil parameters on coating damage evolution of X52 pipeline steel under cathodic protection conditions. In: Corrosion 2014.
- Li, Y., Hasegawa, K., Miura, N. and Hoshino, K., 2017. Failure experiments on pipes with local wall thinning subjected to multi-axial loads. *Journal of Pressure Vessel Technology*, 139(2), 021203
- Li, X., Chen, G. and Zhu, H., 2016. Quantitative risk analysis on leakage failure of submarine oil and gas pipelines using Bayesian network. *Process Safety and Environmental Protection*, 103, 163-173.
- Lins, V. de F.C., Ferreira, M.L.M., Saliba, P.A., 2012. Corrosion resistance of API X52 carbon steel in soil environment. *Journal of Materials Research and Technology*. 1, 161–166.
- Li, Y., Hasegawa, K., Miura, N., & Hoshino, K. , 2017. Failure Experiments on Pipes With Local Wall Thinning Subjected to Multi-Axial Loads. *Journal of Pressure Vessel Technology*, 139(2).
- Liu, Y., Zhang, Z., & Liu, S., 2017. Research on analysis method for lateral displacement of buried pipeline. In *IOP Conference Series: Earth and Environmental Science* (Vol. 59, No. 1, p. 012056).
- Liu, W., & Li, J., 2008. Stochastic seismic response of pipelines with corrosion. *Journal of Earthquake Engineering*, 12(6), 914-931.
- Lund, L. V., 1994. Lifelines performance in the Landers and Big Bear (California) earthquakes of 28 June 1992. *Bulletin of the Seismological Society of America*, 84(3), 562–572.
- Lund, L. V., 1996. Lifeline utilities performance in the 17 January 1994 Northridge, California, earthquake. *Bulletin of the Seismological Society of America*, 86(1B), S350--S361.
- Marhavilas, P.-K., Koulouriotis, D., Gemeni, V., 2011. Risk analysis and assessment methodologies in the work sites: On a review, classification and comparative study of the scientific literature of the period 2000-2009. *Journal of Loss Prevention in the Process Industries*. 24, 477–523.
- Matasovic, N., Kavazanjian, E., & Yan, Y. L., 1997. Newmark deformation analysis with degrading yield acceleration. *Geosynthetics' 97. Proc. Conference, Long Beach, 1997. Vol. 2*, 989–1000.
- Mazumder, R. K., Salman, A. M., and Li, Y, 2020. Failure risk analysis of pipelines using data-driven machine learning algorithms. *Structural Safety*, 89, 102047.
- Melchers, R.E., 2004. Pitting corrosion of mild steel in marine immersion environment part 1: maximum pit depth. *Corrosion* 60 (09).
- Mori, S., Chiba, K., & Koike, T., 2012. Seismic performance analysis of the transmission Gas pipeline in the 2011 Great East Japan earthquake. In *15th World Conference on Earthquake Engineering (15WCEE)*, 24–28.
- Mondal, B. C., & Dhar, A. S., 2019. Burst pressure of corroded pipelines considering combined axial forces and bending moments. *Engineering Structures*, 186, 43-51.
- Muhlbauer, W.K., 2004. Pipeline risk management manual: ideas, techniques, and resources. Elsevier.
- Muthukumar, N., Rajasekar, A., Ponmariappan, S., Mohanan, S., Maruthamuthu, S., Muralidharan, S., Subramanian, P., Palaniswamy, N., Raghavan, M., 2003. Microbiologically influenced corrosion in petroleum product pipelines-a review.

- National Association of Corrosion Engineers (NACE), 2020. Consequences Of Coating Failures As Related To Interaction With Cathodic Protection (NACE TR21447-2020). NACE International, 15835 Park Ten Place, Suite 200, Houston TX 77084, USA.
- Canadian Commission on Building and Fire Codes, and National Research Council of Canada, 2015. National building code of Canada. Ottawa: Associate Committee on the National Building Code, National Research Council.
- Nakhaie, D., Kosari, A., Mol, J.M.C., and Asselin, E, 2020. Corrosion resistance of hot-dip galvanized steel in simulated soil solution: A factorial design and pit chemistry study. *Corrosion Science*, 164, 108310.
- Nataraj, S., 2005. Analytic hierarchy process as a decision-support system in the petroleum pipeline industry. *Issues in Information Systems*. 6, 16–21.
- National Energy Board (NEB), 1996. Public Inquiry Concerning Stress Corrosion Cracking on Canadian Oil and Gas Pipelines. Calgary, AB, Canada.
- Newmark, N. M., 1965. Effects of earthquakes on dams and embankments. *Geotechnique*, 15(2), 139–160.
- Netto, T. A., Ferraz, U. S., & Botto, A., 2007. On the effect of corrosion defects on the collapse pressure of pipelines. *International Journal of Solids and Structures*, 44(22-23), 7597-7614.
- Netto, T. A., Ferraz, U. S., & Estefen, S. F., 2005. The effect of corrosion defects on the burst pressure of pipelines. *Journal of Constructional Steel Research*, 61(8), 1185-1204.
- Netto, T. A., Ferraz, U. S., & Botto, A., 2006. Residual strength of corroded pipelines under external pressure: a simple assessment. In *International Pipeline Conference* (Vol. 42622, pp. 143-156).
- Nešić, S. 2007. Key issues related to modelling of internal corrosion of oil and gas pipelines – A review. *Corros. Sci.* 49, 4308–4338.
<https://doi.org/https://doi.org/10.1016/j.corsci.2007.06.006>
- Norsworthy, R., 2009. Coatings used in conjunction with cathodic protection shielding vs non-shielding pipeline coatings. In *CORROSION 2009*.
- Norsys Software Corp., 2015. Netica TM Application. <http://www.norsys.com>.
- O'Rourke, T. D., Stewart, H. E., Gowdy, T. E., & Pease, J. W., 1991. Lifeline and geotechnical aspects of the 1989 Loma Prieta Earthquake. University of Missouri-Rolla.
- Opeyemi, D.A., Patelli, E., Beer, M., Timashev, S.A., 2015. Comparative studies on assessment of corrosion rates in pipelines as semi-probabilistic and fully stochastic values. University of British Columbia.
- Palaniappan, V., 2018. Pipeline risk assessment using dynamic Bayesian network (DBN) for internal corrosion. PhD Thesis
- Papavinasam, S., 2013. Corrosion control in the oil and gas industry. Elsevier.
- Papavinasam, S., Revie, R.W., 2006. Protective pipeline coating evaluation. In: *CORROSION 2006*.
- Parkins, R.N., 2000. A review of stress corrosion cracking of high pressure gas pipelines. In: *CORROSION 2000*.
- Parkins, R.N., Zhou, S., 1997. The stress corrosion cracking of C-Mn steel in CO₂-HCO₃⁻-CO₃²⁻ solutions. II: Electrochemical and other data. *Corrosion Science*. 39, 175–191.

- Pearl, J., 1988. Probabilistic Reasoning in Intelligent Systems: Networks of Plausible Inference. Morgan-Kaufmann, San Francisco, CA, USA.
- Pearl, J., 2014. Probabilistic reasoning in intelligent systems: networks of plausible inference. Elsevier.
- PRCI, 2009. Guidelines for Constructing Natural Gas and Liquid Hydrocarbon Pipelines Through Areas Prone to Landslide and Subsidence Hazards. In Design, Materials, and Construction Committee of Pipeline Research Council International, Inc. (Issue January). <http://citeseerx.ist.psu.edu/viewdoc/download?doi=10.1.1.250.5780&rep=rep1&type=pdf>
- Quej-Ake, L.M., Contreras, A., Liu, H.B., Alamilla, J.L., Sosa, E., 2018. Assessment on external corrosion rates for API pipeline steels exposed to acidic sand-clay soil. *Anti-Corrosion Methods and Materials*.
- Rathje, E. M., & Bray, J. D., 2000. Nonlinear coupled seismic sliding analysis of earth structures. *Journal of Geotechnical and Geoenvironmental Engineering*, 126(11), 1002–1014. [https://doi.org/https://doi.org/10.1061/\(ASCE\)1090-0241\(2000\)126:11\(1002\)](https://doi.org/https://doi.org/10.1061/(ASCE)1090-0241(2000)126:11(1002))
- Rauch, A. F., & Martin III, J. R., 2000. EPOLLS model for predicting average displacements on lateral spreads. *Journal of Geotechnical and Geoenvironmental Engineering*, 126(4), 360–371.
- Revie, R.W., 2015. Oil and Gas Pipelines: Integrity and Safety Handbook. John Wiley and Sons.
- Ricker, R.E., 2010. Analysis of pipeline steel corrosion data from NBS (NIST) studies conducted between 1922-1940 and relevance to pipeline management. *Journal of research of the National Institute of Standards and Technology*. 115, 373.
- Romanoff, M., 1957. Underground corrosion. US Government Printing Office.
- Sadiq, R., Rajani, B., Kleiner, Y., 2004a. Probabilistic risk analysis of corrosion associated failures in cast iron water mains. *Reliability Engineering & System Safety*. 86, 1–10.
- Sadiq, R., Rajani, B., Kleiner, Y., 2004b. Fuzzy-based method to evaluate soil corrosivity for prediction of water main deterioration. *Journal of Infrastructure Systems*. 10, 149–156.
- Shim, D. J., Choi, J. B., Kim, Y. J., Kim, J. W., & Park, C. Y., 2003. Assessment of local wall thinned pipeline under combined bending and pressure. *International Journal of Modern Physics B*, 17(08n09), 1870-1876.
- Smith, M. Q., & Waldhart, C. J., 2000. Combined loading tests of large diameter corroded pipelines. In 2000 3rd International Pipeline Conference. American Society of Mechanical Engineers Digital Collection.
- Smith, M. Q., Nicolella, D. P., & Waldhart, C. J., 1998. Full-scale wrinkling tests and analyses of large diameter corroded pipes. In *International Pipeline Conference (Vol. 40221, pp. 543-551)*. American Society of Mechanical Engineers.
- Shabarchin O. and Tesfamariam S., 2016. Internal corrosion hazard assessment of oil & gas pipelines using Bayesian belief network model. *Journal of Loss Prevention in the Process Industries* 40, 479-495.
- Shahriar, A., Sadiq, R., Tesfamariam, S., 2012. Risk analysis for oil & gas pipelines: A sustainability assessment approach using fuzzy based bow-tie analysis. *Journal of Loss Prevention in the Process Industries*. 25, 505–523.
- Song, F., 2003. Corrosion of coated pipelines with cathodic protection. Ph. D. Thesis, University of Toronto, Toronto, ON, Canada.

- Sooknah, R., Papavinasam, S., Revie, R.W., 2008. Validation of a predictive model for microbiologically influenced corrosion. In: CORROSION 2008.
- Smith, M., 2018. ABAQUS/Standard User's Manual, Version 2018. Dassault Systèmes Simulia Corp.
- Terasen (2010) Report on 'Regional Seismic Risk Assessment of Terasen Natural Gas Pipelines', prepared for Terasen Gas Inc., Project Team led by D.G. Honegger Consulting, August 2010.
- Tesfamariam, S., Rajani, B., Sadiq, R., 2006. Possibilistic approach for consideration of uncertainties to estimate structural capacity of ageing cast iron water mains. *Canadian Journal of Civil Engineering*. 33, 1050–1064.
- Tesfamariam, S., Sadiq, R., Najjaran, H., 2010. Decision making under uncertainty—An example for seismic risk management. *Risk Analysis: An International Journal*. 30, 78–94.
- Velázquez, J.C., Caleyó, F., Valor, A., Hallen, J.M., 2009. Predictive model for pitting corrosion in buried oil and gas pipelines. *Corrosion* 65, 332–342.
- Walker, A. C., & Williams, K. A. J., 1995. Strain based design of pipelines. American Society of Mechanical Engineers, New York, NY.
- Wang, S., Liu, D., Du, N., Zhao, Q., Xiao, J., 2015. Analysis of the long-term corrosion behavior of X80 pipeline steel in acidic red soil using electrical resistance test technique. *Advances in Materials Science and Engineering*.
- Wang, Y., Zhang, P., Hou, X. Q., & Qin, G., 2020. Failure probability assessment and prediction of corroded pipeline under earthquake by introducing in-line inspection data. *Engineering Failure Analysis*, 115, 104607.
- Wasim, M., Shoaib, S., Mubarak, N.M., Asiri, A.M., 2018. Factors influencing corrosion of metal pipes in soils. *Environmental Chemistry Letters*. 16, 861–879.
- Widaman, K.F., 2006. III. MISSING DATA: WHAT TO DO WITH OR WITHOUT THEM. *Monographs of the Society for Research in Child Development*. 71, 42–64. <https://doi.org/10.1111/j.1540-5834.2006.00404>.
- Wijewickreme, D., Honegger, D.G., and Youd, T.L., 2013, "Characterization of Liquefaction-Induced Lateral Spread Dimensions Based on Past Earthquake Data", From Case History to Practice: 5th International Conference on Earthquake Geotechnical Engineering, Istanbul, Turkey, 17-19 June 2013.
- Wijewickreme, D., Honegger, D., Mitchell, A., & Fitzell, T., 2005. Seismic vulnerability assessment and retrofit of a major natural gas pipeline system: a case history. *Earthquake Spectra*, 21(2), 539-567.
- Wu, J., Zhou, R., Xu, S. and Wu, Z., 2017. Probabilistic analysis of natural gas pipeline network accident based on Bayesian network. *Journal of Loss Prevention in the Process Industries*, 46, 126-136.
- Xiang, W. and Zhou, W., 2021. Bayesian network model for predicting probability of third-party damage to underground pipelines and learning model parameters from incomplete datasets. *Reliability Engineering & System Safety*, 205, 107262.
- Xiang, W. and Zhou, W., 2020. Integrated pipeline corrosion growth modeling and reliability analysis using dynamic Bayesian network and parameter learning technique. *Structure and Infrastructure Engineering*, 16(8), 1161-1176.
- Xu, M.; Liang, H.; Liu, Y. and Asselin, E. 2021. Predicting the external corrosion rate of X60

- pipeline steel: A mathematical model. *Metals*, 11, 583. <https://doi.org/10.3390/met11040583>.
- Yang, S., Lu, M., Liu, B., Hao, B., 2009. A fault diagnosis model for embedded software based on FMEA/FTA and bayesian network. In: 2009 8th International Conference on Reliability, Maintainability and Safety. pp. 778–782.
- Youd, T. L., 2018. Application of MLR Procedure for Prediction of Liquefaction-Induced Lateral Spread Displacement. *Journal of Geotechnical and Geoenvironmental Engineering*, 144(6), 04018033. [https://doi.org/10.1061/\(asce\)gt.1943-5606.0001860](https://doi.org/10.1061/(asce)gt.1943-5606.0001860)
- Youd, T. L., Hansen, C. M., & Bartlett, S. F., 2002. Revised Multilinear Regression Equations for Prediction of Lateral Spread Displacement. *Journal of Geotechnical and Geoenvironmental Engineering*, 128(12), 1007–1017.
- Youd, T. L., & Perkins, D. M., 1987. Mapping of liquefaction severity index. *Journal of Geotechnical Engineering*, 113(11), 1374–1392.
- Yu, X., Liang, W., Zhang, L., Reniers, G. and Lu, L., 2018. Risk assessment of the maintenance process for onshore oil and gas transmission pipelines under uncertainty. *Reliability Engineering & System Safety*, 177, 50-67.
- Yunovich, M., Xia, Z., Szklarska-Smialowska, Z., 1998. Factors influencing stress corrosion cracking of carbon steel in diluted bicarbonate environments. *Corrosion* 54, 155–161.
- Zargarnezhad, H., Asselin, E., Wong, D. and Lam C.N., 2021. A critical review of the time-dependent performance of polymeric pipeline coatings: focus on hydration of epoxy-based coatings. *Polymers*, 13, 1517
- Zhang, Y. and Weng, W.G., 2020. Bayesian network model for buried gas pipeline failure analysis caused by corrosion and external interference. *Reliability Engineering & System Safety*, 203, 107089.
- Zhang, G., Robertson, P. K., & Brachman, R. W. I., 2004. Estimating liquefaction-induced lateral displacements using the standard penetration test or cone penetration test. *Journal of Geotechnical and Geoenvironmental Engineering*, 130(8), 861–871.
- Zhang, Y., & Das, S., 2008. Failure of X52 wrinkled pipelines subjected to monotonic axial deformation. *Journal of pressure vessel technology*, 130(2).
- Zhang, J., & Zhao, J. X., 2005. Empirical models for estimating liquefaction-induced lateral spread displacement. *Soil Dynamics and Earthquake Engineering*, 25(6), 439–450.
- Zheng, W., Elboujdaini, M., Revie, R.W., 2011. Stress corrosion cracking in pipelines. In: *Stress Corrosion Cracking*. Elsevier, pp. 749–771.
- Zimmerman, T.J.E., Cosham, A., Hopkins, P., Sanderson, N., 1998. Can limit states design be used to design a pipeline above 80% SMYS?, In: *OMAE 1998: 17th International Conference on Offshore Mechanics and Arctic Engineering*. p. 1998.

Appendix A: Literature review related to estimation of PGD Capacities of buried pipelines

Title	Author	Year	Remarks
Effect of corrosion on thin-walled pipes under combined internal pressure and bending	Chegeni, Jayasuriya, and Das	2019	<p>Using experimental and numerical methods, this study investigated the effects of corrosion depth, corrosion shape and internal pressure on the performance of corroded thin-walled steel pipes when subject to combined internal pressure and 4-point bending load.</p> <p>Load-displacement curves for intact and different percentage depths of corrosion have been reported on the basis of experimental as well as numerical studies.</p> <ul style="list-style-type: none"> • Four-point bending test conducted • Effect of corrosion depth was studied using three API 5 L X52 grade pipe specimens with a nominal diameter of 8-inches (203 mm) • Effect of corrosion shape was investigated by testing five API 5 L X46 specimens with a nominal diameter of 6-inches (152 mm) • Increase in the corrosion depth drastically decreases the bending capacity of the corroded specimens.
Failure experiments on pipes with local wall thinning subjected to multi-axial loads	Li, Hasegawa, Miura, and Hoshino	2017	Based on the experimental results, a failure estimation method is proposed to be applicable to pipes with local wall thinning due to age-related degradation such as flow-accelerated corrosion subjected to pressure-induced axial forces, bending, and torsion moments due to mechanical or seismic loads.
Evaluation of torsion and bending collapse moments for pipes with local wall thinning	Hasegawa, Li, Bezensek, and Hoang	2011	Finite element analyses were conducted in this paper for 24-inch diameter straight pipes with local wall thinning. The pipe was subject to combined bending and torsion moments. It is shown that the effect of torsion moment on plastic collapse bending moment for the pipes depends on the local wall thinning sizes.
Assessment of local wall thinned pipeline under combined bending and pressure	Shim, Choi, Kim, Kim, and Park	2003	<p>This study provides an assessment procedure for locally wall thinned pipelines subjected to internal pressure and bending moment due to dead-weight loads and seismic loads.</p> <p>In this paper, three-dimensional finite element (FE) analyses in ABAQUS were performed to simulate full-scale pipe tests conducted for various shapes of wall thinned area under internal pressure and bending moment.</p> <p>Additional finite element analyses were performed to investigate the effect of key parameters, such as wall thinned depth, wall thinned angle and wall thinned length, on maximum moment.</p>
Failure of X52 wrinkled pipelines subjected to monotonic axial deformation	Zhang and Das	2008	Current pipeline design standards and practices recommend various limit state design methods for energy pipelines based on noticeable cross-sectional deformation and formation of local buckling/wrinkling that corresponds to material strain of 0.5–2.0%.

			<p>Full-scale tests with two internal pressures carried out under axisymmetric axial compressive deformation on X52 grade NPS12 pipelines with D/t ratio of 45. Detailed parametric study was then undertaken using non-linear FE method to study the influence of internal pressure and D/t ratio on the failure conditions and failure modes of X52 grade pipelines. Both experimental test data and numerical analysis indicate that the X52 grade pipeline usually exhibits high ductility under monotonically increasing axisymmetric axial compressive deformation. This pipeline is able to maintain its integrity much beyond the strain limits recommended by the current design standards and practices.</p>
<p>Burst pressure of corroded pipelines considering combined axial forces and bending moments</p>	<p>Mondal and Dhar</p>	<p>2019</p>	<p>Most of the design codes provide the models of burst pressure for corroded pipeline, assuming that the pipeline is subjected to internal pressure only. However, the pipelines are often subjected to different types of external loads causing a longitudinal bending moment and axial force in addition to the internal pressure. The axial force and the bending moment result in the reduction of burst pressures of the pipelines. This research using FEA presents a detailed study on the effects of axial forces and bending moments on the burst pressures of corroded pipelines.</p>
<p>Research on analysis method for lateral displacement of buried pipeline</p>	<p>Liu, Zhang, and Liu</p>	<p>2017</p>	<p>Deflection equation for lateral movement of buried pipeline is derived based on principle for elastic foundation beam and validated through finite element analysis</p>
<p>Reliability analysis of buried pipes with corrosion and seismic impact</p>	<p>Ebenuwa and Tee</p>	<p>2017</p>	<p>An advanced simulation approach called Line Sampling (LS) combined with Important Sampling (IS) is employed for the assessment of buried continuous pipelines. This study assesses a time-dependent system analysis of a corroded, buried pipeline under earthquake effects. The power law function of time is implemented to model the adverse effect of corrosion pit depth on buried pipe for a service life of 120 years. Designing buried pipelines for critical responses due to longitudinal PGD, transverse PGD and buoyancy due to liquefaction about continuous pipeline failure are discussed.</p>
<p>Stochastic seismic response of pipelines with corrosion</p>	<p>Liu and Li</p>	<p>2008</p>	<p>In this paper, Markov chain with absorbing barrier model is used for simulating the evolution of the pipeline corrosion. Elastic foundation beam method and random perturbation method are used to obtain the seismic response (TGD) of the pipeline with corrosion. However, the uncertainty of the soil around the pipelines and materials conveyed in the pipelines demands the pipelines corrosion to be stochastically described.</p>
<p>Strength and deformation capacity of corroded pipes the joint industry project</p>	<p>Levold, Restelli, Marchionni, Molinari, and Vitali</p>	<p>2013</p>	<p>This paper highlights the need to understand the failure mechanisms and better quantify the strength and deformation capacity of corroded pipelines considering the relevant failure modes under the effect of external pressure as follows:</p>

			<ul style="list-style-type: none"> • Collapse Failure Mode (Col-FM) due to external pressure dominated load conditions; • Local Buckling Failure Mode (LocBuck-FM) due to bending moment load conditions in presence of external and internal overpressure and steel axial force; • Fracture/plastic collapse of defective girth welds under bending moment load conditions in presence of external and internal overpressure and steel axial force. <p>The paper also mentions documents giving recommendations for assessing the capacity of corroded pipelines against external pressure. The study involves performing both experiments as well as FE analysis. The study suggests to fit a corrective equation considering the relevant parameters (d/t, c/D, L/D, position and working factor), to better predict the bending moment capacity and deformation of corroded pipes.</p>
Strength and deformation capacity of corroded pipes	Bartolini, Battistini, Marchionni, and Vitali	2009	Another paper from the same project with a different set of results.
Seismic design of buried steel water pipelines	Karamanos, Keil, and Card	2014	<p>Highlights difference between buried water and oil and gas pipelines.</p> <p>There exist 4 main failure modes for continuous (welded) pipelines, namely:</p> <ul style="list-style-type: none"> • Pipe wall fracture due to excessive tensile strain (base material and butt-welded joints) • Pipe wall local buckling due to excessive compressive strain • Pipeline overall buckling due to compressive loading • Pipeline welded-slip joint failure (fracture or crushing) <p>The failure modes are quantified in terms of strain and deformation capacity</p> <p>The paper provides an overview of available tools and provisions for the structural analysis and design of buried welded (continuous) steel water pipelines in seismic areas, subjected to both transient and permanent ground actions. Specific issues are discussed on the modelling of the interacting pipeline-soil system using either simple analytical models or nonlinear finite elements, and their main advantages and disadvantages are pin-pointed</p>
Reliability of underground pipelines subject to corrosion	Ahammed and Melchers	1994	<p>Probabilistic modeling of the material loss as a nonlinear function of time approach is explored in the present paper, using a nonlinear function first postulated for atmospheric corrosion. This model is incorporated into expressions for stress resulting from externally applied loading and internal pressure to provide a limit state function expressing the boundary between survival and failure of the system.</p> <p>In the paper, a method was presented for the estimation of the structural reliability of underground pipes under the action of both external and internal loading, and incorporating the effect of corrosion. Uncertainties involved in material and soil properties, internal and</p>

			external loads, and corrosion parameters are considered through the use of probability theory. From a numerical investigation of an example pipeline, it was found that there is a very significant long-term contribution of the corrosion parameters to structural reliability deterioration, and that this is directly related to the corrosion parameters (k and n).
--	--	--	--

The Table provides information collected from all the three research domains, viz., experimental, numerical and statistical. Under permanent ground displacements, as the buried pipelines tend to experience either axial or bending type of strains, the investigations wherein, the performance of intact as well as corroded pipelines under axial forces as well as bending moments are reported, have been documented in the Table. Following are the key observations from different types of approaches represented in bulleted format.

Insights from experimental approach

- Considering combined effects of internal pressure and four-point bending load, load-displacement curves are obtained for pipes corroded to different depths
- Small-scale experiments have reported the effect of axial forces and bending moments on the burst pressure of corroded pipes
- Increase in the corrosion depth drastically decreases the bending capacity of corroded specimens

Insights from FE modelling

- Validated FE models developed for studying the effect of corrosion and internal pressure on load carrying capacity of pipelines.
- FE analysis also have been performed to study the effect of axial forces and bending moments on the burst pressure of corroded pipes.

Insights from statistical modeling/ reliability analysis

- Strains in pipe calculated using analytical models for both the failure modes assuming block pattern and hyperbolic model springs (O'Rourke & Liu 1999).
- Transverse or longitudinal strain once is less than a critical value is considered indication of failure.
- Power law is used to estimate corrosion rate and hence the reduced equivalent thickness of pipe.
- Statistical Monte Carlo, Important Sampling and Line Sampling analysis is performed to obtain failure probability and the corresponding PGD.

Insights from stochastic approach

- Markov chain with absorbing barrier technique is used for estimating the corrosion.
- Strains are calculated considering elastic foundation approach wherein the displacements and stresses of pipelines are expressed as the functions of cross section areas of pipelines.
- Random perturbation approach is used to obtain the random seismic response of pipelines with corrosion.

Appendix B Computer code for the estimation of longitudinal strains in buried pipelines subjected to transverse ground movements using closed form solutions by Liu and O'Rourke (1997)

```

%%%%%%%%%%%%%%%%%%%%%%%%%%%%%%%%%%%%%%%%%%%%%%%%%%%%%%%%%%%%%%%%%%%%%%%%
% DATE: Feb 18, 2022
% TO: The User(s)
% FROM: Prajakta Jadhav and Dharma Wijewickreme
% This code is developed by Prajakta Jadhav under the supervision of Dr. Dharma Wijewickreme (Geohazards group at UBC Vancouver) solely for use
% in the Mitacs-funded "Liquefaction-induced Geohazards Data Sets for Training of BBN model for Pipeline Risk Assessment due to
% Liquefaction-induced Permanent Ground Displacements as input to Multi-hazard BBN modeling (IT13626 - Mitacs Accelerate Research Program)".
% This code presents a simplified approach to compute longitudinal strains in buried pipes subjected to transverse ground movements.
% The computations are made in accordance with the closed-form analytical solutions proposed by Liu and O'Rourke (1997). The code was written
% in view of meeting the requirements of the above-mentioned project so as to provide initial datasets as input for training BBN model developed
% through this project. It is to be noted that the computed longitudinal strains from Liu and O'Rourke (1997) are based on certain set of
% assumptions and cannot be considered as the replacement for those obtainable using rigorous finite element analyses. The users are responsible
% for using the code with due quality control checks and assessment of suitability when implementing the algorithm for engineering design and
% research.
%
% It is recommended that this code be used/ referred in conjunction with the technical report (Jadhav and Wijewickreme, 2022)
% related to the above project

% Ref:
% Liu, X., & O'Rourke, M. J. (1997). Behaviour of continuous pipeline subject to transverse PGD.
% Earthquake Engineering & Structural Dynamics, 26(10), 989-1003.
% C-CORE, & , D.G. Honegger Consulting SSD, I. (2009a). Guidelines for Constructing Natural Gas and Liquid Hydrocarbon Pipelines
% Through Areas Prone to Landslide and Subsidence Hazards. Design, Materials, and Construction Committee of Pipeline Research Council
% International, Inc., January.
% Jadhav, P. and Wijewickreme, D., 2021, "Liquefaction-induced Geohazards Data Sets for Training of BBN model for Pipeline
% Risk Assessment due to Liquefaction-induced Permanent Ground Displacements as input to Multi-hazard BBN modeling, Report prepared
% for BC Oil and Gas Commission, 50 pages.

```

```

%%%%%%%%%%%%%%%%%%%%%%%%%%%%%%%%%%%%%%%%%%%%%%%%%%%%%%%%%%%%%%%%%%%%%%%%

```

```

clc
clear all
close all;
% Outer diameter of pipe based on NPS sizes
DD=[0.1016
0.2032
0.3048
0.6096
0.762
1.0668
];
% Thickness of pipe
T=[0.0054
0.0055
0.0064
0.0071
0.0105
0.0091
];

```

```

% corrosion level
f=[0.0 0.1 0.2 0.3];
% Calculation of Tu, Pu based on PRCI (2009) equations
for ii=1:1
    for i1=1:length(f)
        D=DD(ii)-(2*f(i1))*T(ii);
        h=1.0;
        H=h+(D/2);
        t=(1-f(i1))*T(ii);
        d=D-t;
        phi_d=32;
        phi=phi_d*pi/180;
        gamma=18.0*10^3;
        gamma_t=18.0*10^3;
        delta=0.7*phi;
        K=1-sin(phi);
        Tu=pi*D*H*gamma*0.5*(1+K)*tan(delta);
        Nqh_tab=xlsread('Nqh');
        H_D=H/D;
        Lia = ismember(phi_d, [35 40 45]);
        e_elastic=[];
        if Lia==1 || phi_d<35
            Nqh=Nqh_cal(phi_d, Nqh_tab, H_D);
        elseif phi_d>35 && phi_d<40
            Nqh1=Nqh_cal(35, Nqh_tab, H_D);
            Nqh2=Nqh_cal(40, Nqh_tab, H_D);
            Nqh=((phi_d-35)*(Nqh2-Nqh1)/5)+Nqh1;
        elseif phi_d>40 && phi_d<45
            Nqh1=Nqh_cal(40, Nqh_tab, H_D);
            Nqh2=Nqh_cal(45, Nqh_tab, H_D);
            Nqh=((phi_d-40)*(Nqh2-Nqh1)/5)+Nqh1;
        end
        Pu=Nqh*gamma*H*D;
        Nq=exp(pi*tan(phi))*tan((pi/4)+(phi/2))^2;
        Nx=exp((0.18*phi_d)-2.5);
        Qd=(Nq*gamma*H*D)+(0.5*Nx*gamma_t*(D^2));
        if Pu>Qd
            Pu=Qd;
        end
        Nqv=H_D*tan(0.9*phi);
        if Nqv>Nqh
            Nqv=Nqh;
        end
        Qu=Nqv*gamma*H*D;
    end
end

```

```

#####
% Calculation of strains based on Liu and O'Rourke (1997) closed form
% solutions
E=210*10^9;
I=pi*((D^4)-(d^4))/64;
W=100;
dcr_bend=Pu*(W^4)/(384*E*I);
i=1;
e=1;
trial=0.2;
while e>0.01
    del=trial;
    S=Pu*(W^2)/(16*del*pi*D*t);
    d_cr_axial(i)=((4*W/(pi*pi))*((S*W/E)+((2*pi*D*t*S*S)/(2*E*Tu))))^0.5;
    e=abs(d_cr_axial(i)-del);
    trial=d_cr_axial(i);
    i=i+1;
end
dcr_axial=d_cr_axial(i-1);
del_cr=1/((1/dcr_bend)+(1/dcr_axial));
A=pi*((D/2)^2)-((d/2)^2);
if i1=1
    del_cr_i=del_cr;
end
i=1;
for j=0:0.1:17
    if j<=del_cr
        S_E(i)=0.5*pi*j*(Tu/(A*E*W))^0.5;
        e_elastic(i)=S_E(i)+(pi*pi*j*D/(W^2));
        e_elastic_lin(i)=e_elastic(i);
        jjj(i)=j;
    else
        S_E(i)=0.5*pi*del_cr*(Tu/(A*E*W))^0.5;
        e_elastic(i)=S_E(i)+(pi*pi*del_cr*D/(W^2));
    end
    jj(i)=j;
    result1(i,:)=[j e_elastic(i)];
    i=i+1;
end
result(i1,:)=[D t del_cr e_elastic(i-1)];
result1(:,(2*i1)-1:(2*i1))=result1;
plot(jj,e_elastic);
vq(i1)=interpl(e_elastic_lin, jjj, 0.0025);
factor(i1)=vq(i1)/vq(1);
f_delta(i1)=del_cr/del_cr_i;
end
end

```

```

%%%%%%%%%%%%%%%%%%%%%%%%%%%%%%%%%%%%%%%%%%%%%%%%%%%%%%%%%%%%%%%%%%%%%%%%
% DATE: Feb 18, 2022
% TO: The User(s)
% FROM: Prajakta Jadhav and Dharma Wijewickreme
% This subroutine is written for calculating the Nqh values to be used in
% the calculation of lateral soil restraint force, Pu, required for the
% estimation of longitudinal strains in 'Strains_Liu_Rourke.m' subroutine.
%
% Ref:
% C-CORE, & , D.G. Honegger Consulting SSD, I. (2009a). Guidelines for Constructing Natural Gas and Liquid Hydrocarbon Pipelines
% Through Areas Prone to Landslide and Subsidence Hazards. Design, Materials, and Construction Committee of Pipeline Research Council
% International, Inc., January.
%%%%%%%%%%%%%%%%%%%%%%%%%%%%%%%%%%%%%%%%%%%%%%%%%%%%%%%%%%%%%%%%%%%%%%%%

```

```

function [Nqh] = Nqh_cal(phi_d, Nqh_tab, H_D)
for i=1:5
    if phi_d<35
        phi_d1=35;
    else
        phi_d1=phi_d;
    end
    if phi_d1==Nqh_tab(i,1)
        if H_D>Nqh_tab(i,2) && H_D<=Nqh_tab(i,3)
            a=Nqh_tab(i,4);
            b=Nqh_tab(i,5);
            Nqh=a+(b*H_D);
            if Nqh>Nqh_tab(i,6)
                Nqh=Nqh_tab(i,6);
            end
        end
    end
end
end
end

```